INSTITUTO DE TECNOLOGÍA QUÍMICA
(UPV-CSIC)

UNIVERSITAT POLITÈCNICA DE VALÈNCIA

CATALYTIC TRANSFORMATIONS OF OXYGENATED COMPOUNDS DERIVED FROM BIOMASS AQUEOUS EFFLUENTS INTO HIGH-VALUE PRODUCTS

PhD in Sustainable Chemistry

Doctoral candidate:
Alberto Fernández-Arroyo Naranjo

Director:
Dr. Marcelo E. Domine

Obra Social "la Caixa"
EXCELENCIA SEVERO OCHOA

Valencia, September 2018

Agradecimientos

"You cannot hope to build a better world without improving the individuals. To that end, each of us must work for his own improvement"
Marie Curie

"En principio, la investigación necesita más cabezas que medios"
Severo Ochoa

Dicen que el saber no ocupa lugar, pero sí que conlleva mucho tiempo, dedicación y esfuerzo. Esfuerzo que individualmente sería en vano, si no fuera por el apoyo y el trabajo colectivo que es imprescindible alrededor de un trabajo como éste. Por ello, quisiera agradecer a todos aquellos que de una u otra manera me han ayudado durante el desarrollo de esta tesis.

A la Fundación "la Caixa" y al Instituto de Tecnología Química (ITQ) por el contrato pre-doctoral del Programa Internacional de Doctorado "la Caixa"-Severo Ochoa que me ha permitido realizar mis estudios de doctorado.

A mi director Dr. Marcelo E. Domine por mantener la confianza en mí desde que nos conociéramos el verano de 2011 y darme la oportunidad de integrarme en su grupo de trabajo. Por su paciencia, consejos y orientación a lo largo de todo este tiempo.

Durante estos cuatro años, he tenido la suerte de poder colaborar y aprender de otros investigadores, cuya ayuda me ha permitido completar mi formación y ha hecho más fácil todo este trabajo. Quisiera agradecer:

Al Prof. José Manuel López-Nieto, por su capacidad de enseñar y por todas las reuniones y críticas constructivas sobre catálisis. También agradecer a Dani, con quien he compartido muchas horas de trabajo y charlas sobre catálisis, ciencia y la vida en general.

Al Prof. José Antonio Navío y su grupo de investigación en la Universidad de Sevilla, por su amabilidad y su disposición a compartir su experiencia.

Al Prof. Daniel E. Resasco, por su hospitalidad durante mi estancia en EEUU. Por compartir sus ideas y perspectivas en investigación, por incluirme como uno más en su grupo de trabajo y hacer de esos tres meses una experiencia muy enriquecedora.

A todo el personal técnico del Instituto de Tecnología Química y al Servicio de Microscopía de la UPV por toda su colaboración y ayuda.

A mis amigos y compañeros de grupo por todo el tiempo compartido. Chelo, gracias por ser un gran apoyo desde mi primer día en un laboratorio, hasta los últimos días de esta etapa. Marvin, gracias por tu amabilidad, tu sabiduría, tus ganas de compartir y por ser como un segundo jefe. Cristina, gracias por estar siempre dispuesta a ayudar, y por todos los momentos compartidos dentro y fuera del laboratorio. Jaime, gracias por tu ayuda y por las grandes charlas sobre ciencia/fútbol durante este tiempo. Zaher, gracias por tu apoyo. Miriam, gracias también por tu amabilidad, tu cercanía y tu ayuda con la microscopía. Susana, gracias por tu amabilidad y tu ayuda.

A todos los compañeros que me han hecho sentir parte de un grupo más grande. Gracias a cada una de las personas que han compartido su tiempo conmigo durante estos últimos cuatro años, ya sea en el trabajo, haciendo deporte o aquellos, que desde la distancia siempre se han preocupado por mí y me han apoyado durante este tiempo.

A Larisha, por compartir conmigo todo este tiempo, por soportarme, entenderme, animarme y en definitiva, hacerme mejor persona. Gracias por acompañarme en todos estos momentos. Se cierra una etapa, pero se abre un nuevo camino. Y a tu lado, éste siempre será mejor.

A mi familia: mis padres, mis tíos, mi hermana, por el apoyo y el ánimo incondicional. Porque sin la educación y los valores recibidos durante toda mi vida, este trabajo no sería una realidad.

Muchas gracias,

Alberto Fernández-Arroyo Naranjo

The valorisation of lignocellulosic biomass and its derivatives has become a sustainable alternative to the use of fossil sources for the production of fuels and chemicals. In this context, the conversion of light oxygenated compounds present in aqueous effluents derived from primary treatments of biomass (i.e. fast pyrolysis), after a phase separation process via water addition is a key step in the actual bio-refinery scheme processes. The strategy is based on the transformation of these low-value water-soluble oxygenated compounds into a mixture of hydrocarbons and aromatics useful for blending with automotive fuels. In general, the activity of the catalysts employed in these processes is based on their bifunctional character. Nonetheless, their activity in complex aqueous mixtures and their stability under faithful operating conditions close to industrial scenarios are critical challenges to be further applied.

This thesis comprises a detailed work in the design of new solid catalysts with high activity and stability in consecutive aqueous-phase condensation reactions of light oxygenated compounds (C_1-C_4) mixtures under moderated process conditions. In this sense, this work differs from usual probe molecules studies performed even in the absence of water.

Firstly, mixed oxides (including $Ce_xZr_{1-x}O$ and hydrotalcite-derived materials) were employed as they have been widely studied in condensation and ketonization reactions. These materials show good catalytic results in the liquid-phase condensation of light oxygenates, but strong catalysts deactivation was observed due to the active phase partial leaching. Therefore, new heterogeneous acid catalysts must be developed in order to meet these new process requirements: complex aqueous

environments with high contents of organic acids and moderated reaction conditions.

In this sense, the addition of aqueous HF during TiO_2 catalysts synthesis is essential to selectively control the preferential growth of catalytic more reactive {001} TiO_2 facets. Moreover, Lewis acid sites on faceted TiO_2 materials have great stability in condensation reactions, especially in the presence of organic acids and high water contents. Thus, this strategy allows obtaining materials that show better catalytic results and stability than other commercial titanium oxides.

Moreover, hydrothermal synthesized Nb- and WNb-mixed oxides have shown the advantage of having crystalline structure, area and acid properties modified by tailoring their composition and post-synthesis heat-treatments conditions. Optimized NbO_x and WNbO materials show higher activity and stability in the aqueous-phase condensation of oxygenated compounds than other commercial samples, commonly employed in literature

Finally, new acid catalysts prepared via co-precipitation based on tin, titanium and niobium ($Sn_xTi_yNb_zO$) mixed oxides have been developed. These materials mainly present SnO_2 rutile-phase crystalline structure, which has been claimed to have interesting hydrophobic characteristics. Tailoring of composition and calcination conditions allows obtaining mixed oxides with uniform crystalline structures, enhanced surface areas and a higher concentration of Lewis acid sites compared to analogous commercial catalysts. These materials show high activity and stability in the valorisation of oxygenated compounds present in aqueous effluents derived from different biomass processes.

La valorización de biomasa lignocelulósica y de sus derivados supone una alternativa sostenible frente a la utilización de fuentes fósiles para la producción de combustibles y productos químicos. En este contexto, el aprovechamiento de compuestos oxigenados presentes en efluentes acuosos derivados de tratamientos primarios de la biomasa (vía pirólisis rápida), tras un proceso de separación de fases, es fundamental en el esquema actual de bio-refinería. La estrategia consiste en transformar estos compuestos orgánicos en mezclas de hidrocarburos y compuestos aromáticos de utilidad como componentes y/o aditivos en combustibles líquidos. Los materiales catalíticos comúnmente estudiados para este tipo de procesos deben su actividad a sus propiedades multifuncionales. Sin embargo, su actividad en mezclas acuosas complejas y su estabilidad bajo condiciones de reacción más próximas a la realidad industrial continúan siendo un desafío en vistas a su futura aplicación.

La presente Tesis Doctoral se centra en el diseño de nuevos catalizadores heterogéneos que sean activos y resistentes en reacciones de condensación consecutivas en fase acuosa de mezclas de compuestos oxigenados ligeros (C_1-C_4) bajo condiciones de reacción moderadas. En este sentido, este trabajo difiere de los estudios habituales que emplean compuestos modelo de manera individual y en ausencia de agua.

En primer lugar, óxidos mixtos (incluyendo $Ce_xZr_{1-x}O$ e hidrotalcitas), que han sido ampliamente utilizados en reacciones de condensación y cetonización, muestran buenos resultados catalíticos en la condensación en fase acuosa, pero graves problemas de estabilidad debido principalmente al *leaching* de la fase activa de estos materiales. Esto demuestra la necesidad de desarrollar nuevos catalizadores ácidos

capaces de operar en sistemas complejos en presencia de agua y ácidos orgánicos, bajo condiciones de reacción moderadas.

En este sentido, la adición de HF durante la síntesis de catalizadores basados en TiO_2, permite obtener materiales donde se expone mayoritariamente el plano {001}, que es catalíticamente más activo. Además, los sitios ácidos de Lewis presentes en estos materiales de TiO_2 facetados, presentan una gran estabilidad en reacciones de condensación, especialmente en presencia de ácidos y grandes cantidades de agua. Esta estrategia permite desarrollar materiales con mejor actividad catalítica y estabilidad que otros catalizadores comerciales basados en TiO_2.

Por otra parte, la síntesis hidrotermal de óxidos metálicos basados en Nb y W-Nb permite obtener materiales cuya estructura cristalina, propiedades texturales y propiedades ácidas pueden ser modificadas controlando la composición y las condiciones de calcinación aplicadas. Esto permite obtener catalizadores optimizados respecto a los empleados en literatura, que muestran gran actividad y elevada estabilidad en reacciones de condensación de compuestos oxigenados en fase acuosa.

Por último, se han desarrollado nuevos materiales basados en óxidos mixtos de estaño, titanio y/o niobio ($Sn_xTi_yNb_zO$) preparados por co-precipitación que presentan mayoritariamente la estructura tipo rutilo del SnO_2, la cual posee características hidrófobas. El control de la composición y las condiciones de calcinación permite obtener óxidos con estructuras cristalinas uniformes, altas áreas superficiales y mayor densidad de sitios ácidos de Lewis respecto a los respectivos óxidos comerciales. Estos materiales son catalizadores activos y muy resistentes en la valorización de compuestos oxigenados presentes en efluentes acuosos derivados de distintos tratamientos de la biomasa.

La valorització de biomassa lignocel·lulòsica i dels seus derivats suposa una alternativa sostenible enfront de la utilització de fonts fòssils per a la producció de combustibles i productes químics. En aquest context, l'aprofitament de compostos oxigenats presents en efluents aquosos derivats de tractaments primaris de la biomassa (via piròlisi ràpida), després d'un procés de separació de fases, és fonamental en l'esquema actual de bio-refineria. L'estratègia consisteix a transformar aquests compostos orgànics en mescles d'hidrocarburs i compostos aromàtics d'utilitat com a components o additius en combustibles líquids. Els materials catalítics comunament estudiats per a aquest tipus de processos deuen l'activitat a les seues propietats multifuncionals; no obstant això, la seua activitat en mescles aquoses complexes i la seua estabilitat sota condicions de reacció més pròximes a la realitat industrial continuen sent un desafiament amb vista a la seua futura aplicació.

La present tesi doctoral se centra en el disseny de nous catalitzadors heterogenis que siguen actius i resistents en reaccions de condensació consecutives en fase aquosa de mescles de compostos oxigenats lleugers (C_1-C_4) sota condicions de reacció moderades. En aquest sentit, aquest treball difereix dels estudis habituals, que empren compostos model de forma individual i en absència d'aigua.

En primer lloc, òxids mixts (inclosos $Ce_xZr_{1-x}O$ i hidrotalcites), que han sigut àmpliament utilitzats en reaccions de condensació i cetonització, mostren bons resultats catalítics en la condensació en fase aquosa, però greus problemes d'estabilitat a causa principalment de la lixiviació de la fase activa d'aquests materials. Això demostra la necessitat de desenvolupar nous catalitzadors àcids capaços d'operar en sistemes

complexos en presència d'aigua i àcids orgànics, sota condicions de reacció moderades.

En aquest sentit, l'addició d'HF durant la síntesi de catalitzadors basats en TiO_2, permet obtenir materials on s'exposa majoritàriament el plànol {001}, que és catalíticament més actiu. A més, els llocs àcids de Lewis presents en aquests materials de TiO_2 facetats, presenten una gran estabilitat en reaccions de condensació, especialment en presència d'àcids i grans quantitats d'aigua. Aquesta estratègia permet desenvolupar materials amb millor activitat catalítica i estabilitat que altres catalitzadors comercials basats en TiO_2.

D'altra banda, la síntesi hidrotermal d'òxids metàl·lics basats en Nb i W-Nb permet obtenir materials l'estructura cristal·lina, les propietats texturals i les propietats àcides dels quals poden ser modificats controlant la composició i les condicions de calcinació aplicades. Això permet obtenir catalitzadors optimats respecte als emprats en la literatura, que mostren gran activitat i elevada estabilitat en reaccions de condensació de compostos oxigenats en fase aquosa.

Finalment, s'han desenvolupat nous materials basats en òxids mixts d'estany, titani o niobi ($Sn_xTi_yNb_zO$) preparats per coprecipitació, que presenten majoritàriament l'estructura tipus rútil del SnO_2, la qual té característiques hidròfobes. El control de la composició i les condicions de calcinació permeten obtenir òxids amb estructures cristal·lines uniformes, altes àrees superficials i major densitat de llocs àcids de Lewis respecte als respectius òxids comercials. Aquests materials són catalitzadors actius i molt resistents en la valorització de compostos oxigenats presents en efluents aquosos derivats de diferents tractaments de la biomassa.

Index

Chapter 1. Introduction

Chapter 2. Objectives

Chapter 3. Experimental Procedure

Chapter 4. Ceria-Zirconia and hydrotalcite-derived mixed oxides as acid catalysts for the aqueous-phase condensation of oxygenated compounds

Chapter 5. {001} Faceted TiO_2 materials as acid catalysts for the aqueous-phase condensation of oxygenated compounds

Chapter 6. Niobium and Tungsten-Niobium oxides as acid catalysts for the aqueous-phase condensation of oxygenated compounds

Chapter 7. Tin-based mixed oxides as acid catalysts for the aqueous-phase condensation of oxygenated compounds

Chapter 8. General conclusions

Chapter 9. List of Figures and Tables

CHAPTER 1

INTRODUCTION

1.1. The lignocellulosic biomass alternative

For the last 70 years, world population multiplied more rapidly than ever before. In 1950, the world had 2.5 billion people, and in 2017 this number has raised to more than 7.6 billion people[1]. This massive change has been mainly caused by the industrial revolution and medical advances, which have notably increased life expectancy. Simultaneously, human demand for energy and chemical products has suffered from a tremendous expansion. Indeed, energy use (expressed as kg of oil equivalent per capita) has globally risen from 1,336 in 1960 to 1,919 in 2015, whereas more developed countries as Spain have even multiplied this value by four in the last 50 years[2].

The production of fuels and other chemicals such as polymer precursors is predominantly obtained from fossil sources and petroleum refining. The major source of energy also comes from fossil fuels: Coal, natural gas and oil accounted for 81% of the world´s primary energy consumption. However, finite reserves of fossil fuels and their unequally distribution around the world may lead to international conflicts derived from price variability, economic vulnerabilities and energy dependence. In fact, far from going down, Europe´s and Spain´s dependency on the import of fossil sources has dramatically grown (>40%) in the last years. Furthermore, fossil fuels are responsible for great part of CO_2 emissions[3], contributing to global warming and several raising environmental concerns[4].

World Commission on Environment and Development (Bründtland Commission) was the start of a crucial turning point. Its report in 1987[5] introduced the *"Sustainable Development"* concept, which helped to change international perspective towards economic, social and environmental development. Analogously, 12 Principles of Green Chemistry developed by Paul Anastas and John Warner[6] were another important milestone in order to improve sustainability and efficiency from the chemical industry point of view.

Therefore, the future economy must rely on alternative and more sustainable pathways, which include the use of renewable energies and especially of biomass[7,8]. In this sense, the valorisation of biomass and its derivatives has become one of the most promising sustainable alternatives against to the evident economic and environmental concerns of fossil sources for the production of chemical and fuels[9–12].

Biomass refers to any organic or biological matter derived from living or recently living organisms (i.e. plants, animal residues) that is generated through the photosynthesis. Carbon dioxide (CO_2) and water is absorbed by the plants and lately transformed in more complex molecules with higher energy content. Thus, solar energy driving photosynthesis is stored in the chemical bonds of biomass structural components[13]. The wide range of biomass sources available in nature includes feedstock characterised by heterogeneous composition and different physical status (Figure 1.1). These biomass resources can be classified according to the supply sector: Forestry, agricultural (lipid, sugar, starch or lignocelullosic crops), livestock waste, industrial (i.e. wood, food, paper) and urban waste (i.e. municipal solid waste, sewage sludge, among others).

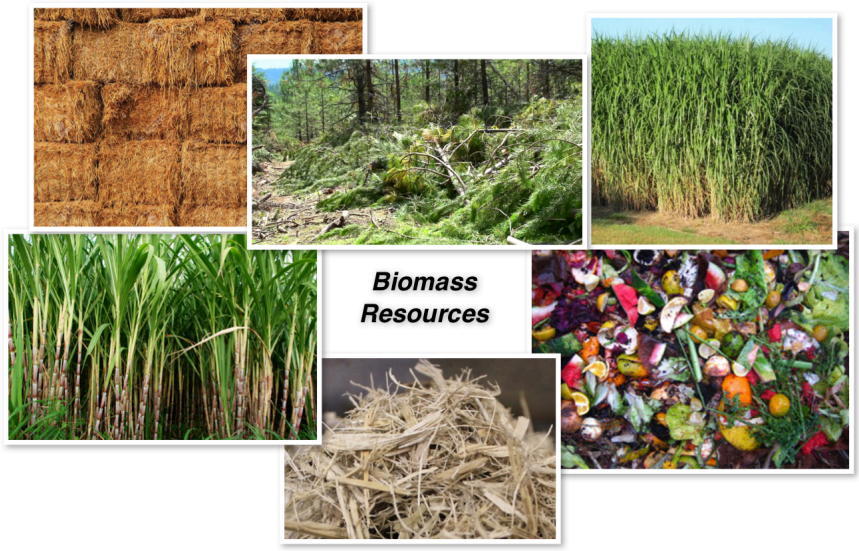

Figure 1.1. Different types of biomass resources.

The efficient transformation of these bio-based resources, which are renewable and come close to CO_2 neutrality scenarios, is a necessity[14,15]. First-generation biofuels produced from agricultural crops were the initial step in this direction[16]. Sugars and carbohydrates-containing plants can be transformed via fermentation into different alcohols, such as methanol, ethanol and butanol[17]. Vegetable oils and fats can be transformed via transesterification to produce biodiesel[15], whereas biogas can be achieved by anaerobic digestion of waste streams or residues[18].

Nonetheless, most of first-generation biofuels have several drawbacks, including competition with food crops, water supply and land occupation. They may also have a negative impact on biodiversity due to intensive farming and experts find several concerns about their carbon footprints. Although these technologies have been widely studied and are easy to process, their associated problems must be solved in order to consider biomass as a sustainable alternative[19].

Therefore, the production of second-generation biofuels from lignocellulosic non-food crops stands as a reasonable solution. The main sources of lignocellulosic biomass are wood from conventional and short-rotation forestry, energy crops such as switch grass and residues from forests, agricultural (i.e. bagasse, corn straw/stubbles, etc.) and industrial processes (i.e. sawdust). Third generation biofuels based on intensive energy crops with high energy density are expected to go beyond these perspectives[20,21].

1.1.1. Lignocellulosic biomass composition

The chemical composition of lignocellulosic biomass varies among species but, in general terms, plants consist of three main components (Figure 1.2): Cellulose, hemicellulose and lignin[22,23]. In particular, wood is essentially composed of 38-50% of cellulose, 23-32% of hemicellulose and 15-25% of lignin.

Cellulose is an unbranched and crystalline polysaccharide consisting of a linear chain of several hundred to thousands of β (1-4) linked D-glucose units[24]. Upon acid hydrolysis, cellulose can be broken into cellotriose (trimer), cellobiose (dimer) or glucose.

Hemicellulose is a branched hetero-polymer with a random structure, shorter than cellulose. This polysaccharide contains five different sugar monomers: glucose, xylose, mannose, galactose and arabinose. Hemicellulose is present as an amorphous matrix that surrounds the crystalline cellulose skeleton[25].

Lastly, lignin is a cross-linked co-polymer formed by three major phenolic monomers, methoxylated to various degrees: p-coumaryl alcohol, coniferyl alcohol and sinapyl alcohol. Lignin fills the spaces in the cell wall between cellulose and hemicellulose conferring mechanical strength and acting as a protective layer. All three components have covalent cross-linkages between the polysaccharides and lignin, making biomass a composite material[26].

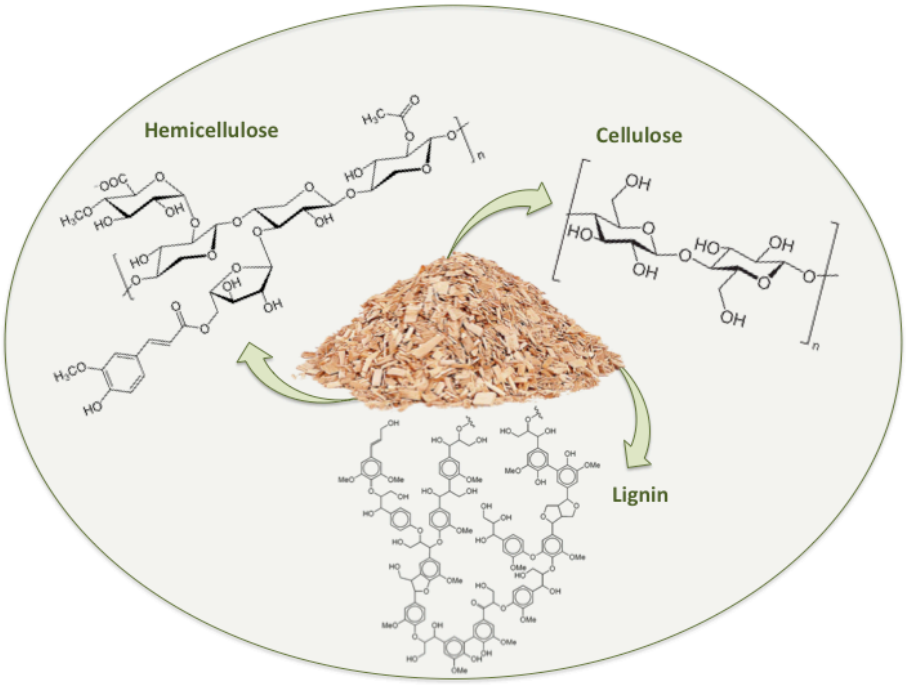

Figure 1.2. Schematic representation of main components of lignocellulosic biomass.

Several physical and chemical pre-treatment processes have been successfully studied as a key step in biomass processing. Subsequently, the environmental and socioeconomic limitations of first generation biofuels, together with these pre-treatment processes, have placed greater interest on lignocellulosic biomass. Biomass without competing with

food production arises as an alternative to reduce the dependency on crude oil, carbon and natural gas[27,28] for the production of fuels[29–31] and high value added chemicals[32–34].

Moreover, lignocellulosic biomass valorisation shows promising reduction of CO_2 emissions[35], while many different biomass resources can be handled including industrial, agricultural and forestry wastes. For instance, in 2005, the United States Department of Agriculture (USDA) and the United States Department of Energy (DOE) released a joint report where they found sufficient land resources in the US for fulfilling the goal of replacing 30% of fossil sources with biofuels by 2030[36]. In the case of Spain, biomass resources availability is also unquestionable. Biomass is currently being underused as other potential renewable energy sources. According to the *"Tercer Inventario Forestal Nacional (IFN3)"*[37], Spanish forestry mass has increased from 597 Mm^3 in 1997 to 928 Mm^3 in 2007. Annual felling, pruning and cleaning of forests are estimated around 15 Mm^3, whereas 10 Mtons of forestry residues are wasted nowadays. Forestry residues valorisation may also help improving the clearing of woodlands and reducing forests fires. Biomass versatility also gives the opportunity of combined heat, power and fuels production; meanwhile distributed generation can be promoted[38].

In conclusion, lignocellulosic biomass valorisation allows producing energy, fuels and chemical products based on cheaper and more abundant feedstock, caring environment (e.g. fossil CO_2 emissions reduction), reducing energy imports and boosting local employment and entrepreneurship.

1.2. Bio-refinery concept

If bio-fuels and bio-products from lignocellulosic biomass are claimed to become an industrial business reality, they must compete against well-established fossil sources technologies. In this context, the term *"bio-refinery"* has emerged as an analogous concept to classic oil refineries, where oil is replaced by biomass as raw material[39]. A bio-refinery can be considered as an integral unit that can deal with all types of renewable biological feedstock and convert them to energy, biofuels and valuable biochemical products.

The efficacy of the oil industry over the last century has been based on the efficient and complete usage of petroleum sources by whole optimized refining technologies like catalytic cracking[40]. The economic viability of current refineries relies on highly integrated industries, where simultaneous production of large volumes of fuels with lower amounts of more valuable chemicals as polymer precursors and fertilizers is managed[31].

Following a similar approach, a biomass-based industry can be achieved by the conversion of a mixture of bio-feedstock into fuels, chemicals and energy through the integrated processing of selected biomass derivatives ("*platform molecules*"). Polyols (glycerol, sorbitol, xylitol), organic acids (succinic, levulinic, itaconic, fumaric, lactic) or other molecules as ethanol, furans and bio-hydrocarbons have been highlighted due to their future potential as raw materials and

intermediates for further industrial processes[41]. Some authors have even claimed the possibility of exploiting synergies and infrastructures between bio- and oil refineries for the production of fuels from biomass, in order to make a more rapid transition to a more sustainable economy[42].

However, biomass and platform molecules composition differs from fossil sources chemical nature, making this direct extrapolation remarkably challenging. Lignocellulosic biomass is characterised by its high versatility and it presents a high degree of oxygenated groups, which make these derivatives water-soluble, low volatile and highly reactive. On the other hand, oil-derived feeds are oppositely characterised: hydrophobicity, high volatility and low reactivity. Thus, different strategies must be considered in order to effectively deal with both resources (Figure 1.3).

Heterogeneous catalysis[43] plays an essential role in chemical industry and especially in current oil refineries, where they have been designed to operate with hydrocarbons. Classical solid catalysts are active and resistant under hydrophobic high-temperature gas-phase processes, wherein their main goal is to activate generally unfunctionalised molecules. Nonetheless, biomass derivatives, usually obtained from aqueous solutions and mild-temperature processes, are preferred to avoid undesired reactivity from highly functionalised molecules. Therefore, new heterogeneous catalysts, catalytic routes and economically feasible technologies must be found to approach these new requirements[44,45].

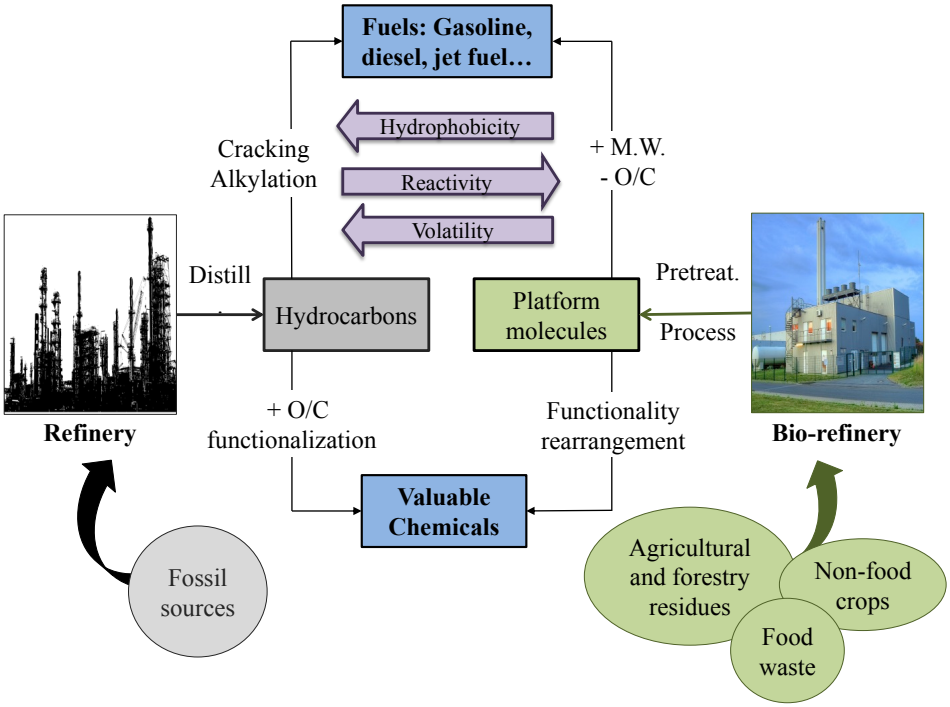

Figure 1.3. Bio-refinery strategy. Adapted from Serrano-Ruiz et al., 2011[31].

At this point, "*Green Chemistry"* stands as a sustainable pathway to attend growing fuels and chemical products demand through the efficient use of renewable resources, waste removal and avoiding the use of toxic/hazardous reactants and solvents[27,46]. The integration of Green Chemistry into bio-refineries and the joint application of low environmental impact conversion technologies can lead into sustainable production chains of biofuels and high value chemicals. Process intensification[47], together with energy optimization strategies are also helpful to make bio-refineries economically competitive and lead to the progressive replacement of current refinery products.

In this new bio-economy, the co-production of biofuels together with valuable chemicals is an inevitable need to increase the efficiency and competitiveness of the processes. Furthermore, the new strategies proposed for innovative processing of 2nd generation lignocellulosic biomass at bio-refineries include the residual currents and aqueous effluents valorisation[48].

1.2.1. Biomass transformation processes

In this context, biomass can be directly used via combustion to produce heat and electricity or indirectly to form bio-fuels, bio-polymers or other bio-products. Lignocellulosic biomass conversion processes[49] can be classified in primary and secondary "*downstream*" processes. Previous treatment methods may be needed (including dilute acid/alkali treatment, ammonia/steam explosion, among others) to break lignin seal and make cellulose and hemicellulose accessible to hydrolysis for conversion to fuels[50,51].

Biomass or its derivatives are handled and transformed into mixtures of intermediate products by primary processes. These intermediates are further processed, upgraded and isolated through secondary processes to obtain the final valuable products. Primary processes have been widely developed and currently have industrial application, whereas secondary processes are still under active research. This explains why biomass is directly used in Europe to produce heat (77%) and electricity (14%), meanwhile small volumes of biodiesel, bio-gasoline or other valuable bio-products are commercialised[52].

The feedstock nature and quality represents a key aspect determining the decision on the most suitable technology to be applied. The main primary lignocellulosic biomass transformation processes are: mechanical processes (fractioning[53], pressing, particle size reduction), biochemical processes (fermentation[54], enzymatic conversion[55]), chemical processes (hydrolysis[56]) and thermochemical processes (gasification[57], pyrolysis[58], liquefaction[59] and combustion).

As above mentioned, electricity and *bio-heating* for individual, district or industrial processes are currently the main lignocellulosic biomass applications. After pelletisation, woody biomass is used by direct combustion or co-combustion with coal. This technology stands by far as the most developed sector in Europe and worldwide. However, biofuels from agriculture and forest residues are emerging sectors, which are drawing much attention[10]. In this sense, gasification stands out as a relevant process to produce CO and H_2 ("*syn-gas*") analogously to carbon gasification technologies. This syn-gas can be further upgraded to produce aliphatic hydrocarbons via Fischer-Tropsch (FT process)[60], methanol and superior alcohols (C_{2+}, via adapted FT catalytic processes) or even H_2 (via Water-Gas-Shift and H_2 purification processes).

Hydrolysis is another widely used method to transform lignocellulosic biomass into sugars. Mainly mineral acids as homogeneous catalysts, together with high temperatures have been traditionally used. Excessive wastes production from further acid neutralisation steps have motivated the use of solid acid catalysts and enzymatic catalysis under moderated temperatures to carry out these processes.

Pyrolysis processes consists in the organic matter thermal decomposition occurring in the complete absence of oxygen. Products distribution including char, gas and liquids (bio-oils) can be modified as a function of reaction temperature, residence time and heating rate.

On the other hand, fermentation consists in anaerobic processes, where biomass-derived sugars are transformed into alcohols and organic acids by yeast or bacteria organisms. These processes also constitute an important source of high-functionalised oxygenated compounds in the bio-refineries process networks.

Pyrolysis processes for bio-oil production and fermentation technologies will be further discussed in detail (Section 1.3 and 1.6 respectively), as derived downstream processes are the main field of this work.

Heretofore, bio-ethanol production from wheat, sugar cane and corn-derived sugar fermentation was the first example of bio-refinery. Afterwards, efforts were made in order to achieve more valuable products (*platform molecules* and bio-oils) from the same raw materials.

The subsequent issues derived from the use of these resources have led to the 3rd type of bio-refineries, where all the three components (cellulose, hemicellulose and lignin) from lignocellulosic biomass must be used to produce advanced fuels and chemical products[61,62] (Figure 1.4). Therefore, conversion processes involve a limited number of reaction, separation and purification steps. Coupling of different catalytic technologies in an integrated bio-refinery design can lead to the development of improved and economical competitive industries[63,64].

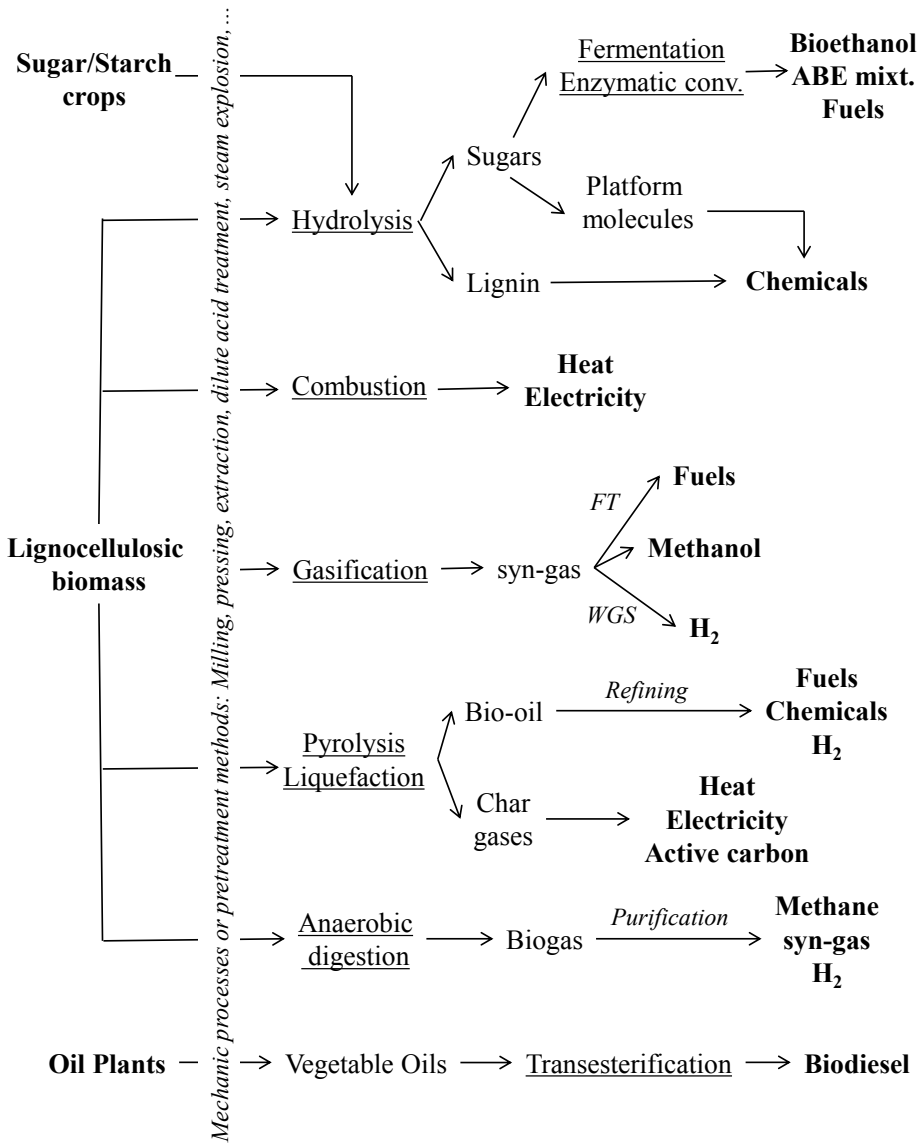

Figure 1.4. Biomass conversion processes in the bio-refinery.

1.3. Bio-oils production from fast pyrolysis processes

Bioethanol, from sugar fermentation processes, has low energetic density and compatibility issues with current hydrocarbon infrastructures and fuel engines. Thus, the development of new technologies capable of producing suitable transport fuels from lignocellulosic biomass has been the subject of great interest in recent years[29,65]. In this context, biomass fast pyrolysis processes stand as an interesting strategy.

Lignocellulosic biomass pyrolysis consists in the organic matter thermal decomposition occurring in the complete absence of oxygen. Biomass suffers diverse transformations including depolymerization, dehydration and C-C cleavage reactions under mild temperature conditions (200-800 ºC)[66,67]. Cellulose, hemicellulose and part of the lignin disintegrate to form smaller molecules, which are gases at the pyrolysis temperatures[68]. Afterwards, some of the vapours condense to form a liquid (which is named bio-oil) and the remaining parts (most of them derived from lignin) keep as a solid (charcoal). Thus, product distributions obtained from different pyrolysis methods include char, gas and liquids. This product yield can be modified as a function of reaction temperature, residence time and heating rate[69]. Slow pyrolysis at low temperature and long residence time increases the production of charcoal. High temperature conditions and short residence times favour gas production, whereas moderate temperature and short vapour residence time maximizes the production of liquids (Table 1.1)[70].

Table 1.1. Product distribution obtained by different pyrolysis methods.

Method (heating rate)	T (ºC)	Residence time	Major products (%)		
			Char	Liquid	Gas
Torrefaction	300	30-60min	**75**	10	15
Carbonisation	400-600	>60min	**40**	30	20
Intermediate	400-600	10-50s	20	50	30
	1000	10-50s	15	60	25
Fast	**400-600**	**<1s**	10	**75**	15
	1000	<1s	10	5	**85**
Flash	400-600	<0.1s	5	65	30
	1000	<0.1s	5	5	**90**

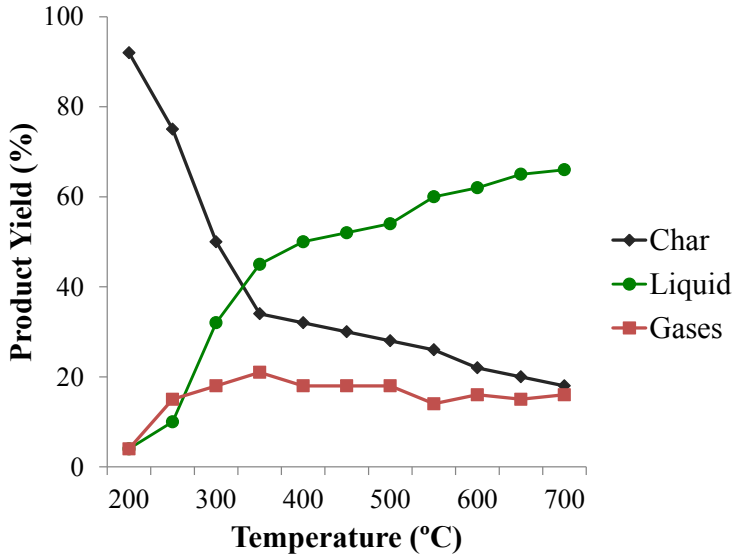

Figure 1.5. Gas, liquid and gas yields from biomass fast pyrolysis.

Meanwhile flash pyrolysis approaches gasification processes and it is usually used to produce gases at mild-temperature conditions, fast pyrolysis is the most interesting option for liquid production (Figure 1.5), as the liquids can be easily transported and storaged. Additionally, these bio-oils are potentially a substitute for petroleum fuels and products.

Rich-carbohydrate (65-80%) lignocellulosic feedstock is preferred for bio-oil production. Some examples of studied biomass resources are bagasse, straw, fruit pits, hulls and shells, forestry residues (i.e. sawdust, bark, stems from shavings/pruning) and several solid wastes. The rapid quenching of flash degradation products from cellulose, hemicellulose and lignin forms the liquid. Cellulose is mainly converted to levoglucosan, carboxylic acids (formic, acetic), hydroxyketones, hydroxyaldehydes, and some furanic derivatives at temperatures among 300-400 ºC[71] (Figure 1.6). Hemicellulose is easy to degrade (200-400 ºC) and it is also transformed to low molecular weight compounds (CO, CO_2, formic acid, acetaldehyde, acetol), furan ring derivatives and other anhydrosugars[72]. On the other hand, lignin degradation occurs at wider temperature ranges obtaining phenolic compounds and high char yields[73]. Thus, rich lignin-biomass feedstock drive to high charcoal production[74,75].

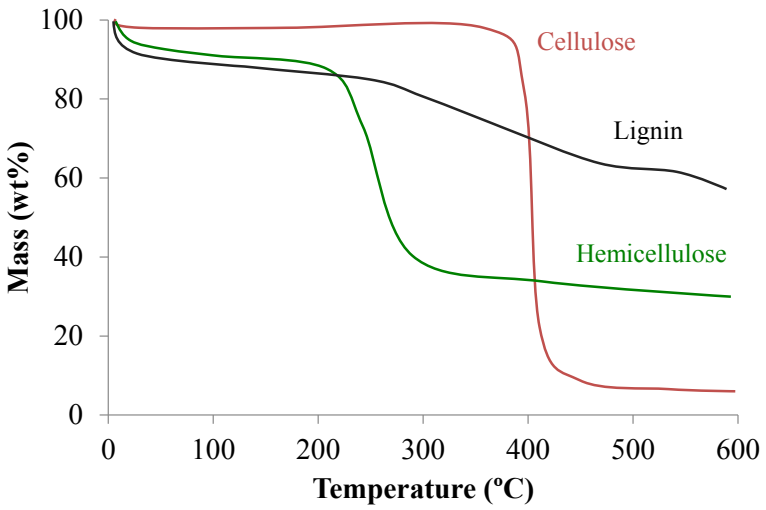

Figure 1.6. Cellulose, hemicellulose and lignin pyrolysis followed by thermogravimetric analysis. Adapted from Yang et al., 2007 [74].

Fast pyrolysis is an advanced process, which takes place in very short residence times, so not only reaction kinetics, but more importantly heat and mass transfer processes are key aspects to control in this technology[76,77]. First of all, biomass particle size needs to be reduced (≈2mm) to achieve high heat transfer rates at the surface and accelerate reaction and further separation steps. Then, optimum temperature conditions (400-500 ºC) and short residence times (0.5-2s) need to be adjusted to maximize bio-oils yields (up to 60-80wt%)[78,79].

Fluid bed and circulating fluid beds reactors allows a good temperature control and a very efficient heat transfer to biomass particles. Additionally, residence time of solids can be carefully controlled by the fluidising gas flow rate[80]. Figure 1.7 shows a scheme of a pyrolysis process. Biomass decomposes into vapour and charcoal. After separation steps, cooling and condensation, a dark brown and viscous liquid is formed. Bio-oil is obtained in yields of up to 60-75%[81] together with biochar and gases, which can be used to self-provide the process heat and electricity requirements[82]. This pyrolysis oil can be directly used for heat and electricity generation in static burners[83] or be further refined to produce transportation fuels[9,84,85].

Bio-oil composition can vary depending on lignocellulosic feedstock and the conditions used in the pyrolytic process. These bio-oils are very complex mixtures containing water (15-40wt%) and more than 200 different oxygenated organic compounds (i.e. sugars, alcohols, aldehydes, ketones, carboxylic acids, esters, furanic derivatives, among others) in varying concentration[86–93].

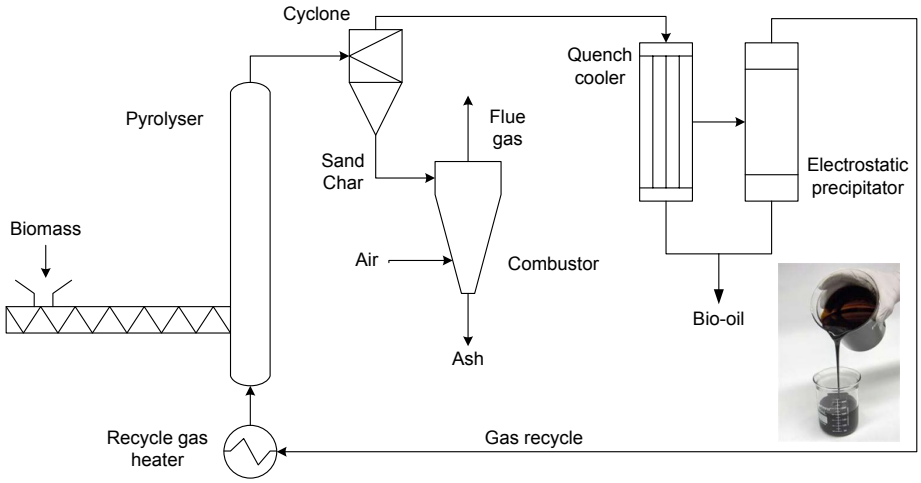

Figure 1.7. Process flow diagram of a pyrolysis plant adapted from Bridgwater et al., 2000 [79].

It should be noted that complete quantitative determination of bio-oil composition is difficult to establish and many analytical techniques are need for its characterization[94–97]. The hundreds of different molecules in bio-oils are grouped into chemical families in order to study upgrading strategies[95]. An approximate bio-oil composition is displayed in Figure 1.8. In particular, light oxygenates, anhydrosugars and monophenols can be easily identified by GC and/or HPLC. Organic acids (i.e. formic, acetic, propanoic, etc.), ketones (i.e. acetone, acetol, cyclopentenone, etc.), aldehydes (i.e. formaldehyde, hydroxyacetaldehyde, propanal, pentanal, furfural, etc.) and alcohols (i.e. methanol, ethanol, ethylenglycol, etc.) are the main components among C_1-C_4 light oxygenates. On the other hand, esters (i.e. methyl acetate), ethers (i.e. tetrahydrofuran), furans (i.e. HMF), phenols (i.e. phenol, methoxyphenol, methylphenol) and sugars (i.e. levoglucosan, cellobiosan, fructose) are usually identified as minor components.

From…	Pyrolysis products	wt%
Carboyhydrate dehydration	Water	15-30
Fragmentation reactions	C1-C4 light oxygenates	10-40
Cellulose pyrolysis	Anhydrosugars	5-10
Cracking and dehydration reactions	Monophenol/monofurans	2-8
Lignin pyrolysis aging	Pyrolytic lignin and oligomers	20-30
Cellulose dehydration	Pyrolytic humins	2-8

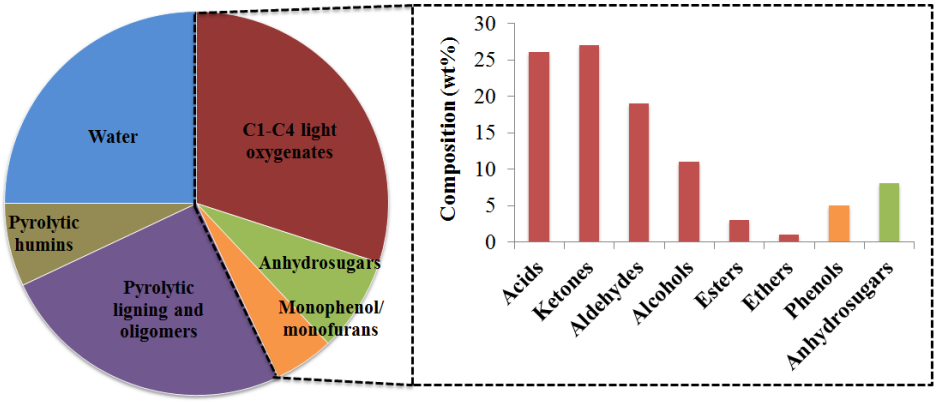

Figure 1.8. Bio-oil composition adapted from Iojoiu et al., 2007; Gayubo et al., 2009 and Stankovikj et al., 2016 [93,94,98].

Therefore, the many and various functional groups confer them the potential of producing wide alternatives of chemicals and fuels[99,100]. However, these heterogeneous physicochemical properties including wide distribution of molecular weights, density, volatility and polarity limit and challenge their direct application as fuels for automotive uses[101].

The average density of the bio-oil is very high (≈1.2 kg/L) and the viscosity can vary from 50 cSt to 800 cSt depending on the feedstock, pyrolysis parameters, etc. The liquid also has a strong smoky odour caused by low molecular weight oxygenated products. Some of these compounds may undergo reactions such as polymerization,

condensation, and etherification, among others. Thus, the viscosity of the liquid may increase during storage (fast "*aging*"). The characteristic high reactivity and thermal instability of these compounds hinder its storage, handling and direct use as liquid fuel[102].

Moreover, the presence of high contents of carboxylic acids makes these mixtures acidic (pH 1-3) and corrosive, which means that more expensive materials must be used in the whole plant. Because of the overall oxygen content (35-40%)[103], the low bio-oil energy density (typically ranging 16-20 MJ/Kg) is lower than fuel oil (40 MJ/Kg), which leads to increased costs for transportation and storage. Thus, upgrading approaches are definitely needed to improve their fuel properties (O content reduction, pH reduction, higher molecular weight, etc.)[94,104–107].

Biomass fast pyrolysis technologies have been demonstrated at small-scale and pilot plants. Bio-oil production and commercialisation still face issues concerning technical barriers during industrial scale-up and cost competitiveness. Nowadays, combustion and co-firing of pyrolysis oils with fossil fuels and even natural gas has meant the easiest and only way to introduce this fuel in the market[108,109]. However, bio-oils need to undergo further upgrading processes in order to meet the requirements for transport fuels[110]. Therefore, more efforts must be done in downstream and refining processes to improve the efficiency of these industries[111,112].

1.4. Bio-oils upgrading processes

1.4.1. Catalytic pyrolysis, vapour upgrading and co-processing

The first possible pathway to improve bio-oil characteristics consists in integrating catalysts in the same pyrolysis reactor system (Figure 1.9)[70]. In fact, catalytic processing has already been efficiently used in several petroleum-derived processes[113]. Biomass can be pyrolized in the presence of a catalyst that changes product distribution. Zeolites and other mesoporous materials have been studied as potential catalysts for this process. These catalysts promote cracking, isomerization and alkylation reactions during pyrolysis. High heating rates and catalyst co-feeding need to be carefully optimized to avoid thermal decomposition and undesired reactions. Moreover, catalytic fast pyrolysis requires catalysts to operate at fixed temperature conditions and materials must be resistant enough to stand complex mechanical environments.

Close-coupled catalytic vapour upgrading (catalytic cracking of bio-oils) can be an alternative to overcome process condition limitations under in-situ catalytic pyrolysis. Then, vapours coming from pyrolysis reactor are upgraded over acidic materials (i.e. HZSM-5, MCM-41, SBA-15) in a separated system (Figure 1.9). Oxygen is eliminated in the form of water and carbon oxides, while olefins and aromatics are produced[114]. This technology was originally developed by Exxon Mobil and has been the main field of study for many researches. Catalysts structural stability is not a problem under these temperature conditions

(400-600 ºC), but catalytic deactivation by coke deposition is still a big concern. Water and inorganic compounds also play an important role on the rapid deactivation of the catalysts[114–116].

Other alternative for the valorisation of bio-oils is the addition of the whole bio-oil, bio-oil fractions or partially upgraded bio-oils to specific petroleum fractions for further processing in conventional refinery units (FCC units)[117,118]. This strategy is commonly named co-processing or co-refining.

Catalytic cracking for co-processing of bio-oils and petroleum fractions has been tested in both lab-scale and demonstration FCC refinery units. Analogously to previous methods, high amounts of char and coke deposition on the catalyst surface lead to the strong deactivation of the catalysts[119,120]. Similar behavior is observed when model oxygenated compounds representative of bio-oil composition are co-processed, as oxygenated compounds deoxygenation reactions lead to important coke deposits[121,122]. However, due to the diverse mixture of compounds present, bio-oil cannot be upgraded using a single technique. Previous de-oxygenation steps are usually required before co-processing to diminish bio-oils reactivity and coke deposition.

1.4.2. Hydrotreating

Most extended and accepted upgrading process includes whole bio-oil hydrotreating. In this context, hydrogenation and hydrocracking are well-known technologies derived from petroleum hydrodesulphurisation processes in refineries[123]. This background has made this technology for bio-oil upgrading to progress rapidly during the last years.

Hydrogenation and hydrodeoxygenation (HDO) processes are usually performed in the presence of catalysts, under high H_2 pressures (>60-70 bar) and high temperatures conditions (300-450 ºC)[124]. Therefore, the main disadvantages are expensive equipment requirements and high operational costs, as H_2 rich environments (>90%) are needed[125].

The most commonly used catalysts for hydrotreating pyrolysis oils are conventional promoted molybdenum sulphides: Co-Mo and Ni-Mo supported on alumina (Al_2O_3)[126]. These catalysts have been widely applied in hydrodesulphurisation petroleum processing technologies[127]. Supported noble metal catalysts (i.e. Ru, Pd, Pt, Rh) over different supports (i.e. carbon, silica, alumina, zirconia, titania, mixed oxides, zeolites)[128,129], together with transition metal phosphides have also been studied[130].

Firstly, both Co-Mo and Ni-Mo/Al_2O_3 show great results but have the great disadvantage of needing sulphur to maintain their activity, whereas traces of other inorganic compounds can cause a strong deactivation[131]. On the other hand, Pd/C materials have been studied for the hydrotreatment of bio-oils[132]. The activity of a wide range of metal catalysts (i.e. Ru/C, Ru/TiO_2, Ru/Al_2O_3 and Pd/C) was also compared to the classic sulfided catalysts[133]. Several reviews about advances in catalytic hydrotreating of bio-oils can be found elsewhere in literature[134–136].

HDO processes lead to a greater removal of oxygen than vapour catalytic cracking technologies. It must be noted that oxygen content must be reduced to 7-10%[70], before the oil can be mixed with petroleum fractions. In this sense, a maximum overall efficiency of 61% has been achieved[137]. Thus, resulting oils possess better fuel properties, lower

acids and water contents, and increased high heating values. Other important characteristics such as volatility and miscibility are also improved. However, significant H_2 and energy consumptions are needed, while low liquid productivities are still achieved as C_1-C_4 highly abundant oxygenated compounds are mainly converted into gases during the process. 40%-60% of the carbon in the bio-oil consists of these light oxygenates. This means that HDO processes can only convert a small fraction of the carbon to gasoline range compounds, while wasting the rest as light gases[87].

The currents efforts focus on fundamental chemistry using model compounds hydroprocessing[135]. Researchers face several concerns about the scale-up of the system (i.e. exothermic reactions, process kinetics, unreactive solids, and metals, among others). In this sense, catalysts stability is once again a key issue when developing potential industrial catalysts. Materials usually suffer from strong deactivation due to the complex composition of the bio-oil including water, acids and oxygenated compounds[138]. Undesirable products including char, coke and tar also deactivate the catalysts reducing the yield of upgraded bio-oil[139,140].

In general, hydrotreatment technologies (HDO, hydrocracking) must be considered as an important alternative to notably reduce O content in pyrolytic bio-oils and enhance their fuel properties. Nonetheless, high operational costs, energy consumption and low yields suggest that other technologies may be jointly applied to increase the efficiency and profitability of the processes.

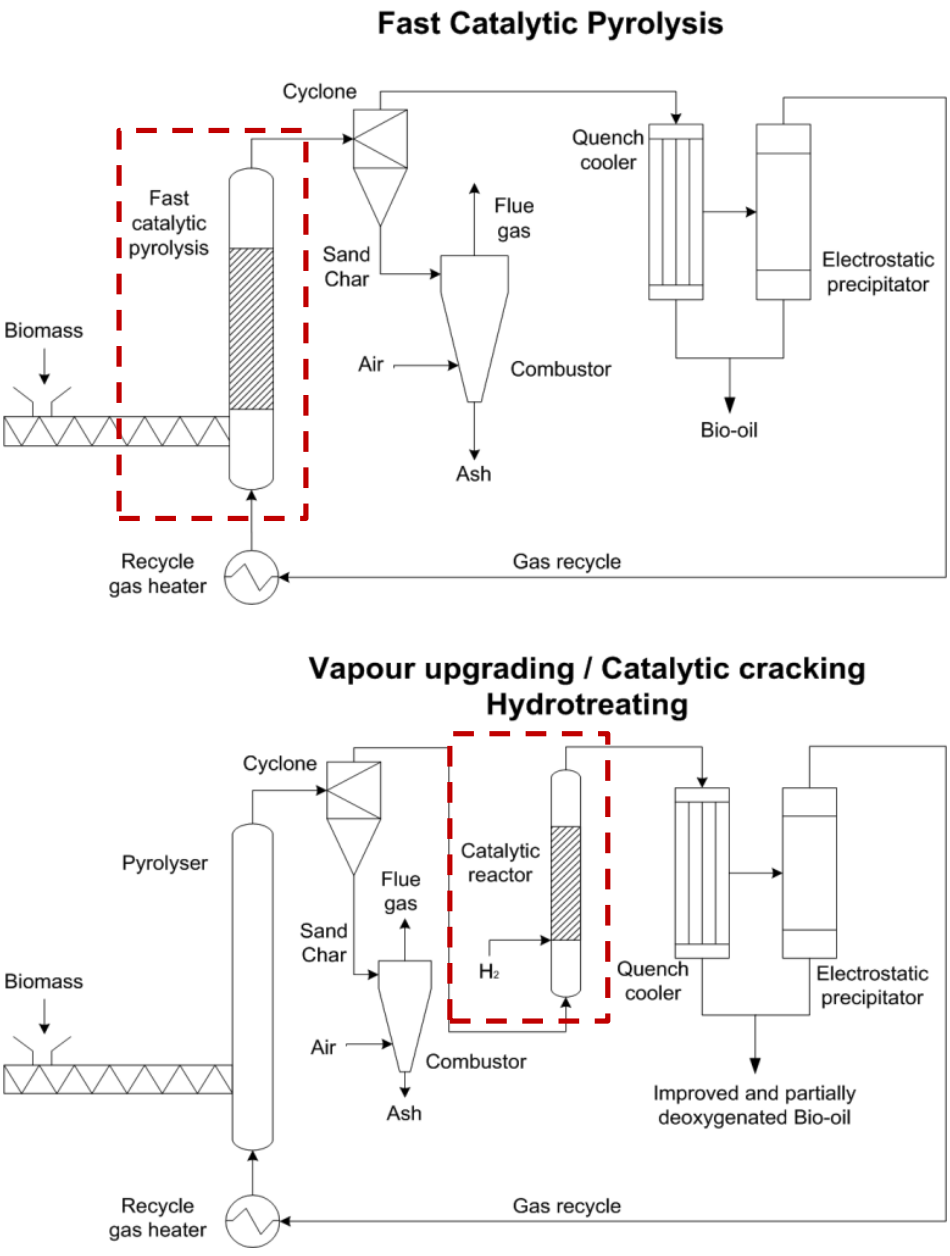

Figure 1.9. Process flow diagram of different upgrading technologies in pyrolysis plants: Fast catalytic pyrolysis, vapour upgrading (catalytic cracking) and hydrotreating.

1.4.3. Bio-oils fractionation and downstream processes

In a standard oil refinery, the first and more important step in order to improve process efficiency is the distillation column. In the case of bio-oils, the presence of high amounts of water and many thermally unstable oxygenated compounds does not make the fractional distillation of bio-oil a reasonable option. High polymerization and oligomerization product yields will be obtained during this process: A solid residue of 50wt% of the original liquid is obtained if it is directly heated to more than 100 ºC[101]. Thus, if bio-oils pretend to be a source of chemicals, alternative separation methods must be developed to generate fractions of similar properties and facilitate their further refining.

In this context, fractional condensation systems consist in a series of condensers at different temperatures that allow separating fractions of the bio-oil based on their boiling points (Figure 1.10)[141,142]. Using the appropriate condenser temperature combination, it is possible to separate fractions with interesting characteristics, which can be further handled and upgraded. Numerous patents and literature can be found involving fractionation of bio-oil using technologies based on condensers, electrostatic precipitators and ionic liquids, among others[143–146]. Fractionation methods may be used to effectively separate individual molecules as acetic acid[147], acetol[148], or hydroxyacetaldehyde[149]. Streams with high contents of sugars (levoglucosan, cellobiosan) can be also achieved[17,150], which can be used in fermentation processes to produce 2nd generation bio-fuels.

However, fractionated condensation involves too many separation steps to efficiently obtain streams pure enough for certain purposes. In this sense, these technologies may find niche markets to achieve specific chemicals or to facilitate further bio-oils refining steps as previous partial pre-treatment strategies.

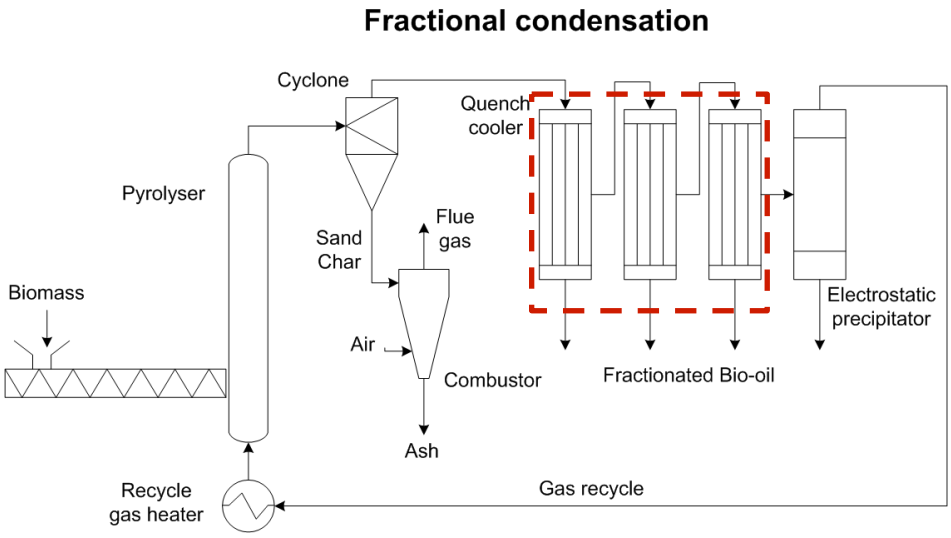

Figure 1.10. Process flow diagram of fractional condensation systems coupled to fast pyrolysis reactor.

1.4.4. Liquid-liquid extraction upgrading

If gaseous products containing true vapours and non-condensable gases are right quenched (rapid cooled down) bio-oils will still have all the above-mentioned disadvantageous characteristics[94,106]. Notwithstanding, this is the simplest and cheapest method to obtain all condensable products in the liquid-phase. Upgrading strategies hereafter will firmly contribute to the economical feasibility of this type of bio-refineries.

On this subject, the use of polar solvents has been claimed as an ingenious and simpler pathway to reduce thermal instability and minimize secondary reactions. Bio-oils are miscible with polar solvents such as methanol, ethanol, acetone, etc; whereas the miscibility of the crude bio-oil with other less polar fuels is negligible. Then, these polar solvents can be used to homogenize and improve bio-liquid properties.

In this sense, bio-oils can be used in standard boilers and engines when mixed to conventional fuels[151]. It is possible to prepare homogeneous blends of bio-oils and biodiesel with the addition of above-mentioned alcohols (Figure 1.11). These blends have been claimed to stabilize whole bio-oils and bio-oils fractions, meanwhile fuel properties are improved[152–154]. For instance, if bio-oils are mixed with methanol and tetraethylene-glycol dinitrate (cetane-improving compound) bio-oil becomes suitable to get used in high-speed diesel engines[100]. Further studies on mixtures of bio-oil and other fuels are available in the literature[155,156].

Additionally, alcohol reactivity with other functional groups present in bio-oil mixtures can be exploited. In particular, esterification of highly abundant organic acids with low-cost alcohols is a very convenient reaction (Figure 1.11)[157]. Bio-oils contain significant amounts of carboxylic acids, which are the main responsible for the high thermal instability, acidity and corrosivity of these mixtures. Catalytic esterification helps to improve these characteristics, together with bio-oils density and viscosity. Several solid acids as zeolites[158], mesoporous silicas[159], ion-exchange resins[160] and mixed oxides[161] have been studied as potential catalysts to stabilize bio-derived carboxylic acids or bio-oil

mixtures. Besides esterification, solid acids can simultaneously promote the addition of alcohols to aldehydes to achieve acetals[162,163].

Diverse alcohols (i.e. methanol, ethanol, butanol, glycerol) under different operation temperature conditions have been studied. This technique has been combined with hydrotreatment and cracking as an alternative way of bio-oil upgrading[164]. One-step hydrogenation-esterification (OHE) using bifunctional catalysts has also been claimed as an effective alternative to transform unstable components (carboxylic acids and aldehydes) to more stable and desirable components (esters)[165]. Nonetheless, the high water content in bio-oils (15-30%) creates equilibrium limitations and neutralization steps cannot usually be completed for bio-oils application in a traditional petroleum refinery[166].

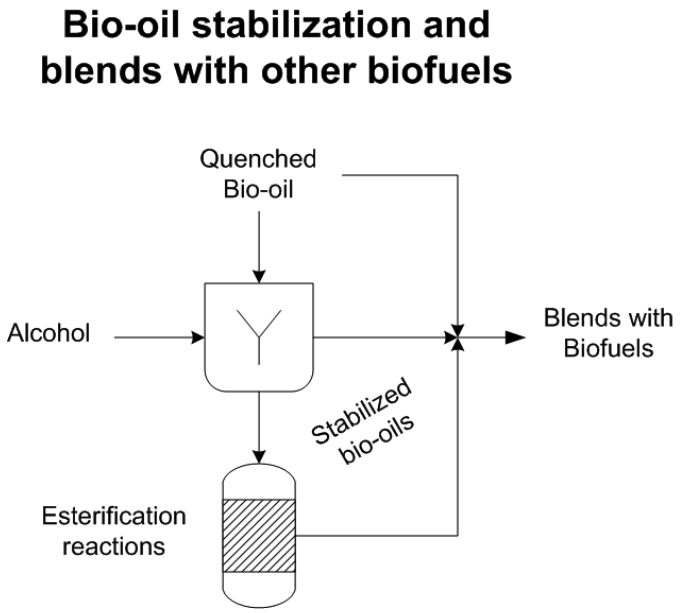

Figure 1.11. Alcohol addition and esterification reactions as useful methods to stabilise bio-oils to further blending with other biofuels.

More interestingly, and due to the complexity of dealing with the whole bio-oil mixture, one of the most suggested strategies is based on a liquid-liquid separation process by water addition to the pyrolytic bio-oils[167]. Bio-oils contain varying amounts of water depending on how it was produced (i.e. biomass feedstock, drying pre-treatment steps, pyrolysis parameters). These liquids usually form a stable single-phase mixture to an upper limit of about 30wt% water. Thus, the addition of extra amounts of water can cause phase separation. On account of this, the main objective is to perceive water as an opportunity rather than a disadvantage. After the addition of water and the resultant phase separation, a water-insoluble fraction and an aqueous fraction can be clearly differentiated[96]. Moreover, the use of water helps reducing the need of auxiliary substances (solvents, separation agents) and particularly influences the reduction of separation operations costs.

Organic fractions usually contain the majority of phenols, furan derivatives (furfural, guaiacol, cresol) and oligomeric compounds, among others. These fractions can be further processed (via hydrotreating) to achieve high quality drop-in fuels. Higher products yields with lower H_2 consumption are achieved when short-chain and high reactive compounds have been previously isolated.

On the other hand, most of light oxygenated compounds, which represent among 10-40wt% of the whole pyrolytic bio-oil[168–171] remain in the water-soluble fraction of bio-oil. These aqueous fractions containing C_1-C_4 acids (i.e. acetic acid), aldehydes, ketones, alcohols, sugars and low amounts of heavier water-soluble compounds, nowadays

are identified as waste effluents at bio-refineries[172]. Following the new bio-economy concept[39], the transformation of these short-chain and low value-added water-soluble compounds would be of considerable relevance. This pathway, together with the subsequent valorisation of these residual currents and waste streams has recently gained more adepts from both academy and industrial sector.

1.5. Aqueous effluents catalytic valorisation

1.5.1. Aqueous phase reforming (APR)

Several strategies for the valorisation of aqueous effluents from bio-refineries have been proposed in the recent years. Aqueous phase reforming (APR) approach developed by Dumesic and co-workers[173,174] could be implemented to produce H_2 from these aqueous fractions (Figure 1.12)[175]. Specifically, APR can be applied in order to transform acetic acid (or aqueous effluents containing light oxygenates) into H_2, syngas or more valuable compounds. In this sense, acetic acid steam reforming has been largely studied in literature[176,177]. Ni/Al_2O_3 catalyst has been used for H_2 production via steam reforming and sequential cracking process (via C-C and C-O bonds cleavage)[178]. In addition, Ni/ and Ni-Ce/$MgAlO_x$ catalysts have been studied employing light oxygenates (i.e. ethanol, acetone, acetic acid, acetol, propanal) as model compounds of pyrolytic aqueous fractions[179,180]. Moreover, Pt supported on CeZrO, CeTiO materials have been considered as effective catalysts for aqueous phase reforming of light oxygenates fractions of bio-oils[181].

Nonetheless, high-energy consumption (250-270 ºC and 25-50 bar) and the process low atom economy make this choice economically objectionable. Specifically, mass transfer limitations, low yields of the desired products and fast catalysts deactivation constitute the main impediments to wide scale application[182].

1.5.2. C-C bond formation reactions

On the other hand, the transformation of these water-soluble compounds by performing "one-pot" C-C bonds formation reactions, such as aldol condensation and ketonization has recently been claimed as a beneficial alternative approach[183–185]. Indeed, they can be further upgraded to generate a mixture of hydrocarbons and aromatics useful for blending with hydrotreated separated organic fractions[186] (Figure 1.12).

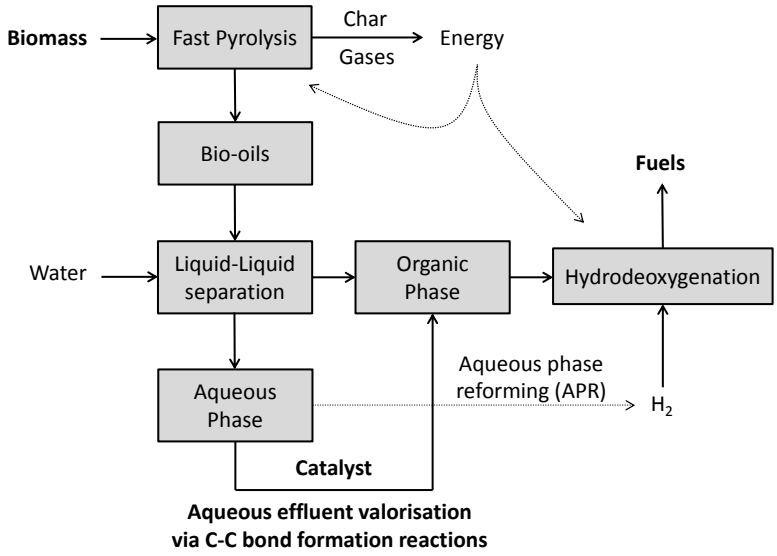

Figure 1.12. Process flow diagram of aqueous effluents catalytic valorisation via aqueous phase reforming (APR) and C-C bond formation reactions.

C-C bond formation reactions are very important processes in organic chemistry as they allow producing complex products from simple molecules. In this sense, these aqueous fractions are mainly composed of $<C_6$ oxygenated molecules derived from the pyrolytic reactions of pentoses and hexoses during biomass fast pyrolysis processes. Then, these light oxygenated compounds could be transformed into hydrocarbons and aromatics in the range of C_6-C_9 compounds (gasoline), C_9-C_{15} (kerosene) or C_9-C_{20} (diesel) for their application as fuels.

This procedure takes advantage from numerous functional groups reactivity to create larger compounds via aldol condensation and ketonization reactions, among others. Thus, the design of bifunctional heterogeneous catalysts is a key point in these processes. The presence of isolated and well-defined active sites, which can operate cooperatively is a need to perform consecutive "one-pot" reactions[187–189]. Moreover, this strategy moves toward more sustainable scenarios and improves the environmental impact of bio-refineries. Indeed, it meets many of The 12 Principles of Green Chemistry[6,190,191]: Catalysis is applied to transform waste streams from renewable feedstock into more valuable products by maximizing "*atom economy*" through reactions under mild-temperature and pressure conditions without using additional solvents.

1.5.2.1. Aldol condensation

Firstly, aldol condensation is a reaction in which a carbonyl compound (aldehyde or ketone) reacts with another carbonyl compound to form a β-hydroxyaldehyde or β-hydroxyketone, followed by dehydration to give a conjugated enone (Scheme 1.1). Water is the only by-product.

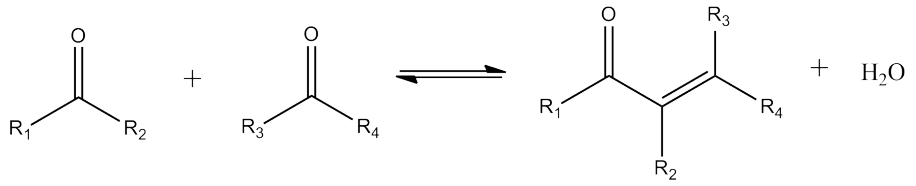

Scheme 1.1. Aldol condensation reaction.

It has been claimed as a key step in the valorisation process of bio-oils and aqueous streams derived from biomass. Abundant light oxygenated compounds can react via aldol condensation producing larger compounds via new C-C bonds formation. Several strategies have been proposed, where "platform molecules" as furfural or HMF (from glucose/xylose dehydration processes) can react with other light oxygenates (acetone, acetol, propanal) to create C_9-C_{15} compounds, which can be lately hydrogenated to gasoline/diesel fuel range[12,29,192].

Aldol condensation mechanism has been largely discussed in literature. Conventional homogeneous strong base catalysts (i.e. NaOH, KOH) have been used to study aldol condensation reactions using different furanic aldehydes and ketones derived from biomass[193–195]. More conveniently, alkaline oxides, and alkaline-substituted zeolites/sepiolites have been traditionally employed to perform these reactions. For instance, basic metallic oxides (i.e. MgO, ZnO) and mixed oxides (i.e. Mg-Al hydrotalcites) have been claimed as active materials for acetone-furfural aqueous phase condensation reactions under moderated conditions[196,197]. In this way, a C_α deprotonation takes place in a basic active site. Then, this enolate ion nucleophilic adds to a C=O of a carbonyl compound to generate an aldol addition product, which lately dehydrates to the final product.

More recently, a cooperative acid-base sites mechanism has been accepted[198]. An acid site can interact with the carbonyl group polarizing the carbon-oxygen bond and making this carbon more susceptible to be attacked by the enolate ion from other carbonyl group (previously formed by the interaction with a basic site). This mechanism opens up the possibility of using amphoteric or acid mixed oxides with well-distributed active sites (cations will act as Lewis acid sites and anions as Brönsted/Lewis basic sites), which can effectively perform these reactions. In this sense, catalysts based on $Ce_xZr_{1-x}O_2$ mixed oxides have been widely considered for the gas-phase conversion of small aldehydes at high temperatures (>300 ºC)[184], whereas TiO_2-based materials have been used for the acetone-furfural condensation under moderated conditions[199]. Moreover, MgO-ZrO_2 oxides have also been used to study furfural/acetone and acetone self-condensation under mild and high temperature conditions (200-300 ºC)[200–204].

Furthermore, cyclopentanone (CPO) has recently been claimed as an interesting linking reactant to produce high-density fuels (C_{10}-C_{18} compounds) via aldol condensation reactions[205–207]. Homogeneous (i.e. NaOH) and heterogeneous (i.e. Mg-Al hydrotalcites) basic catalysts, MgO-ZrO_2 oxides, and other acid catalysts have been applied into these reaction schemes[208,209].

Therefore, aldol condensation is a straightforward reaction, which allows creating new C-C bonds with high atom efficiency, being H_2O the only generated by-product.

1.5.2.2. Ketonization

Ketonic decarboxylation (also known as ketonization) is an organic reaction, where two equivalents of carboxylic acid are converted to one equivalent of ketone, one equivalent of water and one equivalent of carbon dioxide[210] (Scheme 1.2).

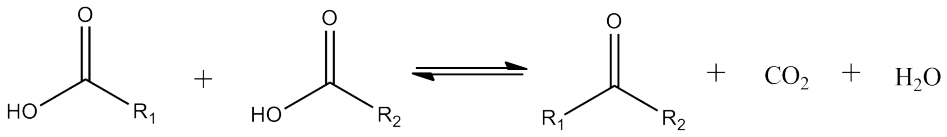

Scheme 1.2. Ketonization reaction.

It is also a C-C bond formation reaction, which creates larger and less reactive compounds, while carboxylic groups are eliminated. It has been considered a very important reaction when dealing with bio-oils due to the amount of carboxylic acids present in them[211]. Indeed, acetic acid is one of the most problematic compounds in bio-oils. Then, this reaction drives to less acid, corrosive and reactive mixtures, where produced ketones have higher energy content. These reactions additionally allow hydrocarbon chain growth by means of ketones consecutive C-C bonds formation via further aldol condensation reactions[212]. Interestingly, oxygen content is significantly reduced by 75%, whereas atom economy is negatively affected, as one carbon is lost in the form of CO_2. One or more carboxylic acids can be involved in ketonization reactions. Symmetric ketones will be formed if only one acid is used, whereas three

possible ketones can be produced (from self- and cross- ketonization reactions), when two different carboxylic acids are employed.

Analogously to aldol condensation, most of research works show that the presence of at least one H_α in any of the molecules is needed to carry out the reaction[213,214]. It should be noted that not only carboxylic acids can react via ketonization: Alcohols, aldehydes and esters can be also transformed into ketones, although these type of reactions have been infrequently considered in literature[215]. On the other hand, ketonization to convert C_1-C_4 acids (i.e. acetic, propionic and butyric acid) into higher molecular weight compounds in the gasoline/diesel range has been widely studied. In such a way, acetone can be produced from acetic acid, this process being of great importance due to its potential applications in biomass upgrading processes.

The first example of ketonization was reported in 1858, when acetone was produced by decomposition of calcium acetate. Following this idea, other low-lattice energy alkaline earth oxides (i.e. MgO, CaO) were found to be effective for producing acetone via the decomposition of the corresponding acetate. The strong interaction between the solid and the carboxylic acid results in the formation of bulk carboxylate salts, which lately decompose upon thermal treatment[211]. Nonetheless, this strategy is not useful in catalysis as solids are disintegrated during this reaction.

On the other hand, later developments have shown that high-lattice-energy metal oxides such as CeO_2, ZrO_2, TiO_2, MnO_2 can act as surface catalysts for the ketonization reaction. However, bulk and surface

ketonization has been observed for different metal oxides (i.e. Fe_2O_3, CeO_2) depending on the temperature conditions[216,217]. In this sense, further and more in deep researches will be needed to fully understand these concerns.

Furthermore, mechanisms and intermediate species have been the subject of large debate. In the last years, β-ketoacid intermediate has been finally accepted as the reliable pathway[210,213]. In this sense, ketonization and aldol condensation mechanisms have been deeply studied by using acetic acid or propanal as probe molecules with TiO_2 and ZrO_2 as catalysts[218–220]. These studies conclude that the activity of these catalysts is based on their bifunctional character (acid/base sites combination), necessary to assist intermediates formation on the surface of the catalysts. Mainly, CeO_2, ZrO_2, $Ce_xZr_{1-x}O_2$[221,222] and rare earth containing catalysts[223–225] have been largely studied for the gas-phase ketonization reactions of C_2-C_5 organic acids at high temperatures (300-500 ºC). Different chain-length organic acids and aqueous mixtures containing acetic acid have been mainly considered as model compounds when studying this approach[226].

In conclusion, C_1-C_4 carboxylic acids ketonization is a relevant reaction for the upgrading of aqueous streams derived from biomass pyrolysis processes. In particular, these acids can be effectively transformed into ketones, which can consecutively form new C-C bonds via aldol condensation. In this sense, an extensive updated review on ketonization can be found in literature[227].

1.5.3. Esterification

On the other hand, carboxylic acids (i.e. acetic acid) can react with different alcohols via esterification to produce the corresponding ester together with H_2O as by-product (Scheme 1.3).

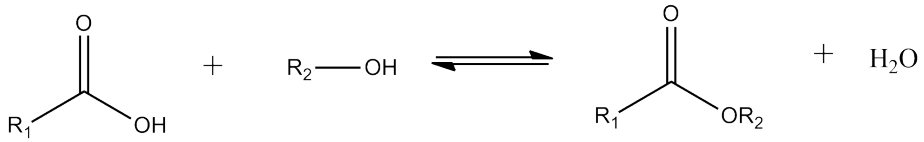

Scheme 1.3. Esterification reaction.

As mentioned in *Section 1.4.4*, this reaction pathway has been considered by other authors in order to "catalytic stabilize" bio-oils fractions or pyrolytic bio-oils themselves. The use of acid catalysts (i.e. zeolites, ionic exchange polymeric resins, among others) together with different alcohols (i.e. methanol, ethanol, butanol) under moderated conditions can reduce carboxylic acid contents (TAN and pH reduction), also decreasing corrosivity and reactivity concerns when using aqueous effluents derived from bio-oils[228,229]. However, traditional distillation, azeotropic water removal or reactive distillation have been used in order to increase this process efficiency, as water limits reaction equilibrium[230,231]. Other authors propose a joint strategy, where acids can react via esterification, whereas formed esters and remaining acids can react via ketonization to produce less reactive compounds[215].

In all events, esterification reactions are one of the alternatives to be considered for the upgrading process, as carboxylic acids and alcohols are always present in aqueous effluents obtained by phase separation of pyrolytic bio-oils.

1.5.4. Reaction conditions

Aldol condensation and ketonization reactions for the valorisation of pyrolytic oils or bio-oils fractions have been traditionally studied in fix-bed reactors under gas-phase conditions. Moreover, most of the reviews and researches so far were performed using individual compounds of bio-oil rather than as a whole, and not many examples of complex mixtures can be found in literature.

Aldol condensation of single small aldehydes and ketones (i.e propanal, butanal, acetone, etc.) have been traditionally studied in liquid and gas phase at mild temperatures conditions[201,232,233]. Nonetheless, potential detrimental effects from the presence of acid and water in the reaction media have been barely reviewed. Gangadharan et al. work is one of the few research papers where the effect of acid and water on propanal condensation over $CeZrO_2$ mixed oxides is carefully considered[184].

On the other hand, great efforts have been accomplished in the ketonization of short-chain carboxylic acids (i.e. acetic and propionic acid). Special attention has been paid to acetic acid, as one of the main components of bio-oils oxygenated compounds. These reactions usually take place at high temperature conditions (>300ºC) in gas-phase reactors.

Complex mixtures have been rarely considered. In particular, furfural, acetol or cresol effects on acetic acid ketonization were studied[234].

Recent exceptions of acetic acid aqueous-phase ketonization can be found in literature. $LaZrO_x$, $ZrMnO_x$ and also carbon-promoted ZrO_2 catalyst have been studied[235–237]. High temperature and pressure conditions (>300 ºC and 100 bar) were needed in order to overcome detrimental effects of water on ketonization reactions[238]. However, these scenarios are distant from realistic operation conditions in bio-refineries.

Water effect on acetic acid ketonization under moderated temperature conditions (180-200 ºC) was studied by Pham et al.[185], where different strategies, even with the incorporation of noble metals on the solid catalyst were attempted to increase catalytic results.

It is well known that traditional support materials (e.g. Al_2O_3) can strongly interact with water and may undergo irreversible surface and structural changes. In addition, many classical metal oxides are also unstable under these conditions and difficulties arise when reactions are carried out at basic or acid pH. For instance, these studies show $CeMO_x$ (where M = Zr, Mn, Al) catalysts to have poor structural stability[217], while TiO_2 and ZrO_2 lose catalytic activity at high temperatures, being this effect enhanced by the presence of water. Nonetheless, the high oxygen content of biomass derivatives makes them water-soluble. Then, these resources would be more conveniently processed at moderate temperatures in aqueous solutions.

Therefore, some key points, which must be considered to strengthen bio-oil upgrading processes, include finding multifunctional catalyst with high activity under complex environments. Some authors have

specifically highlighted the importance of transforming bio-based chemicals into fuels in the aqueous-phase[239,240]. In this context, new requirements on the properties and the stability of these materials under realistic hydrothermal conditions (aqueous mixtures at mild temperatures) have been identified as an area that needs further improvement.

1.6. Fermentation processes

Apart of fast pyrolysis process, different fermentation processes constitute an important source of high-functionalised oxygenated compounds in the bio-refineries process networks. In this context, downstream processing of aqueous fermentation broths is also imperative for the development of the bio-refinery concept. The efficient upgrading of these bio-derived aqueous streams into fuels and added value chemicals has likewise gained more adepts in the recent years[241–243].

Fermentation is an anaerobic process that breaks down carbohydrates and monomeric sugars (e.g. glucose) present in organic materials. Yeast or bacteria organisms are added to the biomass feedstock, and alcohols (and other compounds, i.e. organic acids) can be produced under mild conditions. Sugarcane and corn-derived biomass have traditionally been used to produce ethanol via fermentation processes[244]. Afterwards, ethanol is distilled and dehydrated to obtain a higher concentration stream, useful for blending with automotive fuels.

More recently, the use of lignocellulosic materials such as agricultural wastes and woody materials has been promoted within 3rd generation bio-refineries. Nonetheless, this route requires an additional previous step, as lignin has to be efficiently removed before fermentation takes place (Figure 1.4). In this sense, cellulose and hemicellulose can be transformed into mono- and disaccharides by different processes, such as dilute acid hydrolysis, concentrated acid hydrolysis and enzymatic hydrolysis, among others[245]. The hydrolysis of hemicellulose occurs under moderate conditions, whereas cellulose needs more severe treatments to be transformed. These sugars can be lately used as a feedstock in fermentation processes for the production of renewable fuels (i.e. ethanol, butanol)[246] and interesting platform molecules (i.e. succinic acid and other carboxylic acids)[247]. The formation of furfural, HMF, acetic acid and formic acid during the hydrolysis step is undesired, as these compounds lower the process yield and also inhibit further fermentation processes.

Two main pathways are distinguished within this strategy: the production of carboxylic acids, and the production of ABE (Acetone-Butanol-Ethanol) mixtures for bio-butanol synthesis.

1.6.1. Carboxylic acids production

More importantly, fermentative mono-saccharides (mainly glucose) can be treated via both aerobic and anaerobic fermentation processes to produce a wide range of interesting bio-derived acids depending on the type of microorganism used[248,249]. Some of these sugar-derived acids are: lactic acid (LA), succinic acid (SA), itaconic acid (IA), among others[250].

These bio-acids are considered as important intermediates and platform chemicals for the production of different added value chemicals[41].

In particular, succinic acid (SA) is the conventional name of butanedioic acid, a linear saturated di-carboxylic acid that appears as white crystals under standard conditions. This di-acid compound (SA) is chemically analogous to the maleic anhydride (MAN), thus SA can potentially replace petroleum-derived MAN as a platform chemical for the synthesis of numerous products. In fact, succinic acid (SA) has been described as a compound of a strategic importance in a future chemical industry based upon renewable raw materials, and it can be found in the priority "Top 10" list of biomass-derived compounds[28]. The presence of two carboxylic groups together with SA solubility in water, exhibits succinic acid as one of the key platform molecules for future bio-based products[251,252].

Hydrogenation, esterification and reductive amination, among others, preferably performed in aqueous media, are essential reactions broadening the market perspectives of SA (Figure 1.13). In this sense, the possible applications for SA, which are expected to register continuous demand growth, comprise valued-added chemicals as amides or pyrrolidones, succinic acid esters for its use as plasticizers and its wide application in the manufacture of bio-polymers such as polyesters, poly-butylene succinate (PBS), poly-butylene terephthalate (PBT) or poly-tetramethylene ether glycol (PTMEG). Hydrogenation routes to produce γ-butyrolactone (solvents, adhesives), 1,4-butanediol (films, adhesives, polymers) and THF (solvents, adhesives) have also been widely studied.

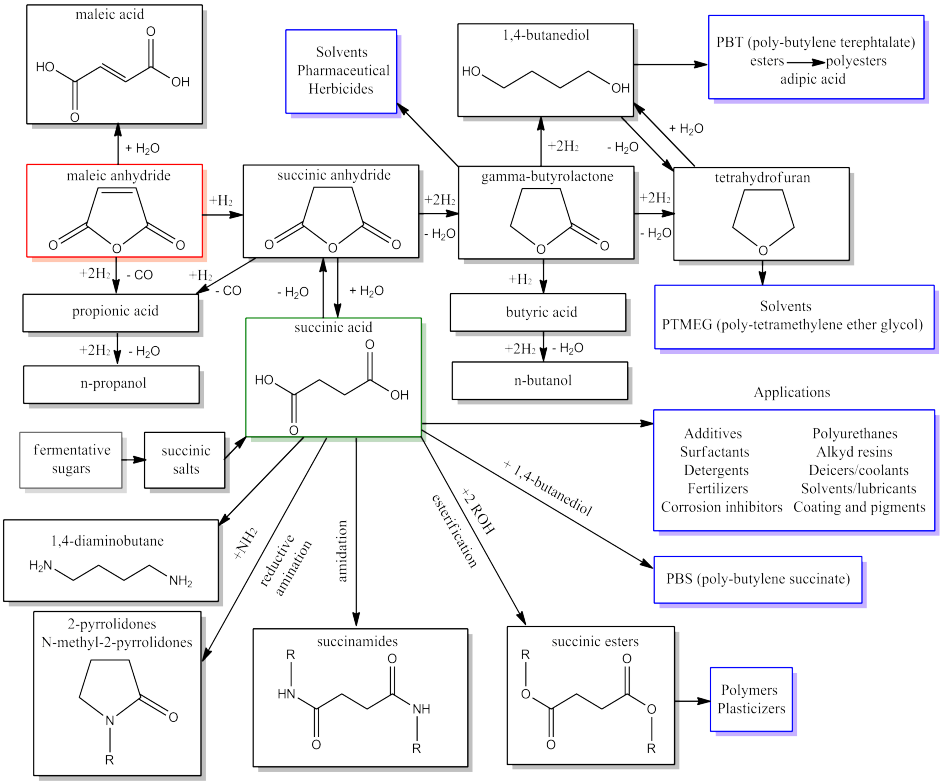

Figure 1.13. Succinic acid as C_4 Platform chemical.

Therefore, the development of selective catalysts is necessary to make the valorisation of SA to products efficient and competitive processes. The activity and stability of these materials under aqueous environments is again a key point for their industrial application.

1.6.2. ABE (Acetone-Butanol-Ethanol) mixtures

Fermentation of biomass to ethanol using the yeast *Saccharomyces cerevisiae* has been largely used for decades. Furthermore, other anaerobic microorganisms as *Solventogenic Clostridias* have been known for producing n-butanol via fermentation processes under

moderated conditions (25-37 ºC and 1 atm). These microorganisms are able to transform different carbohydrates into mixtures of acetone, butanol and ethanol[253–255]. This process is commonly known as ABE fermentation and has recently gained attention, due to this mixture is considered as a potential renewable source of bio-fuels and valuable chemicals products[256,257].

In fact, butanol is widely used as an important industrial solvent and feedstock for chemical production. Moreover, butanol presents superior physical properties compared with ethanol for their blending with gasoline. In particular, butanol has higher energy content, it is less corrosive, it tolerates better water contamination, and it has a better miscibility with gasoline and diesel fuels. Indeed, butanol can be blended up to 30%v/v in traditional engines, without any special pre-treatment. These properties drove ABE fermentation processes to be performed on the industrial scale in US, Russia, South Africa or China[258].

Unfortunately, ABE fermentation processes face several concerns[259]. First of all, a fractionation/hydrolysis pre-treatment step is necessary to enable sugars from lignocellulosic biomass before fermentation takes place. Additionally, main fermentation products are toxic for the yeast, so this fact limits the maximum organic product concentration below 20g/L. This drives to very diluted ABE mixtures, which imply big process volumes, together with the need of recovering/extracting acetone, butanol and ethanol from fermentation media[260–262]. Moreover, other by-products (i.e furfural, HMF, formic acid, acetic acid) have also inhibitory effects on the fermentation processes.

Multiple solutions including genetically modified microorganisms[263] and bio-reactors design[264] have been studied to increase the efficiency of this process. Several methods as distillation, adsorption[265], gas stripping[266], pervaporation[267], liquid-liquid extraction or membrane separation have also been considered as potential recovery operations for acetone, butanol and ethanol from aqueous solutions.

Another potential solution is based on a C-C bond formation strategy. Acetone has a nucleophilic α-carbon, which can react via alkylation[268] (C-C bond formation reaction) with electrophilic alcohols (butanol and ethanol). Moreover, alcohols can also react via Guerbet condensation to produce larger compounds[269–271]. Both mechanisms include a first rate-determining step consisting on the alcohol dehydrogenation to form an aldehyde. Afterwards, aldol condensation and re-hydrogenation steps to form an alkylated ketone or a superior alcohol take place. Water is the only by-product in both reactions; in such a way atom economy is maximized.

In this context, multifunctional catalysts with redox sites (for dehydrogenation – hydrogenation steps) and acid-base sites (for aldol-condensation steps) are necessary. These catalysts should work under aqueous environments, even if previous extracting methods are combined[272]. Therefore, their activity and stability under these complex conditions must be studied. A reaction network based on this strategy is shown in Figure 1.14.

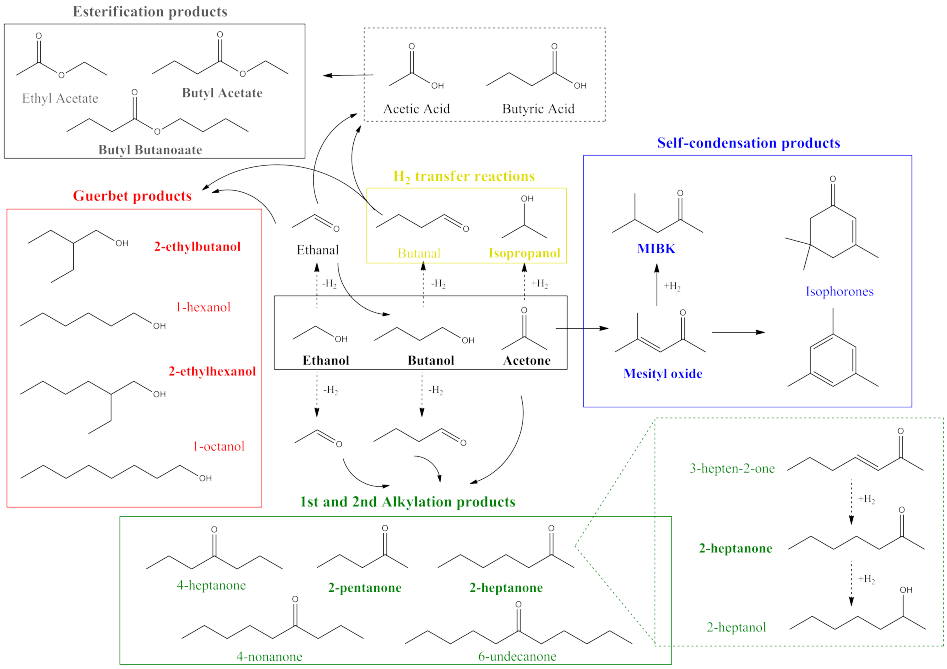

Figure 1.14. ABE mixtures upgrading reaction network.

Therefore, the valorisation of aqueous ABE mixtures via alkylation and Guerbet condensation reactions is an effective way to produce C_6-C_{11} organic compounds useful for fuel applications. In this context, multifunctional catalysts should be active and resistant under extremely diluted mediums and moderated reaction conditions.

Summarizing, the design of new heterogeneous catalysts capable of performing C-C bond formation reactions under complex acid and aqueous environments is a need for the valorisation of several aqueous streams in bio-refineries. Research strategies should focus on the activity and stability of these materials when complex and realistic aqueous mixtures are employed.

1.7. References

1. Worldometers (2017). Available at: http://www.worldometers.info/world-population/.
2. The World Bank DataBank. *Data Bank* (2017). Available at: http://databank.worldbank.org/data/home.aspx.
3. Dlugokencky, E. & Tans, P. *Earth System Research Laboratory* (2017). Available at: http://www.esrl.noaa.gov/gmd/ccgg/trends/global.html.
4. IEA. *Int. Energy Agency* 533 (2016). doi:10.1787/co2_fuel-2016-en.
5. WCED. *Med. War* **4,** 17–25 (1987).
6. Anastas, P.T. & Warner, J.C. *Oxford University Press* **73,** 30 (1998).
7. Mabee, W.E. & Saddler, J.N. *Bioresour. Tech.* **101,** 4806–4813 (2010).
8. Ragauskas, A. J. *et al. Science* **311,** 484–489 (2006).
9. Huber, G.W., Iborra, S. & Corma, A. *Chem.Rev.***106,** 4044–4098 (2006).
10. Tuck, C.O., Pérez, E., Horváth, I. T., Sheldon, R. A. & Poliakoff, M. *Science* **337,** 695–699 (2012).
11. Chheda, J.N., Huber, G.W. & Dumesic, J.A. *Angew. Chem. Int. Ed.* **46,** 7164–7183 (2007).
12. Alonso, D.M., Bond, J.Q. & Dumesic, J.A. *Green Chem.* **12,** 1493-1513 (2010).
13. Zhu, X.G., Long, S.P. & Ort, D.R. *Curr. Opin. Biotechnol.* **19,** 153–159 (2008).
14. Perego, C. & Bosetti, A. *Microp. Mesop. Mater.* **144,** 28–39 (2011).
15. Perego, C. & Bianchi, D. *Chem. Eng. J.* **161,** 314–322 (2010).
16. Dutta, K., Daverey, A. & Lin, J.G. *Renew. Energy* **69,** 114–122 (2014).
17. Lian, J. *et al. Bioresour. Technol.* **101,** 9688–9699 (2010).
18. Holm-Nielsen, J.B., Al Seadi, T. & Oleskowicz-Popiel, P. *Bioresour. Technol.* **100,** 5478–5484 (2009).
19. Naik, S.N., Goud, V.V., Rout, P.K. & Dalai, A.K. *Renew. Sust. Energ. Rev.* **14,** 578–597 (2010).
20. Demirbas, A. *Prog. Energ. Combust. Sci.* **33,** 1–18 (2007).
21. Ho, D.P., Ngo, H.H. & Guo, W. *Bioresour. Technol.* **169,** 742–749 (2014).
22. Kopetz, H. *Nature* **494,** 29–31 (2013).
23. Elliott, D.C. Biomass, Chem. *Encyclopedia of Energy* 163–174 (2004).
24. Klemm, D., Heublein, B., Fink, H.P. & Bohn, A. *Angew. Chem. Int. Ed.* **44,** 3358–3393 (2005).
25. Huber, G.W. & Dumesic, J.A. *Catal. Today* **111,** 119–132 (2006).
26. Hatakeyama, T. & Hatakeyama, H. *Biopolymers : Lignin, Proteins, Bioactive Nanocomposites* **232,** (2010).
27. Clark, J.H. *et al. Green Chem.* **8,** 853-860 (2006).

28. Werpy, T. *et al. Top Value Added Chemicals from Biomass*. *DOE,* 1 (2004).
29. Huber, G.W., Chheda, J.N., Barrett, C.J. & Dumesic, J.A. *Science (80)* **308,** 1446–1450 (2005).
30. Simonetti, D.A. & Dumesic, J. *Catal. Rev.Sci. Eng.* **51,** 441–484 (2009).
31. Serrano-Ruiz, J.C., Luque, R. & Sepúlveda-Escribano, A. *Chem. Soc. Rev.* **40,** 5266-5281 (2011).
32. Bond, J.Q., Alonso, D.M., Wang, D., West, R.M. & Dumesic, J.A. *Science (80)* **327,** 1110–1114 (2010).
33. Corma Canos, A., Iborra, S. & Velty, A. *Chem. Rev.* **107,** 2411–2502 (2007).
34. Climent, M.J., Corma, A. & Iborra, S. *Green Chem.* **13,**520–540 (2011).
35. Jones, S., Valkenburg, C. & Walton, C. *DOE,* 76 (2009).
36. Perlack, R.D. *et al. Agriculture* DOE/GO-102, 78 (2005).
37. Alberdi Ascencio, I., Saura Martínez, S. & M. Millán, F. *Cuaderno de la Sociedad Española Ciencias Forestales* **19,** 11–19 (2005).
38. Ackermann, T., Andersson, G. & Söder, L. *Elect. Pow. Syst. Res.* **57,** 195–204 (2001).
39. Cherubini, F. *Energy Convers. Manage.* **51,** 1412–1421 (2010).
40. Fahim, M.A., Alsahhaf, T.A. & Elkilani, A. *Fundamentals of Petroleum Refining*. *Fundamentals of Petroleum Refining*. Elsevier Science, 2010.
41. Bozell, J.J. & Petersen, G.R. *Green Chem.* **12,** 539–554 (2010).
42. Huber, G.W.& Corma, A. *Angew. Chem. Int. Ed.* **46,** 7184–7201 (2007).
43. Dumesic, J.A., Huber, G.W. & Boudart, M. *Handbook of Heterogeneous Catalysis* 1–27 (2008).
44. Lin, Y.C. & Huber, G.W. *Energy Environ. Sci.* **2,** 68–80 (2009).
45. Zhou, C.H., Xia, X., Lin, C.X., Tong, D.S. & Beltramini, J. *Chem. Soc. Rev.* **40,** 5588–5617 (2011).
46. Poliakoff, M. & Licence, P. *Nature* **450,** 810–812 (2007).
47. Reay, D., Ramshaw, C. & Harvey, A. *Process Intensification: Engineering for Efficiency, Sustainability and Flexibility: Second Edition*. Elsevier Ltd., 2013.
48. Cherubini, F. *et al. Biofuel. Bioprod. Bior.* **3,** 534–546 (2009).
49. Lange, J.P. *Biofuel. Bioprod. Bior.* **1,** 39–48 (2007).
50. Kumar, P., Barrett, D.M., Delwiche, M.J. & Stroeve, P. *Ind. Eng. Chem. Res.* **48,** 3713–3729 (2009).
51. Akhtar, N., Gupta, K., Goyal, D. & Goyal, A. *Environ. Prog. Sustain. Energy.* **35,** 489–511 (2016).
52. Steubing, B., Zah, R. & Ludwig, C. *Environ. Sci. Technol.* **46,** 164–171 (2012).
53. Avellar, B.K. & Glasser, W.G. *Biomass Bioenergy.* **14,** 205–218 (1998).
54. Lee, J. *J. Biotechnol.* **56,** 1–24 (1997).
55. Himmel, M.E. *et al. Science* **315,** 804–807 (2007).
56. Sun, Y. & Cheng, J. *Bioresour. Technol.* **83,** 1–11 (2002).

57. Alauddin, Z.A., Lahijani, P., Mohammadi, M. & Mohamed, A.R. *Renew. Sustain. Energ. Rev.* **14,** 2852–2862 (2010).
58. Maschio, G., Koufopanos, C. & Lucchesi, A. *Bioresour. Technol.* **42,** 219–231 (1992).
59. Huang, H.J. *Energy* **56,** 52–60 (2013).
60. Liu, G., Larson, E.D., Williams, R.H., Kreutz, T.G. & Guo, X. *Energy Fuels* **25,** 415–437 (2011).
61. Stöcker, M. *Angew. Chem. Int. Ed.* **47,** 9200–9211 (2008).
62. Cherubini, F. & Ulgiati, S. *Appl. Energy* **87,** 47–57 (2010).
63. Fernando, S., Adhikari, S., Chandrapal, C. & Murali, N. *Energy Fuels* **20,** 1727–1737 (2006).
64. Fatih Demirbas, M. *Appl. Energy* **86,** S151–S161 (2009).
65. Huber, G.W., Cortright, R.D. & Dumesic, J.A. *Angew. Chem. Int. Ed.* **43,** 1549–1551 (2004).
66. Choi, H.S., Choi, Y.S. & Park, H.C. *Renew. Energy* **42,** 131–135 (2012).
67. Dhyani, V. & Bhaskar, T. *Renew. Energy* 1-22 (2017).
68. Stefanidis, S.D. *et al. J. Anal. Appl. Pyrol.* **105,** 143–150 (2014).
69. Kan, T., Strezov, V. & Evans, T.J. *Renew. Sustain. Energ. Rev.* **57,** 126–1140 (2016).
70. Bridgwater, A.V. *Biomass Bioenergy* **38,** 68–94 (2012).
71. Patwardhan, P.R., Satrio, J.A., Brown, R.C. & Shanks, B.H. *J. Anal. Appl. Pyrol.* **86,** 323–330 (2009).
72. Patwardhan, P.R., Brown, R.C. & Shanks, B.H. *ChemSusChem* **4,** 636–643 (2011).
73. Patwardhan, P.R., Brown, R.C. & Shanks, B.H. *ChemSusChem* **4,** 1629–1636 (2011).
74. Yang, H., Yan, R., Chen, H., Lee, D.H. & Zheng, C. *Fuel* **86,** 1781–1788 (2007).
75. Haiping Yang *et al. Energy Fuels* **20,** 388–393 (2006).
76. Koufopanos, C.A., Papayannakos, N., Maschio, G. & Lucchesi, A. *Can. J. Chem. Eng.* **69,** 907–915 (1991).
77. Babu, B.V. & Chaurasia, A.S. *Energ. Conv. Manage.* **44,** 2251–2275 (2003).
78. Bridgwater, A.V. *Chem. Eng. J.* **91,** 87–102 (2003).
79. Bridgwater, A.V. & Peacocke, G.V.C. *Renew. Sustain. Energ. Rev.* **4,** 1–73 (2000).
80. Bridgwater, A.V. *J. Anal. Appl. Pyrol.* **51,** 3–22 (1999).
81. Singh, N.R., Delgass, W.N., Ribeiro, F.H. & Agrawal, R. *Environ. Sci. Technol.* **44,** 5298–5305 (2010).
82. Catalán-Martínez, D., Domine, M.E. & Serra, J.M. *Fuel* **212,** 353–363 (2018).
83. Bridgewater, A. *J. Therm. Sci.* **8,** 21–50 (2004).
84. Mohan, D., Pittman, C.U. & Steele, P.H. *Energy Fuels* **20,** 848–889 (2006).

85. Vispute, T.P., Zhang, H., Sanna, A., Xiao, R. & Huber, G.W. *Science (80-.).* **330,** 1222–1227 (2010).
86. Yoosuk, B., Boonpo, J., Udomsap, P. & Sukkasi, S. *Kor. J. Chem. Eng.* **31,** 2229–2236 (2014).
87. Resasco, D.E. & Crossley, S.P. *Catal. Today* **257,** 185–199 (2015).
88. Soysa, R., Choi, Y.S., Choi, S.K., Kim, S.J. & Han, S.Y. *Kor. J. Chem. Eng.* **33,** 603–609 (2016).
89. Sipilä, K., Kuoppala, E., Fagernäs, L. & Oasmaa, A. *Biomass Bioenergy* **14,** 103–113 (1998).
90. Branca, C., Giudicianni, P. & Di Blasi, C. *Ind. Eng. Chem. Res.* **42,** 3190–3202 (2003).
91. Bridgwater, A.V. *Prog. in Thermochemical Biomass Conversion* (2008).
92. Zhang, Q., Chang, J., Wang, T. & Xu, Y. *Energ. Convers. Manage.* **48,** 87–92 (2007).
93. Gayubo, A.G., Valle, B., Aguayo, A.T., Olazar, M. & Bilbao, J. *J. Chem. Technol. Biotechnol.* **85,** 132–144 (2010).
94. Stankovikj, F., McDonald, A.G., Helms, G.L. & Garcia-Perez, M. *Energy Fuels* **30,** 6505–6524 (2016).
95. Garcìa-Pérez, M., Chaala, A., Pakdel, H., Kretschmer, D. & Roy, C. *J. Anal. Appl. Pyrol.* **78,** 104–116 (2007).
96. Stankovikj, F., McDonald, A.G., Helms, G.L., Olarte, M.V. & Garcia-Perez, M. *Energy Fuels* **31,** 1650–1664 (2017).
97. Hu, Z., Zheng, Y., Yan, F., Xiao, B. & Liu, S. *Energy* **52,** 119–125 (2013).
98. Iojoiu, E.E., Domine, M.E., Davidian, T., Guilhaume, N. & Mirodatos, C. *Appl. Catal., A. Gen.* **323,** 147–161 (2007).
99. Bridgwater, A.V. & Cottam, M.L. *Energy Fuels* **6,** 113–120 (1992).
100. Czernik, S. & Bridgwater, A.V. *Energy Fuels* **18,** 590–598 (2004).
101. Bridgwater, A.V. *Environ. Prog. Sustain. Energ.* **31,** 261–268 (2012).
102. Diebold, J.P. *Nrel/Sr-570-27613* 59 (2000). doi:NREL/SR-570-27613
103. Karatzos, S. & McMillan, J.D. *The Potential and Challenges of Drop-in Biofuels*. *Task39.Org* (2014).
104. Oasmaa, A., Leppämäki, E., Koponen, P., Levander, J. & Tapola, E. *VTT Publications* (1997). doi:10.1016/S0140-6701(98)97220-4.
105. Oasmaa, A. & Peacocke, C. *VTT Publications*. **731,** 79 (2010).
106. Oasmaa, A., Sundqvist, T., Kuoppala, E., García-Perez, M., Solantausta, Y., Lindfors, C. & Paasikallio, V. *Energy Fuels* **29,** 4373–4381 (2015).
107. Serrano-Ruiz, J.C. & Dumesic, J.A. *Energ. Environ. Sci.* **4,** 83–99 (2011).
108. Oasmaa, A., Kytö, M. & Sipilä, K. *Prog. Therm. Bio. Conv.* 1468–1481 (2008).
109. Solantausta, Y. *et al. Energy Fuels* **26,** 233–240 (2012).
110. Bridgwater, A.V. *Thermochemical Processing of Biomass: Conversion into Fuels, Chemicals and Power* 157–199 (2011).

111. Jacobson, K., Maheria, K.C. & Kumar Dalai, A. *Renew. Sustain. Energ. Rev.* **23,** 91–106 (2013).
112. Gollakota, A.R.K., Reddy, M., Subramanyam, M.D. & Kishore, N. *Renew. Sustain. Energ. Rev.* **58,** 1543–1568 (2016).
113. Holmgren, J., Marinangeli, R., Nair, P., Elliott, D. & Bain, R. *Hydrocarbon Processes* **87,** 95–103 (2008).
114. Gayubo, A.G. *et al. Ind. Eng. Chem. Res.***43,** 2619–2626 (2004).
115. Gayubo, A.G., Aguayo, A.T., Atutxa, A., Valle, B. & Bilbao, J. *J. Chem. Technol. Biotechnol.* **80,** 1244–1251 (2005).
116. Valle, B., Gayubo, A.G., Alonso, A., Aguayo, A.T. & Bilbao, J. *Appl. Catal., B. Environ.* **100,** 318–327 (2010).
117. Fogassy, G., Thegarid, N., Toussaint, G., van Veen, A.C., Schuurman, Y. & Mirodatos, C. *Appl. Catal., B. Environ.* **96,** 476–485 (2010).
118. Fogassy, G., Thegarid, N., Schuurman, Y. & Mirodatos, C. *Energ. Environ. Sci.* **4,** 5068 (2011).
119. Fogassy, G., Thegarid, N., Schuurman, Y. & Mirodatos, C. *Green Chem.***14,** 1367–1371 (2012).
120. Pinho, A.D.R., De Almeida, M.B.B., Mendes, F.L., Ximenes, V.L. & Casavechia, L.C. *Fuel Proces. Technol.* **131,** 159–166 (2015).
121. Domine, M.E., Van Veen, A.C., Schuurman, Y. & Mirodatos, C. *ChemSusChem* **1,** 179–181 (2008).
122. Corma, A., Huber, G.W., Sauvanaud, L. & O'Connor, P. *J. Catalysis* **247,** 307–327 (2007).
123. Elliott, D.C. *et al. Energy Fuels* **26,** 3891–3896 (2012).
124. Bui, V.N., Toussaint, G., Laurenti, D., Mirodatos, C. & Geantet, C. *Catal. Today* **143,** 172–178 (2009).
125. Wright, M.M., Daugaard, D.E., Satrio, J.A. & Brown, R.C. *Fuel* **89,** S2–S10 (2010).
126. Isahak, W.N.R.W., Hisham, M.W.M., Yarmo, M.A. & Yun Hin, T.Y. *Renew. Sustain. Energ. Rev.* **16,** 5910–5923 (2012).
127. Prins, R., de Beer, V. & Somorjai, G. *Catal. Rev. - Sci. Eng.* **31,** 1–41 (1989).
128. Wildschut, J., Iqbal, M., Mahfud, F.H., Cabrera, I., Venderbosch, R.H. & Heeres H.J. *Energ. Environ. Sci.* **3,** 962–970 (2010).
129. De Miguel Mercader, F. *et al. Energ. Environ. Sci.* **4,** 985–997 (2011).
130. Oyama, S.T. *J. Catalysis* **216,** 343–352 (2003).
131. Nava, R., Pawelec, B., Castaño, P, Alvarez-Galván, M.C., Loricera, C.V. & Fierro, J.L.G. *Appl. Catal., B. Environ.* **92,** 154–167 (2009).
132. Elliott, D.C., Hu, J., Hart, T.R. & Neueschwander, G.G. US7425657B1 (2008).
133. Wildschut, J., Mahfud, F.H., Venderbosch, R.H. & Heeres, H.J. *Ind. Eng. Chem. Res.* **48,** 10324–10334 (2009).
134. Elliott, D.C. *Energy Fuels* **21,** 1792–1815 (2007).
135. Wang, H., Male, J. & Wang, Y. *ACS Catal.* **3,** 1047–1070 (2013).

136. Zacher, A.H., Olarte, M.V., Santosa, D.M., Elliott, D.C. & Jones, S.B. *Green Chem.* **16,** 491–515 (2014).
137. Elliott, D.C., Hart, T.R., Neuenschwander, G.G., Rotness, L.J. & Zacher, A.H. *Environ. Prog. Sustain. Energ.* **28,** 441–449 (2009).
138. Pinheiro, A., Hudebine, D., Dupassieux, N. & Geantet, C. *Energy Fuels* **23,** 1007–1014 (2009).
139. Bu, Q. *et al. Bioresour. Technol.* **124,** 470–477 (2012).
140. Kadarwati, S. *et al. J. Anal. Appl. Pyrol.* **118,** 136–143 (2016).
141. Pollard, A.S., Rover, M.R. & Brown, R.C. *J. Anal. Appl. Pyrol.* **93,** 129–138 (2012).
142. Westerhof, R.J.M. *et al. Energy Fuels* **25,** 1817–1829 (2011).
143. Li, X., Kersten, S.R.A. & Schuur, B. *Sep. Purif. Technol.* **175,** 498–505 (2017).
144. Tumbalam Gooty, A., Li, D., Berruti, F. & Briens, C. *J. Anal. Appl. Pyrol.* **106,** 33–40 (2014).
145. Palla, V.S.K.K., Papadikis, K. & Gu, S. *Biomass Bioenergy* **74,** 180–192 (2015).
146. Williams, P.T. & Brindle, A.J. *Fuel* **82,** 1023–1031 (2003).
147. Ijmker, H. M., Gramblička, M., Kersten, S.R.A., van der Ham, A.G.J. & Schuur, B. *Sep. Purif. Technol.* **125,** 256–263 (2014).
148. Vitasari, C.R., Meindersma, G.W. & de Haan, A.B. *Chem. Eng. Res. Des.* **95,** 133–143 (2015).
149. Vitasari, C.R., Meindersma, G.W. & de Haan, A.B. *Green Chem.* **14,** 321–325 (2012).
150. Rover, M.R., Johnston, P.A., Jin, T., Smith, R.G., Brown, R.C. & Jarboe, L. *ChemSusChem* **7,** 1662–1668 (2014).
151. Zhang, L. & Kong, S.C. *Fuel* **95,** 471–480 (2012).
152. Boucher, M.E., Chaala, A., Pakdel, H. & Roy, C. *Biomass Bioenergy* **19,** 351–361 (2000).
153. Alcala, A. & Bridgwater, A.V. *Fuel* **109,** 417–426 (2013).
154. Garcia-Perez, M., Adams, T.T., Goodrum, J.W., Geller, D. & Das, K.C. *Energy Fuels* **21,** 2363–2372 (2007).
155. Garcia-Perez, M., Shen, J., Wang, X.S. & Li, C.Z. *Fuel Proces. Technol.* **91,** 296–305 (2010).
156. Krutof, A. & Hawboldt, K. *Renew. Sustain. Energ. Rev.* **59,** 406–419 (2016).
157. Junming, X., Jianchun, J., Yunjuan, S. & Yanju, L. *Biomass Bioenergy* **32,** 1056–1061 (2008).
158. Milina, M., Mitchell, S. & Pérez-Ramírez, J. *Catal. Today* **235,** 176–183 (2014).
159. Miao, S. & Shanks, B.H. *Appl. Catal., A. Gen.* **359,** 113–120 (2009).
160. Wang, J.J., Chang, J. & Fan, J.. *Energy Fuels* **24,** 3251–3255 (2010).
161. Zhang, Q., Chang, J., Wang, T.J. & Xu, Y. *Energy Fuels* **20,** 2717–2720 (2006).

162. Li, X. *et al. Fuel* **90,** 2530–2537 (2011).
163. Lohitharn, N. & Shanks, B.H. *Catal. Commun.* **11,** 96–99 (2009).
164. Tang, Z., Lu, Q., Zhang, Y., Zhu, X. & Guo, Q. *Ind. Eng. Chem. Res.* **48,** 6923–6929 (2009).
165. Tang, Y., Yu, W., Mo, L., Lou, H. & Zheng, X. *Energy Fuels* **22,** 3484–3488 (2008).
166. Moens, L., Black, S.K., Myers, M.D. & Czernik, S. *Energy Fuels* **23,** 2695–2699 (2009).
167. Radlein, D. & Quignard, A. EP2638129A2 (2014).
168. Venderbosch, R. & Prins, W. *Biofuel.Bioprod.Bioref.* **4,**178–208 (2010).
169. Mullen, C.A., Boateng, A.A., Goldberg, N.M, Lima, I.M., Laird, D.A. & Hicks. K.B. *Biomass Bioenergy* **34,** 67–74 (2010).
170. Talmadge, M.S. *et al. Green Chem.* **16,** 407–453 (2014).
171. Ruddy, D.A., Schaidle, J.A., Ferrel, J.R., Wang, J., Moens, L. & Hensley, J.E. *Green Chem.* **16,** 454–490 (2014).
172. Asadieraghi, M., Wan Daud, W.M.A. & Abbas, H.F. *Renew. Sustain. Energ. Rev.* **36,** 286–303 (2014).
173. Cortright, R.D., Davda, R.R. & Dumesic, J.A. *Nature* **418,** 964–967 (2002).
174. Shabaker, J.W., Huber, G.W. & Dumesic, J.A. *J. Catalysis* **222,** 180–191 (2004).
175. Wang, D., Czernik, S., Montane, D., Mann, M. & Chornet, E. *Ind. Eng. Chem. Res.* **36,** 1507–1518 (1997).
176. Nozawa, T., Mizukoshi, Y., Yoshida, A. & Naito, S. *Appl. Catal., B. Environ.***146,** 221–226 (2014).
177. Chen, G. *et al. Renew. Sustain. Energ. Rev.***79,** 1091–1098 (2017).
178. Davidian, T., Guilhaume, N., Iojoiu, E., Provendier, H. & Mirodatos, C. *Appl. Catal., B. Environ.* **73,** 116–127 (2007).
179. Bimbela, F., Ábrego, J., Puerta, R., García, L. & Arauzo, J. *Appl. Catal., B. Environ.***209,** 346–357 (2017).
180. Trane-Restrup, R., Resasco, D.E. & Jensen, A.D. *Catal. Sci. Technol.* **3,** 3292–3302 (2013).
181. Chen, A., Guo, H., Song, Y., Chen, P. & Lou, H. *Int. J. Hyd. Energ.* **42,** 9577–9588 (2017).
182. Coronado, I., Stekrova, M., Reinikainen, M., Simell, P., Lefferts, L. & Lehtonen, J. *Int. J. Hyd. Energ.* **41,** 11003–11032 (2016).
183. Gaertner, C.A., Serrano-Ruiz, J.C., Braden, D.J. & Dumesic, J.A. *J. Catalysis* **266,** 71–78 (2009).
184. Gangadharan, A., Shen, M., Sooknoi, T., Resasco, D.E. & Mallinson, R.G. *Appl. Catal., A. Gen.* **385,** 80–91 (2010).
185. Pham, T.N., Shi, D., Sooknoi, T. & Resasco, D.E. *J. Catalysis* **295,** 169–178 (2012).
186. Barrett, C.J., Chheda, J.N., Huber, G.W. & Dumesic, J.A. *Appl. Catal., B. Environ.* **66,** 111–118 (2006).

187. Tietze, L.F. & Beifuss, U. *Angew. Chem. Int. Ed.* **32,** 131–163 (1993).
188. Climent, M.J., Corma, A. & Iborra, S. *ChemSusChem* **2,** 500–516 (2009).
189. Climent, M.J., Corma, A., Iborra, S. & Sabater, M.J. *ACS Catal.* **4,** 870–891 (2014).
190. Warner, J.C., Cannon, A.S. & Dye, K.M. *Environ. Imp. Assess. Rev.* **24,** 775–799 (2004).
191. Anastas, P. & Eghbali, N. *Chem. Soc. Rev.* **39,** 301–312 (2010).
192. Chheda, J.N. & Dumesic, J.A. *Catal. Today* **123,** 59–70 (2007).
193. Xing, R. *et al. Green Chem.* **12,** 1933-1946 (2010).
194. West, R.M., Liu, Z.Y., Peter, M., Gärtner, C.A. & Dumesic, J.A. *J. Mol. Catal. A: Chem.* **296,** 18–27 (2008).
195. Deng, Q. *et al. Fuel Proc. Technol.* **148,** 361–366 (2016).
196. Faba, L., Díaz, E. & Ordóñez, S. *Appl. Catal., B. Environ.* **113–114,** 201–211 (2012).
197. Hora, L., Kelbichová, V., Kikhtyanin, O., Bortnovskiy, O. & Kubička, D. *Catal. Today* **223,** 138–147 (2014).
198. Climent, M.J., Corma, A., Fornés, V., Guil-Lopez, R. & Iborra, S. *Adv. Synth. Catal.* **344,** 1090–1096 (2002).
199. Nguyen Thanh, D. *et al. Catal. Today* **277,** 97–107 (2016).
200. Di Cosimo, J. I., Dïez, V. K. & Apesteguía, C.R. *Appli. Catal., A. Gen.* **137,** 149–166 (1996).
201. Faba, L., Díaz, E. & Ordóñez, S. *Appl. Catal., B. Environ.* **142–143,** 387–395 (2013).
202. Sádaba, I., Ojeda, M., Mariscal, R., Richards, R. & Granados, M. L. *Catal. Today* **167,** 77–83 (2011).
203. Shen, W. *et al. Appl. Catal., A. Gen.* **392,** 57–68 (2011).
204. Sádaba, I., Ojeda, M., Mariscal, R., Fierro, J.L.G. & Granados, M. L. *Appl. Catal., B. Environ.* **101,** 638–648 (2011).
205. Wang, W. *et al. ACS Sustain. Chem. Eng.* **5,** 1812–1817 (2017).
206. Cueto, J., Faba, L., Díaz, E. & Ordóñez, S. *ChemCatChem* **9,** 1765–1770 (2017).
207. Hronec, M. *et al. Biomass Bioenerg.* **63,** 291–299 (2014).
208. Liang, D., Li, G., Liu, Y., Wu, J. & Zhang, X. *Catal. Commun.* **81,** 33–36 (2016).
209. Bui, T.V., Sooknoi, T. & Resasco, D.E. *ChemSusChem* **10,** 1631–1639 (2017).
210. Renz, M. *Eur. J. Org. Chem.* 979–988 (2005).
211. Pham, T.N., Sooknoi, T., Crossley, S.P. & Resasco, D.E. *ACS Catal.* **3,** 2456–2473 (2013).
212. Dooley, K.M., Bhat, A.K., Plaisance, C.P. & Roy, A.D. *Appl. Catal., A. Gen.* **320,** 122–133 (2007).
213. Pulido, A., Oliver-Tomas, B., Renz, M., Boronat, M. & Corma, A. *ChemSusChem* **6,** 141–151 (2013).

214. Oliver-Tomas, B., Gonell, F., Pulido, A., Renz, M. & Boronat, M. *Catal. Sci. Technol.* **6,** 5561–5566 (2016).
215. Gaertner, C.A., Serrano-Ruiz, J.C., Braden, D.J. & Dumesic, J.A. *Ind. Eng. Chem. Res.* **49,** 6027–6033 (2010).
216. Snell, R.W. & Shanks, B.H. *ACS Catal.* **3,** 783–789 (2013).
217. Snell, R.W. & Shanks, B.H. *ACS Catal.* **4,** 512–518 (2014).
218. Wang, S., Goulas, K. & Iglesia, E. *J. Catalysis* **340,** 302–320 (2016).
219. Wang, S. & Iglesia, E. *J. Catalysis* **345,** 183–206 (2017).
220. Pacchioni, G. *ACS Catal.* **4,** 2874-2888 (2014).
221. Nagashima, O., Sato, S., Takahashi, R. & Sodesawa, T. *J. Mol. Catal. A. Chem.* **227,** 231–239 (2005).
222. Hasan, M.A., Zaki, M.I. & Pasupulety, L. *Appl. Catal., A. Gen.* **243,** 81–92 (2003).
223. Gliński, M., Kijeński, J. & Jakubowski, A. *Appl. Catal., A. Gen.* **128,** 209–217 (1995).
224. Gliński, M., Zalewski, G., Burno, E. & Jerzak, A. *Appl. Catal., A. Gen.* **470,** 278–284 (2014).
225. Yamada, Y., Segawa, M., Sato, F., Kojima, T. & Sato, S. *J. Mol. Catal. A. Chem.***346,** 79–86 (2011).
226. Snell, R.W., Hakim, S.H., Dumesic, J.A. & Shanks, B.H. *Appl. Catal., A. Gen.* **464,** 288–295 (2013).
227. Kumar, R. *et al. Catal. Today* **302,** 16–49 (2018).
228. Westerhof, R.J.M. *et al. Energ. Technol.* **5,** 205–215 (2017).
229. Schulzke, T., Conrad, S., Kaluza, S. & Van Loo, T. *Biomass Bioenergy* **103,** 11–20 (2017).
230. Qin, F., Cui, H., Yi, W. & Wang, C. *Energy Fuels* **28,** 2544–2553 (2014).
231. Sundqvist, T., Oasmaa, A. & Koskinen, A. *Energy Fuels* **29,** 2527–2534 (2015).
232. Shen, W., Tompsett, G.A., Xing, R., Conner, W.C. & Huber, G.W. *J. Catalysis* **286,** 248–259 (2012).
233. Sharma, S.K., Parikh, P.A. & Jasra, R.V. *J. Mol. Catal. A. Chem.* **278,** 135–144 (2007).
234. Hakim, S.H., Shanks, B.H. & Dumesic, J.A. *Appl. Catal., B. Environ.* **142–143,** 368–376 (2013).
235. Lopez-Ruiz, J.A., Cooper, A.R., Li, G. & Albrecht, K.O. *ACS Catal.* (2017). doi:10.1021/acscatal.7b01071
236. Wu, K. *et al. ACS Sustain. Chem. Eng.* **5,** 3509–3516 (2017)
237. Wu, K. *et al. AIChE Journal* **63,** 2958–2967 (2017).
238. Cai, Q. *et al. ACS Catal.* **8,** 488–502 (2018).
239. Pham, T.N., Shi, D. & Resasco, D.E. *Appl. Catal., B. Environ.* **145,** 10–23 (2014).
240. Wu, K. *et al. ChemSusChem* **9,** 1355–1385 (2016).
241. Sreekumar, S. *et al. ChemSusChem* **7,** 2445–2448 (2014).

242. Koutinas, A. A. *et al. Chem. Soc. Rev.* **43,** 2587 (2014).
243. Pellow, K.J., Wingad, R.L. & Wass, D.F. *Catal. Sci. Technol.* **7,** 5128–5134 (2017).
244. Lin, Y. & Tanaka, S. *Appl. Microbiol. Biotechnol.* **69,** 627–642 (2006).
245. Katzen, R. & Schell, D.J. *Biorefineries-Industrial Processes and Products: Status Quo and Future Directions* **1,** 129–138 (2008).
246. Waldron, K. *Bioalcohol Production: Biochemical Conversion of Lignocellulosic Biomass* (2010).
247. Varadarajan, S. & Miller, D.J. *Biotechnol. Prog.* **15,** 845–854 (1999).
248. Dodds, D.R. & Gross, R.A. *Science* **318,** 1250–1251 (2007).
249. Danner, H. & Braun, R. *Chem. Soc. Rev.* **28,** 395–405 (1999).
250. van Haveren, J., Scott, E.L. & Sanders, J. *Biofuel. Bioprod. Bioref.* **2,** 41–57 (2008).
251. Wang, C. *et al. Biotechnol. Biofuel.* **6:74,** (2013).
252. Du, C., Lin, S.K.C., Koutinas, A., Wang, R. & Webb, C. *Appl. Microbiol. Biotechnol.* **76,** 1263–1270 (2007).
253. Ezeji, T.C., Qureshi, N. & Blaschek, H.P. *Curr. Op. Biotechnol.* **18,** 220–227 (2007).
254. Jones, D.T. & Woods, D.R. *Microbiol. Rev.* **50,** 484–524 (1986).
255. Moon, H. G. *et al. FEMS Microbiol. Lett.* **363,** (2016).
256. Nahreen, S. & Gupta, R.B. *Energy Fuels* **27,** 2116–2125 (2013).
257. Anbarasan, P. *et al. Nature* **491,** 235–239 (2012).
258. Ni, Y. & Sun, Z. *Appl. Microbiol. Biotechnol.* **83,** 415–423 (2009).
259. Jurgens, G. *et al. Biotechnol. Lett.* **34,** 1415–1434 (2012).
260. Qureshi, N. *Biorefineries: Integrated Biochemical Processes for Liquid Biofuels* 101–118 (2014).
261. Kujawska, A., Kujawski, J., Bryjak, M. & Kujawski, W. *Renew. Sustain. Energ. Rev.* **48,** 648–661 (2015).
262. Oudshoorn, A., Van Der Wielen, L.A.M. & Straathof, A.J.J. *Ind. Eng. Chem. Res.* **48,** 7325–7336 (2009).
263. Tracy, B.P., Jones, S.W., Fast, A.G., Indurthi, D.C. & Papoutsakis, E.T. *Curr. Op. Biotechnol.***23,** 364–381 (2012).
264. Maddox, I.S. *Biotechnol. Gen. Eng. Rev.* **7,** 189–220 (1989).
265. Abdehagh, N., Gurnani, P., Tezel, F.H. & Thibault, J. *Adsorption* **21,** 185–194 (2015).
266. Lu, K. M. & Li, S. Y. *J. Taiw. Inst. Chem. Eng.* **45,** 2106–2110 (2014).
267. Qureshi, N., Meagher, M.M., Huang, J. & Hutkins, R.W. *J. Memb. Sci.* **187,** 93–102 (2001).
268. Kwon, M. S. *et al. Angew. Chem. Int. Ed.***44,** 6913–6915 (2005).
269. Gabriëls, D. *et al. Catal. Sci. Technol.* **5,** 3876–3902 (2015).
270. Carlini, C., Macinai, A., Raspolli Galletti, A.M. & Sbrana, G. *J. Mol. Catal. A. Chem.* **212,** 65–70 (2004).
271. Kozlowski, J.T. & Davis, R.J. *ACS Catal.* **3,** 1588–1600 (2013).
272. Xu, G. *et al. ChemSusChem* **7,** 105–109 (2014).

CHAPTER 2

OBJECTIVES

2.1 Main objectives

Lignocellulosic biomass has become a sustainable alternative to the use of fossil sources for the production of fuels and chemicals. In this context, bio-oils obtained via fast pyrolysis of biomass are complex mixtures containing water and a wide range of oxygenated organic compounds, these bio-oils being characterized by their high acidity and reactivity. A liquid-liquid separation upgrading approach by H_2O addition allows obtaining separated organic fractions, which can be processed for their application as liquid fuels; and aqueous streams containing C_1-C_4 water-soluble compounds, which constitute waste effluents at bio-refineries. In the same way, other aqueous effluents derived from fermentation processes (i.e. ABE mixtures) also need to be valorised to increase processes efficiency and competitiveness. The transformation of these low-value water-soluble oxygenated compounds into a mixture of hydrocarbons and aromatics useful for blending with automotive fuels would be of great interest. This can be achieved by performing "one-pot" C-C bond formation reactions, such as aldol condensation and ketonization, among others. In general, the activity of the catalysts employed in these reactions is based on their bifunctional character, although their activity and stability under faithful operating conditions is a critical factor to be further improved.

The design of new heterogeneous catalysts that meet these new process requirements is a need for the valorisation of these aqueous streams. In this sense, this work will focus on the catalytic behaviour of new solid acid catalysts by using an aqueous mixture of representative C_2-C_3 oxygenated compounds, which is closer to the real conditions at the

industry and differing from the usual probe molecules studies performed even in the absence of water.

2.2 Specific objectives

- The activity and stability of bifunctional catalysts widely used in condensation and ketonization reactions will be studied in the liquid-phase condensation of light oxygenates present in an aqueous model mixture. In this sense, $Ce_xZr_{1-x}O$ mixed oxides as reference materials in literature, hydrotalcite-derived mixed oxides, monometallic and mixed metal oxides will be analysed.

- The development of hydrothermally synthesized TiO_2 crystals with specific facets in order to obtain surfaces with higher reactivity will be considered as a feasible strategy to obtain active and resistant TiO_2-based catalysts for these complex reaction mixtures under moderated operation conditions.

- Nb- and WNb-mixed oxides prepared by different synthesis and post-synthesis procedures and their influence on the catalytic performance in the aqueous-phase condensation of oxygenated compounds will be studied. Nb-based materials stability against organic acids and aqueous environments will be discussed.

- The synthesis of new Sn-based mixed oxides via co-precipitation will be studied; being these materials potential Lewis acid catalysts in the aqueous-phase condensation of light oxygenated compounds. In particular, tin combination with resistant metal oxides, such as titania and niobia will be investigated.

CHAPTER 3

EXPERIMENTAL PROCEDURE

3.1 Reactants and commercial catalysts

Reagent-grade chemicals (>95% purity) from Sigma-Aldrich and Scharlab as main providers were used during this research (Table 3.1). All these reactants and solvents were directly used without any pre-treatment or purification steps.

Table 3.1. Organic reactants and solvents used during this work.

Nº	Reactant	Nº	Reactant
1	Methanol	14	2-methyl-2-pentenal
2	Ethanol	15	Mesityl oxide
3	Acetic acid	16	2,3-hexanedione
4	Propanal	17	3-hexen-2-one
5	Acetol	18	3-methylcyclopentanone
6	Acetone	19	2-methylcyclohexanone
7	Isopropanol	20	2-heptanone
8	Butanol	21	4-heptanone
9	Ethyl acetate	22	2,4,4-trimethylcyclopentanone
10	2-pentanone	23	4-nonanone
11	3-pentanone	24	2,3,6-trimethylphenol
12	Furfural	25	2,3,4,5-tetramethyl-2-cyclopentenone
13	Chlorobenzene	26	4-tert-butylcyclohexanone

Many different catalysts were synthesized in this work. Metal precursors and inorganic reactants used for their preparation are detailed in Table 3.2.

Table 3.2. Inorganic reactants used for catalysts preparation.

Nº	Reactant	Nº	Reactant
1	Hydrochloric acid	13	Gallium nitrate hydrate
2	Hydrofluoric acid	14	Manganese (II) nitrate tetrahydrate
3	Sodium hydroxide	15	Titanium (IV) isopropoxide
4	Sodium carbonate	16	Titanium (IV) butoxide
5	Ammonium hydroxide solution	17	Niobium (V) chloride
6	Cerium (III) nitrate hexahydrate	18	Niobium oxalate monooxalate adduct
7	Zirconium (IV) oxynitrate hydrate	19	Ammonium metatungstate hydrate
8	Magnesium nitrate hexahydrate	20	Tin (IV) chloride pentahydrate
9	Aluminum nitrate nonahydrate	21	Tin (II) oxalate
10	Zinc nitrate hexahydrate	22	Titanium (IV) oxychloride-HCl acid solution (15% Ti)
11	Iron (III) nitrate nonahydrate	23	Potassium carbonate
12	Lanthanum nitrate hexahydrate	24	Cesium nitrate

Metallic oxides commercial catalysts and supports used during this work and their main physicochemical characteristics are detailed in Table 3.3.

Table 3.3. Commercial catalysts and supports used during this work.

Nº	Catalyst	Provider	Surface area (m^2/g)	Total pore volume (cm^3/g)
1	ZrO_2 monoclinic	Chempure	98	0.26
2	ZrO_2 tetragonal	Chempure	138	0.20
3	CeO_2 nanopowder	Sigma-Aldrich	22	0.15
4	MgO nanopowder	Chempure	104	0.22
5	ZnO nanoactive	Chempure	47	0.28
6	La_2O_3	Sigma-Aldrich	-	-
7	Al_2O_3 nanopowder	Sigma-Aldrich	134	0.43
8	SiO_2 nanopowder	Sigma-Aldrich	508	0.96
9	TiO_2 aeroxide P25	Degussa	50	0.25
10	TiO_2 anatase	Sigma-Aldrich	100	0.20
11	TiO_2 rutile	Sigma-Aldrich	2	0.00
12	Nb_2O_5	Sigma-Aldrich	13	0.02
13	SnO_2	Sigma-Aldrich	15	0.01

All these catalysts were calcined in air at 400-600 ºC for 2h, with a heating rate of 2 ºC/min, in order to eliminate adsorbed water and contaminants. In this way, commercial catalysts have the same heat-treatment compared to the synthesized materials.

3.2 Catalysts synthesis

3.2.1 Hydrotalcite-derived mixed oxides

The catalysts were prepared through co-precipitation method, following the procedure described in reference[1]. The corresponding gels were achieved by mixing two aqueous solutions: A) acid solution containing the corresponding precursors of trivalent metals: $Al(NO_3)_3.9H_2O$, $Fe(NO_3)_3.9H_2O$, $Ce(NO_3)_3.6H_2O$, $La(NO_3)_3.6H_2O$ or $Ga(NO_3)_3.H_2O$ and bivalent metals: $Mg(NO_3)_2.6H_2O$, $Zn(NO_3)_2.6H_2O$ and B) basic solution containing Na_2CO_3 and NaOH. Both solutions were slowly mixed at 20 mL/h (addition rate) during 3h with vigorous stirring. Basic solution concentration was adjusted to obtain a final pH=12-13. Afterwards, the gels obtained were aged at 60 ºC during 24h; and then filtered and washed with distilled water until pH=7. Finally, the catalysts were dried at 60 ºC overnight and heat-treated in air/N_2 at 450 ºC during 10h, with a heating rate of 2 ºC/min, in order to obtain the hydrotalcite-derived mixed oxides.

3.2.2 Mixed metal oxides via incipient wetness impregnation

An aqueous solution of the metal to be supported was firstly prepared. This solution contains the calculated amount of precursor to obtain a nominal 1-10wt% over each support (0.5-1.0 g). The volume of necessary distilled water was previously calculated for each oxide. Afterwards, the solution was drop by drop added to the commercial solid. After the addition step, the catalyst was dried at 100 ºC overnight.

Finally, synthesized catalysts were calcined in air/N_2 at 400-600 ºC during 2h, with a heating rate of 2 ºC/min. This method has been used for catalysts employed in Chapter 4 (Mg/ZrO_2, Zn/ZrO_2, Mg/TiO_2, Zn/TiO_2), Chapter 6 (W/Nb_2O_5) and Chapter 7 (Sn/Nb_2O_5, Nb/SnO_2, Sn/TiO_2, Ti/SnO_2). Information about metal precursors and commercial supports can be found in Table 3.2 and Table 3.3.

3.2.3 Mixed metal oxides via wet impregnation

This procedure was used in Chapter 6 as an alternative method to synthesize WNbO mixed oxides. An aqueous solution of $(NH_4)_6H_2W_{12}O_{40}.H_2O$ and $C_4H_4NNbO_9.H_2O$ as metal precursors in the desired relation was firstly prepared. The metal salts were dissolved in 15 mL of distilled water and kept under stirring at 70 ºC until the solvent was totally evaporated. Then, the catalyst was dried at 100 ºC overnight. Finally, synthesized catalyst was heat-treated at 550 ºC under air/N_2 during 2h, with a heating rate of 2 ºC/min.

3.2.4 Mixed metal oxides via co-precipitation

Co-precipitation method has been one of the synthesis procedures commonly used during this work, as it is an easy process to produce homogeneous mixed oxides in a wide range of composition.

In this context, $Ce_xZr_{1-x}O_2$ mixed oxides (reference catalysts in this work) have usually been prepared through co-precipitation synthesis[2]. Aqueous solutions of $Ce(NO_3)_3.6H_2O$ and $ZrO(NO_3)_2.H_2O$ were used to obtain the desired Ce-Zr ratio. Once the solutions were mixed, a 28wt%

NH_4OH aqueous solution was slowly added until a pH=10 was reached. Afterwards, the solution was kept under stirring at room temperature during 65h; the solids were separated by filtration, and washed with distilled water. Finally, the catalysts were dried at 100 ºC overnight and heat-treated in air at 450 ºC during 2h, with a heating rate of 2 ºC/min.

A more general co-precipitation procedure was used to synthesize the rest of mixed oxides employed during this work. In this sense, an aqueous solution containing the desired relation of metal precursors was firstly prepared. Metals precursors (25 mmol of metals) were dissolved in 100 mL of distilled water and kept under stirring until homogenization. Afterwards, a 28wt% NH_4OH aqueous solution was slowly added until pH=9 was reached. The resulting slurry was kept at room temperature during 24h before the solids were separated by filtration, washed with distilled water and dried at 100 ºC overnight. Finally, synthesized catalysts were calcined in air/N_2 at 400-600 ºC during 2h with a heating rate of 2 ºC/min. This procedure has been used for catalysts employed in Chapter 4 (Mg-Ti, Zn-Ti, Mg-Zr, Zn-Zr, Mn-Zr), Chapter 6 (W-Nb) and Chapter 7 (Sn-Zr, Sn-Nb, Sn-Ti, Sn-Ti-Nb). Information about metal precursors and commercial supports can be found in Table 3.2 and Table 3.3.

The influence of metal precursor, initial solution concentration, pH during the synthesis and heat-treatment conditions have been studied and optimized for the most promissory catalytic materials (Chapter 6 and Chapter 7).

3.2.5 Faceted TiO_2 materials via hydrothermal synthesis

TiO_2-based materials used in Chapter 5 were prepared in collaboration with the Prof. José A. Navío´s research group by direct hydrothermal treatment of the titanium precursors[3], i.e. 50 mL of titanium (IV) isopropoxide or titanium (IV) butoxide together with the addition of 8 mL of aqueous HF as a capping agent. The solutions were transferred into a Teflon recipient inside of a 125 mL-stainless steel autoclave and hydrothermal treatment was performed at 200 ºC for 24 h. The precipitate obtained was filtered, repeatedly washed with distilled water and dried overnight at 100 ºC.

3.2.6 Nb_2O_5 and WNbO mixed oxides via hydrothermal synthesis

h-WO_3, Nb_2O_5 and WNbO mixed oxides (used in Chapter 6) were prepared in collaboration with the Prof. José M. López-Nieto's research group through hydrothermal synthesis from acidified aqueous solutions containing stoichiometric amounts (H_2O/(W+Nb) molar ratio = 53/1) of the corresponding metal salts: ammonium metatungstate hydrate (>85wt% WO_3 basis, Aldrich) and niobium oxalate monooxalate adduct (Sigma Aldrich). These solutions were introduced into Teflon-lined stainless steel autoclaves, purged with N_2 and heat-treated at 175 ºC during 48h. Resulting solids were filtered, washed with distilled water and dried at 100 ºC during 16h. Finally, they were heat-treated at 550 ºC under air/N_2 flow during 2h. On the other hand, h-WO_3 sample was just heat-treated at 450 ºC to avoid decomposition into m-WO_3.

3.3 Catalysts analysis and characterization

In this section, the fundamental principles of the different characterization techniques used during this work are examined.

3.3.1. Inductively Coupled Plasma Atomic Emission Spectroscopy (ICP-AES)

It is an analytical technique used for the detection and quantification of chemical elements. It is a type of emission spectroscopy technique, where inductively coupled plasma is used to produce excited atoms and ions, which emit electromagnetic radiation at given wavelengths characteristic of each element[4]. The intensity of the energy emitted is proportional to the amount (concentration) of that element in the analysed sample. ICP-AES analysis requires the sample to be in solution. In this sense, solid catalysts (30-50 mg) were dissolved in a 5 mL mixture of acids (HF:HNO_3:HCl), which afterwards was diluted in 50 mL of distilled water. The composition of solid catalysts has been elucidated in an ICP-AES Varian 715-ES equipment.

This fluid sample is pumped into the nebulizer via a peristaltic pump. This nebulizer generates an aerosol mist, while an argon gas current is injected into the chamber along with the sample. The largest mist particles settle down, whereas the finest particles (1-2%) are subsequently transferred into the torch. A radio frequency-generated Ar plasma is formed, which cause the excitation of the electrons. When those return to the ground state, they emit energy at peculiar wavelengths corresponding to the sample´s elemental composition. The light emitted

is focused through lenses and multipliers to the spectrometer. The analysis is usually performed in comparison with reference standards (background corrections). This technique provides flexible and rapid analysis of solid catalysts composition.

3.3.2. X-Ray Fluorescence Spectrometry (XRF)

$Ce_xZr_{1-x}O_2$ mixed oxides were not dissolved in the mixture of acids ($HF:HNO_3:HCl$) during sample preparation for ICP-AES analysis. In addition, fluoride species present in faceted TiO_2 materials (Chapter 5) cannot be analysed as the HF used during the digestion step affects the quantitative results. In this sense, an alternative technique was selected to analyse these catalysts composition.

X-Ray Fluorescence Spectrometry (XRF) technique is based on the quantitative analysis of the characteristic secondary (or fluorescent) X-rays emitted from a material that has been bombed with high-energy X-Rays[5]. When materials are exposed to high-energy radiation, ionization of their component atoms takes place, where one or more electrons from the atom can be ejected. Electrons in higher orbitals "fall" to fill the holes left behind and energy is released in form of a photon. This energy is related to the energy difference among the orbitals involved, which is characteristic of each chemical element. This phenomenon is known as fluorescence. The intensity detected in the spectrophotometer is proportional to the element concentration. $Ce_xZr_{1-x}O_2$ samples XRF measurements were carried out in a MiniPal 4 PANanalytical equipment, where 30 keV radiation was used. On the other hand, fluoride species in

TiO_2-samples were analysed in a PANalytical Axios sequential spectrophotometer using pressed pellets (10wt% of wax).

3.3.3. X-Ray Diffraction (XRD)

X-ray crystallography is a technique commonly used to determine the atomic and molecular structure of a solid catalyst. X-ray wavelength interval goes from 10 to 100 Å, being in a similar order of magnitude to interplanar spacing in most of crystalline structures. Then, when a monochromatic X-ray radiation incises on a solid, dispersion phenomenon may take place. Crystals are regular and periodic arrays of atoms, which can elastically scatter X-ray radiation. Regular scattering produce waves that will cancel each other in most directions through destructive interference, whereas they will add constructively in a few specific directions, determined by Bragg´s law[6]:

$$2d * \sin\theta = n\lambda \qquad \text{(Equation 3.1)}$$

where d is the spacing between diffraction planes, θ is the incident angle, n is any integer and λ is the wavelength of the beam.

Then, X-ray diffraction consists in an incident X-ray beam with varying angle, which cause dispersion phenomenon, whose intensity is measured and transformed into an X-ray diffraction pattern. This pattern allows elucidating a catalyst crystalline structure. In our case, XRD patterns of powder solid samples were performed on a PANalytical Cubix diffractometer equipped with a PANalytical X-Celerator detector, using Cu Kα radiation and a graphite monochromator.

In crystallography, the ordered arrangement of atoms in a crystalline material along the three-dimensional space directions drives to a specific crystal structure. Crystal structures are described in terms of the geometrical arrangement of the particles present in the unit cell (the smallest repeating unit having full symmetry in the structure). In this context, vectors and planes in a crystal lattice are described by the three-value Miller index notation (hkl). All crystalline materials recognized today fit in one of the 14 Bravais lattices, where interplanar spacing (d) between adjacent (hkl) planes is given by known equations depending on the catalyst structure (i.e. cubic, tetragonal, hexagonal).

Then, if λ is experimentally known and (hkl) and θ are known for a specific lattice plane, interplanar spacing can be calculated using Braggs´s Law: $2d_{hkl} * \sin \theta_{hkl} = n\lambda$. Unit cells lattice dimensions (a, b and c) can be elucidated from this data and the corresponding equation for a determined crystal structure. This is useful information in catalysis in order to analyse the incorporation of metals in a crystalline structure during the synthesis of mixed metal oxides.

Moreover, X-ray diffraction gives information about the particle size (D) using Scherrer´s equation[7]:

$$D = K \lambda / B \cos \theta \qquad \text{(Equation 3.2)}$$

where K is a constant, λ is the wavelength of the beam, B is the FWHM (Full Width at Half Maximum) and θ is the angle where this peak appears.

3.3.4. Raman Spectroscopy

It is a spectroscopic characterization technique used to analyse vibrational, rotational and other low-frequency modes in a catalyst sample[8]. It is commonly used to characterize catalyst structure and it gives complementary information to infrared spectroscopy.

Raman spectroscopy is based on inelastic (Raman) scattering of monochromatic light (from a laser in the visible, near infrared or near ultraviolet range: 100-1200 cm^{-1}). The laser interacts with molecular vibrations or other excitations in the system, resulting in the energy of the laser photon being shifted up or down. There are three possible scenarios:

i) Firstly, if the excited molecule returns to the fundamental state, the energy of the incident and dispersed photon is the same (Rayleigh dispersion). This elastic component does not participate in the Raman spectra.
ii) Secondly, if the molecule ends in a higher energy level, less-energy photons are dispersed, which means a wavelength increase and a decrease in the radiation frequency (Stokes dispersion).
iii) On the contrary, if the molecule ends in a lower energy level, a lower wavelength (higher radiation frequency) is observed (anti-Stokes dispersion).

All these energy changes drive to useful information about metal-oxygen bonds (M-O, M-O-M, M=O) in the catalyst structure. This technique is especially relevant when dealing with mixed metal oxides as data about catalyst crystalline structure, homogeneity and stability can be analysed[9].

Raman spectra of hydrothermally synthesized Nb- and WNbO materials (Chapter 6), together with $Sn_xTi_yNb_zO$ mixed oxides (Chapter 7) were achieved in a 1000 inVia Renishaw spectrometer equipped with an Olympus microscope, a CCD detector and a Renishaw HPNIR laser. An exciting wavelength of 514 nm corresponding to light green in the electromagnetic spectra was employed. On the other hand, Raman analyses of TiO_2-based catalysts (Chapter 5) were performed in a LabRAM Horiba Jobin Yvon confocal Raman microscope with three excitation wavelengths (785 nm red, 532 nm green and 325 nm UV) in order to confirm crystalline phases and preferential growth of TiO_2 crystals.

3.3.5. Textural analysis. N_2 adsorption isotherms

Gas adsorption characterization techniques give information about textural properties of solid materials from gas-solid adsorption and desorption processes. Surface area, pore size and pore volume information can be achieved from the adsorption-desorption isotherms interpretation. In this sense, Brunauer-Emmett-Teller (BET) theory explains the physical adsorption of gas molecules on a solid surface and has been traditionally used as a characterization technique for the measurement of the specific surface area of materials[10]. Nitrogen (at 77 K) is the most commonly employed gaseous adsorbate used for surface area determination. This method is an extension of the Langmuir theory, where liquid-phase N_2 monolayer molecular adsorption occurs. The resulting BET equation is:

$$\frac{P}{V\,(P^0-P)} = \frac{1}{V_m*C} + \frac{(C-1)}{V_m*C} * \frac{P}{P^0} \qquad \text{(Equation 3.3)}$$

where V is the adsorbed gas quantity at a determinate relative pressure (P/P^0) and V_m is the monolayer adsorbed gas quantity. C is related to the heat of adsorption for the first layer; and BET surface area is given by:

$$Surface\ area\ (BET) = \frac{V_m*L*A_m}{M} \qquad \text{(Equation 3.4)}$$

where V_m is the monolayer adsorbed gas quantity, L is Avogradro´s number, A_m is the volume of each adsorbed N_2 molecule (0.162 nm^2) and M is the molar volume of the adsorbate gas.

The adsorbed gas quantity (V) versus relative pressure (at fix temperature conditions) is an adsorption isotherm. The IUPAC classification of adsorption isotherms[11] is illustrated in Figure 3.1. The six types of isotherms are characteristic of adsorbents that are microporous (type I), nonporous or macroporous (II, III and VI) or mesoporous materials (types IV and V). Different shape of adsorption hysteresis (IV and V) can give information about pore size distribution, pore geometry and connectivity of mesoporous materials.

N_2 adsorption isotherms were collected in a Micromeritics ASAP 2000 equipment. Samples were degassed in vacuum overnight at a temperature 200 ºC below their calcination temperature. Surface areas were calculated by BET method and pore size distribution and pore volumes were obtained by Barrett-Joyner-Halenda (BJH) method.

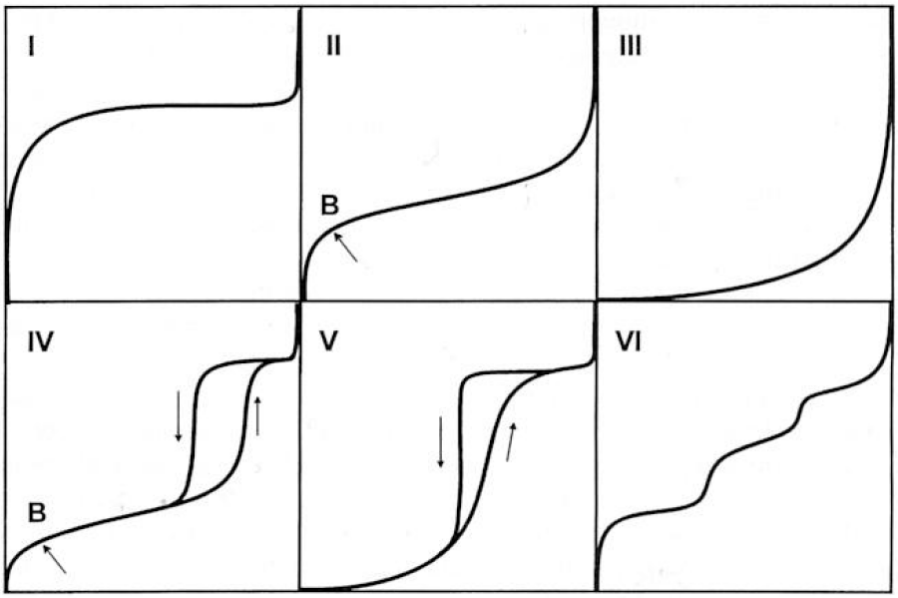

Figure 3.1. IUPAC classification of adsorption isotherms[11].

3.3.6. Fourier Transform Infrared spectroscopy (FTIR-KBr)

Infrared spectroscopy gives information about structural and surface characteristics of solid catalysts. Number, position and intensity of IR bands are associated with M-O bond strength and structural features of IR active species. Analogously to Raman spectroscopy, an IR spectrum is formed from photons interaction (in this case from a radiation in the IR range; 0.78 to 1000 μm), which causes changes in vibrational and rotational modes of a molecule. In this sense, a molecule adsorbs IR radiation at resonant frequencies (when the frequency of the adsorbed radiation matches the vibrational frequency of an atom that implies a polarity deviation in the molecule).

In our case, the FTIR spectroscopy has been used to obtain information about Ti-OH bonds in TiO_2-materials (Chapter 5) when fluoride species are present in the surface. IR spectrums were achieved at ambient temperature using a FTIR Nicolet710 apparatus where 10-20 mg of catalysts were mixed with KBr in the form of a thin wafer.

3.3.7. Fourier Transform Infrared spectroscopy with Pyridine adsorption (FTIR-PY)

Specifically, Infrared (FT-IR) spectroscopy monitoring of adsorbed pyridine is a commonly used characterization technique for evaluating the acidity of solid catalysts. Interestingly, both, Brönsted acid sites (BAS) and Lewis acid sites (LAS) can be distinguished. Characteristic band of pyridine adsorbed on BAS sites (1545 cm^{-1}) corresponding to pyridinium ion, and characteristic band of pyridine adsorbed on LAS sites (1455 cm^{-1}) are used for acid properties discussion. Moreover, the acid strength distribution of acid sites can be investigated by the desorption of pyridine at different temperature conditions.

Infrared spectra of adsorbed pyridine were carried out in a Nicolet 710 spectrometer, where self-supported wafers of 10 $mg.cm^{-2}$ were degassed in vacuum at 200 ºC overnight. Then, pyridine was admitted, and after achieving equilibrium, samples were outgassed at 150 ºC, 250 ºC and 350 ºC, respectively. Concentration of acid sites was calculated from the corresponding band intensities and extinction coefficients applying the method proposed by Emeis et al[12].

3.3.8. Temperature-Programmed Desorption (TPD) of ammonia and carbon dioxide

Temperature-Programmed Desorption (TPD) experiments using NH_3 and CO_2 is a common characterization technique to measure surface acid and base properties, respectively, in solid catalysts. This technique is based on the chemisorption of a gas on the solid surface, and the following study of the gas desorption with a controlled increasing temperature. In this sense, NH_3 can act as a Brönsted/Lewis molecule, so it is used to determine acid characteristics of solid materials[13]. Then, NH_3 molecules interact with acids centers and remain chemisorbed. When temperature is raised, NH_3 progressively desorbs from the surface and is measured in a TCD detector and a mass spectrometer. Therefore, total acid sites (both Lewis and Brönsted) can be analysed using this characterization technique. Moreover, the strength of these acids centres can be studied, as stronger acid sites may drive to a shift in the peak of NH_3 desorption to higher temperatures. On the other hand, and based on the same principles, the use of CO_2 allows studying basic characteristics of solid catalysts.

Temperature programmed desorption of ammonia (NH_3-TPD) was carried out on a Micromeritics TPD/2900 apparatus. Typically, 100 mg of the catalyst sample was pre-treated in an Ar stream at 450 ºC during 1h to eliminate adsorbed contaminants and volatile species, which can interfere during the gas desorption analysis. Afterwards, ammonia was chemisorbed by pulses at 100 ºC until equilibrium was reached. Then, the sample was fluxed with helium stream during 15 min to eliminate the

excess of NH_3, prior to increase the temperature up to 500 ºC in a 100 mL/min He stream with a heating rate of 10 ºC/min. NH_3 desorption was monitored with a thermal conductivity detector (TCD) and a mass spectrometer. Total volumes of adsorbed ammonia are measured under pressure and temperature standard conditions. Then, total moles of adsorbed NH_3 (equivalent to total moles of acid sites) can be calculated using the ideal gas law. Analogously, temperature programmed desorption of carbon dioxide (CO_2-TPD) was carried out following the same procedure, but temperature was increased up to 800 ºC during the gas desorption step.

3.3.9. X-ray Photoelectron Spectroscopy (XPS)

Quantitative and qualitative information about chemical species in the surface of solid catalysts can be achieved by X-ray photoelectron spectroscopy (XPS)[14]. This characterization technique gives data about surface elemental composition, surface structure, chemical and electronic state of the elements that exist in the outer 6nm surface of a material.

This technique relies on the radiation of the surface employing a monochromatic X-ray beam. When X-ray photons interact with elements in the surface, electrons move to internal energy bands and consequently electrons are emitted. To count the number of electrons during the acquisition of a spectrum, XPS detectors must be operated under ultra-high vacuum conditions. Then, a typical XPS spectrum is a plot of the number of electrons detected versus their binding energy. If both, photon radiation energy and the ejected photo-emitted electron kinetic energy are known, electron binding energy can be calculated. Each element

produces a characteristic set of XPS peaks at characteristic binding energy values that directly identify each element that exists on the surface and their chemical and electronic state.

This technique was used to understand surface features of faceted TiO_2 based materials (Chapter 5) and analyse elemental composition and electronic states of the elements that exist on the surface of these catalysts. This study was carried out on a Lybold-Heraeus LHS-10 spectrometer, working with constant pass energy of 50 eV. The spectrometer main chamber, working at a pressure $<2x10^{-9}$ Torr, is equipped with an EA-200 MCD hemispherical electron analyser with a dual X-ray source working with Al K_α ($h\nu$ = 1486.6 eV) at 120 W and 30 mA. C 1s signal (284.6 eV) was used as internal energy reference in all the experiments. Samples were outgassed in the pre-chamber of the instrument at 150 ºC up to a pressure $<2x10^{-8}$ Torr to remove chemisorbed water.

3.3.10. Scanning Electron Microscope with Energy Dispersive X-ray spectroscopy (SEM-EDX)

Electron Microscope techniques give information about catalysts morphology and textural features of the materials. Specifically, materials can be observed from a nano- (nm) and micro-metric (μm) scale using SEM (Scanning Electron Microscopy) technique[15]. Sample images are produced by scanning the surface with a focused beam of electrons (2-50 kV). These electrons interact with atoms in the sample, producing various signals that contain information about sample´s surface. Back-scattered electrons (BSE) and secondary electrons (SE) emitted by atoms

are detected to produce an image. On one hand, the number of BSE depends on the interaction of the electrons with the atomic nucleus, which gives information about elemental composition. SE electrons are generated from the interaction of incident and back-scattered electrons with other electrons that exist in the outer orbital shell of an atom. Secondary electrons give information about catalyst morphology.

Moreover, Energy Dispersive X-ray spectroscopy (EDS-EDX) can be applied together with Scanning Electron Microscopy (SEM-EDX). This characterization technique is based on the detection of emitted X-ray after the samples have been radiated with a focused beam of electrons. X-ray energy radiation is characteristic of each element. Then, elemental composition can be determined from the wavelength of the emitted radiation (qualitative analysis) and the intensity of each signal (quantitative analysis). Elemental mapping of catalysts can be interestingly achieved to study mixed oxides homogeneity.

X-ray energy-dispersive spectroscopy to obtain the bulk composition and elemental mapping of the catalysts (Chapter 6 and 7) was performed in a JEOL 6300 scanning electron microscope, with an Oxford LINK ISIS detector connected. Samples were dispersed on an adhesive mounted rigidly to a carbon sample holder and afterwards, a thin carbon layer is deposited over them. Images were obtained with a focused beam of electrons (20 kV) and a counting time of 50-100s.

Moreover, Field Emission Scanning Electron Microscopy (FESEM) images of TiO_2-based materials (Chapter 5) were obtained in a Hitachi S-4800 microscope used in secondary electron mode with an acceleration voltage of 2 kV (1-3 nm resolution). Samples were dispersed in ethanol using an ultrasonicator and dropped on a carbon grid without any coating of conductive material.

3.3.11. Transmission Electron Microscopy (TEM) and High-Resolution Transmission Electron Microscopy (HRTEM)

In these cases, the beam of electrons is transmitted through the sample to form an image. This sample is most often an ultrathin section less than 100 nm suspended on a metallic grid. An image is formed from the interaction of the electrons with the sample as the beam is transmitted. TEM image contrast is due to the differential absorption of electrons by different element composition or thickness of the material. Then, the signal is magnified and focused to create the final image. TEM and HRTEM microscopes are capable of imaging at significantly higher resolution than SEM images, owing to the smaller wavelength of electrons (high-energy electron beams >200 keV).

Transmission Electron Microscopy (TEM) images of TiO_2 samples (Chapter 5) were performed in a Philips CM200 instrument. Selected TiO_2 sample was also studied by High-Resolution Transmission Electron Microscopy (HRTEM) from FEI Company (model TECNAI G2 F30 S-twin) with scanning-transmission capabilities (STEM). The measurements were conducted at 300 kV (0.2 nm point resolution). The microscope is equipped with a high angle annular dark field (HAADF)

detector from Fischione Instruments (0.16 nm point resolution). The HR micrograph analysis, lattice spacing, First Fourier Transform (FFT) and phase interpretation, were done with the Gatan Digial Micrograph software (Gatan Inc.) and the Java version of the Electron Microscope Software (JEM).

Moreover, selected area electron diffraction (SAED) and high-resolution transmission electron microscopy (HRTEM) of Nb- and WNb-catalysts (Chapter 6) were performed on a JEOL JEM300F electron microscope working at 300 kV (point resolution of 0.17 nm). Crystal-by-crystal chemical microanalysis was performed in the same microscope by energy-dispersive X-Ray spectroscopy with an ISIS 300 X-ray microanalysis system (Oxford Instruments) with a detector model LING "Pentafet" (resolution 135 eV). Samples for TEM images were ultrasonically dispersed in n-butanol and transferred to carbon coated copper grids.

3.3.12. Thermogravimetric analysis (TG)

A thermogravimetric analysis (TG or TGA) provides information about changes in the mass of a sample when it is measured over time under a controlled environment. A typical thermogravimetric analyser consists in a precision balance, where the sample is placed inside a furnace with a programmable temperature control. The temperature is increased at constant rate under fix atmosphere conditions and changes in the mass of the samples are measured derived from phase transition, absorption, desorption or thermal decomposition processes. In our case, TG

experiments were carried out in a TGA/SDTA851 Mettler Toledo apparatus. 10-20 mg of catalyst were heated to 800 ºC using a heating rate of 10 ºC/min in an air stream (50 mL/min). The data collected is usually displayed into a plot of percentage of initial mass on the y axis versus temperature on the x-axis. The first derivative of the TG curve (DTG curve) is useful to determine inflection points and in-depth differential thermal analysis. In this context, valuable information about catalyst thermal stability, water adsorption and coke deposition on the catalyst surface can be obtained by this characterization technique.

3.3.13. Elemental Analysis (EA)

Elemental analysis (EA) is a process where a sample of catalyst is analysed to determine its content in carbon, hydrogen, nitrogen and sulphur. This method consists in an oxidation process, which is accomplished by a combustion analysis. The sample is instantaneously burned in an excess of oxygen and gas combustion products are in-situ reduced to produce N_2, SO_x, CO_2 and H_2O, which will be separated in a chromatographic column and quantified in a TCD detector. Elemental analysis (EA) was carried out in a Fisons EA1108CHN-S apparatus to determine organic matter deposition (C wt%) on the catalysts after their use in condensation reactions.

3.4 Catalytic tests

Catalytic experiments were performed in a 12 mL autoclave-type reactor with PEEK (polyether-ethyl-ketone) interior, equipped with a magnetic bar, pressure control and a valve for either liquid or gas sample extraction. Reactors were placed over a steel jacket individual support equipped with a temperature close loop control system.

The initial feed for most of the experiments consisted of an aqueous model mixture containing oxygenated compounds representing aqueous waste streams obtained by phase separation after biomass fast pyrolysis processes in a bio-refinery. In these cases, the following aqueous model mixture composition was used: water (30wt%), acetic acid (30wt%), propanal (25wt%), ethanol (10wt%) and acetol (5wt%).

Typically, 3.00 g of aqueous model mixture and 0.15 g of catalyst were introduced in the autoclave-type reactor. The reactor was sealed, heated at 180-200 ºC and pressurized at 13 bar N_2, under continuous stirring (800-1000 rpm). These conditions were selected to maintain all the reactants in the liquid phase at these temperature conditions and to avoid mass transfer limitations.

Based on this initial scenario, a reaction network can be established including the main reaction pathways and products observed along the experiments, which are detailed below:

- 2 molecules of acetic acid can react via ketonization to produce one molecule of acetone and CO_2 and H_2O as only subproducts. Acetic acid can also react with ethanol via esterification to produce ethyl acetate.

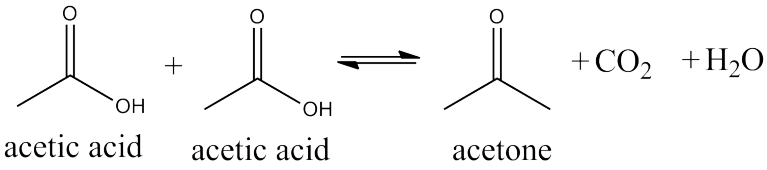

Reaction 3.1. Acetic acid ketonization reaction

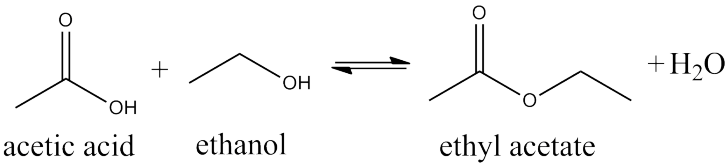

Reaction 3.2. Acetic acid and ethanol esterification reaction

- Acetone, together with propanal and acetol can react via self- or cross- aldol condensation to produce intermediate products as 2-methyl-2-pentenal, mesityl oxide, 3-hexen-2-one, or 2,3-hexanedione. Water is also produced from condensation reactions.

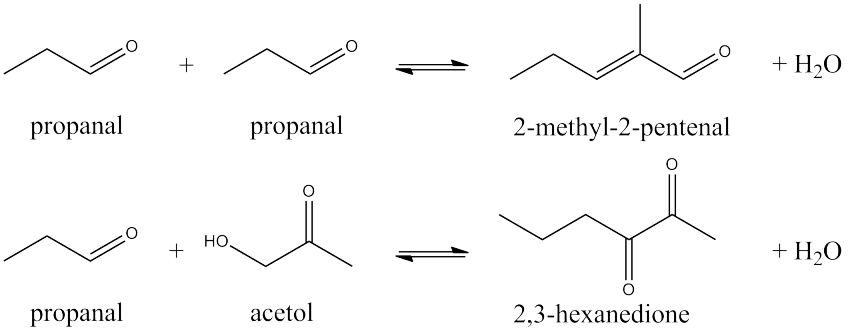

Reaction 3.3. Propanal self- and cross-aldol condensation reaction.

- These intermediate products can keep reacting in a 2nd condensation step to produce larger C_9-C_{10} products. Equimolar amounts of water are likewise generated in these cases.

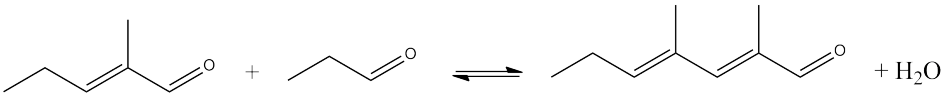

2-methyl-2-pentenal propanal 2,4-dimethyl-2,4-heptadienal

Reaction 3.4. 2nd aldol condensation step reaction.

- Moreover, and due to the mixture complexity (presence of high amounts of water and different functional groups as acids, aldehydes, alcohols and ketones) other reactions can simultaneously occur as alkylations, decarbonylations, and cyclations, among others.

Then, besides first-step condensation products as acetone, 3-pentanone and 2-methyl-2-pentenal, groups of molecules containing from 5 to 10 carbon atom are distinguished and classified in two main groups, namely C_5-C_8 and C_9-C_{10} products, to simplify its quantification.

Taking into account all the above-mentioned reaction pathways, the next reaction network for the overall process is proposed (Figure 3.2).

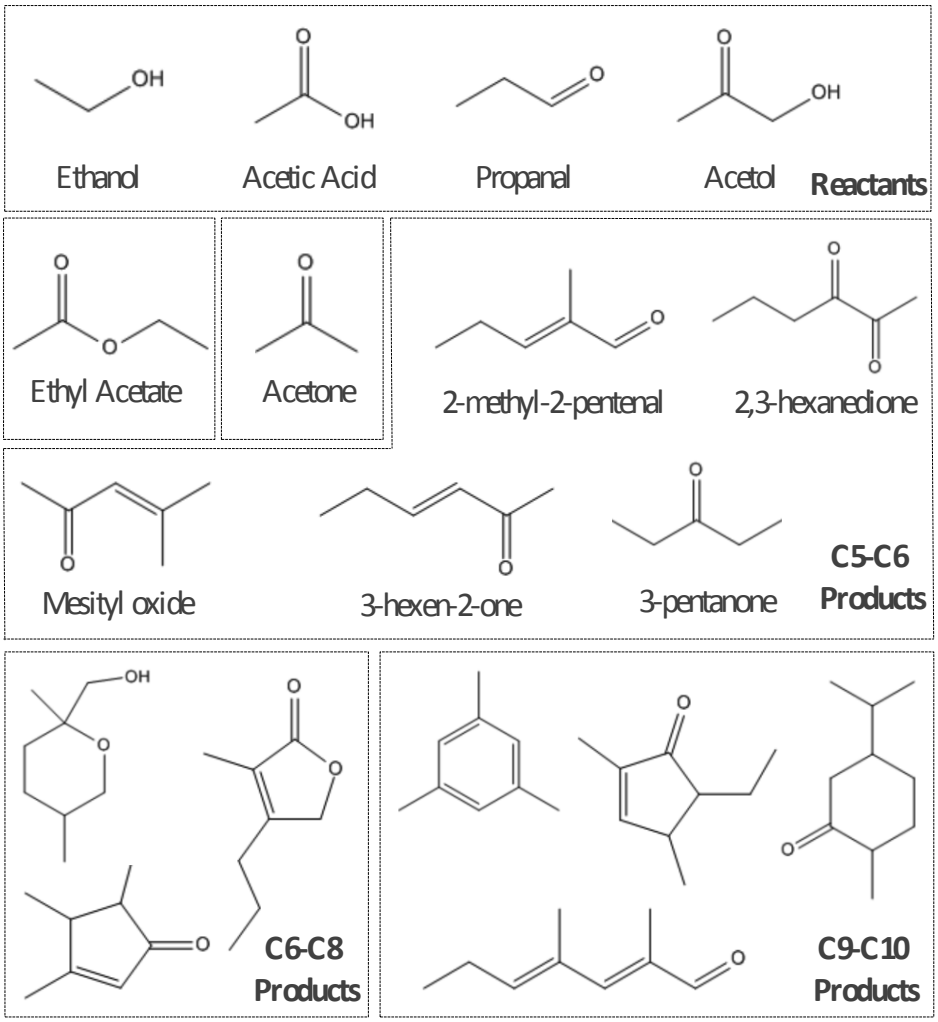

Figure 3.2. General Reaction network: Reactants in the initial aqueous mixture, ethyl acetate (esterification product), acetone (ketonization product) and main condensation products are displayed.

Other reaction mixtures have been studied along this work. On one hand, simpler scenarios as propanal self-condensation, propanal-acetol cross-condensation, non-aqueous mixtures, and carboxylic acid influence on condensation reactions have been employed in order to achieve a better understanding of the reaction network and correlate catalytic activity with catalysts characterization and physicochemical properties. On the other hand, more complex scenarios have been studied: incorporation of heavier compounds (furfural, guaiacol) and more amount of water in the initial mixture to test catalysts stability (Figure 3.3).

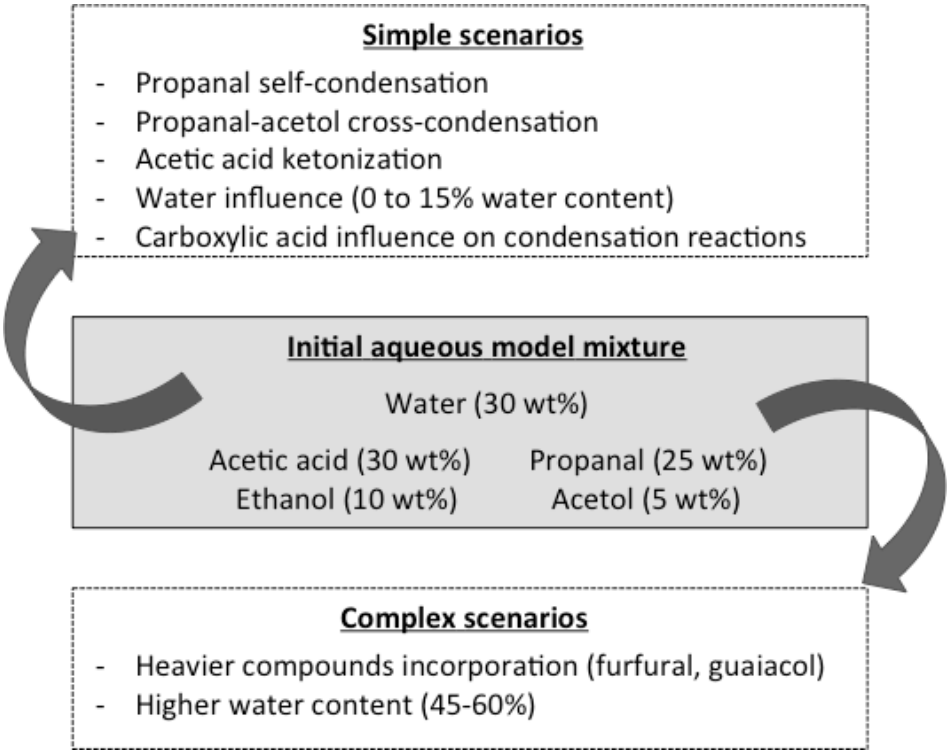

Figure 3.3. "Top-down" and "Bottom-up" scenarios used along this work.

3.5 Reaction mixtures analysis

Gas chromatography (GC) has been used to separate and analyse reactants and products during catalytic tests. In gas chromatography, a known volume of sample is injected into the injector section of the equipment using a micro-syringe installed in an autosampler. This sample is vaporized together with a carrier gas (in our case, N_2 was used as unreactive gas) that forms the mobile phase, which enters into the capillary column. The gaseous compounds interact with the walls of the column, which is coated with the stationary phase. The capillary column is placed inside an oven, where temperature can be modified. These factors cause the compounds to elute at different times (retention time) and finally, as they exit the end of the column, they are detected by means of detector device, which finally produces a registrable electronic signal.

In this work, small liquid aliquots (50-100 μL) were taken at different time intervals (0.5 to 7h) during catalytic tests, filtered off and diluted in 0.5 g of methanol solution containing 2wt% chlorobenzene as external standard. These liquid samples were analysed by a Bruker 430 GC equipped with both a flame ionization detector (FID detector) and a capillary column (TRB-624, 60 m length).

Reactants and intermediate products are quantified from response factors, which are calculated by the use of chlorobenzene as standard, while long-chain products are classified in intervals (C_5-C_8 and C_9-C_{10} products) and group contribution technique was previously used to predict their response factors. In this context, Figure 3.4 shows chemical products used to individually estimate the response factor of reaction C_5-C_{10} products.

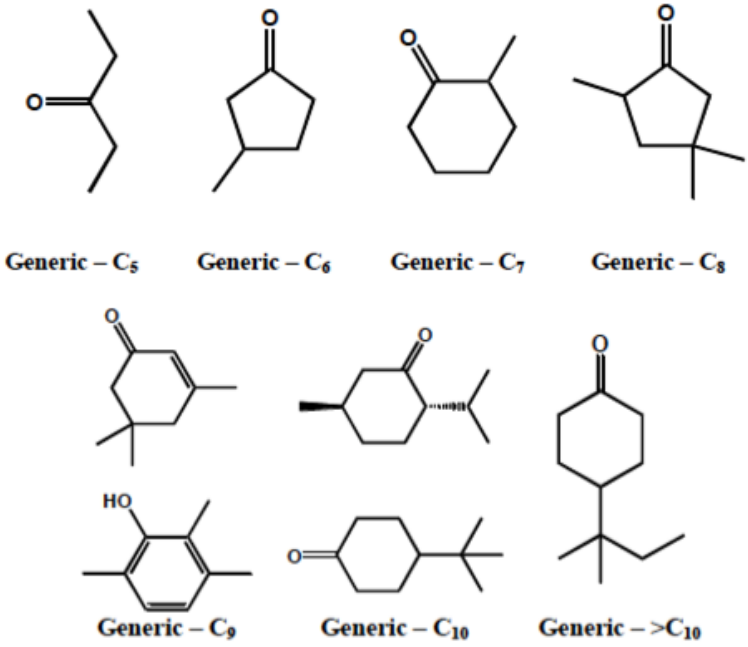

Figure 3.4. Representative molecules used for the response factor estimation of C_5-C_8 and C_9-C_{10} products.

Figure 3.5 shows examples of chromatograms achieved in the GC equipped with a TRB-624 capillary column and a FID detector for the initial aqueous model mixture (0h) and a reaction sample taken at 5h.

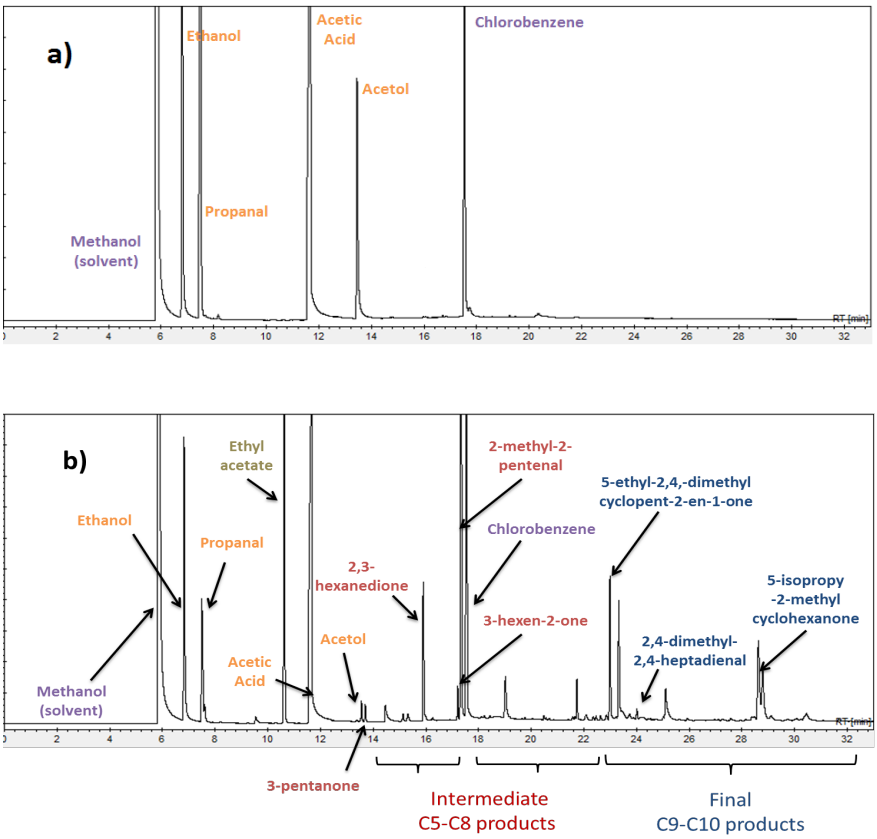

Figure 3.5. Chromatograms obtained by GC-FID with a capillary column (TRB-624, 60 m length). a) Sample at 0h and b) Sample at 5h.

Product identification was done by gas chromatography-mass spectrometry (GC-MS) in an Agilent 6890 N GC System coupled with an Agilent 5973 N mass detector and equipped with a HP-5 MS, 30 m length capillary column.

Catalytic results along this work are discussed in terms of reactant conversion and main reaction products yield. In this context, the following formulas have been used:

- Reaction 3.5: Reactant conversion (mol%) is calculated as:

$$Conversion\ (mol\%) = \frac{(Reactant_x\ initial\ moles - Reactant_x\ final\ moles)}{Reactant_x\ initial\ moles} * 100$$

- Reaction 3.6: Main product yields (wt%) are calculated as:

$$Product_y\ yield\ (wt\%) = \frac{Mass\ of\ Product_y\ in\ the\ reactor}{Total\ mass\ in\ the\ reactor} * 100$$

- Reaction 3.7: Total organic product yield (wt%) is calculated as:

$$Total\ products\ \ yield\ (wt\%) = Yield_{2-methyl-2-pentenal} + Yield_{C5-C8} + Yield_{C9-C10}$$

Based on the aqueous model mixture composition, a theoretical maximum attainable total organic yield can be calculated, assuming that:

- 100% conversion for all reactants is achieved.
- Acetic acid can be equally converted to ethyl acetate and acetone (ketonization product).
- Final products are C_9 compounds (no intermediate or heavier products are present in the final mixture).

Taking into account these ideal assumptions, the composition of the final mixture is calculated as 51.3wt% of water, 19.1wt% of ethyl acetate, and 29.6wt% of organic products. Therefore, results of catalytic experiments (expressed as main product and total organic product yields) are calculated by considering that ≈30% is the maximum attainable value.

Example:

Total organic products yield measured during reaction = 20.0wt%

Maximum total organic products yield attainable = 30.0wt%

Calculated total organic products yield (referred to maximum)=66.7wt%

When other simpler or complex scenarios were studied (Figure 3.3), an analogous calculation was performed. Then, all catalytic results are always expressed considering the maximum attainable product yield for each experiment. High reactants conversion and condensation products yield drive to these heavier products to spontaneously form an upper-phase (Figure 3.6), which reduce further separation and process costs. In this sense, additional characterization of this organic phase was performed to study its possible application.

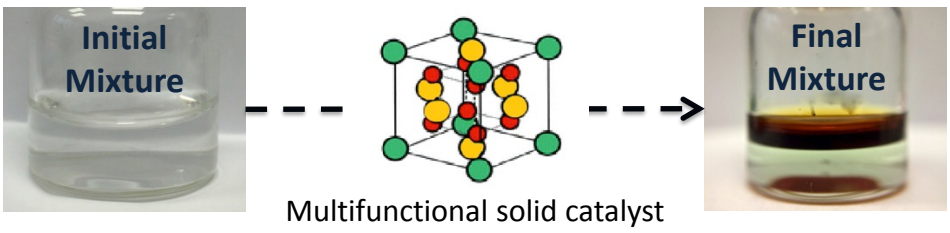

Figure 3.6. Products spontaneous separation from aqueous-phase after the use of active multifunctional solid catalysts.

First of all, partition coefficients (distribution coefficients) were calculated as the ratio of concentration of reactants and products in the mixture of the two immiscible phases (aqueous phase and organic phase). This ratio is a measure of the solubility of the compounds in these two phases. These calculations were performed from gas chromatography analysis of both phases in the Bruker 430 GC equipped with both a FID detector and a capillary column (TRB-624, 60 m length).

Moreover, organic phase was analysed by bi-dimensional gas chromatography (GCxGC) in a 7890 Agilent GC equipped with a HP-INNOWAX column (30 m) and followed by a DB-5 column (5 m) coupled with a FID detector. This technique follows the same fundamentals than common gas chromatography, but the use of two different columns allows separating products in two dimensions, based on their properties (boiling point and polarity).

Organic phase was also analysed by simulated distillation. This technique is a gas chromatography method to control products derived from petroleum refining processes. Samples are analysed in a GC equipped with a non-polar column, where products are separated by their boiling point differences and compared to standard samples assembling oil cuts in a refinery. The aim of this method is to check the similarities among the organic phase obtained and the possibility of blending with different petroleum fractions. These analyses were performed in a Bruker 450 GC equipped with an Agilent J&W GC Columns CP-SimDist (10 m) and ASTM D2887 - Extended 2887 methodologies were followed.

Finally, catalysts stability tests during this work have been one the most relevant field of study. Recycling experiments were performed by using (or reusing) the catalysts several times. Once the catalytic experiment was finished, the solid was separated by centrifugation and washed repeatedly with methanol. Finally, after drying it at 100 ºC overnight, the solid was used again in the condensation of light oxygenates under the same temperature and pressure conditions.

3.6 References

1. Corma, A., Fornés, V. & Rey, F. *J. Catalysis* **148,** 205–212 (1994).
2. Serrano-Ruiz, J.C., Luettich, J., Sepúlveda-Escribano, A. & Rodríguez-Reinoso, F. *J. Catalysis* **241,** 45–55 (2006).
3. Lara, M.A., Sayagués, M.J., Navío, J.A. & Hidalgo, M.C. *J. Mater. Sci.* **53,** 435–446 (2018).
4. Fassel, V.A. & Kniseley, R.N. *Anal. Chem.* **46,** 1110A–1120A (1974).
5. Jenkins, R. *Handbook of Analytical Tech.* 76–82 (1981).
6. Gregory, N.W. *J. Am. Chem. Soc.* **79,** 1773–1774 (1957).
7. Holzwarth, U. & Gibson, N. *Nature Nanotechnology* **6,** 534 (2011).
8. Jestel, N.L. *Process Anal. Technol.* 195–243 (2010).
9. Wachs, I.E. *Catal. Today* **100,** 79–94 (2005).
10. Brunauer, S., Emmett, P.H. & Teller, E. *J. Am. Chem. Soc.* **60,** 309–319 (1938).
11. Donohue, M. & Aranovich, G. *Adv. Coll. Interf. Sci.* **76–77,** 137–152 (1998).
12. Emeis, C.A. *J. Catalysis* **141,** 347–354 (1993).
13. Kapustin, G. ., Brueva, T.R., Klyachko, A.L., Beran, S. & Wichterlova, B. *Appl. Catalysis* **42,** 239–246 (1988).
14. Bubert, H., Rivière, J.C. & Werner, W.S.M. *X-Ray Photoelectron Spectroscopy (XPS)*. *Surface and Thin Film Analysis* (2011).
15. Zhou, W., Apkarian, R., Wang, Z.L. & Joy, D. *Scanning Microscopy for Nanotechnology: Techniques and Applications* 1–40 (2007).

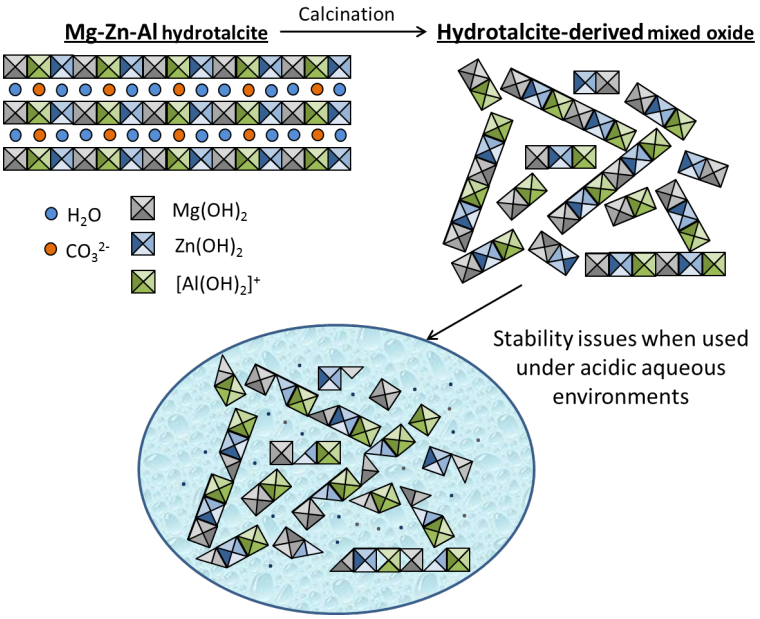

CHAPTER 4

CERIA-ZIRCONIA AND HYDROTALCITE-DERIVED MIXED OXIDES AS ACID CATALYSTS FOR THE AQUEOUS-PHASE CONDENSATION OF OXYGENATED COMPOUNDS

4.1 Introduction

A catalyst is a substance that enables a chemical reaction to proceed at higher rates, without being consumed or altered during this process. Catalysis plays a fundamental role in chemical processes as activation barriers are diminished, while desired products selectivity is maximized. Thus, fewer amounts of sub-products are generated during these less energy-demanding activities[1].

Heterogeneous catalysts are preferred as there is little difficulty in separating and recycling these materials compared to traditional homogeneous catalysts. In this way, further neutralization and separation steps are avoided, so processes costs and complexity are reduced. On the other hand, the main disadvantage is that a lower effective concentration of catalyst is present when heterogeneous catalysts are employed, since the reaction only takes place on the exposed active sites on the pores and surface of the material. In this sense, traditionally, expensive heterogeneous active phases have been supported over abundant and cheap materials such as TiO_2, SiO_2 or Al_2O_3 in order to facilitate the exposition of these active sites. Zeolites (microporous aluminosilicate materials) with large surface areas and various pores sizes have arisen as highly efficient acid solid catalysts in many chemical reactions.

Several zeolites have been studied in different bio-oils upgrading strategies like vapour upgrading, HDO or esterification processes.

Unfortunately, special properties of biomass derivatives and especially of bio-oils have been largely discussed during Chapter 1. The presence of water and a wide range of highly oxygenated organic compounds (i.e. acids, aldehydes, ketones, alcohols, etc.) makes difficult to valorise these bio-oils, and more specifically the aqueous fractions derived from them. These complex characteristics make necessary to design new catalysts, which meet these new process requirements. In this sense, metal and mixed metal oxides emerge as an alternative with numerous advantages compared to traditional supports and zeolite materials.

Metal oxides are ionic solids with a structure conformed by metallic cations (M^{n+}) and oxygen anions (O^{2-}). Metal and mixed metal oxides have been found to present versatile applications in organic synthesis including important C-C bond forming reactions[2]. One of the main characteristics to take into account when dealing with metal oxides is the metal´s electronegativity. Electronegativity is a chemical property that describes the tendency of an atom to attract a shared pair of electrons (or electron density) towards itself. Then, in more electropositive metals, electrons are more attracted to the oxygen atom, as ionic species are well defined. These metals drive to more ionic bonds and correspond to more basic metal oxides, such as MgO. On the other hand, transition metals would normally lead to more amphoteric and acid metal oxides.

Both, metallic cations and oxygen anions on the surface can work as active centres for chemical reactions. In particular, metallic cations can act as electron acceptors (Lewis acid sites), whereas O^{2-} anions can either share a pair of electrons with electrophilic species, (Lewis basic sites) or

act as proton acceptors (Brönsted basic sites). All this active centres are on the surface, which is not completely regular. Figure 4.1 shows a representative scheme of a monometallic or mixed metallic oxide surface structure, where corners, edges, steps and terraces can be found. Then, ions coordination can change depending on the position in the surface. These defects and specific surfaces can drive to different coordination states, which directly affect to active sites characteristics and catalytic properties of these materials. For instance, ions coordination is related to the strength of acid/base sites. Then, stronger acid/basic sites will be found on more isolated (less coordinated) ions in edges, corners and terraces, in this order. The effective understanding of the amount and strength of acid and base active sites is crucial for the design of catalysts for these new applications.

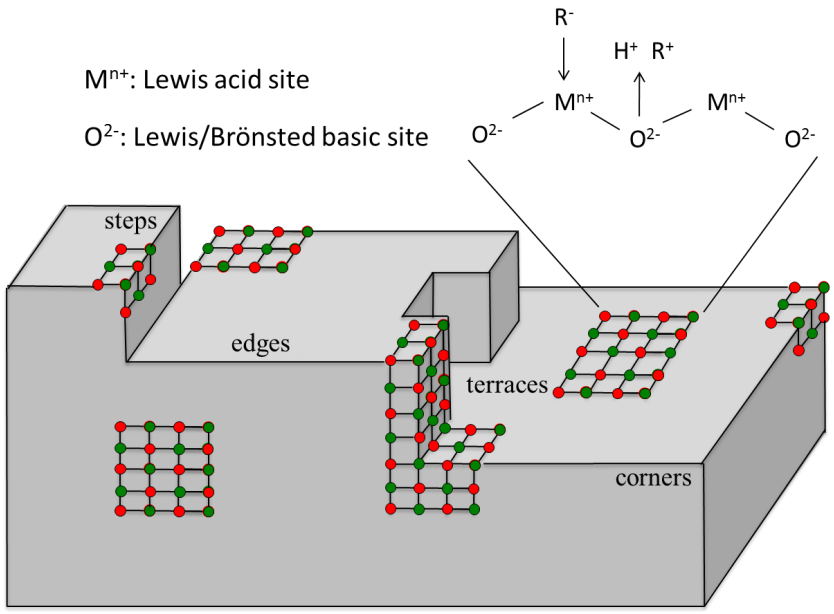

Figure 4.1. Structure and acid-base characteristics of monometallic and mixed metallic oxides.

Once surface structure and active sites characteristics have been discussed, major advantages of mixed metal oxides compared to zeolites for bio-oil (and mainly aqueous fractions derived from bio-oil) upgrading processes should be highlighted. First of all, mixed metal oxides can be easily synthesized in broad range of chemical composition via cheap and easy scale-up processes such as co-precipitation, sol-gel or hydrothermal methods (see Section 3.2). These procedures can drive to metal oxides with high surface areas and controlled acid-base sites characteristics. In particular, moderated density and strength of acid sites is desired for bio-oils upgrading strategies due to the presence of more reactive highly functionalised compounds.

On one hand, zeolites active sites mainly correspond to strong Brönsted acid centres located inside the pores of the materials, whereas Lewis acid centres are usually related to extra-red aluminium species. Zeolites microporous structure can induce internal mass transfer limitations and stability issues by poisoning and pore blocking by coke deposition. Moreover, most of aluminium species responsible for acid characteristics are not stable under hydrothermal and/or acidic conditions, so Si/Al composition limitations may exist when dealing with biomass-derived aqueous mixtures.

On the other hand, and in spite of metal oxides usually have lower surface areas, more interesting intermediate acid-base characteristics can be achieved. Additionally, internal mass transfer limitation is not a problem as most of the metal oxides have negligible microporous structure. Then, metal oxides may be active and more stable solid catalysts for biomass valorisation procedures, mainly when aqueous fractions are involved.

Therefore, the design of metal and mixed metal oxides with the right density and strength of acid-base sites on the surface can drive to potential effective catalysts in C-C bond formation reactions (i.e. ketonization, aldol condensation, among others) for the valorisation of aqueous streams derived from bio-oils production processes in bio-refineries.

4.2 $Ce_xZr_{1-x}O_2$ mixed oxides as reference materials

In this sense, CeO_2, ZrO_2 and $Ce_xZr_{1-x}O_2$ have been extensively studied as efficient catalysts for the valorisation of bio-oil individual compounds and bio-oil fractions or mixtures mainly via ketonization and aldol condensation reactions.

On one hand, CeO_2 is a rare-earth metal oxide that adopts fluorite structure containing 8-coordinate Ce^{4+} and 4-coordinate O^{2-} anions, whereas hexagonal phase, with 7-coordinate Ce^{3+} cations, is the most stable structure for reduced cerium oxide, Ce_2O_3. However, it is well known that fluorite structure is the most stable crystalline phase, where interestingly oxygen vacancies are created and distributed depending on the synthesis procedure, oxide particle size and temperature treatment conditions. These oxygen vacancies confer cerium cations different coordination states, which make this material easily reducible. These redox properties, including cerium varying oxidation and coordination state on the catalytic surface, have grown special interest for its industrial application in diverse processes such as: removal of organic pollutants, hydrocarbon reforming, CO oxidation and methanol production from syngas.

There are several studies that show how CeO_2 reducibility and the high oxygen mobility in the oxide lattice favours the dissociative adsorption of H_2O molecules and light oxygenated compounds. Focused on this last question, CeO_2 has been widely studied in the ketonization of light carboxylic acids as an interesting strategy to upgrade bio-renewable compounds. In particular, most of the research has focused on acetic acid and propionic acid ketonization reactions, as these C_1-C_3 acids are one of the main components in bio-oils from biomass pyrolysis processes. CeO_2, CeO_2/Al_2O_3 and $CeMO_x$ (M: Mg, Mn, Fe, etc.) have been studied for the gas-phase ketonization of acetic and propanoic acid in fix-bed reactors under high temperature conditions (300-400 ºC)[3–7].

On the other hand, ZrO_2 has interesting properties for its application as support or catalyst by itself due to the presence of numerous weak acid and base sites. Then, its bifunctional character and its high stability under thermal conditions and reducing atmospheres make this material suitable for diverse applications such as MTO processes, hydrogenation, dehydration and C-C bond formation reactions as ketonization and aldol condensation of alcohols, aldehydes and carboxylic acids. In this sense, the weak sites promote desired product selectivity and reduce catalyst deactivation by coke deposition, which mostly occur over strong acid and basic sites.

Different zirconium oxides polymorphs can be found including cubic, tetragonal, monoclinic and orthorhombic crystalline phases depending on temperature. Cubic phase has a fluorite-type structure stable above 2370 ºC, tetragonal phase is stable between 1150 and 2370 ºC and finally,

monoclinic phase is stable under 850 ºC. It should be highlighted that monoclinic and tetragonal phases can be stabilized at ambient temperature conditions by doping other agents as Y, Mg or Ca. Then, monoclinic (m-ZrO_2) and tetragonal (t-ZrO_2) phases are the most studied polymorphs of zirconium dioxide.

More interestingly, many studies have shown how the introduction of zirconium atoms in the fluorite-type structure of CeO_2 can drive to $Ce_xZr_{1-x}O_2$ mixed oxides, where surface properties are enhanced. In particular, Zr can promote oxygen movility in $Ce_xZr_{1-x}O_2$ mixed oxides, increasing the formation of intermediate enolate and carboxylate species on the surface. Its bifunctional character has turned this material into a reference catalyst in ketonization and aldol condensation reactions for bio-oils valorisation processes.

In this sense, $Ce_xZr_{1-x}O_2$ (x: 0 to 100) mixed oxides have been tested in the ketonization of individual carboxylic acids as acetic acid and propionic acid under high temperature conditions. $Ce_xZr_{1-x}O_2$ has also been studied in the aldol condensation of small aldehydes (propanal) under high temperatures (300-400 ºC)[8]. This particular research showed that cerium atoms favour ketonization reactions, whereas Zr favours aldol condensation reaction. Then, if both processes are performed in one-pot, equilibrium in the catalyst composition must be found. This study also showed the inhibitory effect of H_2O and carboxylic acids on aldol condensation reactions.

Additionally, these materials have been studied in scenarios that are more realistic; using model compounds mixtures representative of bio-oils composition. Some examples are hexanoic acid, pentanol and 2-butanone mixtures used by C. Gaertner et al.[9,10], or acetic acid, acetol and furfural mixtures used by S. Hakim et al[11]. Both studies are performed in fix bed reactors under 250-350 ºC and confirm the complexity of treating mixtures of compounds with different functional groups and the inhibitory effect of H_2O and CO_2 on ketonization and condensation reactions equilibrium.

Then, as starting point for this work, different $Ce_xZr_{1-x}O_2$ were synthesized assembling those commonly used in literature in this type of reactions. Their catalytic activity in the condensation of aqueous mixtures containing: 30wt% H_2O, 30wt% acetic acid, 25wt% propanal, 10wt% ethanol and 5wt% acetol (See Section 3.4) will be used as reference data for the rest of this work. The catalysts were prepared through co-precipitation synthesis, following the methodology described in literature[12]. Aqueous solutions of $Ce(NO_3)_3.6H_2O$ and $ZrO(NO_3)_2.H_2O$ were used to obtain solids with the desired Ce-Zr ratio, by using a 28wt% NH_4OH aqueous solution as precipitating agent (See section 3.2.4). The attained solids were separated by filtration, and washed with distilled water. Finally, the catalysts were dried at 100 ºC overnight and heat-treated in air at 450 ºC during 2h. The actual bulk CeO_2 and ZrO_2 content was determined by X-ray fluorescence and textural properties by N_2 adsorption isotherms (Table 4.1). Commercial ZrO_2 (from Chempur) and CeO_2 (from Sigma Aldrich) were also tested under the same reaction conditions.

Table 4.1. Main physicochemical and textural properties of $Ce_xZr_{1-x}O_2$ mixed oxides

Composition[a]	Ce	1.00	0.69	0.55	0.28	0.00
	Zr	0.00	0.31	0.45	0.72	1.00
Surface Area (m^2/g)[b]		22	98	112	109	138
Pore volume (cm^3/g)[b]		0.15	0.14	0.09	0.24	0.20

[a] Measured by XRF; [b] Calculated from N_2 adsorption isotherms (BET method and BJH method, respectively).

Catalytic results of $Ce_xZr_{1-x}O_2$ materials in the consecutive condensation of oxygenated compounds in aqueous mixture are shown in Table 4.2 and Figure 4.2. Results are discussed in terms of oxygenated compounds conversion and yield to main reaction products: ethyl acetate, 2-methyl-2-pentenal, C_5-C_8 and C_9-C_{10} products (See Section 3.4).

Table 4.2. Catalytic results of $Ce_xZr_{1-x}O_2$ materials in the consecutive condensation of oxygenated compounds in aqueous mixture.

Catalyst		Zr	1.00[a]	0.72	0.45	0.31	0.00
		Ce	0.00	0.28	0.55	0.69	1.00[b]
Conversion (%)		Acetic acid	7.9	14.0	17.2	43.3	54.7
		Propanal	63.7	78.5	85.2	90.2	91.7
		Ethanol	50.8	44.6	42.2	52.3	47.4
		Acetol	100.0	100.0	100.0	100.0	100.0
Product Yield (%)		Ethyl acetate	23.3	18.5	20.7	15.6	17.6
		2M2P[c]	18.9	29.3	40.1	28.0	34.0
		C5-C8	9.5	16.4	6.7	14.3	5.5
		C9-C10	8.5	15.8	24.1	18.7	16.5
		Total	**36.9**	**61.7**	**70.9**	**61.0**	**56.0**
Carbon balance (%)			86.2	89.3	98.3	74.3	72.5

Reaction conditions: 3 g of aqueous mixture, 150 mg of catalyst; T=200 ºC, P=13 bar N_2, t= 3h. [a]Tetragonal ZrO_2 (Chempur); [b]CeO_2 (Sigma Aldrich); [c]2M2P= 2-methyl-2-pentenal

Table 4.2 shows the variation of the conversion of each reactant in the aqueous model mixture as a function of Ce/(Ce+Zr) atomic ratio achieved at 200 ºC and a time of stream of 3h. The main differences along all the series are observed for both propanal and acetic acid conversion, whereas the conversion of acetol (100%) and ethanol (45-52%) is similar regardless of Ce-content in these catalysts. In this way, commercial t-ZrO_2 displays the lowest propanal and acetic acid conversion, which progressively increase with Ce-content in the catalyst.

However, this conversion enhancement does not drive to a concomitant increment in the selectivity to 2-methyl-2-pentenal (2M2P) via self-aldol condensation of propanal. A maximum yield of 2M2P is observed when balanced atomic ratio is achieved ($Ce_{0.55}Zr_{0.45}O_2$), whereas higher amounts of Ce, and commercial CeO_2 drive to lower amounts of desired products. Selectivity to C_9-C_{10} products shows the same trend, since they are formed mainly via aldol condensation of C_5-C_8 fractions with smaller molecules. Consequently, the selectivity to C_5-C_8 oxygenates decreases when C_9-C_{10} products are maximized, since second condensation reactions are favoured. This product distribution profile can easily be observed in Figure 4.2.

In this context, the performance of $Ce_xZr_{1-x}O_2$ mixed oxides can be interpreted considering the Ce atomic ratio role in catalytic activity and stability for these materials. On one hand, t-ZrO_2 and low Ce-content catalysts ($Ce_{0.28}Zr_{0.72}O_2$) lead to low acetic acid and propanal conversion. Additionally, carbon balances were observed to be peculiarly low (86-89%) for both catalysts, this behaviour possibly explained by the interaction of oxygenated compounds with hydroxylated acid sites on

abundant Zr centres on the surface of the material. On the other hand, high Ce-content ($Ce_{0.69}Zr_{0.31}O_2$) materials and commercial CeO_2 drive to higher propanal conversions (90-92%) and excellent acetic acid conversions (43-55%). Unfortunately, acetic acid is not being converted into acetone via ketonization, but forming cerium acetate species by metal carboxylate formation. Then, acetic acid drives to the partial or total dissolution of the catalyst crystalline phase by Ce species decomposition.

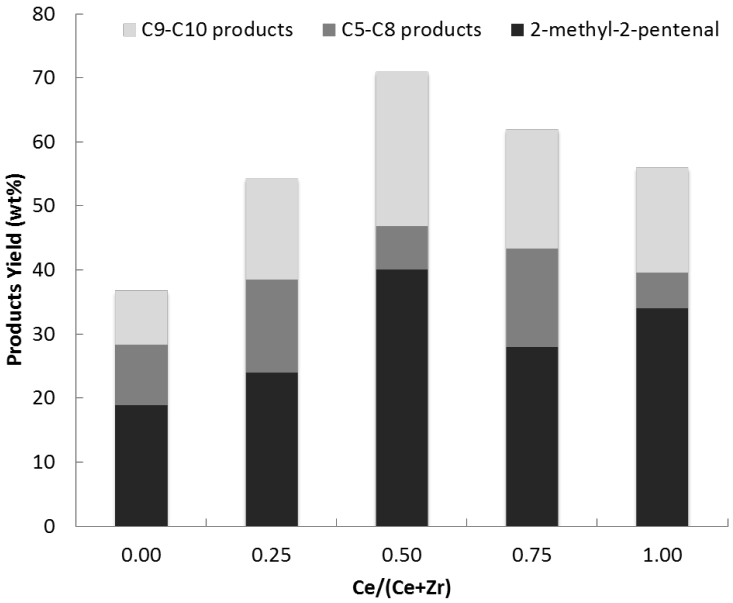

Figure 4.2. Catalytic results of $Ce_xZr_{1-x}O_2$ materials in the condensation of oxygenated compounds in an aqueous model mixture (at 200 ºC, P_{N2}=13 bar during 3h).

This aspect matches previous reports about $CeMO_x$ catalysts stability in the condensed phase. In spite of CeO_2 oxide has a relatively high lattice energy (9627 KJ/mol), CeO_2 has been claimed to act via two different pathways on ketonization reaction depending on temperature

conditions. “Surface” carboxylic acid ketonization will occur under high temperature conditions (>300 ºC), whereas “bulk” ketonization (cerium acetate formation and further catalyst decomposition) takes place when temperature is below 200 ºC[4,6]. Therefore, it seems that balanced Ce-Zr atomic ratio drives to maximum product yields and carbon balances in these reaction conditions, although its stability should be studied.

In this way, $Ce_{0.55}Zr_{0.45}O_2$ catalyst was selected as the reference material for this work, being this solid characterized in detail. Pyridine adsorption FT-IR measurements and NH_3-TPD/CO_2-TPD experiments were performed to quantify total acid and basic sites.

XRD pattern of co-precipitated $Ce_{0.55}Zr_{0.45}O_2$ mixed oxide is depicted in Figure 4.3. This solid presents characteristics Bragg peaks of the fluorite-type cubic structure derived from CeO_2 crystalline structure, although additional small signals corresponding to the presence of t-ZrO_2 phase are also observed. Textural properties of this material were studied by means of N_2 adsorption isotherms (BET method), showing a solid with a surface area of 112 m^2/g, value in a typical range for these materials[12].

Finally, acid and basic properties for this catalyst were also elucidated and shown in Table 4.3. NH_3 and CO_2 temperature programmed desorption experiments showed an interesting balanced amount of acid (194.4 $\mu mol_{NH3}/g$) and basic sites (208.9 $\mu mol_{CO2}/g$) on the catalyst surface. Pyridine adsorption FT-IR measurements were performed to further understand the nature of the acid sites in this material. This experiment shows a higher presence of Lewis acid sites (87.6 μmol/g) compared to a lower amount of Brönsted acid sites (17.4 μmol/g).

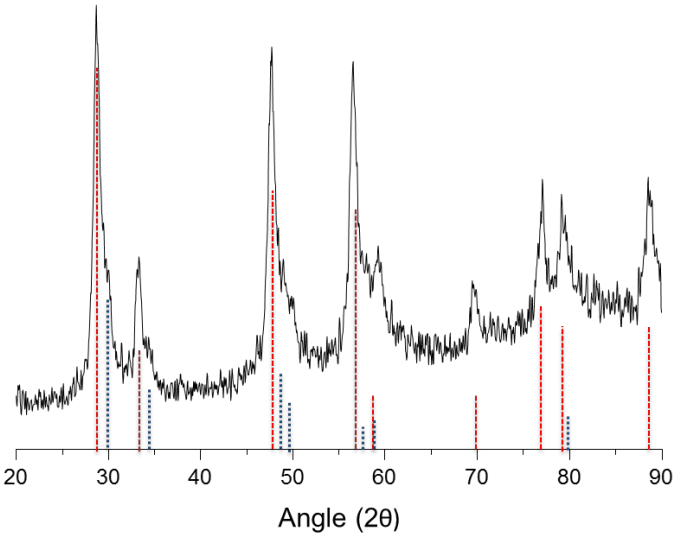

Figure 4.3. XRD pattern of $Ce_{0.55}Zr_{0.45}O_2$ mixed oxide. $Ce_{0.55}Zr_{0.45}O_2$ cubic structure derived from CeO_2 cubic crystalline structure is indicated by red lines, whereas blue lines indicate the presence of t-ZrO_2 structure.

Table 4.3. Main physicochemical properties of $Ce_{0.55}Zr_{0.45}O_2$ oxide.

Composition[a]		Surface area (m^2/g)[b]	Acid sites[c] ($\mu mol_{PY}/g$)		Total acid sites[d] ($\mu mol_{NH3}/g$)	Total basic sites[d] ($\mu mol_{CO2}/g$)
Ce (%)	Zr (%)		Lewis	Brönsted		
55	45	112	87.6	17.4	194.4	208.9

[a] Atomic ratio measured by X-Ray Fluorescence; [b] Calculated from N_2 adsorption isotherms (BET method); [c] Values were calculated by pyridine adsorption FT-IR measurements; [d] Total acid and basic sites were calculated from NH_3-TPD and CO_2-TPD experiments, respectively.

Therefore, the activity of this catalyst is based on its acid/base bifunctional character, although its stability under realistic operation conditions (mainly due to Ce leaching) will be studied under consecutive reuses (see Section 4.4.4), as it is a critical factor to be further improved.

4.3 Hydrotalcite-derived mixed oxides

4.3.1 Hydrotalcite-derived mixed oxides characteristics

Hydrotalcites (HTs) are layered double hydroxides (LDH) that have the general formula $[M^{2+}_{x}M^{3+}_{y}(OH)_{2(x+y)}][A^{n-}_{y/x}.mH_2O]$, where M^{2+} and M^{3+} correspond to metal components with divalent and trivalent cations, respectively, and A^{n-} is an intercalated anion. Magnesium is the most common divalent metal component, although other metal species such as Co, Cu, Ni, Ca, Zn and Mn are possible. On the other hand, aluminium is usually the trivalent metal component, although Fe, Cr and Ga can also be employed. These compounds belong to a class of anionic clay minerals, which structurally are formed by brucite-like $Mg(OH)_2$ sheets. Octahedra of Mg^{2+} (6-fold coordinated to OH^-) share edges to form a layered structure. These sheets are held together by hydrogen bondings.

When isomorphous substitution of Mg^{2+} by a trivalent cation like Al^{3+} occurs, a positive charge is generated in the hydroxyl sheet. This excessive positive charge leads to available anions, such as CO_3^{2-}, NO_3^-, Cl^- and OH^- to be located in the interlayer to compensate this charge. In the free space of the interlayer, water from crystallization also finds a place (Figure 4.4)[13,14].

When these materials are air-treated over 450 ºC, H_2O, CO_3^{2-} and NO_3^- anions are evolved, and a hydrotalcite-derived mixed oxide is formed from the hydrotalcite layered structure decomposition. These materials present a particular characteristic that is “memory effect”: When they are exposed to water environments a hydrotalcite phase reconstruction via

rehydration takes place. The reversion of the mixed oxide to hydrotalcite upon contact with water vapour is complete and very fast at room temperature. Many authors have used this "memory effect" of hydrotalcites for improving the catalytic activity of these materials in diverse applications[15].

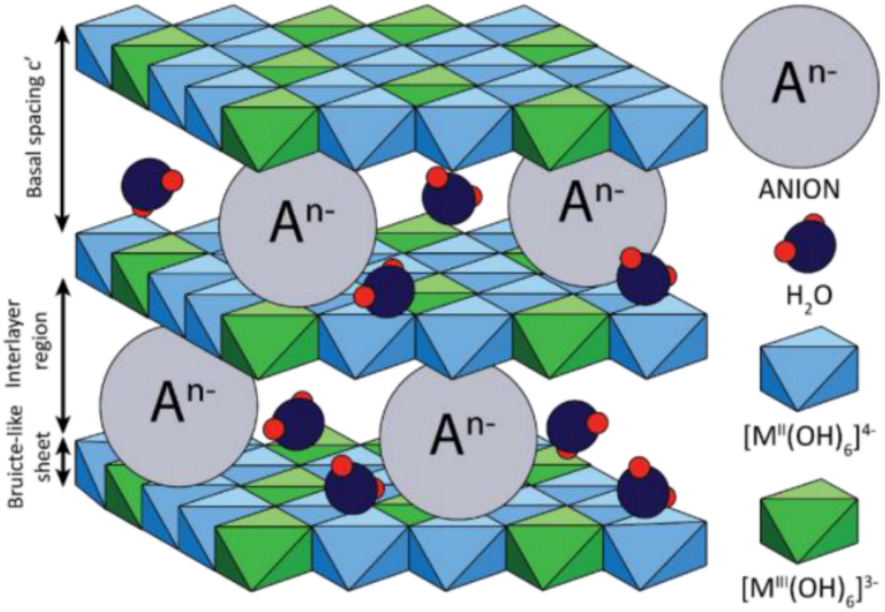

Figure 4.4. Representative scheme of a hydrotalcite structure from R. Debek et al[14].

Then, hydrotalcite-derived mixed oxides have gained increasing attention in the design of new environmentally friendly catalysts due to their high surface area, acid-base properties, as well as because they can be easily and cheaply synthesized. These materials can be synthesized in a wide range of composition via simple co-precipitation procedures, having many possible metal components highly dispersed promoting complex bifunctional reactions. In particular, synthesis conditions such as temperature, pH or metal composition have been widely studied as

they can modify HTs properties, including particle size, surface area and more importantly acid and base properties of the mixed oxides. In this sense, acid-base properties of Mg-Al mixed oxides strongly depend on the chemical composition and synthesis procedures. For instance, the number of active sites can be tuned by modifying the surface area of the material, whereas changing the number of defects in the framework can control the strength of those centres.

These unique properties have meant HTs to have a wide range of applications including anion exchangers, absorbing agents, stabilizer and especially in catalysis. These calcined and rehydrated Mg-Al hydrotalcites have found numerous applications as basic catalysts in organic reactions such as aldol condensation[16,17], Knoevenagel and Claisen-Schmidt condensations[18], Michael addition, alkylation[19], olefin epoxidation, among others.

In this way, hydrotalcite-derived mixed oxides have also been studied in aldol condensation and ketonization reactions as important C-C bond formation reactions to valorise biomass-derived oxygenated compounds.

Different Mg-Al hydrotalcite-derived mixed oxides have been employed in the condensation reaction of biomass derivatives such as furfural, HMF, propanal, ethanol and acetone[20–23]. Others authors have reported the use of Mg/Al and Zn/Al mixed oxides for acetic acid ketonization under high temperature conditions (300-400 ºC)[24,25].

In all these cases, the catalytic performance of hydrotalcite-derived mixed oxides is explained in terms of structural features and specific bifunctional (acid-base) characteristics of the materials. Nevertheless,

studies concerning the transformation of these light oxygenates under more realistic scenarios (acid complex aqueous mixtures) are unavailable. In this sense, it would be interesting to test the activity and stability of these catalytic systems under highly demanding conditions to understand whether they could be implemented.

4.3.2 HT-Mg/Al and HT-Zn/Al hydrotalcite-derived mixed oxides

Different series of HT-Mg/Al and HT-Zn/Al were synthesized to study their catalytic activity in the condensation of aqueous mixtures containing: 30wt% H_2O, 30wt% acetic acid, 25wt% propanal, 10wt% ethanol and 5wt% acetol (See Section 3.4).

The catalysts were prepared through co-precipitation synthesis, following the methodology described in literature[26]. Gels were achieved by mixing (via slowly addition) two aqueous solutions: A) containing $Al(NO_3)_3.9H_2O$, $Mg(NO_3)_2.6H_2O$ and/or $Zn(NO_3)_2.6H_2O$ and B) containing Na_2CO_3 and NaOH (See Section 3.2). Once the solids were filtered and washed with water, the catalysts were dried at 60 ºC overnight and heat-treated in air/N_2 at 450 ºC during 10h, in order to obtain the hydrotalcite-derived mixed oxides.

Both, Mg/Al and Zn/Al atomic ratio was varied from 1 to 4, and these solids were analyzed by ICP, XRD and N_2 adsorption measurements. Main physicochemical and textural properties are shown in Table 4.4. HT-Mg/Al mixed oxides show higher surface areas (>200 m^2/g) and pore volumes (>0.5 cm^3/g) than HT-Zn/Al mixed oxides, the latter showing a further decrease when Zn/Al relation rises.

Table 4.4. Main physicochemical and textural properties of hydrotalcite-derived mixed oxides.

Catalyst	Composition	HT-Mg/Al			HT-Zn/Al		
	Ratio	1	2	4	1	2	4
Composition (M^{2+}/M^{3+})[a]		55/45	69/31	80/20	57/43	71/29	82/18
Surface Area (m^2/g)[b]		218	209	208	91	46	45
Pore volume (cm^3/g)[b]		0.52	0.62	0.55	0.24	0.31	0.16

[a] *Measured by ICP;* [b] *Calculated from N_2 adsorption isotherms (BET method).*

Catalytic results of HT-Mg/Al and HT-Zn/Al materials in the consecutive condensation of oxygenated compounds in aqueous mixture are shown in Table 4.5. Results are discussed in terms of oxygenated compounds conversion and yield to main reaction products: ethyl acetate, 2-methy-2-pentenal, C_5-C_8 and C_9-C_{10} products (See Section 3.4).

All materials show complete conversion of acetol, high conversions of propanal and medium conversions of ethanol and acetic acid. It can be seen in both cases, that if magnesium and zinc composition increases, higher conversion of propanal, ethanol and acetic acid are observed, while specifically HT-Mg/Al materials show higher acetic acid conversion.

However, analogously to the behaviour observed in $Ce_xZr_{1-x}O_2$ mixed oxides, this conversion enhancement does not drive to a concomitant increment in the yield to 2-methyl-2-pentenal (2M2P) and total organic products. Both, MgO and ZnO species generated after hydrotalcite heat-treatment are basic oxides with low lattice energy, whose basic active centres can be easily neutralized by the presence of acetic acid under this

operation conditions. High amounts of Mg and Zn species on the surface can lead to the formation of magnesium and zinc acetate and the decomposition of the catalyst. Moreover, detrimental polymerization reactions might be occurring at this range of composition, as C_9-C_{10} yield also decreases when M^{2+}/M^{3+}=2 is overcome.

Table 4.5. Catalytic results of hydrotalcite-derived mixed oxides in the condensation of oxygenated compounds in aqueous mixture.

Catalyst		Composition	HT-Mg/Al			HT-Zn/Al		
		Ratio	1	2	4	1	2	4
Conversion	(%)	Acetic acid	30.0	41.1	45.8	16.3	22.6	26.5
		Propanal	90.8	91.2	91.2	84.4	93.9	93.7
		Ethanol	31.9	41.3	40.9	40.3	47.4	51.1
		Acetol	100.0	100.0	100.0	100.0	100.0	100.0
Product Yield	(%)	Ethyl acetate	23.0	15.7	16.7	19.7	15.7	16.7
		2M2P[a]	40.0	36.0	30.3	38.0	32.0	30.3
		C5-C8	7.7	8.0	5.4	9.7	7.0	5.4
		C9-C10	26.0	29.7	24.3	23.0	23.7	23.6
		Total	**73.7**	**73.7**	**60.0**	**70.7**	**62.7**	**59.3**
Carbon balance (%)			98.1	92.3	80.0	99.6	90.0	84.0

Reaction conditions: 3 g of aqueous mixture, 150 mg of catalyst; T=200 ºC, P=13 bar N_2, t= 3h. [a]2M2P= 2-methyl-2-pentenal.

Therefore, hydrotalcite-derived mixed oxide optimum composition seems to be between ratios 1-2, when total organic yield is maximized (>70%). On the other hand, Mg/Al and Zn/Al ratios over 2 increase reactant conversion; meanwhile total organic yield and carbon balances decrease. Tuning HTs composition can control Mg and Zn leaching, although partial leaching of these active species is always observed along the catalytic experiments.

Once the activity of these materials had been checked, catalysts were optimized. In this sense, not only the nature of the basicity, but also the simultaneous presence of acidic and basic sites is a key point in order to favour the formation of aldol condensation intermediates. In the case of HT-Mg/Al derived mixed oxides, the acid-base properties can be tuned by playing with different parameters. First of all, Mg/Al ratio influence has already been studied. Then, thermal treatment of the samples (450 ºC, 550 ºC and 600 ºC) was considered[27], without observing notably differences on catalytic results.

Finally, the insertion of different M^{2+} cations in the LDH structure to form tertiary hydrotalcite-derived mixed oxides was studied. In this sense, we decided to modify a HT-Mg/Al hydrotalcite by inserting Zn^{2+} cations during the synthesis procedure. HT-Zn/Al materials had already shown promising results even when lower surface areas were achieved during their synthesis. In this sense, Zn^{2+} is a well-known Lewis acid centre and its incorporation into the structure of the hydrotalcite was expected to modify the balance between acid and base sites on the final catalyst[28].

A HT-$Mg_xZn_{2-x}Al$ catalyst (with low Zn-content) was synthesized and heat-treated under the same conditions. In this sense, HT-MgZnAl (1-1-1) was observed to show better catalytic results than both HT-Mg/Al and HT-Zn/Al with the same M^{2+}/M^{3+} ratio. These results are displayed and compared in Table 4.6 and Figure 4.5.

It can be observed that tertiary HT-MgZnAl synthesis drives to a solid with intermediate textural and physicochemical characteristics. Although reactants conversions are similar to those achieved with HT-Mg/Al=2, both 2M2P and total organic product yield are slightly increased using this composition. This result can be partially explained due to carbon balance is also higher (95%). Then, Zn incorporation may be reducing undesired polymerization reactions on the catalyst surface. When catalytic results of HT-MgZnAl (1-1-1) mixed oxide are compared to those obtained with HT-Mg/Al=2 and HT-Zn/Al=2 materials at different reactions times, this behaviour can be also observed (Figure 4.5).

Table 4.6. Catalytic results in the condensation of oxygenated compounds in aqueous mixture after the optimisation of hydrotalcite-derived mixed oxide composition

Catalyst		Composition	HT-Mg/Al	HT-MgZnAl	HT-Zn/Al
		Ratio	2	1-1-1	2
Composition (M^{2+}/M^{3+})			69/31	34/33/33	71/29
Surface Area (m^2/g)			209	155	46
Pore volume (cm^3/g)			0.62	0.30	0.31
Conversion	(%)	Acetic acid	41.1	42.4	22.6
		Propanal	91.2	89.8	93.9
		Ethanol	41.3	33.8	47.4
		Acetol	100.0	100.0	100.0
Product Yield	(%)	Ethyl acetate	15.7	17.3	15.7
		2M2P[a]	36.0	42.0	32.0
		C5-C8	8.0	6.7	7.0
		C9-C10	29.7	29.3	23.7
		Total	**73.7**	**78.0**	**62.7**
Carbon balance (%)			92.3	95.2	90.0

Reaction conditions: 3 g of aqueous mixture, 150 mg of catalyst; T=200 ºC, P=13 bar N_2, t= 3h. [a]2M2P= 2-methyl-2-pentenal.

Condensation reactions take place in relative short reaction times (1h), from when second condensation steps occur. For instance, HT-MgZnAl (1-1-1) composition maximized total organic yield at 3h (78%), but even a total value of 68% was achieved at 1h of reaction. Although conversions do not significantly increase after 1h, it is interesting to reach 3 hours on stream to maximize C_9-C_{10} compounds (≈30%). In this sense, in all three materials, it is important to stop reaction before 3h, because longer reaction times cause products polymerization, as more consecutive condensation reactions take place.

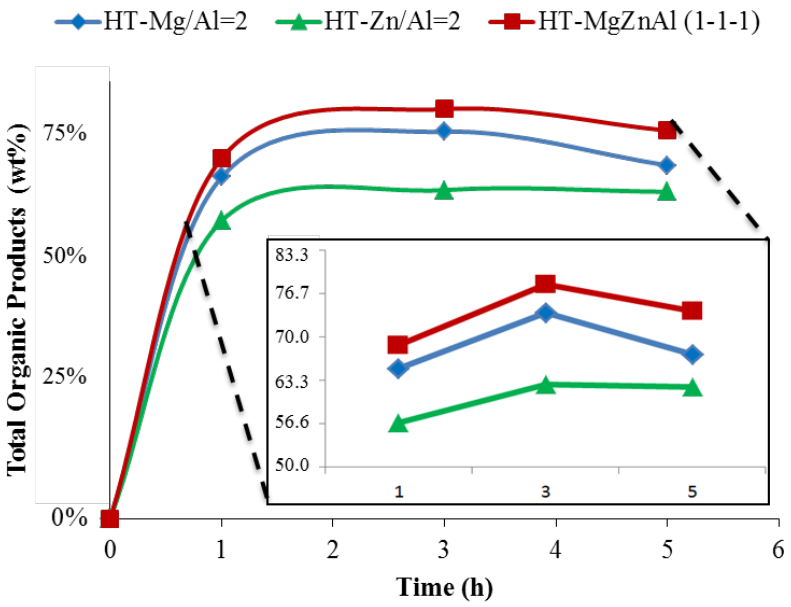

Figure 4.5. Catalytic results in the condensation of oxygenated compounds in aqueous mixture of HT-MgZnAl (1-1-1), HT-Mg/Al=2, and HT-Zn/Al=2 materials. Reaction conditions: 3 g aqueous mixture, 150 mg catalyst; 200 ºC, 13 bar N_2.

This cooperative effect observed in HT-MgZnAl hydrotalcite-derived mixed oxide can be also explained by catalyst crystalline structure analysed by XRD (Figure 4.6). On one hand, magnesium-containing hydrotalcites show a typical crystalline structure for a hydrotalcite-type material, whereas zinc-containing hydrotalcites show additional peaks corresponding to other crystalline phases as zinc oxide, zinc carbonate, among others. Moreover, the presence of Zn in the structure of hydrotalcites was found to cause a huge decrease in the surface area of the calcined materials due to the partial segregation of the ZnO phase when Zn/Al ratios >1 were used[29]. Nonetheless, when HT-MgZnAl is synthesized in 1-1-1 ratio, X-ray pattern is almost identical to that observed for pure HT-Mg/Al hydrotalcite-derived mixed oxides, and no additional peaks are observed. Therefore, Zn can be fully incorporated into the hydrotalcite structure up to this range of zinc composition and an intermediate surface area of 155 m^2/g is reached.

In this sense, a faster kinetics and improved yield to 2M2P and total products is favoured by the right incorporation of Lewis acid and basic sites on the structure of a hydrotalcite-derived mixed oxide, this meaning by incorporation of the Zn^{2+} cations in the MgAl mixed oxide structure.

When the optimum composition for the HT-MgZnAl mixed oxide was selected, reaction conditions were optimized. In this sense, temperature was varied from 170 ºC to 230 ºC to study the effect on product distribution and total organic product yield. Catalytic results in the condensation of oxygenated compounds in aqueous mixture for experiments performed at different temperature conditions are displayed in Figure 4.7.

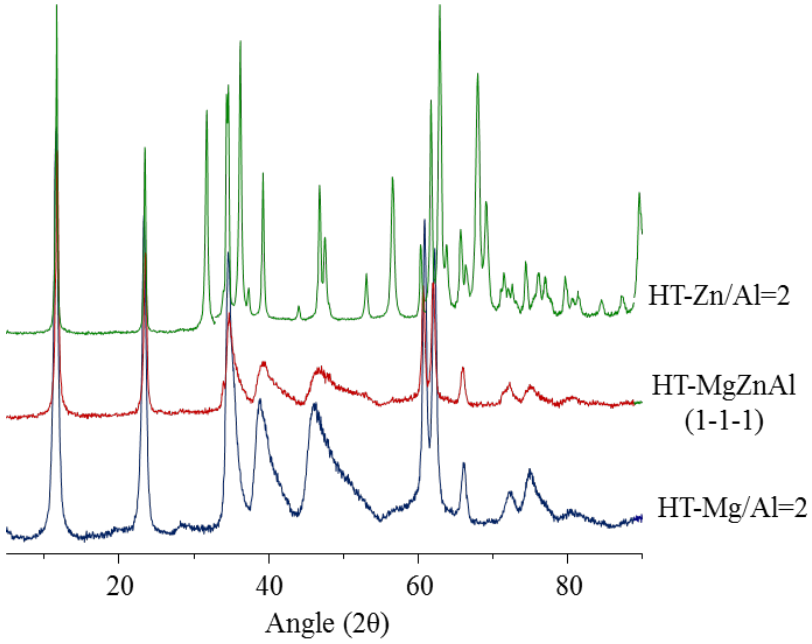

Figure 4.6. XRD patterns of HT-MgAl=2, HT-MgZnAl (1-1-1), and HT-Zn/Al=2 hydrotalcites.

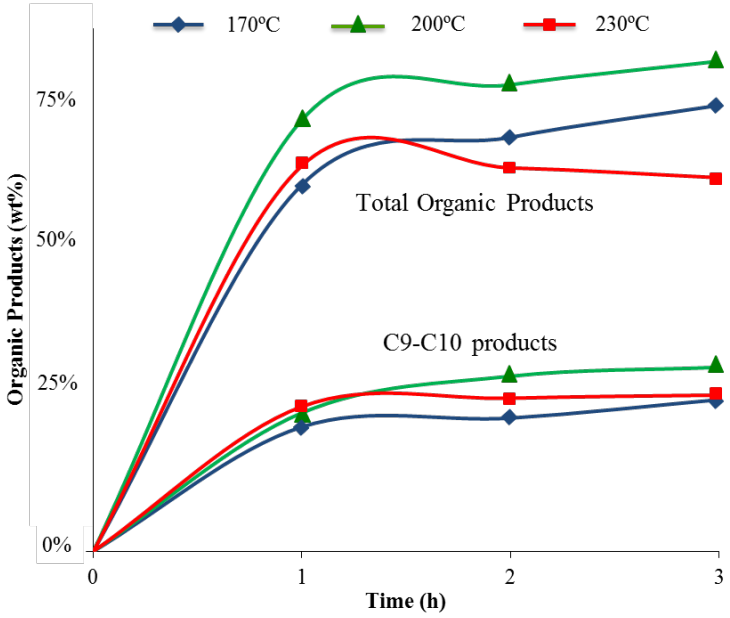

Figure 4.7. Catalytic results of HT-MgZnAl (1-1-1) mixed oxide in the condensation of oxygenated compounds in aqueous mixture under different temperature conditions.

It can be observed that maximum total organic product yield was achieved at 200 ºC. The main difference in activity compared to the experiment at 170 ºC is due to the increase of C_9-C_{10} products yield, when a higher temperature is used. On the other hand, higher temperature conditions (up to 230 ºC) lead to rapid polymerization reactions to occur as total organic products yield decreased even after short reaction times (1h).

4.3.3 HT-MgZnAl (1-1-1) mixed oxide vs. $Ce_{0.55}Zr_{0.45}O_2$

Afterwards, and with the intention of applying these catalysts in more realistic and demanding conditions, different experiments were carried out to study the effect of water content and the presence of heavier compounds in the consecutive condensation of oxygenated compounds present in aqueous mixtures for both, HT-MgZnAl and $Ce_{0.55}Zr_{0.45}O_2$ as reference material. Catalytic results are summarized in Table 4.7.

Firstly, it can be seen that if water content is increased from 30% to 60%, similar acetol, propanal and ethanol conversion is achieved in the case of the hydrotalcite-derived mixed oxide. However, acetic acid conversion is strongly affected when higher amounts of water are used in the model mixture. Then, total organic product yield decreases from 68.6% to 58.6% when HT-MgZnAl is employed. On the other hand, the reference material already showed lower reactant conversion when 30% of water was used, but even, catalytic results are much disfavoured when water content is increased (51.7% to 17.7%). Therefore, differences between hydrotalcite-derived mixed oxides and Ce-Zr mixed oxides become more evident.

A similar behaviour is observed when heavier compounds are added to the initial aqueous model mixture. Furfural was selected as a representative molecule of heavier compounds possible present in these aqueous effluents. Then, when 10% of furfural is added, acetic acid conversion is strongly affected for both catalysts, whereas propanal conversion is favoured compared to the initial scenario. This can be explained as furfural can easily react with propanal to directly produce the C_9 condensation product. This is the reason why lower amounts of 2-methyl-2-pentenal (from propanal self-condensation) are observed, while C_9-C_{10} products are favoured for both materials. Hydrotalcite-derived material still shows better catalytic results than Ce-Zr mixed oxide.

Table 4.7. HT-MgZnAl (1-1-1) mixed oxide vs. $Ce_{0.55}Zr_{0.45}O_2$ in the condensation reaction of aqueous model mixtures.

Catalyst		HT-MgZnAl (1-1-1)			$Ce_{0.55}Zr_{0.45}O_2$		
Aqueous model mixture		30% H_2O	60% H_2O	10% furfural	30% H_2O	60% H_2O	10% furfural
Conversion (%)	Acetic	41.9	22.6	14.9	14.8	0.0	0.0
	Propanal	85.9	88.5	92.0	63.5	33.1	65.5
	Ethanol	33.5	31.8	36.8	39.0	16.3	28.8
	Acetol	100.0	100.0	100.0	82.2	33.2	93.9
	Furfural	-	-	94.5	-	-	64.7
Product Yield (%)	Ethyl	17.3	8.3	14.7	15.7	3.3	11.0
	2M2P[a]	40.0	30.0	25.3	28.7	10.0	16.0
	C5-C8	6.6	4.4	3.0	5.3	2.2	4.0
	C9-C10	22.0	22.2	30.3	17.7	5.5	21.7
	Total	**68.6**	**56.6**	**58.6**	**51.7**	**17.7**	**41.7**
Carbon balance (%)		98.0	83.6	82.2	93.2	93.3	88.3

Reaction conditions: 3 g of aqueous mixture, 150 mg of catalyst; T=200 ºC, P=13 bar N_2, t= 1h. [a]2M2P= 2-methyl-2-pentenal.

Notwithstanding, HT-MgZnAl still suffers from leaching of Mg and Zn species, which progressively deteriorates the catalyst structure. In this sense, and following the strategy of incorporating different cations in the LDH structure to form tertiary hydrotalcite-derived mixed oxides, additional possible cations were studied.

4.3.4 Tertiary hydrotalcite-derived mixed oxides

Among the multiple possibilities, iron, cerium and lanthanum were considered the most interesting options in a first attempt. On one hand, Fe^{2+}/Fe^{3+} can be easily incorporated into the hydrotalcite structure due to its ionic radius and can enhance redox characteristics and oxygen vacancies on the catalyst surface. On the other hand, rare-earth metals have been widely considered to perform ketonization and condensation reactions under high temperature conditions[30,31].

5% Fe-, 5% Ce- and 5% La- HT-Mg/Al=2 hydrotalcite-derived mixed oxides were prepared following the same co-precipitation synthesis procedure (See Section 3.2). These catalysts were tested in the condensation reaction of an aqueous model mixture containing light oxygenated compounds under the same operational conditions. Main catalytic results are shown in Table 4.8.

Acetol, propanal and ethanol conversion are very similar to the results achieved with non-doped HT-Mg/Al=2 catalyst. However, acetic acid conversion decreases when these cations are incorporated in the catalyst structure. More importantly, intermediate products (2M2P, C_5-C_8) and final products (C_9-C_{10}) decrease when Fe, Ce and La are added in the

structure. Furthermore, all of them (even when incorporated in small amounts <5%) have detrimental effects on reaction carbon balances.

Therefore, the incorporation of these reported active species into hydrotalcite structures is not a solution for the enhancement of both activity and stability of these materials. In fact, it seems that atoms with bigger atomic radius, such as Ce^{4+} and La^{3+}, negatively affect catalyst structure and promote the leaching of active species. A white precipitate corresponding to the formation of cerium and lanthanum acetate was observed at the end of reactions when employing both Ce- and La-doped catalysts. This effect can also be related to the reported ability of cerium and other rare-earth metals to accelerate rehydration and restructuration processes in hydrotalcite-derived mixed oxides[32].

Table 4.8. Catalytic results of tertiary hydrotalcite-derived mixed oxides in the condensation of oxygenated compounds in aqueous mixture.

Catalyst		Composition	HT-Mg/Al=2			
		Doping	-	5% Fe	5% Ce	5% La
Conversion (%)		Acetic acid	41.1	29.7	29.7	27.4
		Propanal	91.2	91.1	89.7	90.2
		Ethanol	41.3	41.6	35.4	43.2
		Acetol	100.0	100.0	100.0	100.0
Product Yield (%)		Ethyl acetate	15.7	16.7	16.2	15.8
		2M2P[a]	36.0	29.7	28.9	29.3
		C5-C8	8.0	7.4	6.4	4.6
		C9-C10	29.7	23.7	23.3	21.4
		Total	**73.7**	**60.8**	**58.6**	**55.3**
Carbon balance (%)			92.3	87.0	85.4	77.0

Reaction conditions: 3 g of aqueous mixture, 150 mg of catalyst; T=200ºC, P=13 bar N_2, t= 3h. [a]2M2P= 2-methyl-2-pentenal.

In conclusion, iron, cerium and lanthanum incorporated in the hydrotalcite structure are not effective catalysts for this application, as both, activity and stability of the materials are disfavoured.

Finally, gallium incorporation in HTs structure was attempted, as Ga^{3+} has been reported to stabilize hydrotalcite crystalline structure when added in small amounts during the co-precipitation synthesis procedure. Different catalysts with varying Ga content among 1-4% were synthesized to study the effect of the incorporation of this cation on the catalyst structure. Figure 4.8 shows an XRD pattern of a Ga containing hydrotalcite-derived material compared to a non-doped HT-Mg/Al=4. This catalyst shows the typical XRD profile of Mg-Al LDH, which indicates that Ga cations are completely incorporated into the hydrotalcite structure.

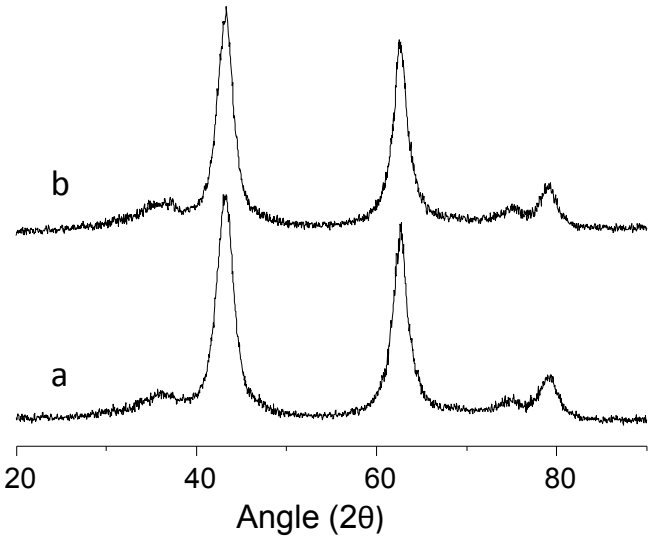

Figure 4.8. XRD profiles of a) HT-MgAl=4 and b) 1%Ga-HT-Mg/Al=4 hydrotalcite-derived mixed oxides.

The more relevant catalytic results obtained for Ga-based hydrotalcite-derived materials in the condensation of oxygenated compounds in aqueous mixtures are highlighted in Table 4.9.

As can be seen, small amounts of Ga^{3+} (<2%) can effectively promote the yield to the desired products. This cation somehow interacts with acid/base active sites in the materials increasing both, the yield to desired C_9-C_{10} and final products; and increasing carbon balance during the reaction. This last effect must be related to the blocking of stronger acid/base sites, which promote consecutive condensation steps. Unsuccessfully, when these materials were analysed by ICP after their use in reaction, similar leaching of Mg and Zn species was observed, so no beneficial stability effect was achieved when Ga^{3+} was added.

Table 4.9. Catalytic results of Ga-doped hydrotalcite-derived mixed oxides in the condensation of oxygenated compounds in aqueous mixture.

Catalyst		Composition	HT-Mg/Al=4			HT-MgZnAl (1-1-1)		
		Ga% Doping	-	1	3	-	2	4
Conversion	(%)	Acetic acid	45.8	44.3	36.8	42.4	38.2	44.0
		Propanal	91.2	94.8	91.7	89.8	93.3	93.5
		Ethanol	40.9	53.2	58.7	33.8	45.9	50.0
		Acetol	100.0	100.0	100.0	100.0	100.0	100.0
Product Yield	(%)	Ethyl acetate	16.7	14.3	11.3	17.3	15.3	14.3
		2M2P[a]	30.3	40.0	34.3	42.0	41.7	36.3
		C5-C8	5.4	7.0	7.1	6.7	7.6	6.1
		C9-C10	24.3	33.0	27.3	29.3	34.0	33.3
		Total	**60.0**	**80.0**	**68.7**	**78.0**	**83.3**	**75.7**
Carbon balance (%)			80.0	96.0	86.0	95.2	95.8	88.0

Reaction conditions: 3 g of aqueous mixture, 150 mg of catalyst; T=200ºC, P=13 bar N_2, t= 3h. [a]2M2P= 2-methyl-2-pentenal.

In conclusion, remarkably catalytic properties of this type of materials have been shown in the condensation of oxygenated compounds in aqueous mixtures at lab scale. On the contrary, the stability issues related to the leaching of great amounts of magnesium and zinc species from the catalysts make their reusability completely unfeasible under these reaction conditions.

There are two alternatives for its future use as catalysts in this application. On one hand, if acetic acid is previously isolated using some of the fractional condensation techniques (Section 1.4.3), stability issues will be reduced, although water role on catalyst durability related to their "memory effect" ability has not been studied and remain unclear.

On the other hand, high temperature conditions can promote ketonization to occur under surface conditions instead of via "bulk" metal decomposition. HTs stability under 350-400 ºC should be tested to be able to apply these catalysts in the valorisation of aqueous streams derived from bio-oils production. Nonetheless, these reactions conditions would lead to unreasonable process costs, which open the door for the development of new active and stable catalysts for the valorisation of complex bio-refineries aqueous waste streams.

4.4 Monometallic and mixed metal oxides

4.4.1. Monometallic oxides

Commercial monometallic oxides have also been tested in the condensation of oxygenated compounds present in an aqueous model mixture in the same reaction conditions previously applied in this research to check the activity and stability of reported materials under realistic operation conditions. Catalytic results attained for some of the most relevant metal oxides are summarized in Table 4.10 and Figure 4.9.

Table 4.10. Catalytic results of monometallic oxides in the condensation of oxygenated compounds in aqueous mixture.

Catalyst			SiO_2	ZrO_2	Al_2O_3	TiO_2	CeO_2	La_2O_3
Conversion	(%)	Acetic acid	0.0	7.9	0.0	12.6	54.7	0.0
		Propanal	51.8	63.7	68.3	44.6	91.7	81.0
		Ethanol	44.4	50.8	47.7	47.2	47.4	31.7
		Acetol	69.7	100.0	94.0	100.0	100.0	100.0
Product Yield	(%)	Ethyl acetate	26.5	23.3	19.8	21.8	17.6	16.3
		2M2P[a]	21.0	18.9	17.6	24.6	34.0	31.1
		C5-C8	11.9	9.4	8.7	11.3	5.5	5.9
		C9-C10	4.6	8.5	15.3	9.4	16.5	22.3
		Total	**37.5**	**36.8**	**41.6**	**45.3**	**56.0**	**59.3**
Carbon balance (%)			96.0	86.0	100.0	95.0	72.5	77.0

Reaction conditions: 3 g of aqueous mixture, 150 mg of catalyst; T=200 ºC, P=13 bar N_2, t= 3h. [a]2M2P= 2-methyl-2-pentenal

Traditional commercial supports including SiO_2, ZrO_2, Al_2O_3 and TiO_2 drive to low reactants conversion and thus, low total products yield after 3h in stream (Table 4.10). On the other hand, commercial CeO_2 and

La_2O_3 catalysts drive to higher propanal conversion values, but they are completely dissolved in reaction media. Then, homogeneous catalysis occurs and carbon balances are very low (<77%) as polymerization reactions take place and high amounts of cerium and lanthanum acetate are formed. α-Al_2O_3 used in these preliminary tests also suffers from structural changes and catalytic activity decrease if the catalyst is reused.

Therefore, TiO_2 and ZrO_2 catalysts are the only reference metals oxides with enough stability under these hydrothermal environments. Nonetheless, further improvements must be made on the design of these catalysts as the monometallic oxides still show poor catalytic results.

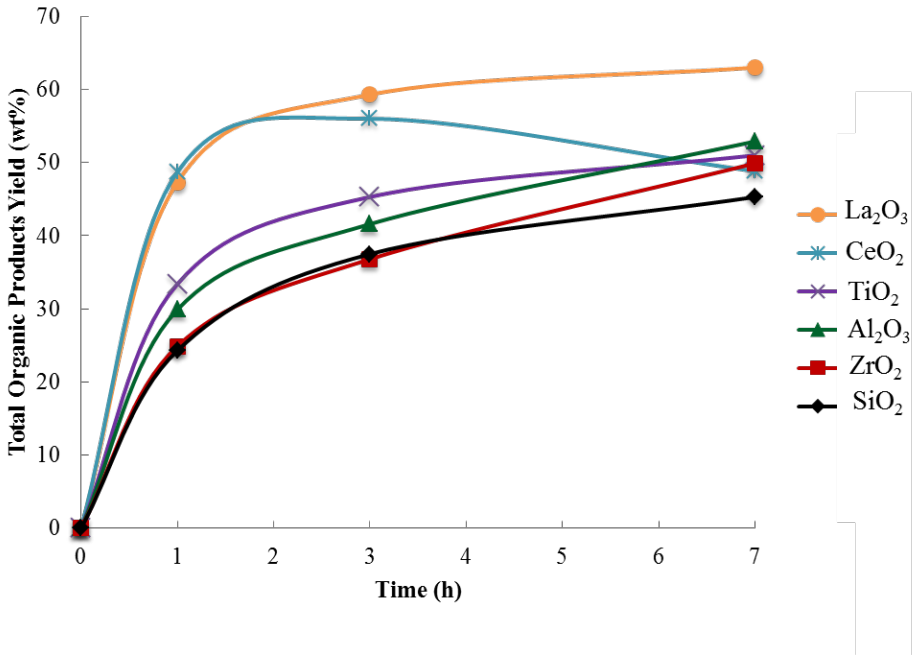

Figure 4.9. Catalytic results of monometallic oxides in the condensation of oxygenated compounds in aqueous mixture. Reaction conditions: 3 g aqueous mixture, 150 mg catalyst; 200 ºC, 13 bar N_2.

In this sense, and taking into account the activity shown by magnesium and zinc species in previous experiments, the stabilization of these active centres into stable TiO_2 and ZrO_2 matrix was attempted in order to improve both the activity and stability of the materials.

4.4.2. $A_xTi_{1-x}O$ mixed oxides (A: Mg, Zn)

Firstly, 5-10% Mg/TiO_2 and Zn/TiO_2 catalysts were prepared via incipient wetness impregnation. Small differences in the catalytic results were observed, while Mg^{2+} and Zn^{2+} species leaching was detected, after measuring final liquid samples by ICP.

Afterwards, different Mg-Ti-O and Zn-Ti-O mixed oxides were prepared via co-precipitation, following the procedure shown in Section 3.2. Mg/(Mg+Ti) and Zn/(Zn+Ti) ratio was varied from 0.1 to 0.5 and catalytic results of these mixed oxides were compared to TiO_2, MgO and ZnO commercial catalysts. In particular, propanal conversion and carbon balance of reactions performed at 200 ºC during 3h are shown in Figure 4.10, in order to analyse catalysts activity and stability.

Propanal conversion increases when Mg and/or Zn are progressively incorporated in the catalyst composition. When Mg/Zn atomic ratio is among 0.10-0.25, propanal conversion is remarkably improved, while carbon balances are still over 90-93%. Moreover, C_9-C_{10} products yield from consecutive condensation steps are maximized from 9% to 14-17% depending on Mg/Zn content in the catalyst. On the other hand, higher Mg-Zn addition and MgO/ZnO commercial catalysts drive to higher

propanal conversions, but very low reaction carbon balances. This is an unequivocally signal of catalyst instability. Thus, partial or total dissolution of the catalysts was observed in both cases after the reaction.

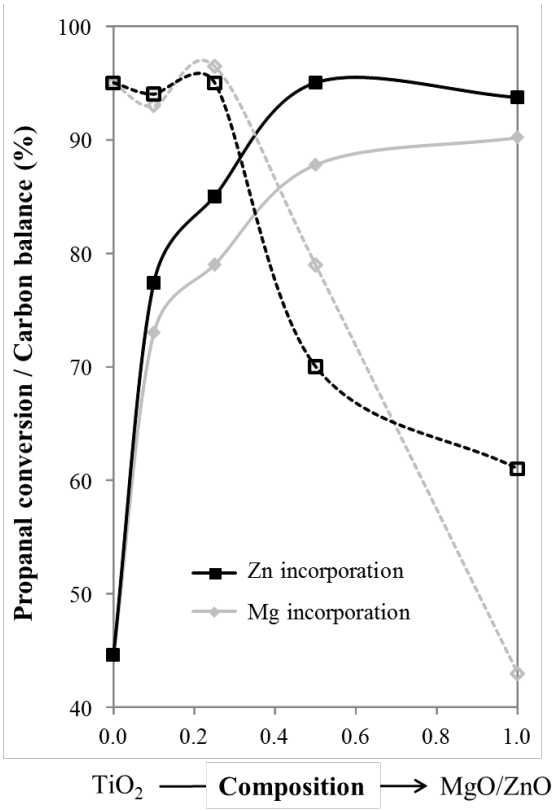

Figure 4.10. Catalytic results of $(Mg/Zn)_xTi_{1-x}O$ mixed oxides in the condensation of oxygenated compounds in aqueous mixture. Propanal conversion (solid lines) and carbon balance (dashed lines).

When catalysts structure is analysed by XRD (see Figure 4.11), intense Braggs signals assigned to TiO_2 anatase crystalline phase are observed for commercial anatase TiO_2 sample (Figure 4.11a). Mg-Ti and Zn-Ti mixed oxides present less intense and much broader peaks assigned to

TiO_2 cyrstalline phase, together with additional peaks corresponding to MgO - ZnO structures, which progressively appear when these species are incorporated during the catalyst synthesis (Figure 4.11b-c).

Then, MgO and ZnO cannot be fully incorporated into TiO_2-anatase crystalline structure and ICP measurements were performed to study Mg^{2+} and Zn^{2+} leaching in this reaction conditions. Mg^{2+} and Zn^{2+} partial leaching is still observed in Mg-Zn/Ti contents below 0.25, even though these catalysts seem to maintain reaction carbon balance. Therefore, Mg and Zn cannot be stabilized in TiO_2 catalysts by incipient wetness impregnation or co-precipitation methods even in small quantities (<5%) and all catalysts resulted unstable under these operation conditions.

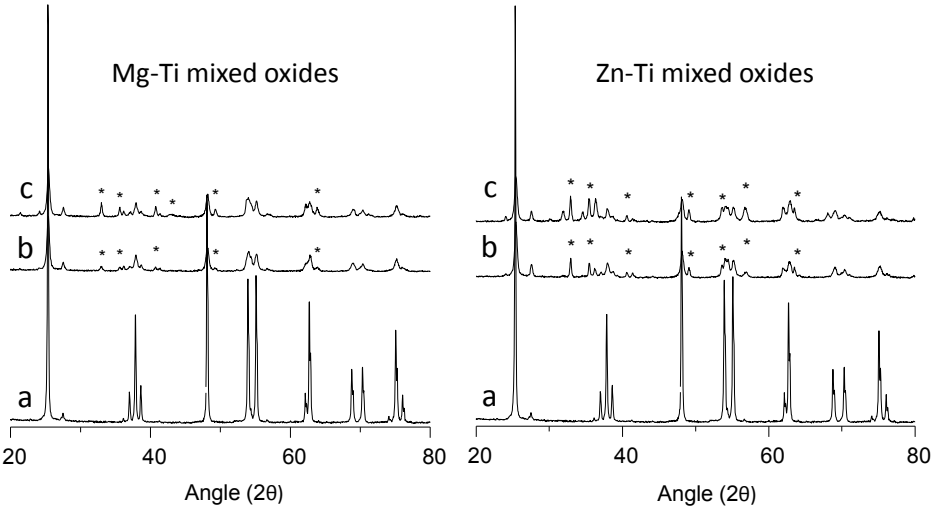

Figure 4.11. XRD profiles of Mg-Ti mixed oxides: a) ANA-TiO_2, b) MgTi-0.10, c) MgTi-0.25; and Zn-Ti mixed oxides: a) ANA-TiO_2, b) ZnTi-0.10, c) ZnTi-0.25.

4.4.3. $A_xZr_{1-x}O$ mixed oxides (A: Mg, Mn, Zn)

The same procedure of magnesium, zinc and manganese incorporation in monometallic oxide was followed in the case of ZrO_2-based catalysts.

Firstly, 5-10% Mg/ZrO_2 and Zn/ZrO_2 catalysts were prepared via incipient wetness impregnation. In these cases, Mg^{2+} and Zn^{2+} species leaching was again detected, after measuring final liquid samples by ICP.

Afterwards, different Mg-Zr-O, Mn-Zr-O and Zn-Zr-O mixed oxides were prepared via co-precipitation, following the procedure shown in Section 3.2. These mixed oxides have been claimed to possess interesting acid-base characteristics useful for aldol-condensation reactions. Thus, Mg, Mn and Zn atomic ratio in the ZrO_2-based materials was varied from 0.1 to 0.5 and the catalytic results of these mixed oxides in the condensation of oxygenated compounds in aqueous mixture were compared to the corresponding commercial catalysts.

$Mg_xZr_{1-x}O$ mixed oxides have been recently used as active catalysts for cyclopentanone condensation reactions[33,34]. Braggs signals assigned to Periclase MgO (JCPDS 00-001-1235) and tetragonal ZrO_2 (JCPDS 00-042-1167) phases were clearly appreciated in XRD analysis of these samples[35,36]. Then, in the presence of acetic acid in the aqueous mixtures used in our studies, Mg^{2+} leaching was observed, even when molar ratios <0.1 were studied.

$Mn_xZr_{1-x}O$ mixed oxides have even been claimed as active catalysts for the aqueous-phase ketonization of acetic acid[37]. Manganese species are more stable than Mg^{2+} sites in ZrO_2-based catalysts. Nonetheless, manganese species leaching is still observed in our experiments as its molar ratio increase in the catalysts composition. Thus, $Mn_{0.34}Zr_{0.66}O$ maintains its catalytic activity (after 1 reuse) better than $Mn_{0.64}Zr_{0.36}O$, which suffers from more Mn species leaching.

Finally, $Zn_xZr_{1-x}O$ have been widely studied as active catalysts in diverse condensations reactions due to their bifunctional character, where acid and base sites can be controlled tailoring catalysts composition and calcination conditions[38–41]. These materials were studied more in detail as Zn incorporation into ZrO_2-based materials seems to be more feasible.

In this sense, different $Zn_xZr_{1-x}O$ mixed oxides were synthesized by co-precipitation, following the procedure found in literature, by varying Zn/(Zn+Zr) ratio from 0.1 to 0.6. These mixed oxides were calcined at 400 ºC (optimal heat-treatment conditions to maximize acid/base active sites), and tested as catalysts in the condensation of oxygenated compounds in aqueous mixture in comparison to the corresponding t-ZrO_2 and ZnO commercial catalysts. The most relevant catalytic results of these $Zn_xZr_{1-x}O$ co-precipitated materials are displayed in Table 4.11 and Figure 4.12.

Table 4.11. Catalytic results of $Zn_xZr_{1-x}O$ mixed oxides in the condensation of oxygenated compounds in aqueous mixture.

Catalyst	Zr	1.00[a]	0.90	0.78	0.64	0.37	0.00
	Zn	0.00	0.10	0.22	0.36	0.63	1.00[b]
Conversion (%)	Acetic acid	7.9	0.4	11.2	11.3	23.9	77.7
	Propanal	63.7	67.7	69.4	80.4	89.7	93.7
	Ethanol	50.8	45.9	37.8	41.9	43.6	50.3
	Acetol	100.0	100.0	100.0	100.0	100.0	100.0
Product Yield (%)	Ethyl	23.3	21.4	21.3	21.0	18.8	15.7
	2M2P[c]	18.9	25.0	28.3	36.9	40.5	31.0
	C5-C8	9.4	11.5	11.2	9.7	7.1	4.7
	C9-C10	8.5	16.4	16.0	20.4	24.0	21.0
	Total	**36.9**	**52.9**	**55.5**	**66.9**	**71.7**	**56.7**
Carbon balance (%)		86.2	98.0	97.0	100.0	95.0	61.0

Reaction conditions: 3 g of aqueous mixture, 150 mg of catalyst; T=200 ºC, P=13 bar N_2, t= 3h. [a]Tetragonal ZrO_2 (Chempur); [b]ZnO (Sigma Aldrich); [c]2M2P= 2-methyl-2-pentenal

Both, acetic acid and propanal conversion increase when Zn is progressively incorporated into the catalyst structure. Thus, higher 2-methyl-2-pentenal, C_5-C_8, and more importantly, C_9-C_{10} products yields increase with higher Zn contents. Moreover, high carbon balances (>95%) are achieved when all $Zn_xZr_{1-x}O$ mixed oxide are used. Oppositely, ZnO, as it had been previously shown, is completely dissolved in reaction media.

$Zn_{0.36}Zr_{0.64}$ and $Zn_{0.63}Zr_{0.37}$ maximized both 2M2P and C_9-C_{10} products (Figure 4.12A) but the latest one, additionally promotes polymerization reactions after 1h, driving to lower total organic products yields at longer reaction times (Figure 4.12B). Total product yields progressively

increase when the other catalysts are employed, all of them showing high carbon balances (>92%) even after 7h on stream.

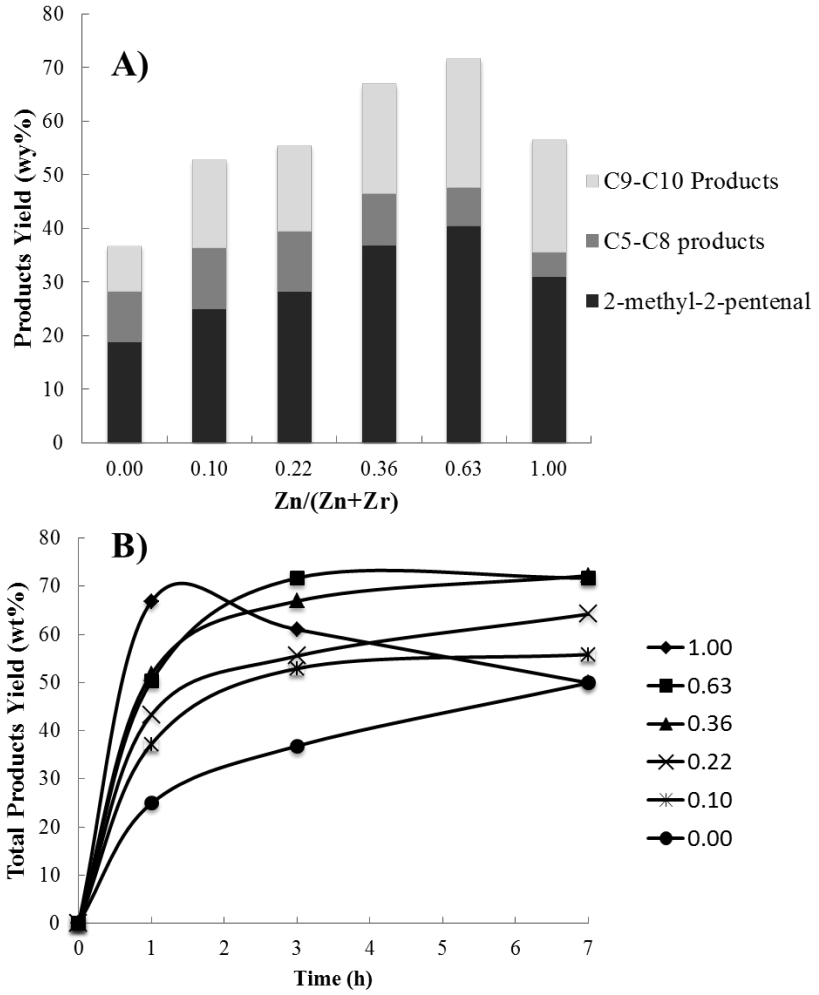

Figure 4.12. Catalytic results of $Zn_xZr_{1-x}O$ mixed oxides in the condensation of oxygenated compounds in aqueous mixture. A) Product yield profile at t=3h. B) Evolution of total organic product yield with time.

Differences in the catalyst structure depending on the composition can be observed when calcined samples are analysed by XRD. Low content Zn samples (<0.22) only show Braggs signals corresponding to t-ZrO_2 crystalline structure (JCPDS 00-042-1167), analogous to the peaks observed for a commercial t-ZrO_2 catalyst (Figure 4.13a), while additional peaks assigned to ZnO phase are progressively identified when high content Zn samples are analysed (>0.36) (see Figure 4.13b).

After the reaction, all catalysts were washed with methanol, dried at 100 ºC overnight and their composition measured by ICP to compare to the one obtained prior to their use in reaction. The composition for all of them was comparable to $Zn_{0.10}Zr_{0.90}$ sample, being Zn content among 10-15%. Therefore, only the one with the lowest amount of Zn was stable under this process conditions. The rest of $Zn_xZr_{1-x}O$ mixed oxides suffer from Zn^{2+} leaching, this increasing when higher Zn contents are used.

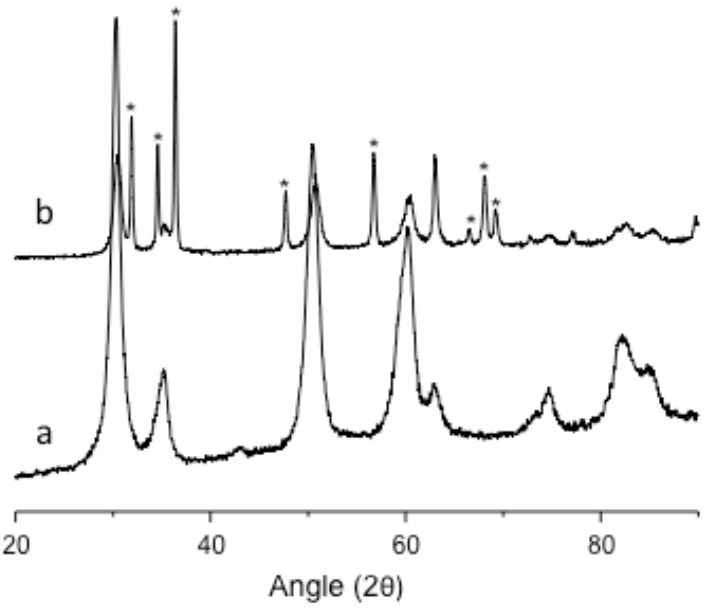

Figure 4.13. XRD profiles of a) tetragonal-ZrO_2 and b) $Zn_{0.63}Zr_{0.37}$ *mixed oxide.*

Finally, the stability of these metal mixed oxides, which have shown better catalytic results was analysed by consecutive reuses. In this sense, both $Ce_xZr_{1-x}O$ and $Zn_xZr_{1-x}O$ representative mixed oxides were employed and the results are discussed in the next section.

4.4.4. Stability study of $Ce_xZr_{1-x}O$ and $Zn_xZr_{1-x}O$ mixed oxides

Stability tests of the solid materials under reaction conditions were performed by using the catalysts several times. Once the catalytic experiment was finished, the solid was separated and washed repeatedly with methanol. Finally, after drying at 100 ºC overnight, the catalysts were tested again in the condensation of oxygenated compounds present in an aqueous model mixture. The effect of the reuses of $Ce_xZr_{1-x}O$ and $Zn_xZr_{1-x}O$ representative samples is shown in Figure 4.14.

$Ce_{0.55}Zr_{0.45}O_2$ was selected, as it was the sample with better products yield and carbon balance among the tested $Ce_xZr_{1-x}O$ mixed oxides (see Section 4.2). It can be seen that this catalyst suffers from progressive deactivation mainly due to partial Ce leaching, and also by the organic matter deposition (measured by EA and TG) on the catalyst surface. In the case of $Zn_xZr_{1-x}O$ mixed oxides, only the one with low content of Zn (0.10) maintains its activity after the first reuse (little decrease due to coke deposition), while Zn leaching was not detected. On the contrary, as it had been previously commented, large amounts of Zn leached from other $Zn_xZr_{1-x}O$ mixed oxides with higher Zn content. This leads to the high deactivation of these catalysts after the first reuse, being this effect analogously observed for other catalysts studied during this section (i.e. $Mg_xZr_{1-x}O$, $Mn_xZr_{1-x}O$, $Mg_xTi_{1-x}O$, among others)

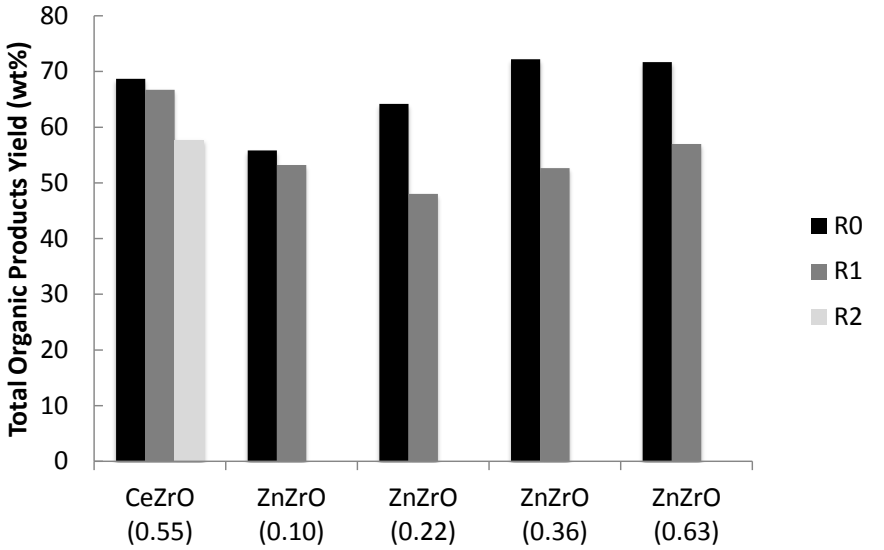

Figure 4.14. Effect of the reuses of $Ce_xZr_{1-x}O$ and $Zn_xZr_{1-x}O$ catalysts on the total organic yield (wt%) attained during the condensation of oxygenated compounds in an aqueous model mixture (at 200 ºC, P_{N_2}=13 bar over 7h).

Summarizing, bifunctional catalysts as $Ce_xZr_{1-x}O$ mixed oxides have been widely used in literature for their application in aldol condensation and ketonization reactions. Hydrotalcite-derived mixed oxides, Mg-based and Zn-based catalysts are alternative materials combining acid and base active sites, which show good catalytic results in these organic reactions. Nonetheless, most authors have studied their activity employing single reactants, without considering their stability against more realistic aqueous mixtures of oxygenated compounds. In this sense, all these catalysts have shown stability concerns, regardless the synthesis procedure followed for their preparation, when employed in this process conditions. Thus, the design of new heterogeneous catalysts is a must for their application in these acidic aqueous environments in order to valorise biomass-derived aqueous streams.

4.5 Conclusions

- $Ce_{0.55}Zr_{0.45}O_2$ catalyst was selected as the reference material for this work as it shows high activity in the aqueous-phase condensation of light oxygenates derived from biomass pyrolytic processes. Nonetheless, this catalyst deactivation by Ce partial leaching and coke deposition is an issue for its application under these operation conditions.
- Hydrotalcite-derived mixed oxides show better catalytic results than $Ce_xZr_{1-x}O_2$ reference material. In particular, HT-MgZnAl (1-1-1) was the optimum composition to maximize total products yield under complex aqueous environments, even with higher amounts of water or the addition of heavier compounds (i.e. furfural) in the model mixture.
- Unfortunately, Mg^{2+} and Zn^{2+} leaching is observed in all these type of samples, even when the composition is optimized. The addition of tertiary metals (Fe, Ce, La) does not improve catalytic results. On the contrary, higher products yields are achieved by the addition of small amounts of Ga (<2%), although the stability of these materials is still a concern under these conditions.
- Poor catalytic results are obtained when traditional mixed oxides (SiO_2, ZrO_2, Al_2O_3, TiO_2) are used. The stabilization of Mg^{2+}, Zn^{2+} and Mn^{2+} active species on resistant ZrO_2 and TiO_2 supports by different synthesis methods has been attempted. Catalytic results have been improved compared to initial metal oxides, but catalyst stability mainly due to metal leaching avoids their use as heterogeneous catalysts in this application.

4.6 References

1. Horváth, I.T. & Anastas, P.T. *Chem. Rev.* **107,** 2169–2173 (2007).
2. Gawande, M.B., Pandey, R.K. & Jayaram, R.V. *Catal. Sci. Technol.* **2,** 1113-1125 (2012).
3. Nagashima, O., Sato, S., Takahashi, R. & Sodesawa, T. *J. Mol. Catal. A: Chem.* **227,** 231–239 (2005).
4. Snell, R.W. & Shanks, B.H. *ACS Catal.* **4,** 512–518 (2014).
5. Snell, R.W., Hakim, S.H., Dumesic, J.A. & Shanks, B.H. *Appl. Catal., A. Gen.* **464–465,** 288–295 (2013).
6. Snell, R.W. & Shanks, B.H. *ACS Catal.* **3,** 783–789 (2013).
7. Dooley, K.M., Bhat, A.K., Plaisance, C.P. & Roy, A.D. *Appl. Catal., A. Gen.* **320,** 122–133 (2007).
8. Gangadharan, A., Shen, M., Sooknoi, T., Resasco, D.E. & Mallinson, R.G. *Appl. Catal., A. Gen* **385,** 80–91 (2010).
9. Gaertner, C.A., Serrano-Ruiz, J.C., Braden, D.J. & Dumesic, J.A. *J. Catalysis* **266,** 71–78 (2009).
10. Gaertner, C.A., Serrano-Ruiz, J.C., Braden, D.J. & Dumesic, J.A. *Ind. Eng. Chem. Res.* **49,** 6027–6033 (2010).
11. Hakim, S.H., Shanks, B.H. & Dumesic, J.A. *Appl. Catal., B. Environ.* **142–143,** 368–376 (2013).
12. Serrano-Ruiz, J.C., Luettich, J., Sepúlveda-Escribano, A. & Rodríguez-Reinoso, F. *J. Catalysis* **241,** 45–55 (2006).
13. Lee, G., Kang, J.Y., Yan, N., Suh, Y.W. & Jung, J.C. *J. Mol. Catal. A: Chem.* **423,** 347–355 (2016).
14. Dębek, R., Motak, M., Grzybek, T., Galvez, M. & Da Costa, P. *Catalysts* **7,** 32-57 (2017).
15. Cavani, F., Trifirò, F. & Vaccari, A. *Catal. Today* **11,** 173–301 (1991).
16. Climent, M.J., Corma, A., Iborra, S., Epping, K. & Velty, A. *J. Catalysis* **225,** 316–326 (2004).
17. Debecker, D.P., Gaigneaux, E.M. & Busca, G. *Chem. - A Eur. J.* **15,** 3920–3935 (2009).
18. Climent, M.J., Corma, A., Iborra, S. & Primo, J. *J. Catalysis* **151,** 60–66 (1995).
19. Velu, S. & Swamy, C.S. *Appl. Catal., A. Gen.* **119,** 241–252 (1994).
20. Hora, L., Kelbichová, V., Kikhtyanin, O., Bortnovskiy, O. & Kubička, D. *Catal. Today* **223,** 138–147 (2014).
21. Ordóñez, S., Díaz, E., León, M. & Faba, L. *Catal. Today* **167,** 71–76 (2011).

22. Faba, L., Díaz, E. & Ordóñez, S. *Appl. Catal., B. Environ.* **142–143,** 387–395 (2013).
23. León, M., Díaz, E. & Ordóñez, S. *Catal. Today* **164,** 436–442 (2011).
24. Parida, K. & Das, J. *J. Mol. Catal. A: Chem.* **151,** 185–192 (2000).
25. Das, J. & Parida, K. *React. Kinet. Catal. Lett.* **69,** 223–229 (2000).
26. Corma, A., Fornés, V. & Rey, F. *J. Catalysis* **148,** 205–212 (1994).
27. Kuśtrowski, P. *et al. Microp. Mesop. Materials* **78,** 11–22 (2005).
28. Hernández, W.Y., Aliç, F., Verberckmoes, A. & Van Der Voort, P. *J. Mater. Sci.* **52,** 628–642 (2017).
29. Sánchez-Cantú, M. *et al. Chem. Papers* **68,** 638–649 (2014).
30. Lopez-Ruiz, J.A., Cooper, A.R., Li, G. & Albrecht, K.O. *ACS Catal.* **7,** 6400-6412 (2017).
31. Yamada, Y., Segawa, M., Sato, F., Kojima, T. & Sato, S. *J. Mol. Catal. A: Chem.* **346,** 79–86 (2011).
32. Soares Dias, A.P., Bernardo, J., Felizardo, P. & Neiva Correia, M.J. *Energy* **41,** 344–353 (2012).
33. Liang, D., Li, G., Liu, Y., Wu, J. & Zhang, X. *Catal. Commun.* **81,** 33–36 (2016).
34. Cueto, J., Faba, L., Díaz, E. & Ordóñez, S. *ChemCatChem* **9,** 1765–1770 (2017).
35. Faba, L., Díaz, E. & Ordóñez, S. *Appl. Catal., B. Environ.* **113–114,** 201–211 (2012).
36. Aramendía, M.A. *et al. J. Mol. Catal. A: Chem.* **218,** 81–90 (2004).
37. Wu, K. *et al. AIChE Journal* **63,** 2958–2967 (2017).
38. Silva-Calpa, L. del R., Zonetti, P.C., de Oliveira, D.C., de Avillez, R.R. & Appel, L.G. *Catal. Today* **289,** 264–272 (2017).
39. Silva-Calpa, L. del R. *et al. J. Mol. Catal. A: Chem.* **425,** 166–173 (2016).
40. Liu, C., Sun, J., Smith, C. & Wang, Y. *Appl. Catal., A. Gen.* **467,** 91–97 (2013).
41. Sun, J. *et al. J. Amer. Chem. Soc.* **138,** 507–517 (2016).

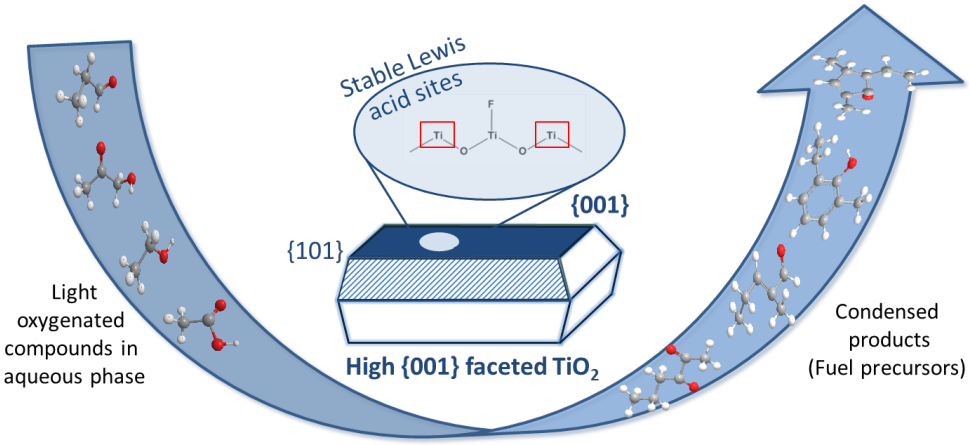

CHAPTER 5

{001} FACETED TiO_2 MATERIALS AS ACID CATALYSTS FOR THE AQUEOUS-PHASE CONDENSATION OF OXYGENATED COMPOUNDS

5.1 Introduction

The activity of mixed metal oxides tested in the condensation of oxygenated compounds present in aqueous mixtures in Chapter 4 is based on their bifunctional character, although their stability under faithful operation conditions is a critical factor to be further improved. In this context, these mixed oxides had been widely considered in the gas-phase conversion of small aldehydes and carboxylic acids at high temperatures (>300 ºC)[1,2]. On the contrary, catalysts including Ce, Zn, Mg or La species have shown to suffer from moderate to strong deactivation due to the leaching of these active species in acidic aqueous mixtures (pH < 2) in liquid-phase reactions. Therefore, hydrothermally resistant acid catalysts must be specifically designed for this application.

In this sense, and in order to overcome stability issues, Ti (IV) oxides have been studied as catalysts for condensation reactions using acetic acid or propanal as probe molecules[3,4]. The number and nature of acid sites are determinant for this type of reactions. Specifically, titanium oxide crystalline phase and associated Ti-Ti and Ti-O distances have been proved to be decisive on the reaction mechanism (Figure 5.1). Then, the existence of coordinatively unsaturated Ti-O-Ti sites with intermediate acid-base strength, together with catalysts geometry are necessary requirements for the formation of reactive intermediate species. In this context, activation barriers for condensation have been found to be much larger on TiO_2-rutile than on TiO_2-anatase phases.

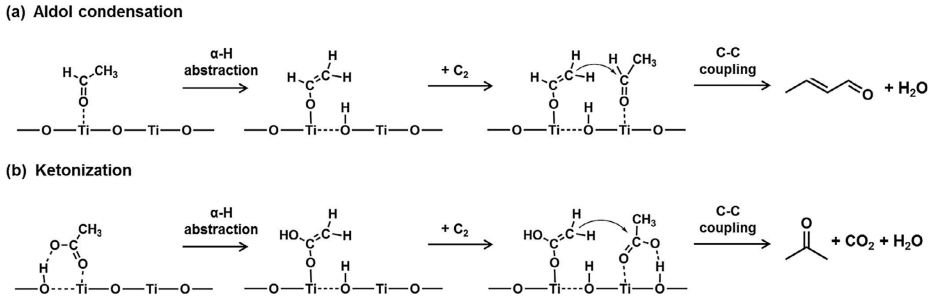

Figure 5.1. Elemental steps involved in condensation and ketonization reactions on acid-base pairs of TiO_2 surface[4].

In addition, TiO_2 has been studied on gas-phase condensation and ketonization reactions under high temperature conditions (300-450 ºC) to produce olefins[5] and even with the incorporation of noble metals as ruthenium on the solid catalyst[6,7]. The presence of Ru is believed to facilitate the formation of surface reduced Ti^{3+} species, which can favour the ketonization reaction in the presence of liquid water. The use of noble metals together with the necessity of pre-reducing materials at high H_2 pressures makes this option economically unfeasible. In this context, an alternative cost-effective approach is actually needed to improve the activity of these TiO_2 based materials in the condensation of light oxygenated compounds in aqueous systems.

In light of all the above-mentioned, the development of TiO_2 crystals with specific facets, in order to obtain surfaces with higher reactivity could be a feasible strategy. It has been suggested that {001} facets of anatase TiO_2 exhibit higher reactivity than thermodynamically stable {101} facets, due to a higher concentration of unsaturated five-coordinated Ti (Ti_{5c}) centres[8–13].

The relevant activity of {001} surfaces on catalytic applications was studied several years ago by M.A. Barteau and cowork[14–19]. Experiments were performed in ultrahigh-vacuum chambers, where TiO_2 {001} single-crystal surfaces and ion-sputtered (reduced) surfaces containing Ti sub-oxides were studied in C-C bond formation reactions. Nonetheless, it was not until recent years that faceted TiO_2 has been easily prepared by different methods, where normally fluorine is used as a capping agent in order to selectively control the preferential growth of catalytic more reactive {001} facets[20]. F atoms with low bonding energies (D_0^{F-F}=158.8 $kJmol^{-1}$) and with strong bonding to Ti (D_0^{F-Ti}=569.0 $kJmol^{-1}$) can effectively decrease high surfaces energies (γ), but also make {001} surfaces more stable than {101} surfaces (Figure 5.2)[21]. Moreover, recent studies have shown the ability of residual fluorine species on faceted TiO_2 surface to improve the photocatalytic activity of these oxides[22–24].

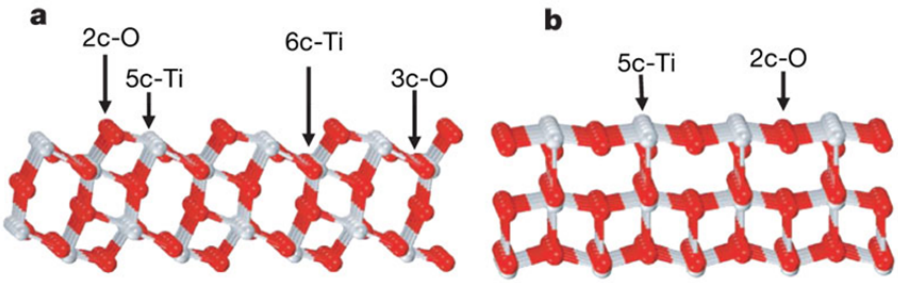

Figure 5.2. a) {101} and b) {001} surfaces of anatase-TiO_2[21].

In this Chapter, the synthesis and characterization of hydrothermally synthesized faceted titanium oxides is presented and their catalytic activity is evaluated in the valorisation of representative light (C_2-C_3) oxygenated compounds present in an aqueous model mixture, which

simulates the complexity of a real bio-refinery aqueous stream (see Section 3.4). The effect of tailoring crystal facets of TiO_2 and the presence of residual fluorine species on catalytic activity in this type of reactions is studied for the first time. Complex reaction mixtures together with moderated operation conditions used during this work also differ from usual single molecule studies performed even in the absence of water in most of the cases. Activity and stability results attained with these {001} faceted TiO_2 samples are also compared with other commercial titanium oxides.

5.2 Results and discussions

5.2.1 Synthesis of faceted TiO_2 materials

Materials were prepared by direct hydrothermal treatment of the titanium precursors, i.e. 50 mL of titanium (IV) isopropoxide or titanium (IV) butoxide, together with the addition of 8 mL of aqueous HF as a capping agent. The solutions were transferred into a Teflon recipient inside of a 125 mL-stainless steel autoclave from Parr Instrument Company and hydrothermal treatment was performed at 200 ºC for 24 h. The precipitate obtained was filtered, repeatedly washed with distilled water and dried overnight at 100 ºC (for more information see Section 3.2.5). Thus, two different samples depending on the titanium precursor were obtained and named as ISO and BUT.

5.2.2 Catalysts characterization

XRD pattern of the different TiO_2 samples used in this work are depicted in Figure 5.3. Both, ISO and BUT TiO_2-based samples present anatase as only crystalline phase. These samples can be compared to commercial anatase, rutile and P25 TiO_2-type catalysts, which show the expected and characteristic XRD patterns in each case. Anatase TiO_2 commonly presents a tetragonal bi-pyramidal structure where thermodynamically stable {101} facets are predominantly observed. However, the presence of {001} facets is desired as they are considered to exhibit higher reactivity due to a higher concentration of unsaturated five-coordinated Ti centers[8–13].

In fact, hydrothermally synthesized TiO_2 ISO and BUT samples exhibit varying relative intensity of XRD peaks. These differences give information of a different preferential growth of the TiO_2 crystals related to the addition of fluorine as a capping agent during materials synthesis. XRD relative peak intensity ratios for different lattice planes are shown in Table 5.1. As it can be observed, relative intensity corresponding to (004) peaks decreases, while relative intensity for (200) and (211) peaks increases for both ISO and BUT samples. The addition of HF during hydrothermal synthesis is believed to have dual roles: to retard hydrolysis of the titanium precursor and to reduce surface energy to promote the growth along the [010] and [100] axes[21]. Then, HF allows obtaining titanium oxides exposing the {001} facet in a higher degree than commercial TiO_2-anatase.

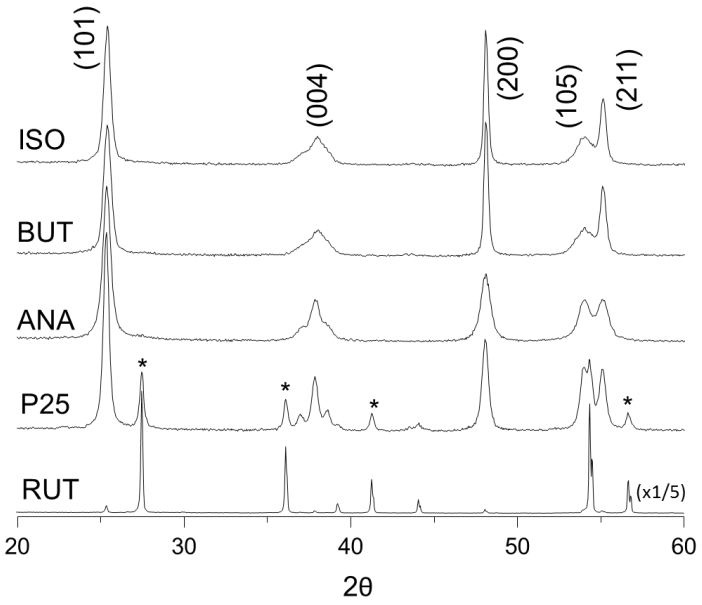

Figure 5.3. XRD patterns of the different TiO_2 samples. Main peaks corresponding to different lattice planes of TiO_2-anatase structure are highlighted, whereas signals corresponding to rutile phase are marked with an asterisk (*).

Raman spectroscopy was performed for TiO_2 ISO and BUT materials in order to confirm their crystalline structure, being their corresponding spectra shown in Figure 5.4. The peaks appearing at 144, 394, 514 and 636 cm^{-1} for both samples corroborate the anatase phase in agreement with XRD patterns. Moreover, some authors have used Raman spectroscopy as an approach for measuring the percentage of exposed {001} facets by using the ratio of Raman vibrational modes between E_g and A_{1g}[25]. These values are shown in Table 5.1 and the resulting estimated percentages of exposed {001} facets for the samples are 69% and 55% for BUT and ISO samples, respectively. On the other hand, {001} facet is ≈29% and ≈20% exposed for anatase and P25 samples, respectively (Figure 5.5).

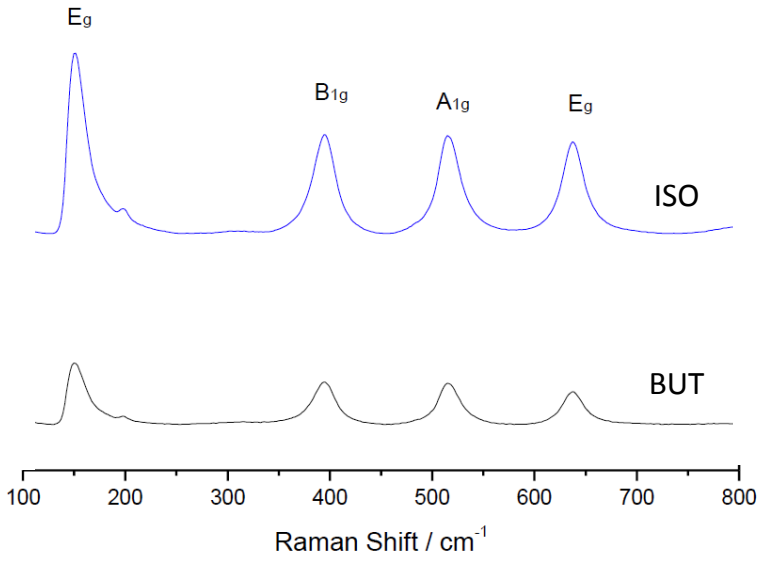

Figure 5.4. Raman spectra for TiO_2-ISO and BUT samples.

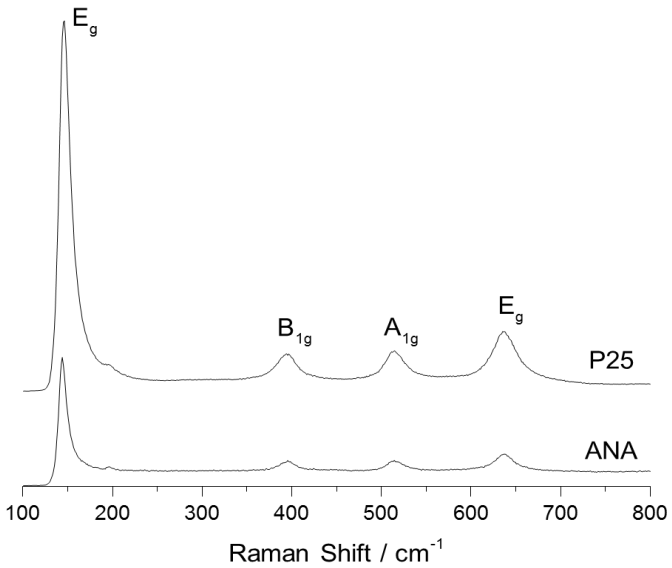

Figure 5.5. Raman spectra for TiO_2-Anatase and P25 samples.

Representative SEM and TEM pictures for ISO and BUT TiO_2-based samples are shown in Figure 5.6, where a regular morphology composed by agglomerated nanoparticles in the shape of square and rectangular nano-platelets with dimensions ranging from 20 to 80 nm, with some larger particles up to 70-80 nm can be observed in both cases[24]. Platelets deposited either flat or on their side can be easily recognized in TEM pictures (Figure 5.6C and 5.6D). The contrast in the images is directly proportional to the thickness of the particle: platelets are clearer because their thickness is very low (<5 nm); while elongated particles deposited on their side are darker as it thickness corresponds to the side of the square platelet (3-50 nm).

HRTEM micrographs of TiO_2-ISO sample were obtained in order to confirm that F preferentially directs {001} facet growth. Indeed, Figure 5.7 shows a set of four-side platelet projection, where the third dimension of the platelets (approx. 5 nm) can be clearly observed. Moreover, the corresponding FFT of each side platelet are also inset in this figure. This information is in line with XRD and Raman spectroscopy data, although F could not be directly ascribed to a specific facet, as EDX analyses could not be performed under HRTEM conditions. Finally, from these SEM, TEM and HRTEM studies, average size dimensions of the platelets could be estimated. Thus, average length of the platelets in TiO_2-ISO was 42 nm, while in TiO_2-BUT was 35 nm. Differences in particle sizes estimation from SEM/TEM studies with those obtained from XRD data using Scherrer´s equation were noticed (Table 5.2), although similar trends were observed from both characterization techniques.

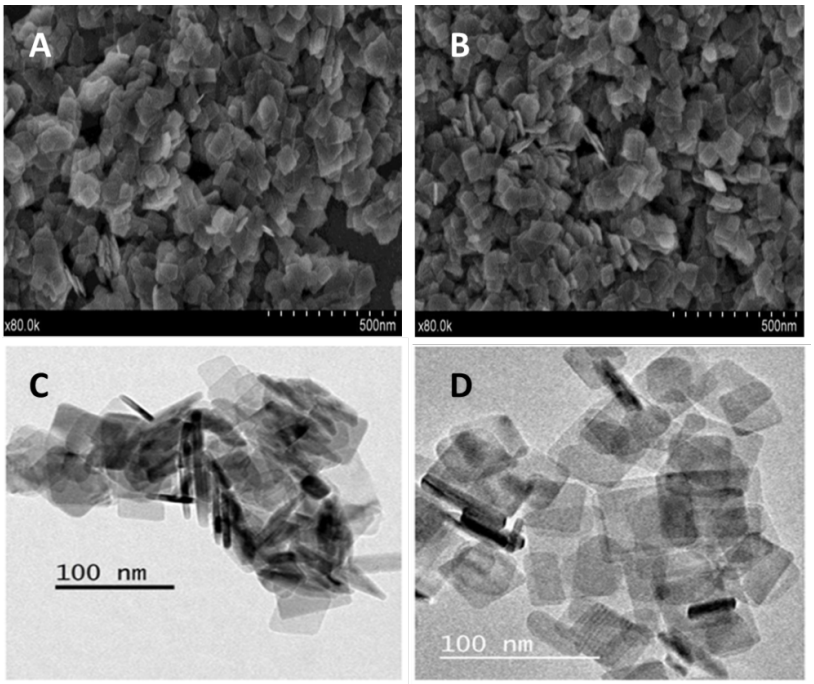

Figure 5.6. Representative FESEM pictures of ISO (A) and BUT (B) TiO_2 samples and TEM pictures of ISO (C) and BUT (D) TiO_2 samples.

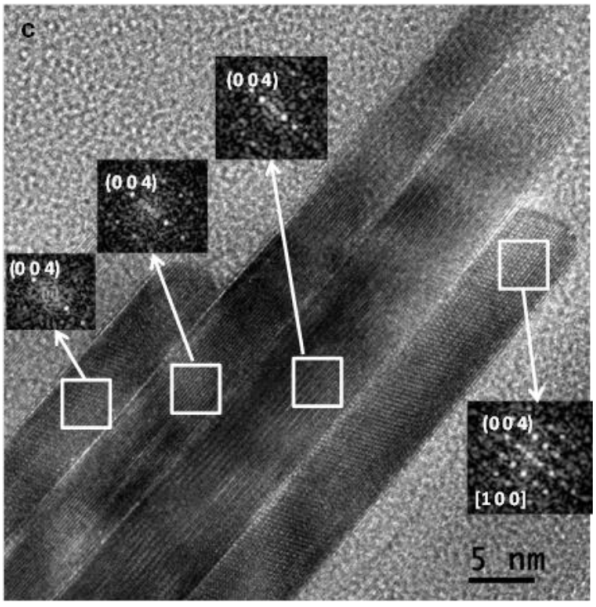

Figure 5.7. Representative HRTEM picture of TiO_2-ISO sample.

More interestingly, TiO_2 ISO and BUT samples exhibit high values of surface area (≈100 m^2/g) and propitious acid properties (see Table 5.3 and Figures 5.8 and 5.9). In particular, acid characteristics for these materials are based on Lewis acid sites, whereas no Brönsted acid sites are observed by FT-IR with pyridine as probe molecule (Figure 5.8). Anatase TiO_2 samples present high number of Lewis acid sites, wherein ISO and BUT samples show values around 90-100 μmol/g (Table 5.3). On the other hand, TiO_2 P25 and RUT samples exhibit lower amounts of acid sites.

In general, anatase TiO_2 samples here used (ISO, BUT, P25 and ANA, respectively) present most of the Lewis acid sites (≈60%, Table 5.3) with weak acidity strength, and between 25-30% of the acid sites possess moderate acidity strength. Interestingly, while ANA and P25 only have ≤10% high strength acid sites, this proportion is slightly higher for ISO and BUT TiO_2 samples (≥15%), this enhancing their acid capacities and becoming more appropriate for their use as catalysts under disadvantageous conditions (i.e. in the presence of water). More importantly, the total density of acid sites calculated for ISO and BUT TiO_2 samples are close to 1.0 (Table 5.3), similarly to the values encountered for the CeZrO catalyst, which have shown excellent activities in condensation reactions in aqueous phase (see Table 4.2).

Table 5.1. Main physico-chemical and textural properties of TiO_2 materials used in this study.

TiO_2	Surface area (m^2/g)[a]	XRD relative peak intensity ratio			Raman		% F[c]
		(004) / (101)	(200) / (101)	(211) / (105)	E_g/A_{1g}	% {001}[b]	
ISO	91	0.24	0.97	2.10	1.85	55	3.6
BUT	96	0.23	1.01	2.20	1.49	69	5.1
P25	50	0.30	0.48	0.88	5.04	20	0.0
ANA	100	0.29	0.46	1.01	3.47	29	0.0
RUT	2	-	-	-	-	-	0.0

[a] Calculated values from N_2 adsorption isotherms (BET method). [b] %{001} facet exposition is estimated by the ratio of Raman vibrational modes between E_g and A_{1g}[25]. [c] Calculated by X-Ray fluorescence spectrometry (XRF).

Table 5.2. Average size dimensions estimation (nm) for faceted TiO_2 nanoparticles.

Catalyst	Scherrer´s equation from XRD data	SEM, TEM and HRTEM studies
TiO_2-ISO	26	42
TiO_2-BUT	22	35

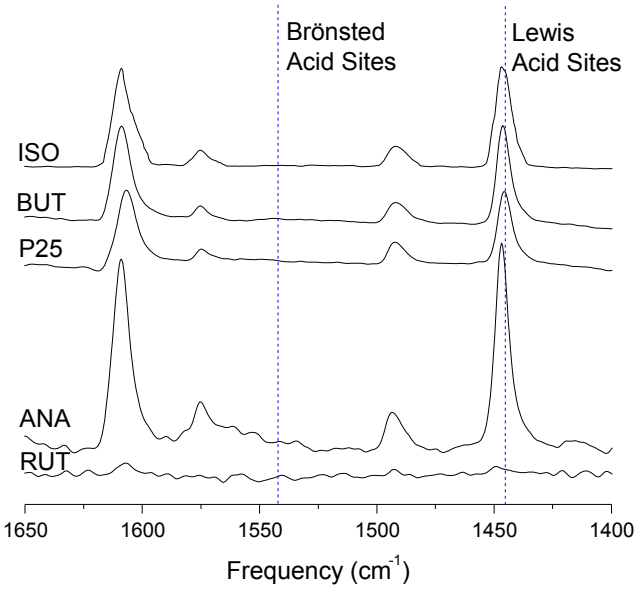

Figure 5.8. FT-IR (pyridine) spectra of the TiO_2 samples measured after pyridine desorption at 150 ºC.

Table 5.3. Acid properties of TiO_2 materials measured by FT-IR with pyridine adsorption and desorption at different temperatures.

TiO_2	Surface area (m^2/g)[a]	Lewis Acid Sites, LAS[b] (µmol/g)			Density of LAS[c] (µmol/m^2)
		150 ºC	250 ºC	350 ºC	
ISO	91	101	25	14	1.1
BUT	96	89	18	13	0.9
P25	50	64	23	8	1.3
ANA	100	187	62	17	1.9
RUT	2	12	0	0	5.6

[a] Calculated values from N_2 adsorption isotherms (BET method). [b] Values calculated from pyridine adsorption/desorption FT-IR measurements. [c] Density of Lewis acid sites (LAS).

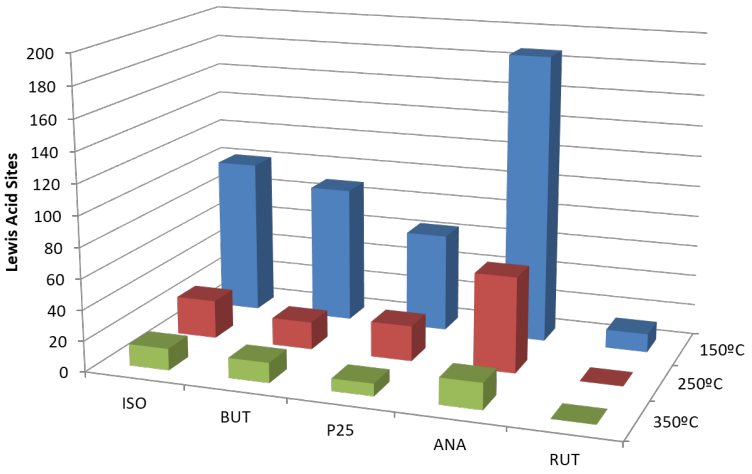

Figure 5.9. Lewis acid sites (LAS) of the different TiO_2 samples measured by FT-IR with pyridine adsorption and desorption at different temperatures.

In addition, X-ray fluorescence measurements reveal that residual fluorine species are present in both ISO and BUT TiO_2-based samples, in amounts of 3.6% and 5.1%, respectively (Table 5.1). Afterwards, XPS measurements were performed over these TiO_2-based samples. F(1s), O(1s) and Ti(2p) XPS spectra are shown in Figure 5.10. First of all, a very symmetric and well-defined single peak at ≈683.9±0.2 eV can be observed, ascribed to fluoride in Ti-F on the TiO_2 surface. Any signal at 688.5 eV ascribed to substituted F^- can be noticed. Therefore, fluorine ions are all adsorbed on TiO_2 surface and atomic incorporation of F atoms in the crystalline lattice can be ruled out. This data is also consistent with the presence of high-energy F-Ti bonds in the surface, which significantly lower the surface energies and make {001} facet more stable during the catalyst synthesis.

Additional information about titanium and oxygen species arises from XPS measurements. On one hand, Ti(2p) spectra shows symmetric peaks at 458.6±0.2 eV and 464.3±0.2 eV ascribed to Ti $2p^{3/2}$ and $Ti2p^{1/2}$, respectively. Both peaks correspond to Ti^{4+} species, whereas Ti^{3+} is not observed in any of the analyzed samples (Figure 5.10 and Table 5.4). On the other hand, O(1s) spectra shows two different contributions: a major contribution at 529.6±0.2 eV ascribed to structural O^{2-} and a minor contribution at 531.2±0.2 eV ascribed to surface hydration/hydroxylation oxygen species. Surface atomic composition is calculated (Table 5.4) and Ti:O ratio on the surface of TiO_2 samples is estimated. Both faceted ISO and BUT samples present Ti:O ratios slightly higher than P25 and anatase commercial catalysts, previously estimated from literature[26].

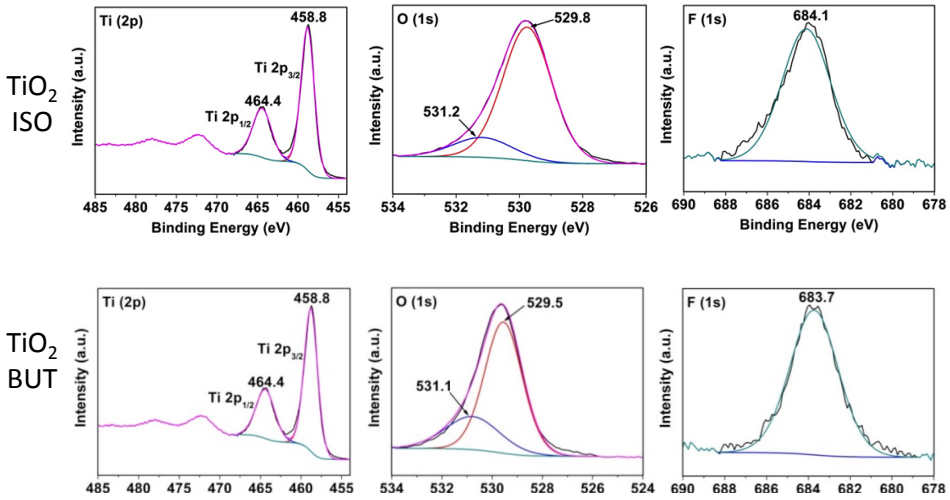

Figure 5.10. X-ray photoelectron spectroscopy (XPS) Ti_{2p}, O_{1s} and F_{1s} of TiO_2 ISO and BUT samples.

Table 5.4. Surface atomic composition of TiO_2 samples measured by XPS.

Catalyst	Surface atomic composition (%)					
	Ti (2p)	O (1s) Structural O^{2-}	O (1s) Hydration OH	F (1s)	Ti:O ratio	Ti^{4+} / Ti^{3+} (%)
	458.8 eV	529.8 eV	531.2 eV	683.9 eV		
ISO	26.65	55.10	9.85	8.40	0.48	100
BUT	24.22	49.32	18.15	8.31	0.49	100
P25[a]	28.37	64.47	7.16	-	0.44	100
ANA[a]	29.26	66.50	4.24	-	0.44	100

[a] *Values from literature*[26].

TiO_2 samples were also characterized by IR-KBr measurements to identify Ti-OH signals. Characteristics signals ascribed to Ti-OH bonds on the catalyst surface were observed at 3480 cm^{-1}, but quantitative differences were not clearly distinguished among anatase and faceted TiO_2 samples. This fact is consistent with Ti-F signals not being detected during Raman spectroscopy measurements.

All these physicochemical and textural properties of faceted TiO_2 samples (mainly summarized in Table 5.1 and 5.3) make these materials become promising catalysts for condensation reactions of oxygenated compounds in aqueous phase. In particular, the importance of {001} facet exposition and the influence of fluorine species in the surface will be discussed along the activity and stability tests.

5.2.3 *Catalytic performance of TiO_2 samples in the condensation reaction of a mixture of oxygenated compounds in aqueous phase*

Selected TiO_2–based samples, such as ISO, BUT, ANA, P25 and RUT were tested as catalysts in the transformation of oxygenated compounds present in an aqueous model mixture including acetic acid (30wt%), ethanol (10%wt), propanal (25wt%) and acetol (10wt%). The liquid phase system was introduced in an autoclave reactor at 200 ºC and P_{N2} = 13 bar during 7h. Moderate temperature and pressure conditions have always been used along this work (see also Section 3.4).

Catalytic results obtained for the different TiO_2–based materials expressed in terms of total organic yield and yield to the main reaction products are shown in Table 5.5. In particular, results are discussed in terms of conversion of each one of the oxygenated compounds used as reactants and yields to intermediates (2-methyl-2-pentenal and C_5-C_8 fractions) and C_9-C_{10} hydrocarbons fractions, as the main reaction products and finally, ethyl acetate as the main by-product. A schematic reaction network, analogous to that shown in Chapter 3 is provided in Figure 5.11 as a reminder, while more information about reactions taking place is detailed in Chapter 3.

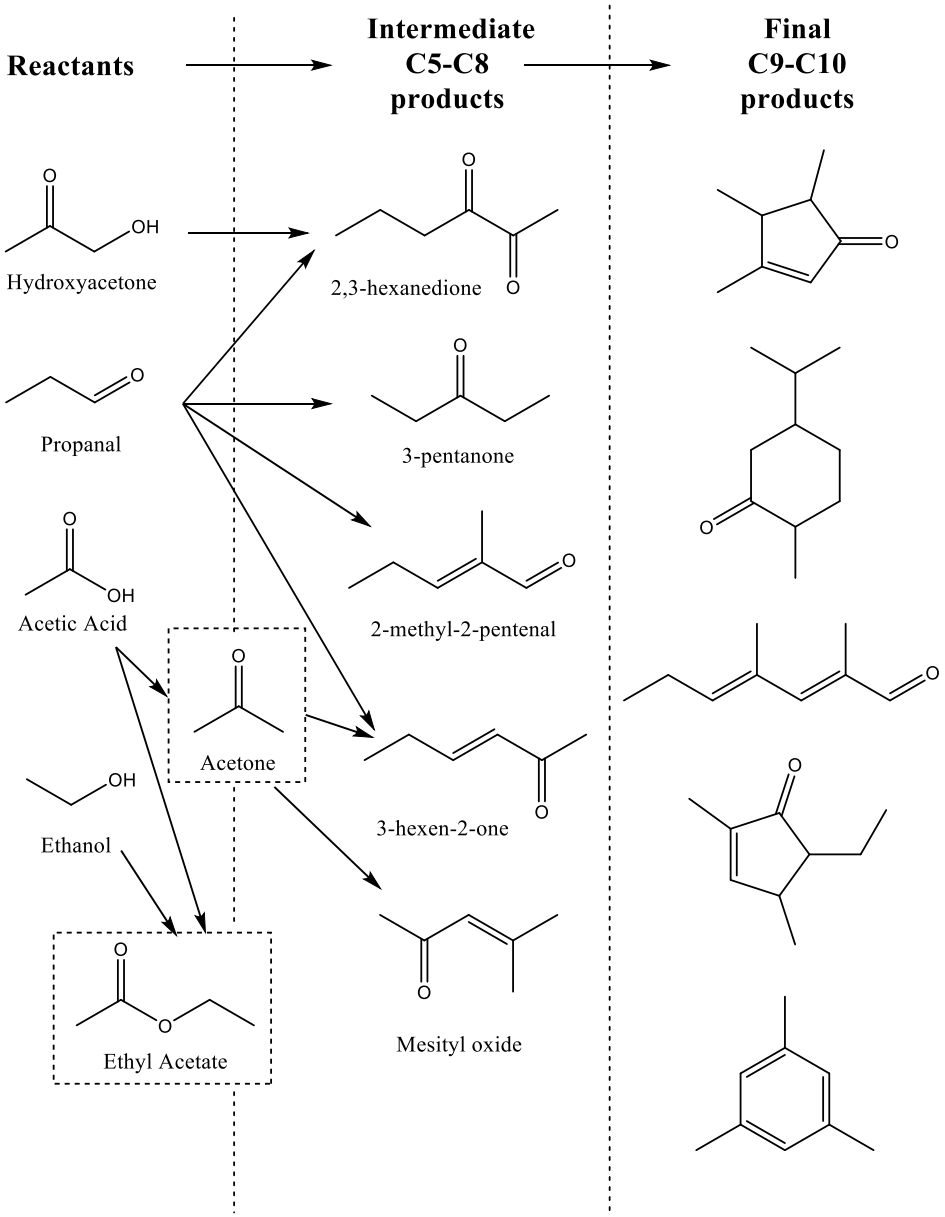

Figure 5.11. Reaction network for the condensation of oxygenated compounds in aqueous-phase catalysed by TiO_2-based materials.

As can be seen in Table 5.5, faceted TiO_2 materials (ISO and BUT TiO_2-based samples) exhibit higher total organic product yields than TiO_2-P25, these results being much higher when compared to anatase (ANA) and rutile (RUT) TiO_2 commercial catalysts. In particular, ISO and BUT TiO_2 samples present total acetol conversion, high propanal conversion (>83%) and medium ethanol (≈50%) and acetic acid (≈20%) conversion. Acetic acid mainly reacts via esterification to produce ethyl acetate, while low amounts of acetone are detected. Then, main reaction products come from consecutive aldol condensation reactions. This data is consistent with previous reports in literature, where carboxylic acids strongly bind at acid-base pairs and convert via ketonization at much lower rates than aldol condensation reactions of other carbonyl compounds. Moreover, moderated temperature conditions used along these experiments even maximize this catalytic behaviour.

In this sense, the most important differences among products yields are observed in intermediate products. A strong increase on 2-methyl-2-pentenal yields (derived from propanal self-aldol condensation) is observed when faceted TiO_2 materials are employed. On the contrary, the yields of C_9-C_{10} products (from 2nd condensation steps) are practically the same for all the TiO_2 samples employed, with the exception of TiO_2-RUT, which shows much lower values of these final products. This data is also consistent with previous reports, which show a higher activation barrier for condensation on rutile than on anatase surfaces[3,4]. The same trend is observed for ethyl acetate (acetic acid and ethanol esterification product), its yield keeping more or less constant on all the samples studied after 7h reaction (Table 5.5).

Table 5.5. Data of reactants conversions and organic products yields for TiO_2 materials in the condensation reaction of oxygenated compounds in aqueous phase.

	Catalyst	ISO	BUT	P25	ANA	RUT
Conversion (%)	Acetic acid	21.8	19.4	20.0	16.4	9.8
	Propanal	85.2	83.4	79.2	66.4	58.4
	Ethanol	48.1	51.6	41.6	46.0	39.0
	Acetol	100.0	100.0	100.0	100.0	100.0
Product Yield (%)	Ethyl acetate	20.8	21.2	23.3	28.1	23.4
	2M2P[a]	37.4	37.9	31.4	28.9	25.0
	C5-C8	14.4	14.8	13.8	8.4	15.0
	C9-C10	13.2	12.6	16.0	13.7	8.2
	Total	**65.0**	**65.3**	**61.2**	**51.0**	**48.2**
Carbon balance (%)		95	94	95	97	98

Reaction conditions: 3 g of aqueous mixture, 150 mg of catalyst; T=200 ºC, P=13 bar N_2, t= 7h. [a]2M2P=2-methyl-2-pentenal.

When total organic products yields are plotted against reaction time (Figure 5.12), differences in catalytic activity can be analogously observed. A sharp increase in total product yield is observed at short reaction times (1-3h), whereas total yields practically reach a *plateau* after 5h for most of the samples. Reaction was held until 7h to increase the amount of C_9-C_{10} products in the final mixture. It is worth noting that phase separation occurs after this reaction time, especially when faceted TiO_2 and P25 samples are employed. An organic fraction enriched in heavier and long-chain products is interestingly obtained, this fact being very useful for further processing.

From catalytic results at short reaction times, reaction rates at 1h can be calculated (Table 5.6). ISO and BUT TiO_2 materials present higher reaction rates and total organic products yields in only 1h when compared to commercial catalysts. If these values are normalized taking into account the density of acid sites (see also Table 5.3), the differences between catalysts can be more easily observed as both faceted TiO_2 materials exhibit higher activity than the rest of commercial titanium oxides (Table 5.6). Moreover, if total organic products yields at 1h are normalized taking into account the number of acid sites (μmol/g) for comparable structures (ISO, BUT and ANA samples), both faceted TiO_2 materials exhibit much higher activity per acid site under these reaction conditions than commercial TiO_2 anatase catalyst.

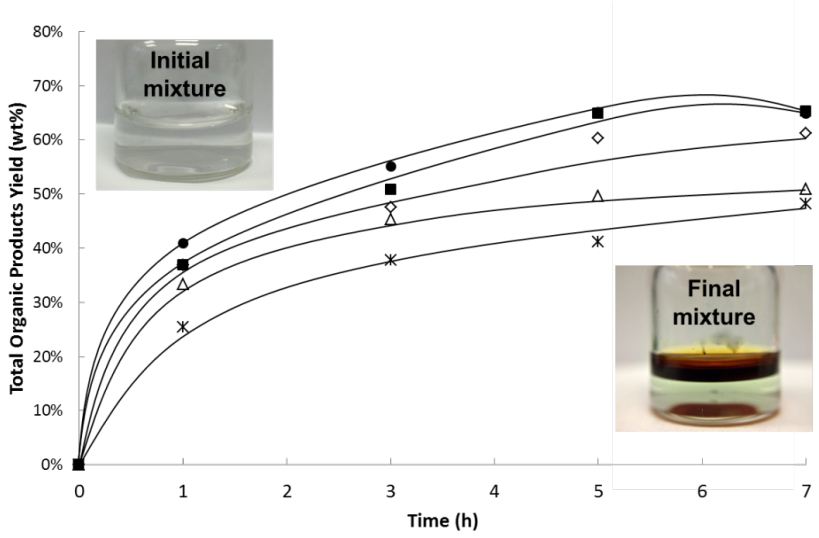

Figure 5.12. Total organic products yield in function of reaction time. ISO (●), BUT (▪), P25 (◊), ANA (Δ) and RUT (*) TiO_2 samples. Reaction conditions: aqueous model mixture (3.00 g) and catalyst (0.15 g) at 13 bar N_2 and 200 ºC under continuous stirring during 7 h.

Table 5.6. Main catalytic results and reaction rates at 1h for TiO_2 materials in the condensation reaction of oxygenated compounds in aqueous phase.

TiO_2	Reaction rate at 1h ($\mu molmin^{-1}g^{-1}$)	Total Products Yield (wt%)	Total Products Yield /($\mu mol/m^2$)
ISO	1345	40.9	36.9
BUT	1387	36.8	39.6
P25	1232	36.9	28.8
ANA	1086	33.4	17.9
RUT	942	25.4	4.5

Reaction conditions: aqueous model mixture (3.00 g) and catalyst (0.15 g) in autoclave-type reactor, at 13 bar N_2 and 200 ºC under continuous stirring during 1h.

At this point, it was interesting to ascertain the role of fluorine species in the catalytic activity observed for faceted TiO_2 materials. In this sense, and in order to rule out the possibility of the action of HF species dissolved in the reaction medium (by leaching of F^- to the aqueous solution), a catalytic experiment was carried out using Anatase TiO_2 (ANA) material with the addition of 2.9wt% of HF into the aqueous solution (ANA+HF). The attained results are detailed in Table 5.7 and compared with both ISO and ANA TiO_2 catalysts. As can be seen, the yields to the intermediates (2M2P and C_5-C_8) and final products (C_9-C_{10}), as well as the total organic products yield achieved with the incorporation of HF in the reaction medium are much lower than those reached with the ISO TiO_2 sample. Moreover, carbon balance is lower in this case, as HF acts as a strong homogeneous catalyst and promotes polymerization reactions.

In addition, the Anatase TiO_2 sample was impregnated with HF attaining 3.6wt% of F^- species in the solid, and then used as catalyst in the oxygenated compounds condensation in aqueous phase. As can be seen in Table 5.7, even in this case, the results obtained are lower when comparing with ISO TiO_2 catalyst, this meaning that the method of fluorine incorporation by hydrothermal synthesis leads not only to the formation of the desired {001} faceted TiO_2, but also to the correct incorporation of fluorine species in the solid. Indeed, the presence of these fluorine species was detected by XRF and XPS measurements, as it was previously commented, and ascribed to Ti-F type moieties.

Table 5.7. Influence of HF incorporation method on the catalytic activity of TiO_2-ANA catalyst in the conversion of oxygenated compounds present in aqueous model mixtures.

Catalyst		ISO	ANA+HF	ANA+HF	ANA
F content (wt%)		3.6	2.9	3.6	0.0
Incorporation method		Hydrot.[a]	Added[b]	Impreg.[c]	-
Product Yield (%)	Ethyl acetate	20.8	25.3	29.6	28.1
	2M2P[a]	37.4	29.4	27.0	28.9
	C5-C8	14.4	13.9	9.0	8.4
	C9-C10	13.2	10.8	14.3	13.7
	Total	**65.0**	**54.1**	**50.3**	**51.0**
Carbon balance (%)		95	90	93	97

Reaction conditions: 3 g of aqueous mixture, 150 mg of catalyst; T=200 ºC, P=13 bar N_2, t= 7h. [a]2M2P=2-methyl-2-pentenal. [a] Hydrothermal synthesis of TiO_2-ISO with HF. [b] HF added into the aqueous solution. [c] TiO_2-ANA impregnated with HF.

Summarizing, the high surface area and the presence of adequate acid sites in the TiO_2-based materials play an important role in this type of condensation reactions. Lewis acid centers on faceted TiO_2 materials

seem to show an outstanding activity in the condensation of light organic compounds in complex aqueous mixtures. The relevance of {001} facet exposition and the stability of acid centers in the presence of organic acids and water will be discussed in detail.

5.2.4 Effect of H_2O and acetic acid on catalytic results of TiO_2-based materials

Catalytic studies using complex reaction mixtures containing diverse oxygenated compounds in water are necessary to test materials under realistic conditions. Moreover, single molecule studies are required to gain better understanding about catalysts behaviour. In this sense, reactions with varying concentration of water and acetic acid were performed in order to analyze differences between TiO_2-ISO and TiO_2-ANA materials at short reaction times (1h). Details of the different scenarios considered for this study are given in Table 5.8.

Table 5.8. Composition (wt%) of different mixtures used in this section.

Scenario	Propanal (wt%)	H_2O (wt%)	Acetic Acid (wt%)	Acetol (wt%)	Ethanol (wt%)
Initial 1	-	-	30	-	70
Initial 2	25	-	-	-	75
A	36	-	43	7	14
B	25	-	30	5	40
C	25	30	-	-	45
D	25	30	30	-	15
E	25	30	30	5	10

Firstly, two initial scenarios are considered, where acetic acid and propanal reactivity are individually studied in the absence of water, using ethanol as solvent and no additional organic compounds. Both TiO_2-ISO and TiO_2-ANA show comparable results. On one hand, acetic acid is remarkably converted (96% and 88% respectively) via esterification to produce ethyl acetate. On the other hand, propanal is also highly converted (92% and 89% respectively) with a similar product distribution profile for both TiO_2 materials.

Subsequently, the effect of water is studied. It is worth noting, that water is produced in all the desired reactions, so its concentration directly affects equilibrium and reaction rates. Three different scenarios (Table 5.8) are considered: A) water is eliminated and relative concentration of all reactants is kept constant, B) the amount of water is replaced by ethanol and E) reference aqueous model mixture is used. As can be seen in Figure 5.13, high conversion of propanal is reached in only 1 hour and 68.3% of total organic products yield is achieved when TiO_2-ISO is used in the absence of water in the reaction medium (Scenario A, Table 5.9). Propanal conversion and total organic yield results slightly decrease (from 86.7 to 72.4%, ≈16% decay) when a higher concentration of ethanol is added (Scenario B) as esterification reactions are maximized (notice that acetic acid conversion increase from 46.0 to 56.6%). Finally, when 30wt% of water is added to the mixture, a drastic decrease on propanal conversion (from 86.7 to 42.9%, ≈50% decay, Figure 5.13) is observed. Moreover, C_9-C_{10} products from second condensation reaction steps are also influenced by the amount of water (being reduced from 10.7% yield in Scenario A to 2.9% yield in Scenario E).

In the case of anatase TiO_2 sample, propanal conversion only reaches 71.0% in 1 hour of reaction when water is not added (Scenario A, Table 5.10), while a strong decay in propanal conversion c.a. 28% (from 71.0 to 47.6%) is observed with higher ethanol concentration in the medium (Scenario B). More importantly, the presence of water in the system has a tremendous impact on the catalytic activity of TiO_2 anatase, with a relative decrease in propanal conversion of ≈64% (from 71.0 to 24.8%, Figure 5.13). Thus, although similar detrimental effects are detected in both samples (see Table 5.9 and 5.10), the catalytic activity decay is more pronounced in the case of anatase TiO_2 sample.

Table 5.9. Catalytic activity in the conversion of oxygenated compounds of TiO_2-ISO catalyst using different aqueous model mixtures.

TiO_2-ISO / Scenario		A	B	C	D	E
Conversion (%)	Acetic acid	46.0	56.6	-	25.0	17.1
	Propanal	86.7	72.4	73.6	58.0	42.9
	Ethanol	75.4	36.8	0.0	36.3	33.9
	Acetol	100.0	100.0	-	-	87.8
Product Yield (%)	2M2P[a]	37.6	32.6	60.5	34.8	23.9
	C5-C8	20.0	25.8	6.2	6.5	14.1
	C9-C10	10.7	7.0	3.0	1.7	2.9
	Total	**68.3**	**65.4**	**69.7**	**43.0**	**40.9**
Carbon balance (%)		95	100	100	98	100

Reaction conditions: 3 g of aqueous mixture, 150 mg of catalyst; T=200ºC, P=13 bar N_2, t= 1h. [a]2M2P=2-methyl-2-pentenal.

Table 5.10. Catalytic activity in the conversion of oxygenated compounds of TiO_2-ANA catalyst using different aqueous model mixtures.

TiO_2-ANA / Scenario		A	B	C	D	E
Conversion (%)	Acetic acid	49.1	56.9	-	28.5	20.5
	Propanal	71.0	47.6	66.4	37.7	24.8
	Ethanol	71.7	31.2	0.0	28.8	29.6
	Acetol	100.0	100.0	-	-	78.5
Product Yield (%)	2M2P[a]	26.5	16.5	52.3	22.5	15.2
	C5-C8	18.6	22.0	8.5	5.0	12.6
	C9-C10	9.6	4.1	3.0	0.8	5.6
	Total	**54.6**	**42.6**	**63.8**	**28.3**	**33.4**
Carbon balance (%)		94	96	100	92	98

Reaction conditions: 3 g of aqueous mixture, 150 mg of catalyst; T=200ºC, P=13 bar N_2, t= 1h. [a]2M2P=2-methyl-2-pentenal.

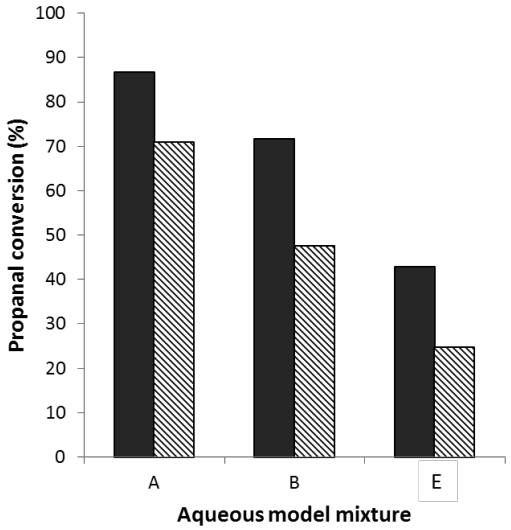

Figure 5.13. Effect of water content on propanal conversion for TiO_2-ISO (filled) and TiO_2-ANA (striped). Reaction conditions: aqueous model mixture (3.00 g) and catalyst (0.15 g) at 13 bar N_2 and 200 ºC under continuous stirring during 1h.

From these data, it is quite clear that catalytic activities in the oxygenated compounds condensation are higher in the case of TiO_2-ISO, mainly when water is present in the reaction medium. Under these circumstances, Lewis acid sites created by facet exposition together with fluorine concentration on TiO_2-ISO surface play an essential role on catalytic behaviour.

In this sense, thermogravimetric (TG) analyses of fresh samples were performed in order to study water adsorption in both ISO and ANA TiO_2 samples (Figure 5.14). Firstly, a first mass loss is detected under 100 ºC corresponding to water adsorption on the surface of both materials. A stronger decay is observed for anatase TiO_2 sample, which is in accordance with the above-mentioned results. An additional mass loss is noticed in the case of TiO_2-ISO among 300-400 ºC probably related to fluorine species leaching from catalyst surface. On the other hand, experiments using anatase TiO_2 sample impregnated with equivalent amounts of HF or even with direct addition of the acid in the reaction media already discussed, evidenced that any beneficial catalytic effect is observed in both cases (see Table 5.7).

Consequently, the importance of fluorine species (stable at temperature reaction conditions) on faceted TiO_2 materials relies on its function as capping agent to selectively control the growth of more reactive {001} facets during the hydrothermal synthesis, together with the slightly useful hydrophobic effect they seem to create.

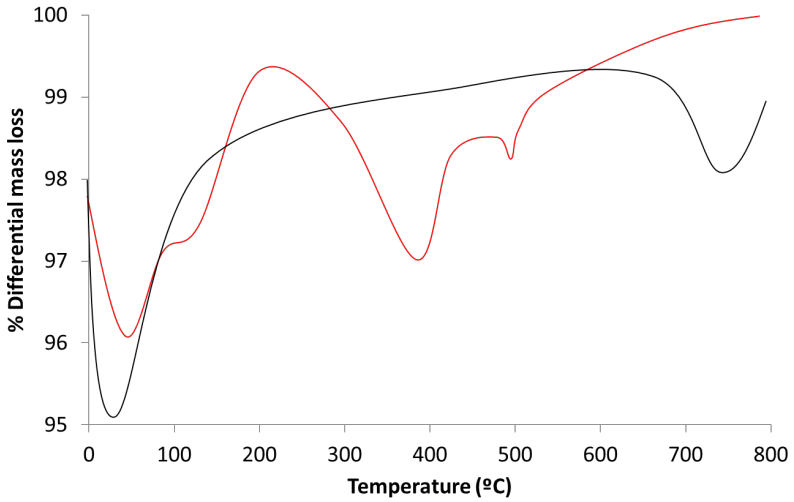

Figure 5.14. % Differential mass loss (first derivative curve) measured by TG of fresh samples. TiO_2-ISO (red) and TiO_2-ANA (black).

In the same way, three different scenarios are considered to study the effect of acetic acid on condensation reactions: C) propanal condensation without acetic acid, D) propanal condensation in the presence of 30wt% of acetic acid and E) reference aqueous model mixture are compared.

Primarily, detrimental effect of water on condensation reactions over TiO_2-based materials is once more confirmed if Scenario C (with water) and the initial scenario (without water) are compared. Propanal conversion decreases from 92 to 74% in the case of TiO_2-ISO and from 89 to 66% when TiO_2-ANA is used (see Figure 5.15).

Moreover, substantial differences in products distribution profiles can be observed among these scenarios: When acetol is not present in the initial mixture (Scenarios C and D), low amounts of other C_5-C_8 products are observed because 2-methyl-2-pentenal (propanal self-condensation) is the main intermediate product. In addition, lower C_9-C_{10} products yields

are observed under these scenarios compared when cross-condensation reactions are taking place.

Fundamentally, as it can be seen in Figure 5.15, propanal conversion progressively decreases when acetic acid is added and complex mixtures are used. While propanal conversion (at 1h) varies from 74 to 43% when TiO_2-ISO is employed (Figure 5.15A), more evident differences (66 to 25%) are observed when TiO_2-ANA is used (Figure 5.15B).

Therefore, Lewis acid centers present in faceted titanium oxides are more resistant to the presence of organic acids. These results can explain why faceted titanium oxides exhibit higher total organic products yields when a complex aqueous mixture is studied in the consecutive condensation of light oxygenated compounds. This is a crucial fact if these materials want to be applied in a real bio-refinery effluent.

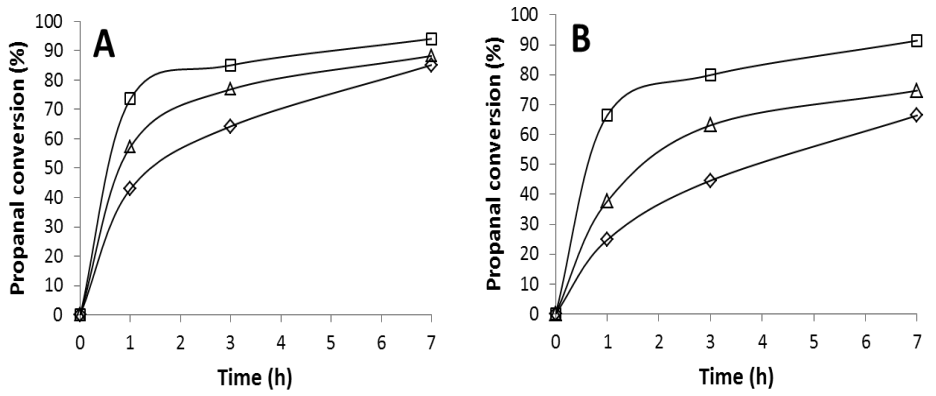

Figure 5.15. Effect of the presence of acetic acid on propanal conversion for TiO_2-ISO (A) and TiO_2-ANA (B). Reaction conditions: aqueous model mixture (3.00 g) and catalyst (0.15 g) at 13 bar N_2 and 200 ºC under continuous stirring during 7 h. Aqueous mixture composition: 25wt% propanal, 30wt% H_2O and 45wt% ethanol (Scenario C; □), 25wt% propanal, 30wt% H_2O, 30wt% acetic acid and 15wt% ethanol (Scenario D; Δ) 25wt% propanal, 30wt% H_2O, 30wt% acetic acid, 5wt% acetol and 10wt% ethanol (Scenario E; ◊).

5.2.5 Effect of heat-treatments and facet exposition on catalytic results of TiO_2-based materials

Once the effect of residual fluorine species has been mainly defined on the preferential growth of {001} facets on TiO_2, the importance of tailoring crystal facets on these materials must be confirmed. In this sense, it is well known that post-synthesis heat-treatments can modify crystalline structure and physicochemical properties of metal oxides. Thus, the following step is to study the influence of post-synthesis heat-treatment on the facet exposition and the catalytic performance of TiO_2-ISO. This material is employed under three additional conditions and it is compared to TiO_2-ANA as a reference material. TiO_2-ISO sample is treated during 2h under an air atmosphere at 250 ºC, 400 ºC and alternatively under a hydrogen atmosphere at 400 ºC.

XRD relative peak intensity ratios and hence, the crystalline structure of faceted titanium oxides progressively vary when stronger heat-treatment conditions are applied (Figure 5.16 and Table 5.11). Higher temperature conditions and hydrogen atmosphere cause a reversion in the {001} facet exposition. As it can be seen in Figure 5.17, total organic products yield also decrease when heat-treatment conditions are applied. Therefore, catalytic results are unequivocally directly related to {001} facet exhibition.

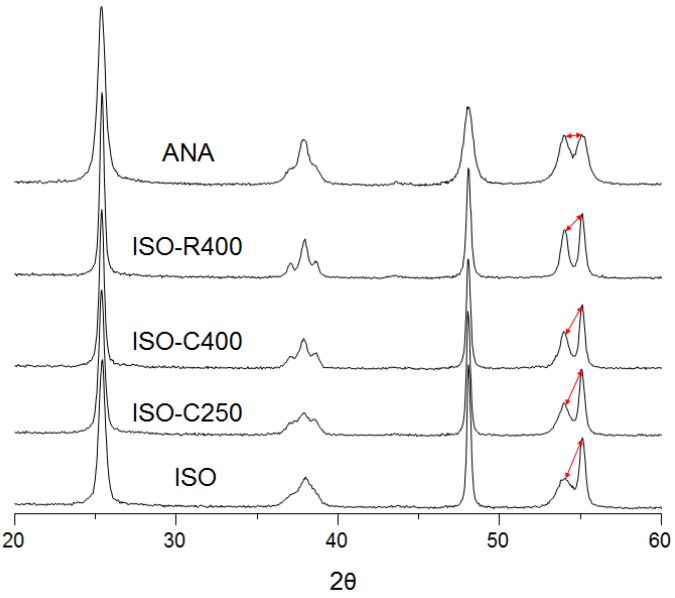

Figure 5.16. XRD pattern of TiO_2-ISO under different heat-treatment conditions and TiO_2-ANA as reference material.

Table 5.11. XRD relative peak intensity ratio and catalytic results when different heat-treatment conditions are applied.

	Catalyst	ISO	ISO	ISO	ISO	ANA
	Heat treatment	-	C250	C400	R400	-
Catalysts characterization	(004)/(001)	0.24	0.19	0.22	0.24	0.29
	(200)/(101)	0.97	0.86	0.70	0.61	0.46
	(211)/(105)	2.10	1.84	1.62	1.32	1.01
	F content (wt%)	3.6	-	0.7	0.7	0.0
Product Yield (%)	Ethyl acetate	20.8	21.3	26.6	23.1	28.1
	2M2P[a]	37.4	32.4	31.9	30.5	28.9
	C5-C8	14.4	16.9	16.2	12.6	8.4
	C9-C10	13.2	12.4	10.4	10.2	13.7
	Total	**65.0**	**61.7**	**58.5**	**53.3**	**51.0**
Carbon balance (%)		95	93	97	93	97

Reaction conditions: 3 g of aqueous mixture, 150 mg of catalyst; T=200 ºC, P=13 bar N_2, t= 7h. [a]2M2P=2-methyl-2-pentenal.

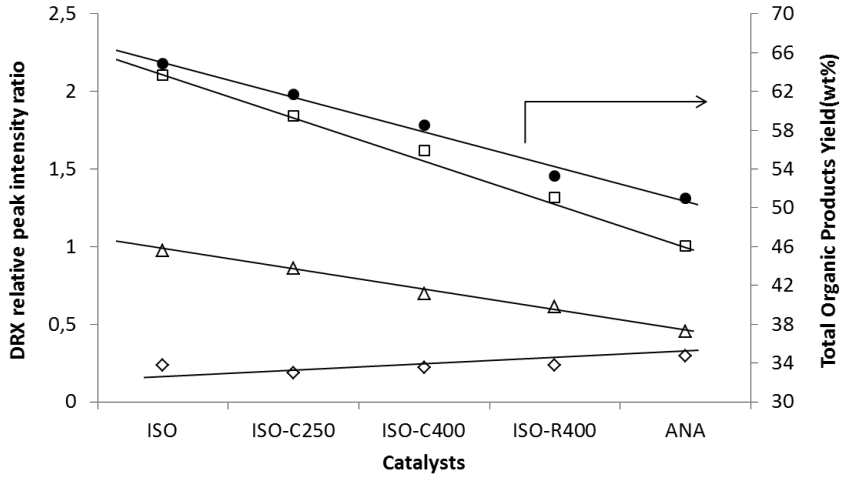

Figure 5.17. Correlation between {001} facet exposure measured by XRD relative peak intensity ratios (004/001 (◊), 200/101 (Δ) and 211/105 (□)) and total organic products yield (●). Reaction conditions: aqueous model mixture (3.00 g) and catalyst (0.15 g) at 13 bar N_2 and 200 ºC under continuous stirring during 7 h.

Moreover, additional catalyst characterization was performed after the different heat-treatment conditions. In particular, UV-Visible and XPS measurements were carried out to elucidate titanium oxidation state and possible changes in fluoride species present in the materials (Figure 5.18 and Figure 5.19).

Firstly, UV-Visible measurements show that titanium species stay invariable regardless of H_2 heat-treatment conditions. It could be say that, in general, similar UV-Visible spectra and derived E_{gap} values are obtained for the three TiO_2 based samples studied. Moreover, these titanium species do not suffer any variation after their use in condensation reactions in aqueous phase, whether or not a previous calcination or reduction procedure has been applied to the samples.

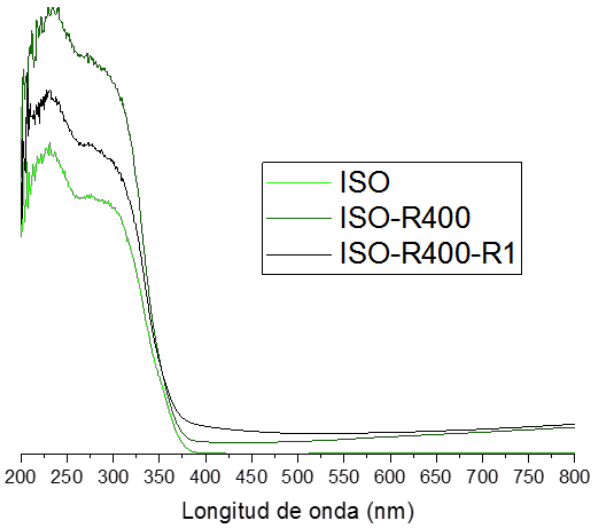

Figure 5.18. UV-Visible measurements of ISO, ISO-R400 and ISO-R400 after one re-use in the condensation of oxygenated compounds.

Analogous information can be achieved by XPS Ti(2p) spectra shown in Figure 5.19. Ti species stay invariable regardless of different heat-treatment conditions. Ti(2p) spectra shows symmetric peaks at 458.7±0.2 eV and 464.3±0.2 eV ascribed to Ti $2p^{3/2}$ and $Ti2p^{1/2}$ respectively. Both peaks correspond to Ti^{4+} species, whereas Ti^{3+} is not observed in any of the analyzed samples. Then, reduced centers do not form during H_2 treatment at 400 ºC, consistent with the higher temperatures typically required to form O vacancies in TiO_2-anatase samples. O(1s) spectra always shows the two different contributions previously observed: one at 529.6±0.2 eV ascribed to structural O^{2-} and one at 531.2±0.2 eV ascribed to surface hydration O^{2-} species. Nonetheless, slight quantitative differences can be observed depending on the heat-treatment. TiO_2-ISO sample initially shows a 15% of 531.2 eV signal assigned to hydration O^{2-}, which is reduced to 12% when the sample is calcined at 250 ºC, due

to the elimination of adsorbed water molecules. On the contrary, this signal increases to 29% after the H_2-treatment, although O/Ti ratio close to 2 is always observed, surface not suffering any stequiometric variation regardless of heat-treatments. Finally, F(1s) spectra shows a symmetric single peak at 683.9±0.2 eV for ISO and ISO-C250 samples, ascribed to fluoride species (Ti-F) on the TiO_2 surface. On the contrary, reduction treatment at 400 ºC drives to two different effects: On one hand, high temperatures cause fluorine species decomposition (see Figure 5.14 and Table 5.11) and F^- species decrease from 3.6 to 0.7 wt%. Moreover, the nature of remaining F^- species is different as two peaks at 683.7 eV and 685.9 eV are observed ascribed to different Ti-F adsorbed species, whereas any signal at 688.5 eV ascribed to substituted F^- can be noticed.

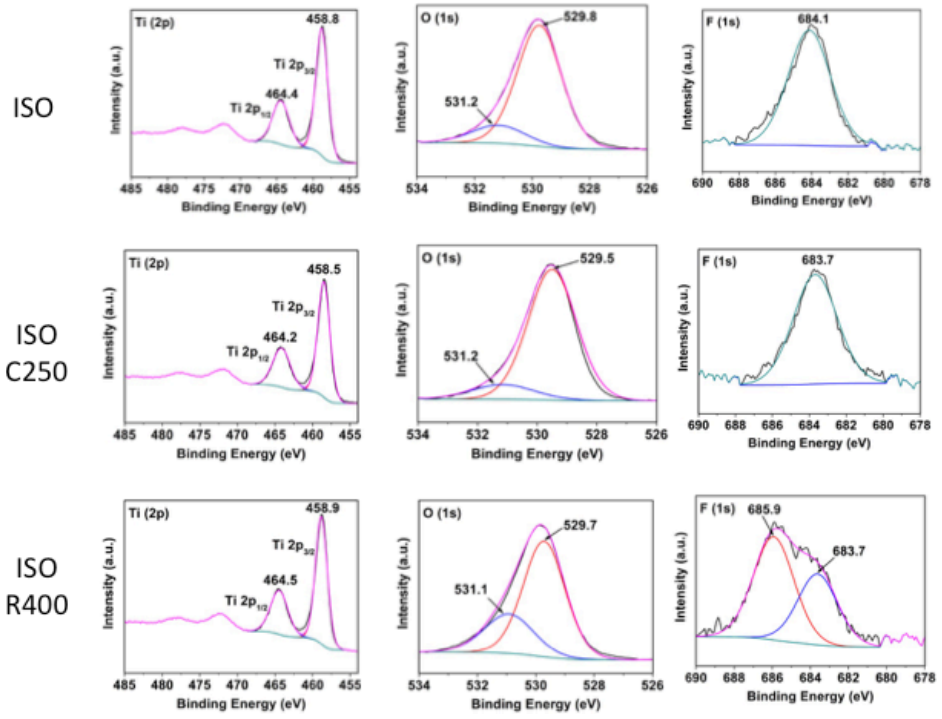

Figure 5.19. X-ray photoelectron spectroscopy (XPS) Ti_{2p}, O_{1s} and F_{1s} of ISO, ISO-C250 and ISO-R400 TiO_2 samples.

5.2.6 Stability tests

Catalysts stability is essential when dealing with the processing of aqueous effluents, especially those containing organic acids and several oxygenated organic compounds. Moreover, the maintenance of crystalline structure and {001} facet exposition is crucial to maintain catalytic activity in TiO_2-based materials. Therefore, recycling experiments are performed testing selected TiO_2-ISO catalyst to corroborate its resistance under reaction conditions in the oxygenated compounds condensation in aqueous phase.

Stability tests are performed by using the catalyst several times. Once the catalytic experiment is finished, the solid is separated and washed repeatedly with methanol. Finally, after drying at 100 ºC overnight, the solid is analyzed by elemental analysis (EA), thermogravimetric (TG) measurements and X-Ray fluorescence to determine the organic compounds deposition in the surface of the catalyst and fluorine species composition, respectively (Table 5.13). FT-IR studies of pyridine adsorbed on used TiO_2-ISO sample were also performed to confirm that the same Lewis acid sites remain responsible for the catalytic activity even though water and acidic medium were used.

Catalytic results in terms of total organic products yield attained are given in Table 5.12 and Figure 5.20. As it can be clearly seen, TiO_2-ISO catalyst maintains its catalytic performance practically invariable after four consecutive reuses.

Table 5.12. Reuse of TiO_2-ISO catalyst in the transformation of oxygenated compounds present in aqueous model mixture.

	Catalyst	REF	R0	R1	R2	R3
Conversion (%)	Acetic acid	21.8	22.6	17.1	14.5	15.0
	Propanal	85.2	85.0	82.5	82.6	82.6
	Ethanol	48.1	44.1	46.6	47.3	46.2
	Acetol	100.0	100.0	100.0	100.0	100.0
Product Yield (%)	Ethyl acetate	20.8	23.9	24.0	23.2	22.9
	2M2P[a]	37.4	36.8	35.9	34.4	33.9
	C5-C8	14.4	15.1	14.8	14.5	16.1
	C9-C10	13.2	12.6	13.7	14.7	13.4
	Total	**65.0**	**64.5**	**64.4**	**63.6**	**63.4**
Carbon balance (%)		95	94	97	97	96

REF (reference results), R0 (1st use), R1 (2nd use), R2 (3rd use) and R3 (4th use). Reaction conditions: 3 g of aqueous mixture, 150 mg of catalyst; T=200 ºC, P=13 bar N_2, t=7h. [a]2M2P=2-methyl-2-pentenal.

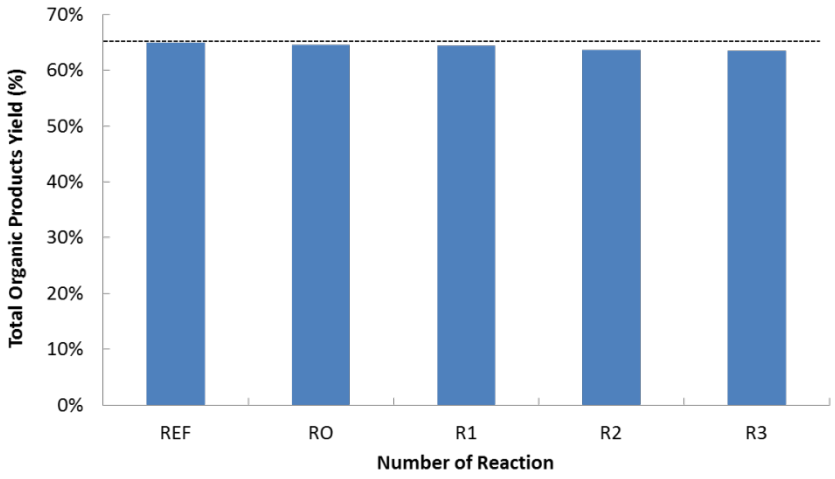

Figure 5.20. Stability tests of TiO_2-ISO catalyst in oxygenated compounds condensation in aqueous phase. Reaction conditions: aqueous model mixture (3.00 g) and catalyst (0.15 g) in autoclave-type reactor, at 13 bar N_2 and 200 ºC under continuous stirring during 7h.

The great stability shown by the faceted TiO_2-ISO catalyst is mainly due to the structure preservation. XRD pattern of the used catalysts after four reuses show the maintenance of crystalline structure for faceted TiO_2 samples (Figure 5.21).

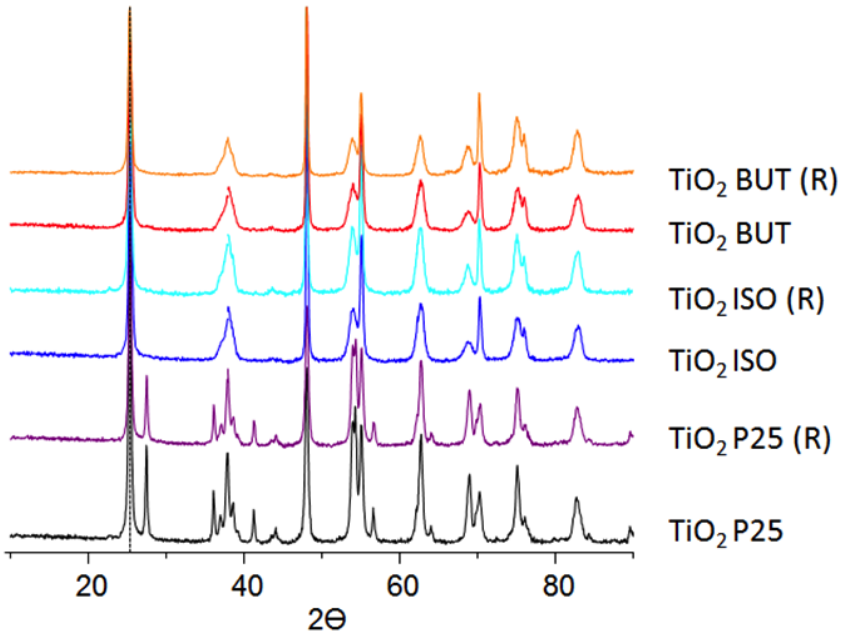

Figure 5.21. XRD pattern of TiO_2-ISO, TiO_2-BUT and TiO_2-P25 after four consecutive reuses in the condensation of organic compounds present in an aqueous model mixture.

Moreover, {001} facet exposition remains essentially unchanging and only narrow differences can be observed even when the catalyst have been used in reaction for 7 hours during four consecutive cycles (Table 5.13). Moreover, only a small amount of carbon (<1%) mainly due to carbonaceous compounds deposition is measured by EA and TG, this explaining the slight deactivation observed in the catalyst.

More interestingly, both amount and strength of Lewis acid sites remain stable and responsible for the catalytic activity after four consecutive reuses (see Table 5.14 and Figure 5.22). These catalysts show much better stability results to those obtained with CeZrO materials, which suffered from a deeper catalytic deactivation when used in the same operation conditions (see Chapter 4).

Table 5.13. Characterization data of TiO_2-ISO material after four consecutive reactions in the transformation of oxygenated compounds present in aqueous model mixture.

TiO_2	DRX relative peak intensity ratio			Organic compounds deposition (%)		F content (%)[c]
	(004) / (001)	(200) / (101)	(211) / (105)	TG[a]	EA[b]	
ISO-R0	0.24	0.97	2.10	-	-	3.6
ISO-R3	0.23	0.90	1.98	0.9	1.9	1.8

[a] *TG: Mass loss (wt%) measured by thermogravimetric analysis.*
[b] *EA: Carbon deposition (wt%) measured by elemental analysis.*
[c] *Amount of fluorine species determined by X-Ray fluorescence.*

Table 5.14. Acid properties of TiO_2-ISO fresh and used catalysts measured by FT-IR with pyridine adsorption/desorption at different temperatures.

TiO_2	Lewis Acid Sites, LAS [a] (µmol/g)		
	At 150 ºC	At 250 ºC	At 350 ºC
ISO-RO	101	25	14
ISO-R1	99	38	39

[a] Values calculated from pyridine adsorption/desorption FT-IR measurements.

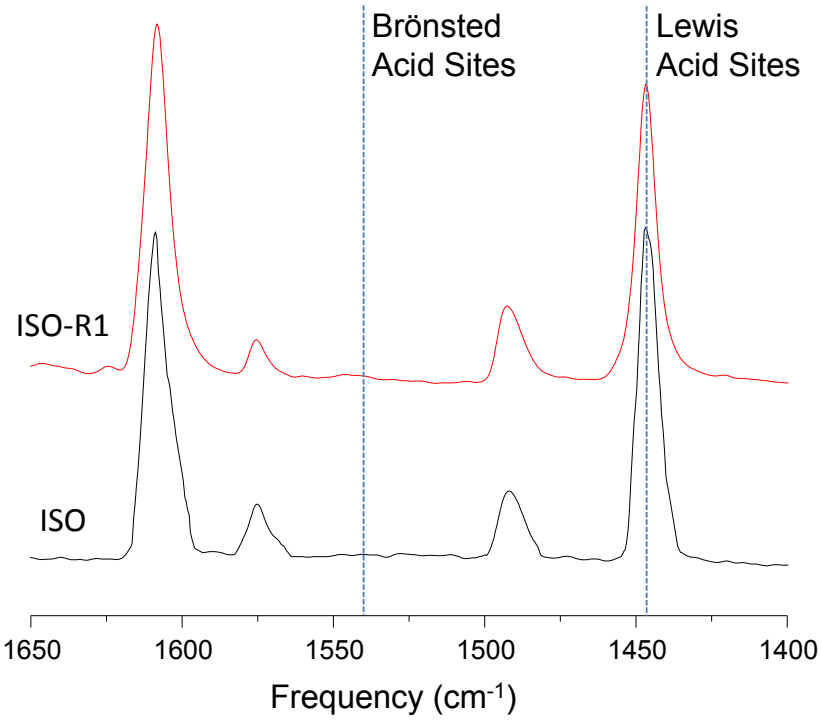

Figure 5.22. FT-IR spectra for TiO_2-ISO catalyst, measured after pyridine desorption at 150 ºC, for both TiO_2-ISO fresh and reused samples.

From the above-mentioned results, it can be concluded that TiO_2-ISO catalyst shows outstanding stability under reaction conditions, maintaining practically unaltered its activity after several re-uses. In particular, Lewis acid sites present in the faceted TiO_2 material are more stable in the presence of organic acids under aqueous environments. This opens new possibilities for the application of this type of materials in the valorisation of light oxygenated compounds present in biomass-derived aqueous effluents.

5.3 Conclusions

- Hydrothermally synthesized faceted titanium oxides have shown great catalytic activity and outstanding stability results in the valorisation of representative light oxygenated compounds present in an aqueous model mixture.

- The addition of aqueous HF during the TiO_2-based catalyst synthesis is essential to selectively control the preferential growth of catalytic more reactive {001} facets.

- Residual fluorine species seem to have a slight useful hydrophobic effect on TiO_2 surface, but not any particular beneficial catalytic effect during condensation reactions. On the contrary, catalytic results are totally influenced by tailoring of crystal facets of titanium oxide.

- Lewis acid sites on faceted TiO_2 have great stability in condensation reactions, especially in the presence of organic acids under aqueous environments. Thus, these materials have shown better results than other commercial titanium oxides when complex reaction mixtures are tested under moderated operation conditions. Precise control of crystalline structure and morphology opens up a new strategy to improve titanium oxides as effective catalysts in the upgrading of aqueous biomass-derived effluents.

5.4 References

1. Gangadharan, A., Shen, M., Sooknoi, T., Resasco, D. E. & Mallinson, R. G. *Appl. Catal., A. Gen.* **385,** 80–91 (2010).
2. Hakim, S.H., Shanks, B.H. & Dumesic, J.A. *Appl. Catal., B. Environ.* **142–143,** 368–376 (2013).
3. Wang, S., Goulas, K. & Iglesia, E. *J. Catalysis* **340,** 302–320 (2016).
4. Wang, S. & Iglesia, E. *J. Catalysis* **345,** 183–206 (2017).
5. Oliver-Tomas, B., Renz, M. & Corma, A. *J. Mol. Catal. A: Chem* **415,** 1–8 (2016).
6. Pham, T.N., Shi, D., Sooknoi, T. & Resasco, D.E. *J. Catalysis* **295,** 169–178 (2012).
7. Aranda-Pérez, N., Ruiz, M. P., Echave, J. & Faria, J. *Appl. Catal., A. Gen.* **531,** 106-118 (2017).
8. Wang, Z., Lv, K., Wang, G., Deng, K. & Tang, D. *Appl. Catal., B. Environ.* **100,** 378–385 (2010).
9. Luan, Y., Jing, L., Wu, J., Xie, M. & Feng, Y. *Appl. Catal., B. Environ.* **147,** 29–34 (2014).
10. Pan, X., Zhang, N., Fu, X. & Xu, Y.-J. *Appl. Catal., A. Gen.* **453,** 181–187 (2013).
11. Liu, G. *et al. Chem. Rev.* **114,** 9559–9612 (2014).
12. Jiang, H.B. *et al. Angew. Chem. Int. Ed.* **50,** 3764–3768 (2011).
13. Gong, X.Q. & Selloni, A. *J. Phys. Chem. B* **109,** 19560–19562 (2005).
14. Kim, K.S. & Barteau, M.A. *J. Mol. Catal.* **63,** 103–117 (1990).
15. Kim, K.S. & Barteau, M.A. *J. Catalysis* **125,** 353–375 (1990).
16. Idriss, H., Pierce, K. & Barteau, M.A. *J. Am. Chem. Soc.* **113,** 715–716 (1991).
17. Idriss, H., Kim, K.S. & Barteau, M.A. *J. Catalysis* **139,** 119–133 (1993).
18. Idriss, H., Lusvardi, V. S. & Barteau, M. A. *Surf. Sci.* **348,** 39–48 (1996).
19. Idriss, H. & Barteau, M.A. *Catal. Lett.* **40,** 147–153 (1996).
20. Grabowska, E., Diak, M., Marchelek, M. & Zaleska, A. *Appl. Catal., B. Environ.* **156–157,** 213–235 (2014).
21. Yang, H. G. *et al. Nature* **453,** 638–641 (2008).
22. Dozzi, M. & Selli, E. *Catalysts* **3,** 455–485 (2013).
23. Iervolino, G. *et al. J. Catalysis* **339,** 47–56 (2016).
24. Lara, M.A., Sayagués, M.J., Navío, J.A. & Hidalgo, M.C. *J. Mater. Sci.* **53,** 435–446 (2018).
25. Tian, F., Zhang, Y., Zhang, J. & Pan, C. *J. Phys. Chem. C* **116,** 7515–7519 (2012).
26. Sola, A.C. *et al. Catal. Today* **266,** 53–61 (2016).

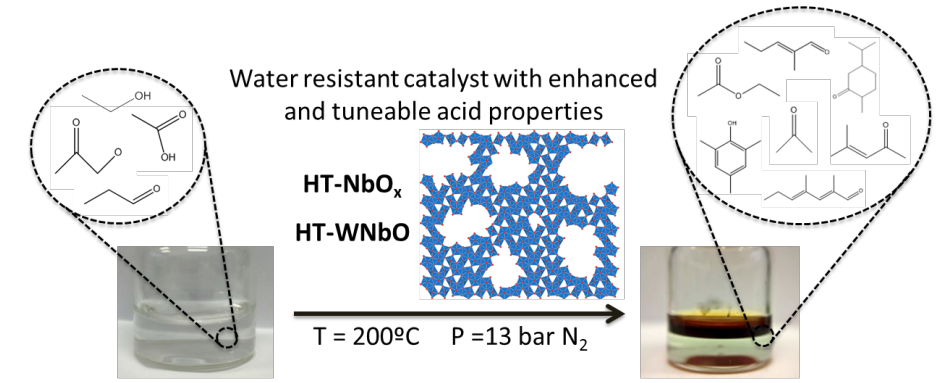

CHAPTER 6

NIOBIUM AND TUNGSTEN-NIOBIUM OXIDES AS ACID CATALYSTS FOR THE AQUEOUS-PHASE CONDENSATION OF OXYGENATED COMPOUNDS

6.1 Introduction

Faceted TiO_2 materials with enhanced acid properties discussed in Chapter 5 have improved the catalytic activity of TiO_2 anatase materials. Nevertheless, these results have also shown the need to design new hydrothermally resistant acid catalysts to meet demanding requirements present in biomass-derived aqueous mixtures valorisation processes.

Based on these considerations, the stability and acid properties of niobium oxides at high reaction temperatures (even in the presence of water) make these materials attractive for industrial use as heterogeneous catalysts[1–3]. While several inorganic oxides including zeolites and other metal oxides have their Lewis acid sites partially/totally deactivated in the presence of water (due to the formation of Lewis acid-base adducts), niobic acid ($Nb_2O_5.nH_2O$) has shown Lewis acid sites with potential activity in aqueous environments.

$Nb_2O_5.nH_2O$ is usually an amorphous metal oxide composed mainly of distorted NbO_6 octahedra and NbO_4 tetrahedra (Figure 6.1)[1]. These last Lewis acid sites work in water due to NbO_4 tetrahedra still have effective positive charges as Lewis acid sites even after the formation of NbO_4-H_2O adducts[1]. Therefore, even when this M^+-H_2O adducts are formed, an oxygenated compound can still get coordinated and react via Lewis acid catalysis.

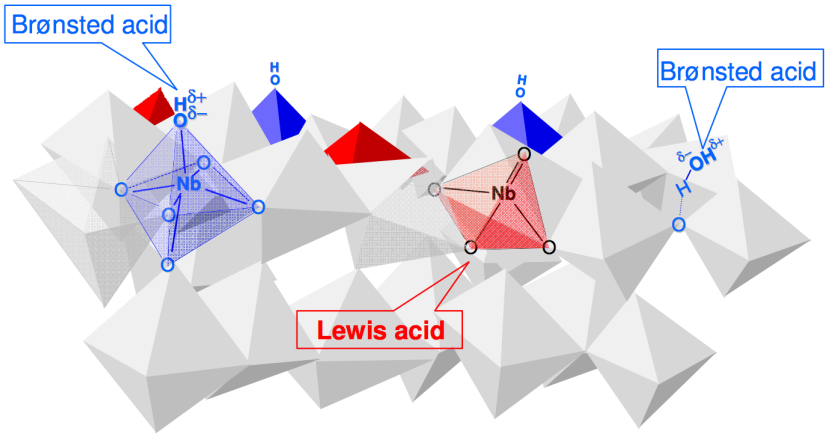

Figure 6.1. Schematic structure of $Nb_2O_5.nH_2O$ from Nakajima et al. [1].

In this sense, most of their Lewis acid sites remain active even in aqueous environments when tested in different reactions (i.e. acetalization, isomerization, allylation)[4,5]. More interestingly, niobium oxides also show great stability against organic acids. This is also a very important feature, due to the acid character of bio-oil derived aqueous streams, which is based on the presence of C_1-C_4 organic acids (i.e. formic, acetic and propionic acid, among others). Moreover, Nb_2O_5 crystalline structure, surface area and acid properties can be modified depending on the synthesis procedure and/or the post-synthesis thermal treatment[6,7]. These abilities can be exploited in order to synthesize Nb-based metal and mixed metal oxides with the adequate textural and physicochemical characteristics for a specific catalytic application.

With these ideas in mind, in a first section of this chapter, the influence of synthesis and post-synthesis procedures of different niobium oxides on their catalytic performance in the aqueous phase condensation of oxygenated compounds is studied.

Then, in a second part, the influence of synthesis and post-synthesis procedures of different tungsten-niobium mixed oxides on their catalytic performance in the same aqueous phase condensation of oxygenated compounds is studied. Moreover, reactions at different temperature conditions and with varying amount of water are carried out in order to achieve a deeper understanding of the reaction network and the advantages of niobium as water-resistant Lewis acid sites.

6.2 NbO_x-based materials

6.2.1 Synthesis of NbO_x-based materials

Nb-oxide based catalysts were prepared by two different synthesis procedures. On one hand, NbO_x-based materials were prepared by hydrothermal synthesis (HT-series) from acidified aqueous solutions containing niobium oxalate monooxalate adduct, following the procedure explained in Section 3.2.6. Specifically, 30.6 g of niobium oxalate were dissolved in 63.2 g of distilled water and kept 10 minutes under stirring at 80 ºC. Afterwards, this mixture was kept during 2 days in an autoclave-type reactor at 75 ºC, and the solid obtained was dried at 100 ºC during 16h.

On the other hand, niobium oxides were also prepared by conventional precipitation procedure (PR-series) using $NbCl_5$ as niobium precursor. The synthesis method is described in Section 3.2.4. For comparative purposes, commercial Nb_2O_5 catalyst from Sigma-Aldrich (C-series) was also tested.

Finally, all the niobium-based samples (including commercial catalysts) were heat-treated in air or N_2 at 300-550 ºC during 2h, with a heating rate of 2 ºC/min to obtain the final catalysts. In this sense, the influence of both the synthesis procedure and the heat-treatment conditions on the catalytic performance of different niobium oxides in the condensation of oxygenated compounds present in aqueous effluents (obtained by liquid phase separation of pyrolytic bio-oils) was studied.

The catalysts are named as HT-xy, PR-xy and C-xy (for hydrothermal, precipitation or commercial materials, respectively), where x is temperature and y is A or N, depending on the atmosphere (air or N_2, respectively) used during the heat-treatment. In addition, a $Ce_{0.55}Zr_{0.45}O_2$ mixed oxide (CeZrO) was used as the reference material in literature (as explained during Chapter 4).

6.2.2 Catalysts characterization

X-Ray diffraction patterns of HT-, PR- and C-series of samples calcined in N_2 at 450 ºC are shown in Figure 6.2. Significant differences in the crystallinity and the particle size of the different niobium oxides can be observed depending on the preparation procedure.

In this sense, HT-series and PR-series materials heat-treated at 450 ºC in N_2, tend to form a pseudo-crystalline (Figure 6.2a) or an amorphous phase (Figure 6.2b) respectively, while C-series sample gives rise to a well-ordered T-Nb_2O_5 phase (JCPDS: 00-027-1313) (Figure 6.2c). In addition, niobium oxides prepared by hydrothermal method show the lowest particle size (ca.10-20 nm) compared to other synthesis procedures (TEM images in Figure 6.2).

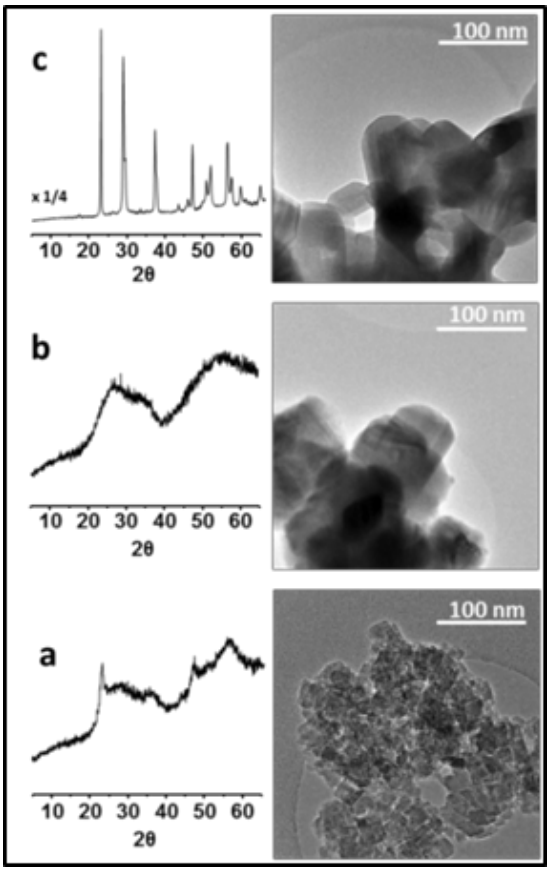

Figure 6.2. XRD patterns and TEM images of representative NbO_x-based catalysts, heat-treated in N_2 at 450 ºC: a) HT-450N; b) PR-450N; and c) C-450N.

Specifically, TEM images of HT-, PR- and C-series of samples calcined at 450 ºC in N_2 are shown in Figure 6.3, where clear differences in the crystalline structure can be distinguished.

Then, X-Ray diffraction patterns of HT-, PR- and C-series of samples for all the different heat-treatment conditions are shown in Figure 6.4, where the effect of calcination temperature and atmosphere on the NbO_x structure can be easily observed.

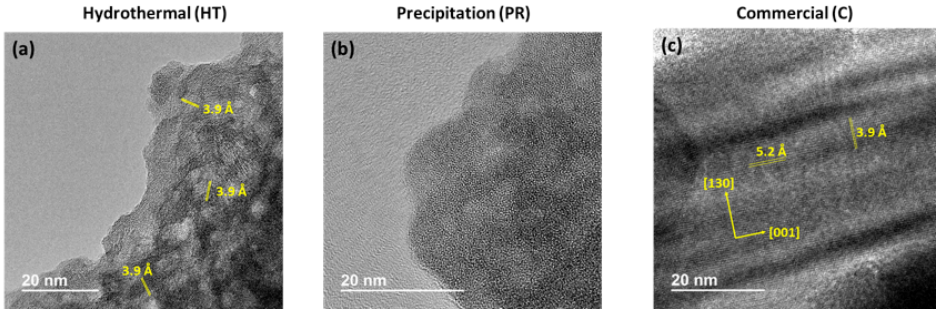

Figure 6.3. TEM images of pseudo-crystalline HT-450N (a), amorphous PR-450N (b) and crystalline C-450N (c) niobium oxide catalysts.

Pseudo-crystalline materials obtained through hydrothermal procedure present Bragg signals corresponding to (001) and (002) planes in a crystal structure ordered along c-axis (c = 3.9 Å), which is related to ReO_3-type structure (Figure 6.4 and Figure 6.3a), as it has been observed in other NbO_x-based materials[8,9]. It is noteworthy to mention that heat-treatments in air promote the crystallization, at least partially of the orthorhombic T-Nb_2O_5 phase (JCPDS: 00-027-1313) (Figure 6.4e).

On the other hand, PR-Nb_2O_5 samples show amorphous phase when calcined at 450-550 ºC in N_2, meanwhile a well-ordered structure arises when heat-treatment is realized under an air atmosphere (Figure 6.4i). Finally, C-Nb_2O_5 samples show a well-ordered crystal structure regardless the heat-treatment atmosphere (Figure 6.4j-l and Figure 6.3c).

Catalysts were also characterized by N_2 adsorption experiments to study the effect of synthesis procedure and calcination conditions on the surface area and pore volume of NbO_x samples. Main textural properties of these catalysts are shown in Table 6.1.

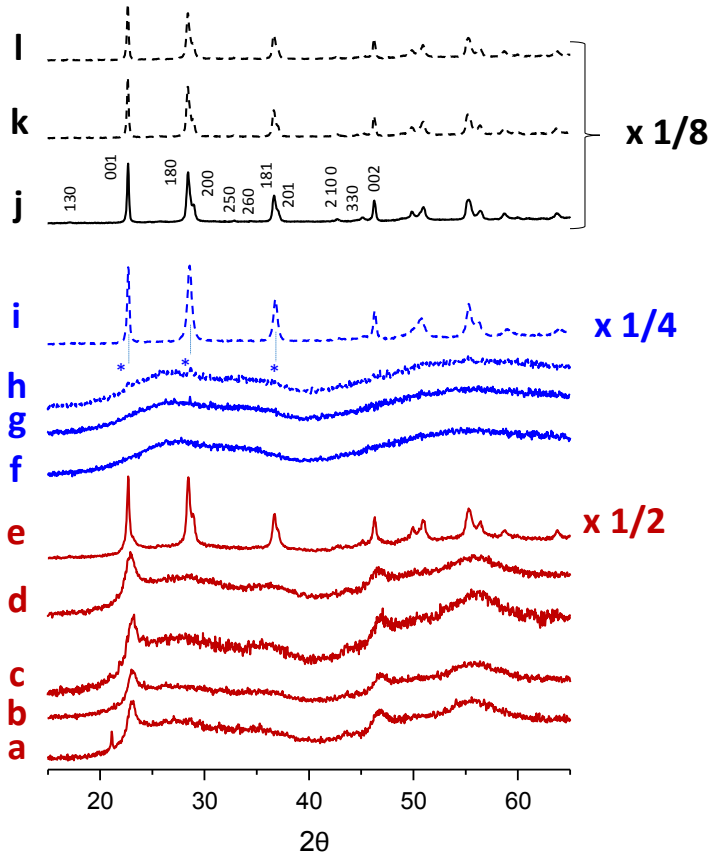

Figure 6.4. XRD profiles of NbO_x-based catalysts: a) HT-300N; b) HT-400N; c) HT-450N; d) HT-550N; e) HT-550A; f) PR-400N; g) PR-450N; h) PR-450A; i) PR-550A; j) C-450N; k) C-450A; and l) C-550A. Dashed lines: Samples heat-treated in air.

Pseudo-crystalline HT-NbO_x materials obtained through hydrothermal procedure after calcination at 550 ºC show higher surface areas (70 m^2/g) and pore volumes (0.075 cm^3/g) compared to PR- and C-series, which show low surface areas (10-40 m^2/g) and negligible porosity regardless the heat-treatment conditions. In particular, lower calcination conditions (300 ºC) drive to larger surface areas (150-160 m^2/g) and higher pore volumes (>0.1 cm^3/g) in the case of HT-samples. Moreover, a fraction of these pore volumes is assigned to the range of mesopores.

Table 6.1. Textural properties of catalysts used in this section.

Samples	Calcination Conditions	Surface Area (m^2/g)[a]	Pore Volume (cm^3/g)[b]	Mesopore Volume (cm^3/g)[b]
HT-series	300 ºC (N_2)	163	0.131	0.059
	400 ºC (N_2)	152	0.107	0.068
	450 ºC (N_2)	108	0.104	0.074
	550 ºC (N_2)	70	0.075	0.061
	550 ºC (air)	27	0.083	0.081
C-series	450 ºC (N_2)	13	0.012	0.009
	450 ºC (air)	13	0.011	0.007
	550 ºC (air)	13	0.011	0.008
PR-series	450 ºC (N_2)	26	0.022	0.021
	450 ºC (air)	36	0.023	0.022
	550 ºC (air)	9	0.023	0.021
CeZrO	450 ºC (air)	112	0.093	n.d.[c]

[a] *Calculated values from N_2 adsorption isotherms (BET method).* [b] *Calculated by BJH method.* [c] *n.d. = Non determined.*

Additionally, the type, both the amount and the nature of acid sites present in niobium oxide catalysts prepared by hydrothermal synthesis (HT-series), and heat-treated in the 300 to 550 ºC temperature range were studied and compared with those present in C- and PR-series by means of FT-IR spectroscopic measurements through pyridine adsorption and desorption at different temperatures. The calculated values for pyridine adsorption-desorption in the solids are given in Table 6.2. NbO_x-samples obtained through hydrothermal procedure (HT-series) show higher amounts of both Lewis and Brönsted acid sites compared to PR- and C-series, where minor acid properties are observed.

Table 6.2. Acid properties of catalysts used in this section.

Samples	Calcination Conditions	Acidity Measurements			
		LAS [a]	BAS [a]	BAS/LAS	Total Acidity[b]
HT-series	300 ºC (N_2)	135.3	41.5	0.31	1.08
	400 ºC (N_2)	54.7	57.4	1.05	0.74
	450 ºC (N_2)	65.4	33.5	0.51	0.92
	550 ºC (N_2)	20.6	16.1	0.78	0.52
	550 ºC (air)	-	-	-	-
C-series	450 ºC (N_2)	4.5	3.0	0.68	0.58
	450 ºC (air)	6.9	2.7	0.39	0.74
	550 ºC (air)	10.3	4.9	0.48	1.17
PR-series	450 ºC (N_2)	-	-	-	-
	450 ºC (air)	10.6	5.0	0.47	0.44
	550 ºC (air)	10.0	7.4	0.74	1.94
CeZrO	450 ºC (air)	87.6	17.4	0.20	0.94

[a] Values calculated by pyridine adsorption FT-IR measurements, in (μmol/g). [b] Total acidity (BAS + LAS) or density of acid sites, in μmol/m^2.

Additionally, as can be seen in Figure 6.5, the IR band assigned to the Lewis acid sites (LAS) is particularly well defined for all the hydrothermally prepared samples (HT-series), being the intensity of this IR band (assigned to LAS) much higher by lowering the heat-treatment temperature in these HT-Nb-based materials. Acid characteristics of HT-550A sample were not measured as it shows low surface area (see Table 6.1) and air heat-treatments drive to lower products yields (see Fig. 6.6).

In this sense, the density of total acid sites (expressed in μmol/m^2) increases when low heat-treatment conditions are applied. Both, the amount and density of actives sites are known to be relevant in condensation and ketonization reaction rates.

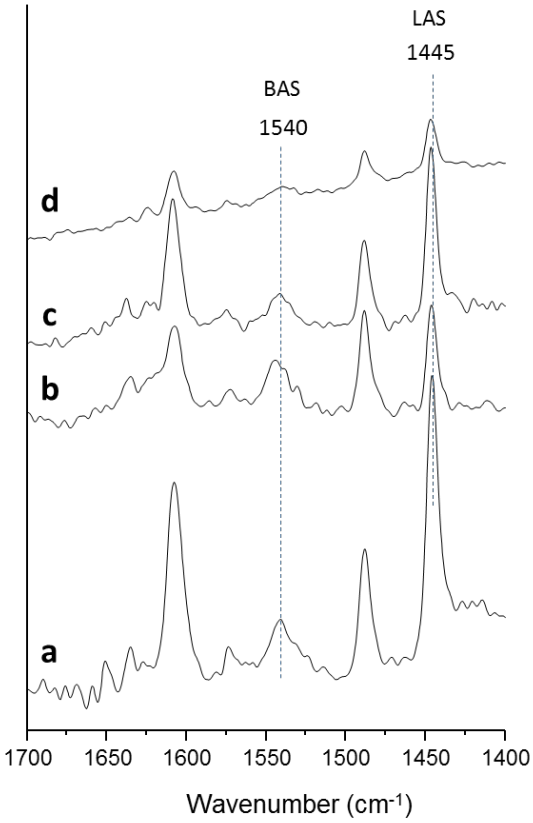

Figure 6.5. Pyridine IR adsorption spectra for samples prepared through hydrothermal method calcined under N_2 atmosphere: a) HT-300N; b) HT-400N; c) HT-450N; and d) HT-550N.
BAS: Brönsted acid sites; LAS: Lewis acid sites

In summary, niobium oxide based materials prepared by hydrothermal synthesis with a pseudo-crystalline structure (ordered just along c-axis) show higher surfaces areas, pore volumes and acid properties than other niobium oxides prepared by precipitation or commercial Nb_2O_5 catalysts. More interestingly, these HT-samples show tunable textural and acid properties when changing post-synthesis heat-treatment conditions.

6.2.3 Catalytic performance in the condensation reaction of a mixture of oxygenated compounds in aqueous phase

The catalytic behaviour of NbO_x-catalysts prepared by hydrothermal synthesis and using different post-synthesis heat-treatment conditions in the condensation of oxygenated compounds in an aqueous mixture is investigated. In this case, and similarly to reactions carried out in previous Chapter 4 and 5, an aqueous mixture of C_2-C_3 representative oxygenated compounds, closer to the real conditions at industry is used (see also Chapter 3). Catalytic results of HT-series of NbO_x catalysts are shown in Table 6.3, while comparative data obtained for PR- and C-series of samples are provided in Table 6.4. Results expressed in terms of reactants conversion and yield to the main reaction products are shown for experiments carried out at 200 ºC during 7h on stream.

In general, commercial Nb_2O_5 catalysts (with well-ordered structure) and PR-samples (presenting an amorphous nature) present the lowest catalytic activity (Table 6.4), whereas samples prepared hydrotermally (HT-series, with a pseudocrystalline structure) present the highest catalytic activity in aqueous-phase condensation reactions (Table 6.3).

In particular, hydrothermally synthesized niobium oxides (HT-series) reached higher propanal conversion (>90%) and 2-methyl-2-pentenal (2M2P) yields (Table 6.3), thus achieving the highest total organic products yields (see also Figure 6.6). The best results for HT-series of NbO_x catalyst are reached with HT-400N and HT-450N samples, which offer total organic product yields close to 70%.

Table 6.3. Data of reactants conversions and organic products yields for HT-NbO_x materials in the condensation reaction of oxygenated compounds in aqueous phase.

Catalyst	HT-	300N	400N	450N	550N	550A
Conversion (%)	Acetic acid	7.8	9.9	16.5	6.5	1.0
	Propanal	91.7	94.0	92.6	92.0	88.8
	Ethanol	53.3	45.5	44.1	51.9	52.4
	Acetol	100.0	100.0	100.0	100.0	100.0
Product Yield (%)	Ethyl acetate	19.3	22.3	25.0	20.3	20.0
	2M2P[a]	32.7	39.4	41.0	35.3	34.3
	C5-C8	10.3	12.3	11.0	10.7	10.7
	C9-C10	16.0	18.0	17.3	19.3	19.0
	Total	**59.0**	**69.7**	**69.3**	**65.3**	**64.0**
Carbon balance (%)		90	98	97	96	96

Reaction conditions: 3 g of aqueous mixture, 150 mg of catalyst; T=200 ºC, P=13 bar N_2, t= 7h. [a]2M2P=2-methyl-2-pentenal

Table 6.4. Data of reactants conversions and organic products yields for PR- and C-series of Nb-materials in the condensation reaction of oxygenated compounds in aqueous phase.

Catalyst		PR-series			C-series		
		450N	450A	550A	450N	450A	550A
Conversion (%)	Acetic acid	14.3	14.2	23.4	6.2	8.6	15.4
	Propanal	74.5	74.4	61.8	80.0	76.4	70.6
	Ethanol	44.5	53.5	47.7	47.9	53.5	50.7
	Acetol	100.0	100.0	100.0	100.0	100.0	100.0
Product Yield (%)	Ethyl	23.3	21.0	24.0	21.7	20.7	22.3
	2M2P[a]	26.4	25.6	25.0	31.0	27.0	26.7
	C5-C8	11.3	8.0	7.7	8.3	7.3	6.0
	C9-C10	14.3	16.7	15.6	21.7	18.0	16.3
	Total	**52.0**	**50.3**	**48.3**	**61.0**	**52.3**	**49.0**
Carbon balance (%)		97	87	85	97	91	86

Reaction conditions: 3 g of aqueous mixture, 150 mg of catalyst; T=200 ºC, P=13 bar N_2, t= 7h. [a]2M2P=2-methyl-2-pentenal

Moreover, hydrothermally synthesized niobium oxides (HT-series) reached higher carbon balances compared to PR- and C-series of catalysts. In this sense, heat-treatments under N_2 atmosphere promote better carbon balances in this type of samples.

Additionally, the effect of changing the atmosphere (air or N_2) used during heat-treatment of the different series of NbO_x-materials on the catalytic activity has also been studied. As can be seen in Figure 6.6, slight higher total organic products yields are observed when the heat-treatment is carried out in N_2 atmosphere, this behaviour being observed in the three different HT-, PR- and C-series of samples.

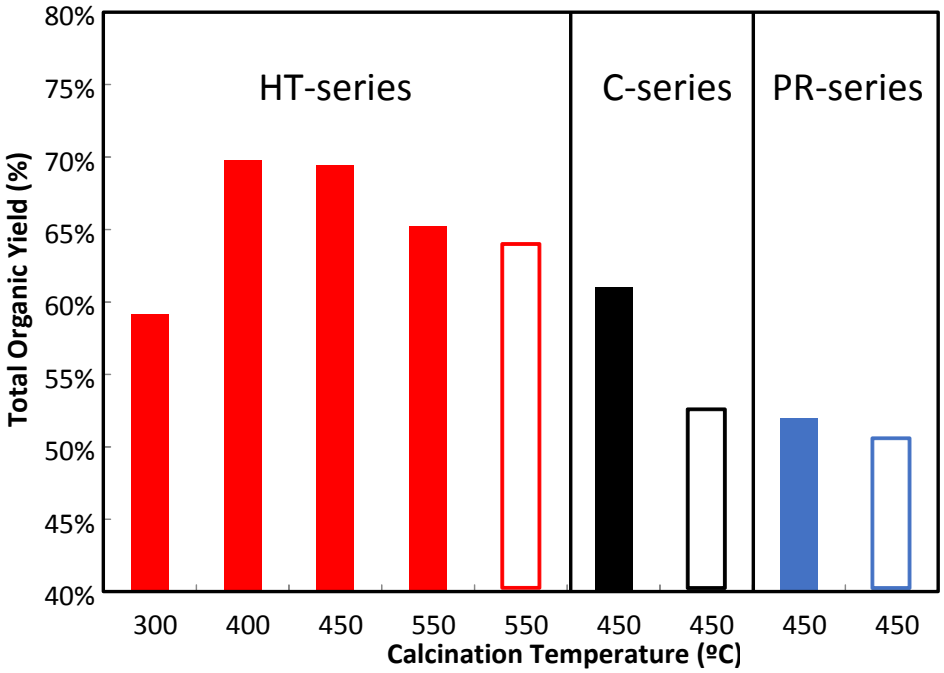

Figure 6.6. Catalytic activity (in total organic products yield) in the conversion of oxygenated compounds in aqueous model mixture of HT-, PR- and C-series of catalysts heat-treated under different conditions: N_2 (filled column) or air (empty column).

A deeper understanding about HT-series activity can be achieved by individually studying the behaviour of reactants conversion present in the aqueous model mixture (Figure 6.7a). Complete conversion of acetol and high conversion of propanal are reached in short times, while ethanol and acetic acid exhibit lower conversion (≈50% and 15%, respectively).

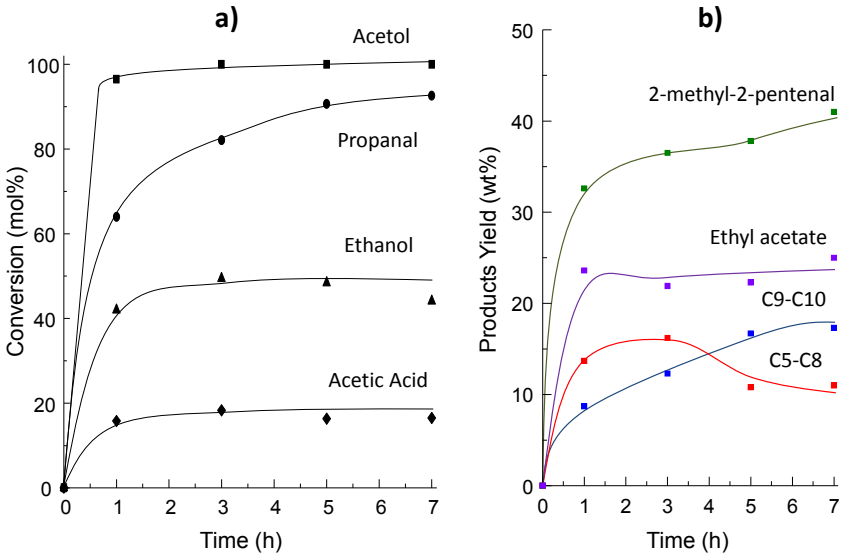

Figure 6.7. a) Conversion of acetic acid, ethanol, propanal and acetol; and b) evolution of products yields vs reaction time over HT-450N catalyst. Reaction conditions: 3.0 g of aqueous model mixture, 0.15 g of catalyst at 200 °C and PN_2 = 13 bar during 7h.

Note that a low acetic acid conversion is expected under the moderate reaction conditions used here, mainly due to the strong competition for the active sites of more reactive molecules (i.e. propanal and acetol). In addition, the identification of main reaction products by GC and GC-MS allow us to draw the evolution of products yield with reaction time when HT-450N sample was used (Figure 6.7b). Accordingly, a reaction network is once again proposed (Figure 6.8), in which the main intermediate (C_5-C_8) and final (C_9-C_{10}) products have been highlighted.

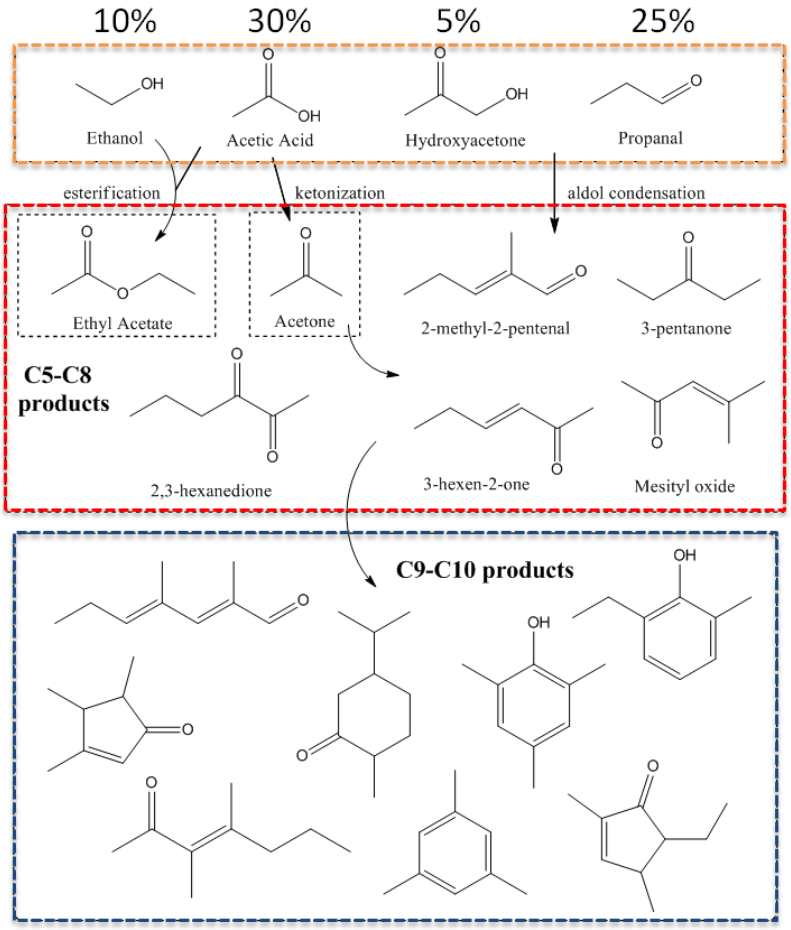

Figure 6.8. Reaction network for the condensation of oxygenated compounds in aqueous-phase catalysed by NbO_x-based materials.

Then, as can be seen in Figure 6.7b, high products yields are reached within 3 hours of time on stream due to fast condensation reactions among propanal and acetol, whereas ethyl acetate is produced from acetic acid and ethanol esterification. At higher reaction times, the products from the first condensation stage (C_5-C_8 intermediates, mainly formed by cross-condensation between acetol and propanal) are formed, which can continue to react with propanal or other intermediates

(acetone, 3 pentanone, etc.) to generate C_9-C_{10} products (Figure 6.7b and Figure 6.9). However, the ethyl acetate yield remains constant over time, suggesting that this reaction probably only takes place at the beginning of the experiment.

This same behaviour was observed for all NbO_x-samples regardless from the synthesis procedure (see Figure 6.9). As can be seen, products distribution curves in Figure 6.9b show that C_5-C_8 intermediates initially formed during reaction are consumed to produce the corresponding C_9-C_{10} final products via consecutive condensations, independently of the type of NbO_x-based materials used. Nevertheless, the catalytic activity data observed for the different types of NbO_x materials (Figure 6.9a) clearly demonstrate that the HT-series catalysts are rather more active than the corresponding PR- and C-series of samples.

The better catalytic performance of pseudocrystalline HT-samples can be explained in terms of their improved acid and textural properties. Thus, they show an increase in total acidity, surface areas (>70 m^2/g) and pore volumes, which probably favours a higher accessibility of reactants to active sites (Table 6.1 and Table 6.2).

The different crystalline structures of the materials seem to have only minor effects on the catalytic activity, being acid and textural properties more decisive in this case, thus giving rise to higher reaction rates (Table 6.5). In fact, it is more interesting to correlate physicochemical properties with catalytic results this way, as primary condensation reactions mainly take place at short reaction times (1-3h) as seen in Figure 6.7a.

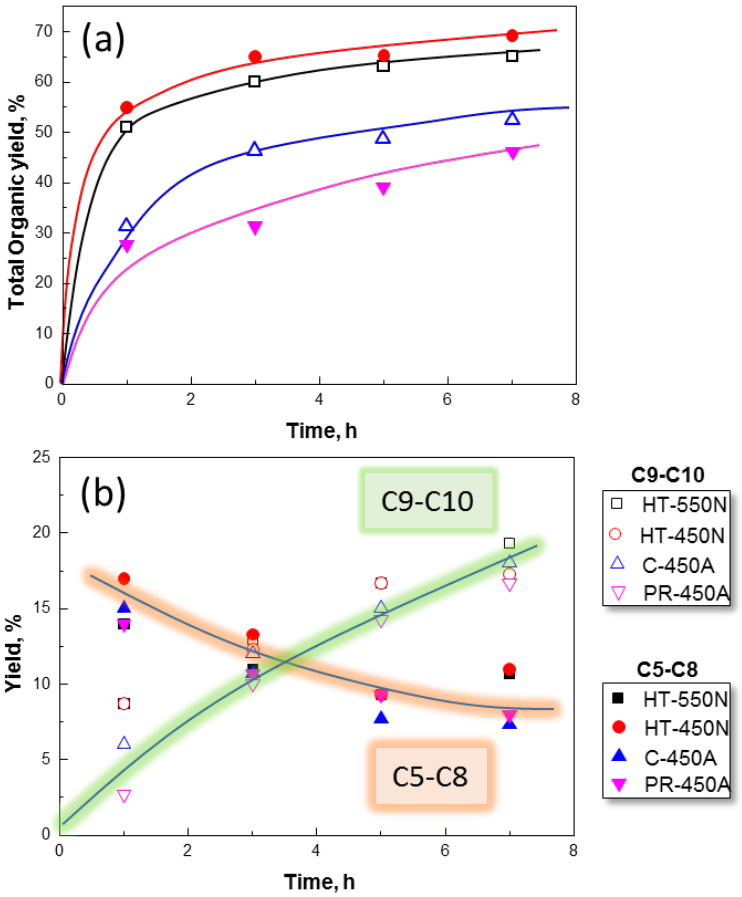

Figure 6.9. Catalytic activity in total organic products yield (a); intermediates (C_5-C_8) and C_9-C_{10} product yields (b) in the conversion of oxygenated compounds in aqueous model mixture of different HT-, PR- and C-series catalysts.

In particular, if total organic products yields at 1h of reaction are normalized to the density of acid sites (Table 6.2), the differences among all the materials can easily be noticed. Thus, hydrothermally synthesized NbO_x-based catalysts (HT-series) display a better catalytic performance than C- and PR-series samples (Table 6.5). Moreover, these HT-samples show comparable reaction rates and better yield values per acid sites density compared to CeZrO reference catalyst.

Table 6.5. Reaction rates and total organic products yields normalized taking into account density of acid sites for NbO_x catalysts after 1h of reaction.

Catalyst	Reaction rate ($\mu molmin^{-1}g^{-1}$)	Total Products Yield (1h)	Total Products Yield (1h) / $\mu mol/m^2$
HT-300N	1881	58.7	54.4
HT-400N	1644	53.0	71.6
HT-450N	1667	55.0	59.8
HT-550N	1577	51.0	98.1
C-450N	1051	31.7	58.7
C-450A	1051	31.3	16.1
C-550A	872	32.3	55.7
PR-450A	1029	27.7	37.4
PR-550A	912	24.0	20.5
CeZrO	1650	51.7	55.0

Reaction conditions: 3 g of aqueous mixture, 150 mg of catalyst; T=200 ºC, P=13 bar N_2, t= 1h.

More interestingly, textural and acid properties of HT-samples can be modified applying different heat-treatment conditions. In this sense, the density of acid sites increases when decreasing the heat-treatment temperature, despite the increment of the surface area observed (Table 6.1 and Table 6.2). Indeed, the higher amount of total acid sites and their right distribution on catalyst surface leads to increase the organic products yields during the process (Figure 6.10). The optimal combination of these parameters has been found for HT-400N and HT-450N samples, which lead to a better catalytic behaviour in terms of total organic yield than CeZrO reference catalyst (Table 6.5 and Figure 6.10)

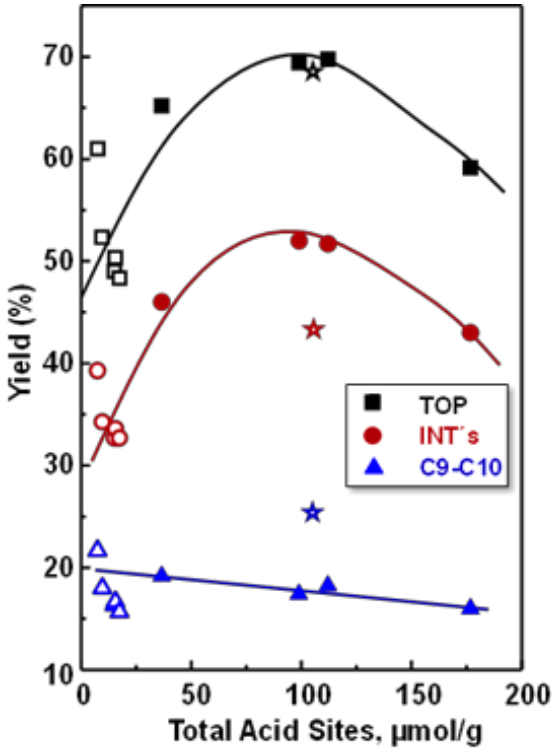

Figure 6.10. Variation of total organic products yield, TOP (black) and intermediates, INT´s (red) and C_9-C_{10} products (blue) yields with the density of acid sites for all catalysts: HT-series (filled symbols); PR-series and C-series (empty symbols). Results over CeZrO sample (star symbols) are also included.

Remarkably, in spite of the higher density of acid sites and reaction rates observed for the sample heat-treated at the lowest temperature (i.e. sample HT-300N), its higher acidity could also favour undesired polymerization reactions during the process; thus lowering the final total organic products found in the liquid reaction mixture at 7h on stream (Figure 6.10). This effect can be also observed by the decrease of the carbon balance when HT-300N was used (see Table 6.3).

6.2.4 Stability tests

Finally, recycling experiments in the catalytic condensation of oxygenated compounds in aqueous mixture were performed testing selected catalysts during three consecutive reuses to corroborate the resistance of Nb-oxides under reaction conditions, and the results in terms of total organic products yield attained are given in Figure 6.11.

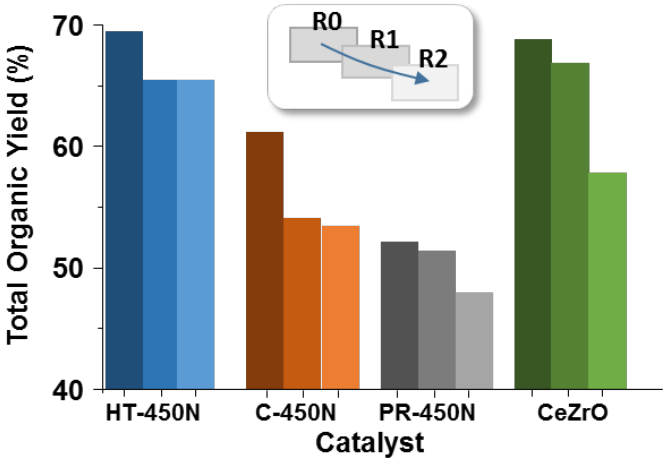

Figure 6.11. Effect of the re-uses (R0, R1 and R2) of different catalysts on the total organic products yield (%) attained during the condensation of oxygenated compounds in aqueous model mixture (at 200 ºC and P_{N2}=13 bar during 7h).

On one hand, it was observed that HT-450N catalyst maintained its catalytic performance practically invariable after reuses due to its structure preservation. Then, the slight catalytic deactivation observed after reuses is mainly related to coke deposition on the catalyst surface measured by TG and EA (Table 6.6).

On the other hand, C-450N and PR-450N samples exhibited high stability (low carbon deposition), although in the first material its catalytic activity decreased probably due to surface reconstruction and changes processes after being used in aqueous solutions. In fact, Raman spectroscopy of C-450N before and after reaction (Figure 6.12) confirms a change in the intensity of the band at 550-750 cm^{-1} assigned to Nb-O-Nb bonds. In the case of PR-type sample, a very low activity is observed even with the fresh catalyst (R0).

In all the Nb-based catalysts used in the re-cycling experiments, no leaching of Nb was observed (Table 6.6). Remarkably, hydrothermally prepared catalyst (HT-450N) still showed much better stability than CeZrO mixed oxide, which suffered a bigger loss of activity due to carbon deposition as it was measured by TG and EA, but mostly due to the significant leaching of Ce (>30 wt.% lost from the initial content in solid) clearly detected in liquids after reaction (Table 6.6). These stability issues were previously explained in Chapter 4.

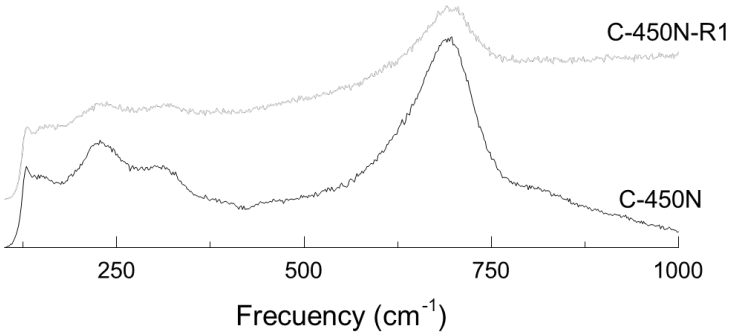

Figure 6.12. Raman spectroscopy analysis for C-450N (fresh catalyst) and C-450N-R1 (used catalyst).

Table 6.6. Catalysts post-reaction characterization: Organic compounds deposition and active sites leaching.

Catalyst	TG[a]	EA[b]	Metal Lost[c]
CeZrO	13.8%	4.8%	>30.0%
HT-550N	6.9%	1.9%	Non det.
HT-450N	11.9%	3.7%	Non det.
C-450N	0.6%	0.3%	Non det.

[a] *TG: Mass loss (wt.%) measured by thermogravimetric analysis.*
[b] *EA: Carbon composition (wt%) measured by elemental analysis.*
[c] *Amount of metal lost (in wt%) from the solid catalyst determined by ICP measurements of metal concentration in liquids after first use (R0).*

Summarizing, niobium oxide based materials prepared by hydrothermal synthesis with a pseudo-crystalline structure (ordered just along c-axis) and showing tuneable acid properties, have resulted to be active catalysts for the condensation of light oxygenated compounds in aqueous mixtures. These optimized NbO_x-materials present higher stability (after several reuses) and catalytic activity than other NbO_x-catalysts prepared by other procedures or reference materials as CeZrO, mainly due to they are highly water resistant catalysts. All these characteristics make affordable the use of these optimized HT-NbO_x materials as solid catalysts for the valorisation of aqueous effluents obtained by phase separation of pyrolytic bio-oils.

6.3 WNbO mixed oxides

Analogously to the case of NbO_x-based materials, acid–base properties of WNbO mixed oxides can likewise be strongly changed by tailoring composition and catalyst preparation procedure. Specifically, we have found that both the Brönsted/Lewis ratio and the total number of acid sites in niobium-containing materials can be tuned by an appropriate combination of hydrothermal synthesis and post-synthesis treatments, thus improving both the acid characteristics and the catalytic performance of NbO_x-based catalysts, as seen in Section 6.2.

Based on these considerations, the use of mixed metal oxides, especially those containing W and Nb was examined for this process. In this section, the catalytic performance of hydrothermally synthesized WNbO bronzes in the condensation of light oxygenated compounds present in aqueous effluents obtained by liquid phase separation of pyrolytic bio-oils is studied. In line with previous research, the catalytic behaviour is investigated by using a mixture of C_2-C_3 representative oxygenated compounds in water, closer to the real conditions at industry and differing from usual probe molecules studies performed even in the absence of water in most of the cases. The determining influence of the synthesis procedure is thoughtfully examined. Catalytic differences are analysed in detail when hydrothermally synthesized WNbO catalysts are employed. Moreover, reaction pathways are specifically discussed with the use of these catalysts due to their importance when dealing with complex mixtures.

6.3.1. Synthesis of WNbO mixed oxides

WNbO mixed oxides have been prepared by different procedures in order to study the importance of the synthesis, the crystalline structure and the textural and physicochemical properties of these mixed oxides, which are decisive characteristics for their catalytic activity. In addition, h-WO_3 and NbO_x materials have been prepared and characterized for comparative purposes.

On one hand, WNbO mixed oxides were synthesized via hydrothermal method from acidified aqueous solutions containing stoichiometric amounts (H_2O/(W+Nb) molar ratio: 53/1) of the corresponding metal salts: ammonium metatungstate hydrate and niobium oxalate monooxalate adduct. These solutions were introduced into Teflon-lined stainless steel autoclaves, purged with N_2 and heat-treated at 175 ºC for 48 h. After filtering, washing and drying steps, the resulting solids were finally heat-treated at 550 ºC under N_2 flow for 2 h. Samples are named as HT-W_xNb_y, x and y expressing catalyst molar ratio composition.

On the other hand, examples of WNbO mixed oxides via co-precipitation synthesis (COP-$W_{50}Nb_{50}$), wet impregnation (WI-$W_{50}Nb_{50}$) and incipient wetness impregnation synthesis (IWI-$W_{34}Nb_{66}$) were prepared as means of comparison. All catalysts were also heat-treated at 550 ºC under air during 2h, with a heating rate of 2 ºC/min. Additional details of these synthesis procedures can be found in Section 3.

6.3.2. Catalysts characterization

Firstly, WNbO mixed oxides were characterized by X-ray diffraction (XRD) to study their crystalline structure. XRD patterns of WNbO materials are depicted in Figure 6.13. On short notice, huge differences in crystallinity can be observed among materials depending on the synthesis procedure: hydrothermal (blue), co-precipitation (green), wet impregnation (purple) and wetness impregnation (red).

On one hand, HT-WNbO series with varying composition can be compared. Firstly, non-doped tungsten oxide (i.e. HT-$W_{100}Nb_0$) presents characteristic Bragg peaks of the hexagonal tungsten bronze-type structure h-WO_3 (HTB JCPDS: 01-85-2459) (Fig.6.13, a)[10], in which WO_6 octahedra share their vertices along the three crystallographic directions, displaying trigonal and hexagonal channels along c-axis. Then, isomorphic substitution of W by Nb causes some changes in the diffraction profiles (Fig.6.13, b-d). As the Nb content increases, the intensity of the Bragg signals progressively decreases. At relatively low Nb/(W+Nb) contents (HT-$W_{71}Nb_{29}$), HTB structure is maintained, although the intensity of these diffraction peaks becomes notably lower (Fig.6.13, b). Moreover, for higher Nb/(W+Nb) ratios (Fig.6.13, c-d), only two sharp Bragg signals, that can be assigned to the (002) and (004) reflections of the HTB structure can be observed. Additional broad diffraction peaks at 27˚, 35˚, 50˚ and 55˚ are also present (Fig.6.13, c-d). This process is promoted by the introduction of Nb within h-WO_3 structure, which finally gives rise to a pseudo-crystalline mixed oxide phase already observed in other Mo, Nb and W-based systems[11].

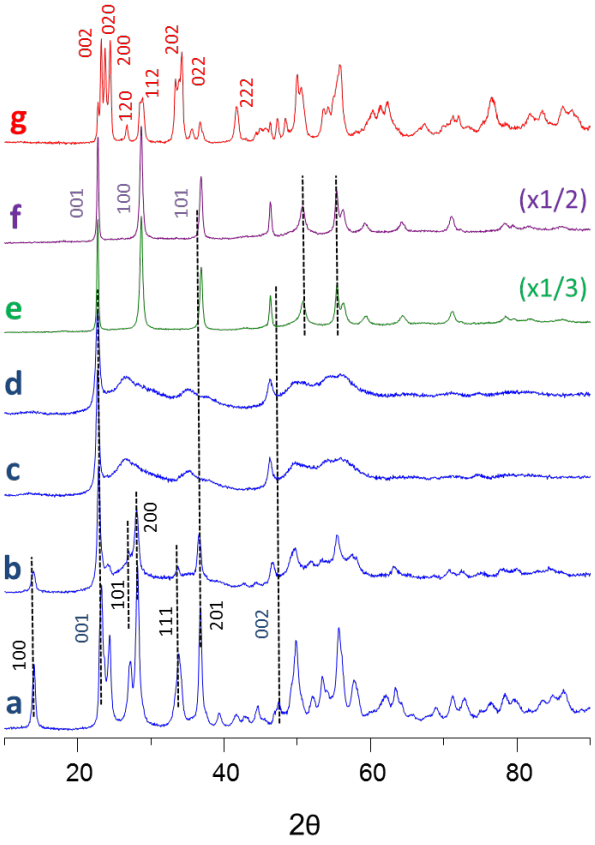

Figure 6.13. XRD patterns of WNbO catalysts. a) HT-$W_{100}Nb_0$, b) HT-$W_{71}Nb_{29}$, c) HT-$W_{47}Nb_{53}$, d) HT-$W_{38}Nb_{62}$, e) COP-$W_{50}Nb_{50}$, f) WI-$W_{50}Nb_{50}$ and g) IWI- $W_{34}Nb_{66}$.

On the other hand, WNbO samples prepared by coprecipitation (Fig.6.13, e) or wet impregnation (Fig.6.13, f) exhibit a well-ordered crystalline hexagonal structure, similar to H-Nb_2O_5 (JCPDS: 00-007-0061). In both patterns, Bragg signals are slightly displaced to the right, unequivocally indicating tungsten is being introduced into H-Nb_2O_5 structure. Finally, catalyst prepared by wetness impregnation, IWI-$W_{34}Nb_{66}$ (Fig.6.13, g) shows diffraction peaks corresponding to H-Nb_2O_5 structure, together with additional sharp peaks related to monoclinic WO_3 structure (JCPDS: 00-020-1323).

Structural features of HT-WNbO materials were also analysed by Raman spectroscopy (see Figure 6.14). Main bands centred at 780, 691 and 648 cm^{-1} assigned to O-W-O stretching vibrations in the HTB structure of h-WO_3 and low frequency deformation modes at 331, 291 and 261 cm^{-1}, progressively disappear after the substitution of Nb for W. By contrast, a new broad signal at 900-1000 cm^{-1} appears, which is related to M=O type stretching vibrations (M: W, Nb). Likewise, another band at 709 cm^{-1} ascribed to symmetric stretching mode of slightly distorted NbO_6 octahedra in bulk niobium oxides is observed (Fig. 6.14, c-e), together with low frequency Nb-O-Nb deformation modes due to the increasing disorder in the crystalline structure.

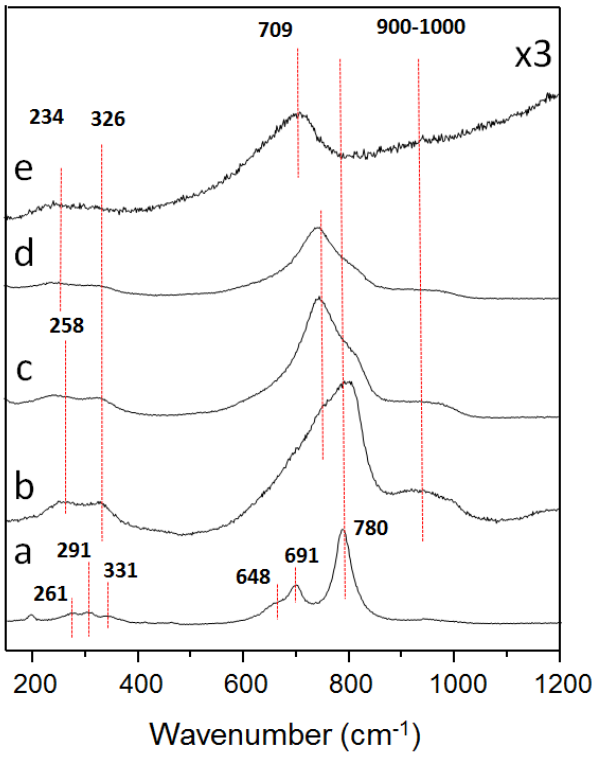

Figure 6.14. Raman spectra of WNbO catalysts. a) HT-$W_{100}Nb_0$, b) HT-$W_{71}Nb_{29}$, c) HT-$W_{47}Nb_{53}$, d) HT-$W_{38}Nb_{62}$, and e) HT-W_0Nb_{100}.

Textural properties of WNbO mixed oxides were studied by means of N_2 adsorption (Table 6.7). Firstly, HT-WNbO materials present larger surface areas than WNbO prepared by other methods. In particular, surface area increases from 28 m^2/g for HT-$W_{100}Nb_0$ to 124 m^2/g for HT-$W_{38}Nb_{62}$. Moreover, a transition between type II isotherms for Nb/(Nb+W)≤0.53 to type IV for higher Nb contents (typical of mesoporous materials) is observed. Indeed, these changes are also accompanied by a concomitant variation in average pore sizes and pore volumes (see Table 6.7). In this sense, materials with Nb/(Nb+W) lower than 0.53 present a broad pore size distribution, whereas for higher Nb concentrations narrower distributions are observed. Likewise, average pore size of the catalysts decreases from 17.2 nm for HT-$W_{100}Nb_0$ to 5.9-3.5 nm for HT-$W_{38}Nb_{62}$ and HT-W_0Nb_{100}. On the contrary, WNbO synthesized by other procedures show small surface areas (<30 m^2/g) and insignificant pore volumes (<0.01 cm^3/g).

Table 6.7. Main textural properties of WNbO materials.

Samples	S_{BET} ($m^2.g^{-1}$)[a]	Pore data[b]	
		Pore size (nm)	Mesopore volume (cm^3/g)
HT-$W_{38}Nb_{62}$	124	5.9	0.216
HT-$W_{47}Nb_{53}$	102	14.6	0.176
HT-$W_{71}Nb_{29}$	38	11.1	0.050
HT-$W_{100}Nb_0$	28	17.2	0.045
COP-$W_{50}Nb_{50}$	29	-	-
WI-$W_{50}Nb_{50}$	16	-	-
IWI- $W_{34}Nb_{66}$	8	-	-

[a] *Calculated values from N_2 adsorption isotherms (BET method).*
[b] *Calculated values from BJH method.*

Considering the acid properties of the materials, HT-samples remarkably exhibit higher number of acid sites per gram than other WNbO samples (Table 6.8 and Figure 6.15). In particular, acidity of HT-WNbO catalysts increases with Nb content, reaching a maximum of 331 $\mu molNH_3 g^{-1}$ for HT-$W_{38}Nb_{62}$. On the contrary, the density of acid sites (i.e. number of acid sites per m^2/g) decreases when increasing Nb content, due to the higher surface areas observed (Table 6.8).

Figure 6.15 specifically shows the TCD signal of NH_3-TPD experiments for the different WNbO samples prepared by different procedures. Huge differences on the total number of acid sites per gram can be observed among HT-WNbO and other WNbO mixed oxides synthesized via co-precipitation, wet impregnation or incipient wetness impregnation.

Moreover, acid properties of a whole series of HT-samples were elucidated by means of FT-IR measurements with pyridine adsorption (Figure 6.16) to achieve additional information. In this sense, considering the concentration of acid sites in terms of the total number of acid sites per gram of catalyst, the acidity of HT-WNbO oxides increases with Nb content (reaching a maximum, Figura 6.16a) whereas the surface density of acid sites decreases when increasing Nb content (Figure 6.16b). This information is equivalent to those values achieved by NH_3-TPD experiments. Finally, the Brönsted/Lewis acid sites ratio (BAS/LAS) decreases as Nb concentration in the catalysts increases (Figure 6.16c).

Table 6.8. Main physicochemical properties of WNbO materials.

Samples	Total acid sites (NH_3-TPD)	
	($\mu mol_{NH3} g^{-1}$)[a]	($\mu mol_{NH3} m^{-2}$)[b]
HT-$W_{38}Nb_{62}$	331	2.6
HT-$W_{47}Nb_{53}$	217	2.1
HT-$W_{71}Nb_{29}$	139	3.7
HT-$W_{100}Nb_0$	124	4.4
COP-$W_{50}Nb_{50}$	53	1.8
WI-$W_{50}Nb_{50}$	41	2.5
IWI- $W_{34}Nb_{66}$	15	1.9

[a] *Values calculated by pyridine adsorption NH_3-TPD experiments, in (μ mol/g).*
[b] *Density of acid sites, in µmol/m^2.*

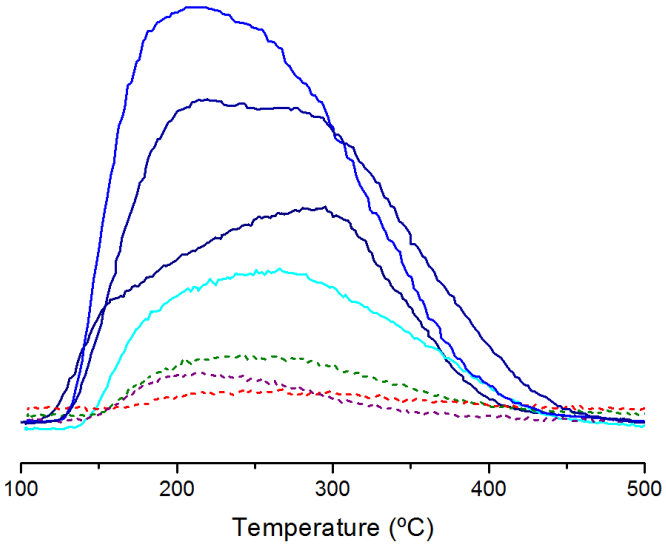

Figure 6.15. TCD signal (NH_3-TPD) of WNbO catalysts. HT-$W_{38}Nb_{62}$, HT-$W_{47}Nb_{53}$, HT-$W_{71}Nb_{29}$, HT-$W_{100}Nb_0$ (blue lines), COP-$W_{50}Nb_{50}$ (green), WI-$W_{50}Nb_{50}$ (purple) and IWI- $W_{34}Nb_{66}$ *(red).*

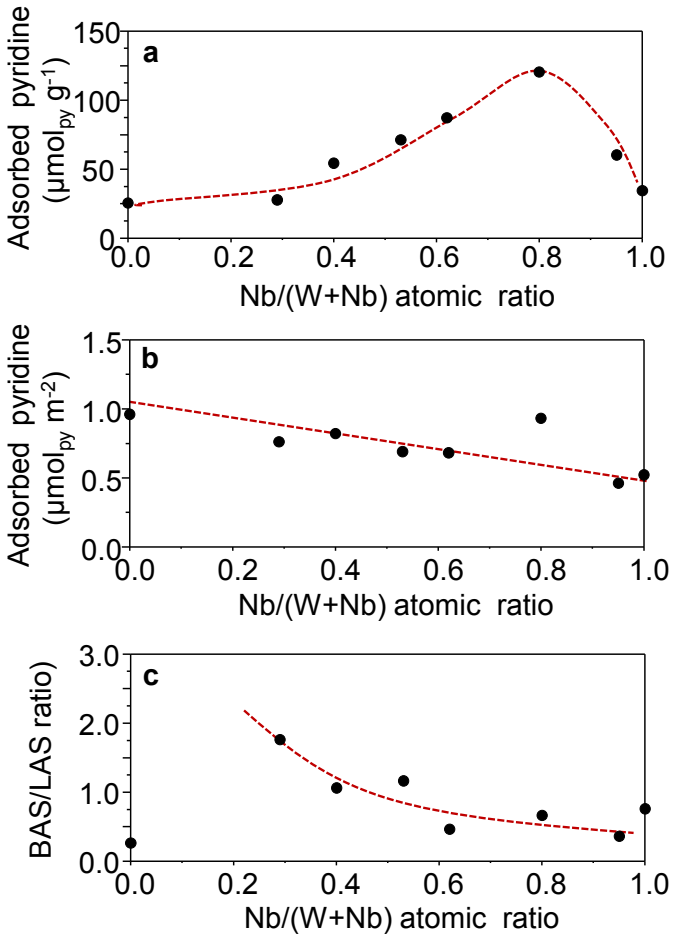

Figure 6.16. Acid features of HT-WNbO mixed oxides catalysts obtained by FTIR of adsorbed pyridine: a) Concentration of acid sites sites (in μmol_{py} g^{-1}); b) Surface density of acid sites (in μmol_{py} m^{-2}); and c) BAS/LAS ratio (BAS: Brönsted Acid Sites; LAS: Lewis Acid Sites).

Summarizing, hydrothermally synthesized tungsten-niobium bronzes (HT-WNbO) have shown the advantage of having crystalline structure, textural and acid properties (nature, concentration and density of acid sites) modified by tailoring the Nb composition. On the other hand, other synthesis methods lead to WNbO catalysts with low surface areas and poor acid properties, which limit their catalytic applications.

6.3.3. Catalytic results: Experiments at 180 ºC

Firstly, the performance of WNbO materials was tested in aqueous-phase condensation reactions of oxygenated compounds at 180 ºC (Table 6.9 and Table 6.10). All HT-WNbO catalysts show better results than WNbO prepared by other methods. HT-samples exhibit high total organic products yield (49 to 68%), whereas values under 39% are observed when other WNbO materials prepared by co-precipitation, wet impregnation or incipient wetness impregnation are used (see Table 6.10). In particular, higher propanal and ethanol conversion are achieved if HT-WNbO samples are employed. In all these cases, larger amounts of intermediate products (2M2P and C_5-C_8 products) and final C_9-C_{10} products are observed. On the other hand, similar poor catalytic results and low total organic products yield are obtained for other WNbO materials.

Meanwhile, big differences can be distinguished when different HT-WNbO samples are tested. In this sense, a whole series of HT-WNbO catalysts were examined in these process conditions. The main difference along all the series is observed for propanal conversion, being the conversion of acetol (100%), ethanol (37-47%) and acetic acid (13-18%) similar regardless Nb-content in the catalysts (Table 6.9 and Figure 6.17a). Primarily, non-doped HT-$W_{100}Nb_0$ catalyst and low Nb content catalysts (i.e. HT-$W_{71}Nb_{29}$) display low conversion of the different oxygenated compounds. Thus, lower 2-methyl-2-pentenal, C_9-C_{10} products and total organic products yields are observed in these cases.

However, propanal conversion increases with Nb content, reaching maximum values for Nb/(W+Nb) of ca. 0.62 (i.e. 90% propanal conversion). In this way, a concomitant increment in the selectivity to 2-methyl-2-pentenal (2M2P, via self-aldol condensation of propanal) can be observed when increasing Nb content in the catalysts. Selectivity to C_9-C_{10} products shows the same trend, since they are formed mainly via aldol condensation of C_5-C_8 fractions with smaller molecules. Consequently, the selectivity to C_5-C_8 oxygenates decreases when increasing Nb content, since second condensation reactions are favoured at high Nb concentration (Figure 6.17b).

The selectivity to ethyl acetate also decreases with Nb-content. However, this effect seems to be more related to an increase in the yield to condensation products rather than an effective decrease in ethyl acetate formation. In fact, ethyl acetate yield remains almost constant in all the series (Table 6.9). This observation is in agreement with the specific acid properties of the materials, in which BAS/LAS ratio decreases when increasing Nb content (Figure 6.16c), what would benefit the reactivity via condensation reactions instead of esterification reactions. In the case of WNbO oxides prepared by different methods, ethyl acetate formed from the esterification of acetic and ethanol also shows similar yield values. This data confirms that esterification reactions take place under thermal conditions regardless the number and density of acid sites on the WNbO employed.

Table 6.9. Data of reactants conversions and organic products yields for HT-WNbO catalysts in the condensation reaction of oxygenated compounds in aqueous phase.

Catalyst		HT-	$W_{100}Nb_0$	$W_{71}Nb_{29}$	$W_{47}Nb_{53}$	$W_{38}Nb_{62}$
Conversion	(%)	Acetic acid	17.2	15.2	13.3	17.8
		Propanal	61.2	77.8	84.5	90.1
		Ethanol	40.4	38.4	43.4	47.2
		Acetol	100.0	100.0	100.0	100.0
Product Yield	(%)	Ethyl acetate	25.1	23.5	24.2	23.8
		2M2P[a]	28.3	29.0	34.7	39.0
		C5-C8	14.5	15.9	16.0	16.2
		C9-C10	6.4	6.6	11.5	13.2
		Total	**49.2**	**51.5**	**62.2**	**68.4**
Carbon balance (%)			96.5	94.8	92.1	96.7

Reaction conditions: 3 g of aqueous mixture, 150 mg of catalyst; T=180 ºC, P=13 bar N_2, t= 7h. [a]2M2P=2-methyl-2-pentenal

Table 6.10. Data of reactants conversions and organic products yields for WNbO oxides prepared by different procedures in the condensation reaction of oxygenated compounds in aqueous phase.

Catalyst			COP-$W_{50}Nb_{50}$	WI-$W_{50}Nb_{50}$	IWI- $W_{34}Nb_{66}$
Conversion	(%)	Acetic acid	20.2	22.1	25.9
		Propanal	65.4	56.5	56.2
		Ethanol	24.4	33.1	45.5
		Acetol	100.0	100.0	100.0
Product Yield	(%)	Ethyl acetate	21.6	22.1	24.6
		2M2P[a]	17.8	18.8	20.7
		C5-C8	12.3	11.5	9.1
		C9-C10	8.3	7.4	8.8
		Total	**38.4**	**37.7**	**38.6**
Carbon balance (%)			91.6	90.5	90.2

Reaction conditions: 3 g of aqueous mixture, 150 mg of catalyst; T=180 ºC, P=13 bar N_2, t= 7h. [a]2M2P=2-methyl-2-pentenal

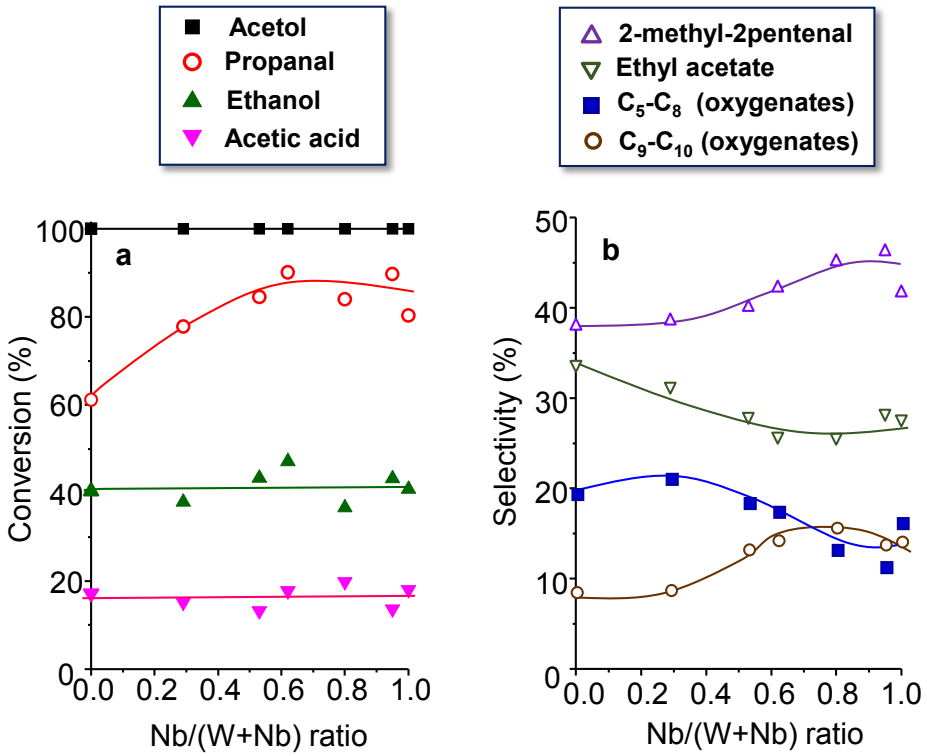

Figure 6.17. Variation of the conversion of each reactant in the aqueous model mixture (a) and selectivity to the main products (i.e. 2-methyl-2-pentenal, ethyl acetate, C_5-C_8 and C_9-C_{10} oxygenates) (b) as a function of Nb content in HT-WNbO catalysts. Reaction conditions: 3 g of aqueous mixture, 150 mg of catalyst, at 13 bar N_2 and 180 ºC during 7 h.

In this context, the catalytic performance of HT-WNbO oxides should be interpreted considering the concentration and the nature of acid sites on the surface of catalysts. Figure 6.18a displays the total organic yield (i.e the sum of 2M2P, C_5-C_8 and C_9-C_{10} products), the yield to intermediates products (i.e. 2M2P and C_5-C_8 oxygenates) and the yield to final products (i.e. C_9-C_{10} products) as a function of the concentration of acid sites.

As it can be seen, an increase of the concentration of acid sites in the samples gives rise to an increase in the yield to both the intermediate oxygenates (2M2P and C_5-C_8) and final (C_9-C_{10}) products, thus increasing the total organic yield (Figure 6.18a).

However, an important point to take into account in order to increase the yield to condensation products is the control of BAS/LAS ratio in the catalysts. On one hand, a very high BAS/LAS ratio does not favour the condensation reactions, neither to reaction intermediates nor to final (C_9-C_{10}) products, leading mainly to esterification and other Brönsted acid catalysed reactions. On the other hand, higher concentration of Lewis acid sites (i.e. low BAS/LAS ratios) favours the desired condensation reactions to produce C_5-C_8 and C_9-C_{10} products, being these conditions attained on catalysts with Nb/(W+Nb) ratios higher than 0.53.

Nevertheless, much higher content of Lewis acid sites in the catalysts produces the over-condensation of C_9-C_{10} oxygenated compounds with indiscriminate growing of the carbon chain to give heavier compounds (i.e. polymers), thus decreasing the amount of the desired C_5 to C_{10} range products obtained in the final mixture. Accordingly, an adequate BAS/LAS ratio with an optimized amount of Lewis acid sites is required in the catalyst for the desired condensation reaction, the optimum value being achieved at a Nb/(W+Nb) atomic ratio of ca. 0.62, or in the 0.62-0.80 range (Figure 6.18b). Nevertheless, it seems that higher concentration of Lewis sites (i.e. low BAS/LAS ratios, at increasing Nb contents) favours these reactions, being these conditions attained at Nb/(W+Nb) > 0.53 (i.e. HT-$W_{47}Nb_{53}$ and HT-$W_{38}Nb_{62}$ catalysts).

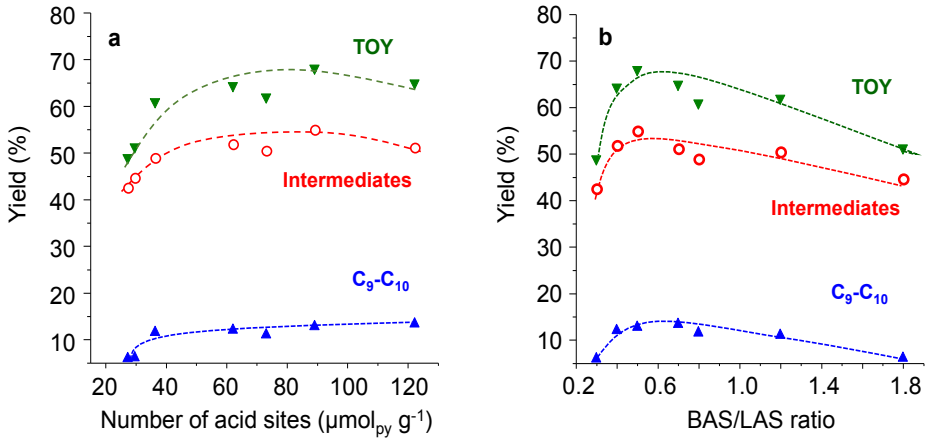

Figure 6.18. Variation of the Total Organic Yield (TOY), yield to intermediates (2M2P and C_5-C_8 products) and yield to final products (i.e. C_9-C_{10} products) as a function of the number of acid sites (a) and the BAS/LAS ratio (b) in HT-WNbO catalysts. Reaction conditions: 3 g aqueous mixture, 150 mg of catalyst, at 13 bar N_2 and 180 ºC during 7 h.

6.3.4. Catalytic results: Experiments at 200 ºC

Afterwards, experiments of oxygenated compounds condensation in aqueous phase under higher temperature conditions (200 ºC) were carried out to maximize C_9-C_{10} products. Results obtained for the HT-WNbO series of catalysts are shown in Table 6.11, while the data attained for WNbO oxides prepared by other methods are detailed in Table 6.12. As can be seen, and in comparison with results obtained in the experiments at 180 ºC, increasing the reaction temperature improves 2nd condensation reaction steps. Then, yields to intermediates (2M2P and C_5-C_8) decrease, while C_9-C_{10} products yields are optimized. This is the general trend observed for the HT-WNbO catalysts, and also for the WNbO samples prepared by other synthesis procedures. Nevertheless, big differences are once more detected among hydrothermally synthesized catalysts and the rest of WNbO mixed oxides (see Table 6.11 and Table 6.12).

The lowest 2M2P and C_9-C_{10} yields are still achieved when non-doped HT-$W_{100}Nb_0$ sample and WNbO materials synthesized by other procedures are employed. As Nb content further increases in HT-WNbO series of samples, both conversion and products yield repeatedly increase. Complete conversions of acetol, together with high conversion of propanal (>90%) are reached from HT-$W_{47}Nb_{53}$ catalyst; reaching maximum 2-methyl-2-pentenal yields (36%) for HT-$W_{38}Nb_{62}$ material. More interestingly, a change in product distribution is found when higher niobium contents are used among HT-WNbO samples. A logic decrease in C_5-C_8 products is observed while C_9-C_{10} products are maximized (17-18% at 7h, see Table 6.11).

Moreover, it is worth noting that high-Nb content HT-WNbO samples (i.e. HT-$W_{38}Nb_{62}$ catalyst) show better total organic products yield at 180 ºC than when higher temperature conditions are applied. This fact can be explained as consecutive condensation reactions are taking place. C_9-C_{10} products from 2nd condensation steps are maximized but polymerization reactions might be occurring at the same time. Although inferior values of C_9-C_{10} products are achieved under lower temperature conditions, undesired polymerization reactions are partially supressed and total organic products yield are optimized.

Additionally, a slight decrease in the carbon balance is also observed at 200 ºC, due to polymerization and over-condensation reactions, that giving rise to higher molecular weight oxygenates, which are not detected by gas chromatography or are retained as coke in the catalyst surface. Therefore, equilibrium must be found between temperature and reaction time to maximize both C_9-C_{10} and total products yields without inducing undesired polymerization reactions.

Table 6.11. Data of reactants conversions and organic products yields for HT-WNbO catalysts in the condensation reaction of oxygenated compounds in aqueous phase at 200 ºC.

Catalyst		HT-	$W_{100}Nb_0$	$W_{71}Nb_{29}$	$W_{47}Nb_{53}$	$W_{38}Nb_{62}$
Conversion	(%)	Acetic acid	0.0	8.2	8.0	9.8
		Propanal	86.6	85.1	93.8	90.0
		Ethanol	49.8	50.8	56.7	51.3
		Acetol	100.0	100.0	100.0	100.0
Product Yield	(%)	Ethyl acetate	22.3	19.0	19.4	19.2
		2M2P[a]	29.3	32.5	32.7	35.6
		C5-C8	12.4	13.4	13.5	11.2
		C9-C10	11.2	10.7	18.0	17.7
		Total	**52.9**	**56.6**	**64.2**	**64.5**
Carbon balance (%)			90.0	87.2	90.8	94.0

Reaction conditions: 3 g of aqueous mixture, 150 mg of catalyst; T=200 ºC, P=13 bar N_2, t= 7h. [a]2M2P=2-methyl-2-pentenal.

Table 6.12. Data of reactants conversions and organic products yields for WNbO oxides prepared by different procedures in the condensation reaction of oxygenated compounds in aqueous phase at 200 ºC.

Catalyst			COP-$W_{50}Nb_{50}$	WI-$W_{50}Nb_{50}$	IWI- $W_{34}Nb_{66}$
Conversion	(%)	Acetic acid	14.7	12.5	16.3
		Propanal	75.7	73.4	62.9
		Ethanol	48.0	53.3	45.2
		Acetol	100.0	100.0	100.0
Product Yield	(%)	Ethyl acetate	23.4	21.7	25.1
		2M2P[a]	25.3	27.4	26.1
		C5-C8	16.8	12.5	9.0
		C9-C10	10.0	9.1	12.0
		Total	**52.2**	**49.0**	**47.1**
Carbon balance (%)			90.0	89.3	91.8

Reaction conditions: 3 g of aqueous mixture, 150 mg of catalyst; T=200 ºC, P=13 bar N_2, t= 7h. [a]2M2P=2-methyl-2-pentenal.

In line with Section 6.3.3, the activity of these catalysts in C-C bond formation reactions is directly related to their textural and acid properties. On one hand, the better catalytic results of HT-WNbO samples can be explained in terms of their improved surface areas (>100 m^2/g) and pore volumes, which favours a higher accessibility of reactants to active sites. More interestingly, HT-WNbO samples also show an increase in total acidity (Table 6.8) compared to other WNbO materials synthesized by different methods. Moreover, if total organic products yields are normalized to the density of acid sites for WNbO catalysts with a similar Nb content, the differences among the synthesis procedure influence on catalytic results can easily be noticed (Table 6.13).

Table 6.13. Catalytic results of different WNbO catalysts in oxygenated compounds condensation reactions in aqueous phase.

Catalysts	Surface area ($m^2.g^{-1}$)[a]	Total acid sites ($\mu mol_{NH3}g^{-1}$)[b]	Total Organic Products Yield /($\mu mol_{NH3}m^{-2}$)	
			180 ºC	200 ºC
HT-$W_{47}Nb_{53}$	102	217	29.2	30.2
COP-$W_{50}Nb_{50}$	29	53	21.0	28.5
WI-$W_{50}Nb_{50}$	16	41	14.7	19.1
IWI- $W_{34}Nb_{66}$	8	15	20.6	25.1

[a] *Calculated values from N_2 adsorption isotherms (BET method).* [b] *Values calculated by NH_3-TPD adsorption measurements, in (μmol/g).*

Therefore, all these improved textural and acid characteristics for HT-WNbO samples lead to the best catalytic results. Specifically, if total organic products yields are displayed versus total acid sites, a clear linear correlation can be observed (Figure 6.19). As total acid sites increase, all main products including 2-methyl-2-pentenal, intermediate C_5-C_8 and

C_9-C_{10} products also increase. Furthermore, the change in product distribution profile previously mentioned for HT-$W_{47}Nb_{53}$ and HT-$W_{38}Nb_{62}$ samples is also related to an increase in the total acidity of the materials.

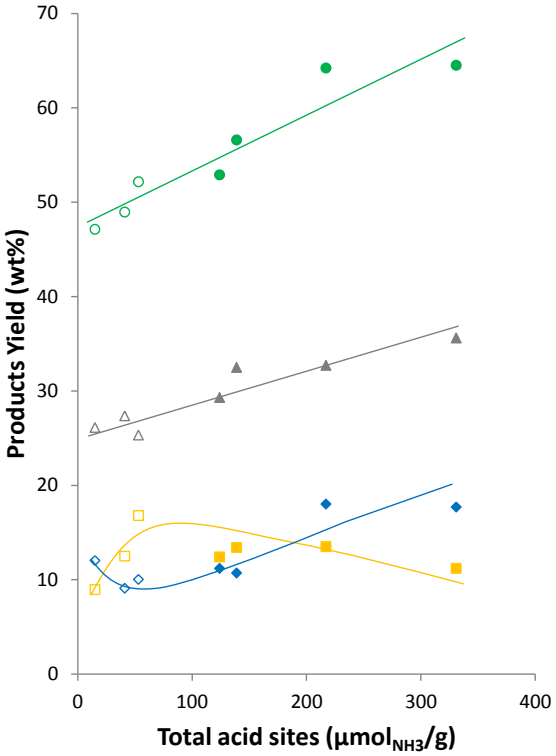

Figure 6.19. Products yield distribution profile with total acid sites: Total organic products (green), 2-methyl-2-pentenal (grey), C_5-C_8 products (yellow) and final C_9-C_{10} products (in blue) are represented. HT-WNbO (full symbols) and WNbO prepared via other methods (empty symbols) are distinguished. Reaction Conditions: 3 g aqueous mixture, 150 mg of catalyst, at 13 bar N_2 and 200 ºC during 7 h.

Therefore, WNbO materials preparation via hydrothermal synthesis is essential in order to obtain pseudo-crystalline mixed oxides with high surface areas and adequate acid properties, necessary in processes involving condensation reactions.

6.3.5. Reaction network and mechanism discussion

The employment of complex mixtures and the effect of temperature on consecutive condensation reactions and products distribution profiles allow obtaining a deeper understanding of the reaction network by both: A) Individually studying the behaviour of reactants conversion in the aqueous model mixture at different temperatures; and B) studying products yield evolution profile with time.

A) Reactants conversions at 180 ºC and 200 ºC.

Complete conversion of acetol and high conversion of propanal are reached in 7h under 180 ºC, while ethanol and acetic acid exhibit lower conversion values (40-45% and 15-20%, respectively). On the other hand, when experiments are carried out at 200 ºC, complete conversion of acetol and higher conversion of propanal are reached even in shorter reaction times, while ethanol and acetic acid continue exhibiting lower conversion values (50-55% and 4-10% respectively).

The lower acetic acid conversions at higher temperature conditions can be explained by oxidation reactions are possibly taking place (Figure 6.20). At lower temperature conditions (180 ºC) acetic acid is larger converted and higher amounts of ethyl acetate (esterification product) are observed in the final mixture (21-24%). When temperature is raised to 200 ºC, ethanol is largely converted, while lower acetic acid conversions (from ≈17% to ≈10%) and lower ethyl acetate yields (from ≈24% to ≈19%) are observed. Therefore, esterification reaction is favoured at 180

ºC, whereas oxidation reaction contribution is noticed from 200 ºC, where ethanol is being partially oxidized to acetic acid.

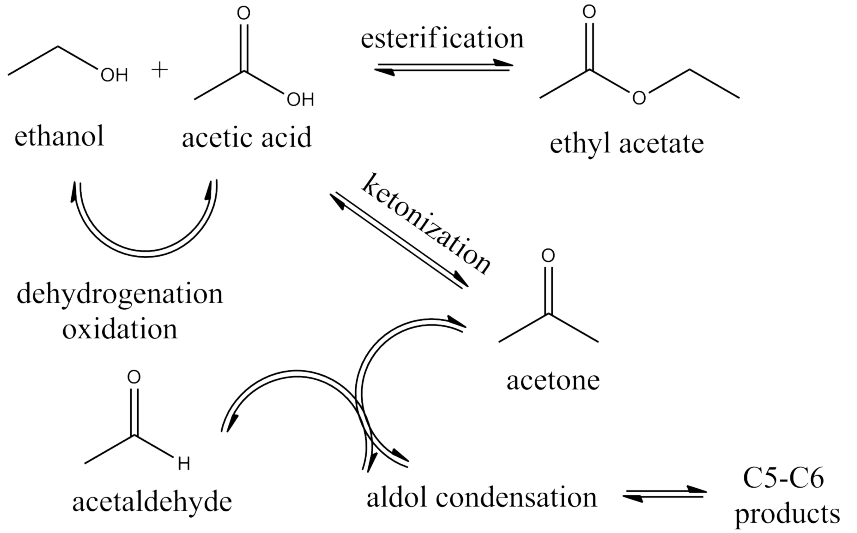

Figure 6.20. Ethanol reaction network.

B) Products yield evolution profile

The identification of reaction products and their distribution profile observed by GC and GCMS allowed us to draw the evolution of products yield with reaction time (see Figure 6.21). HT-WNbO samples and the results reached with reactions at 200 ºC were selected in order to analyse products evolution profiles from 1st and 2nd reaction steps.

As can be seen in Figure 6.21, the product yield evolution profile is similar for all selected HT-WNbO samples. As previously mentioned, as Nb content in the materials increases (from Fig.6.21A to Fig.6.21D), both conversion and products yield also increase. Higher reaction rates are also observed when Nb content increases and constant total organic

product yields are achieved from HT-$W_{47}Nb_{53}$ catalyst within 3h of reaction time (Figure 6.21C and Figure 6.21D). Moreover, introduction of higher amounts of Nb in the material (i.e. HT-$W_{38}Nb_{62}$ catalyst) drives to a faster increase in C_9-C_{10} products yield, while this C_9-C_{10} products yield is always below C_5-C_8 intermediate products yield when HT-WNbO catalysts with low Nb content are analyzed (Fig.6.21A and Fig. 6.21B).

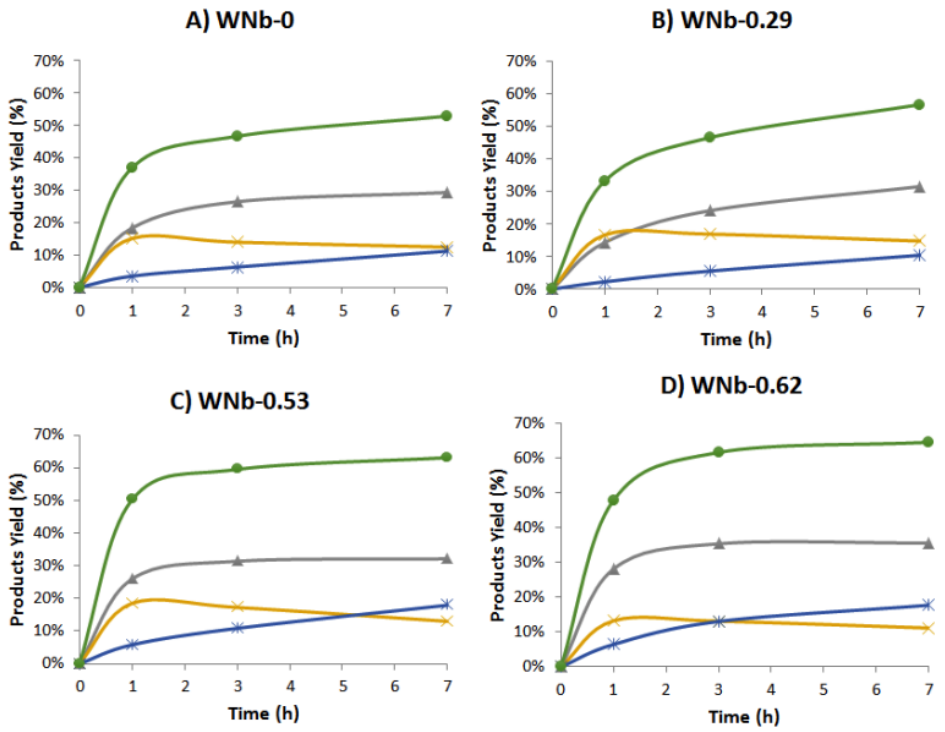

Figure 6.21. Products yield distribution profile with reaction time: A) HT-$W_{100}Nb_0$, B) HT-$W_{71}Nb_{29}$, C) HT-$W_{47}Nb_{53}$ and D) HT-$W_{38}Nb_{62}$. Total organic products (green), 2-methyl-2-pentenal (grey), main intermediate C_5-C_8 products (yellow) and final C_9-C_{10} products (in blue) are displayed. Reaction Conditions: 3 g aqueous mixture, 150 mg of catalyst, at 13 bar N_2 and 200 ºC during 7 h.

Moreover, the effect of temperature conditions on HT-WNbO samples yield to C_5-C_8 products, C_9-C_{10} products and carbon balance as a function of Nb content can be observed in Figure 6.22. Experiments at 180 ºC allow determining the optimum W-Nb composition to maximize products yield, meanwhile similar catalytic results are obtained when experiments are carried out at 200 ºC. Higher temperature conditions promote the change in product distribution (C_5-C_8 and C_9-C_{10} products yield) and drive to lower carbon balances in all the range of composition.

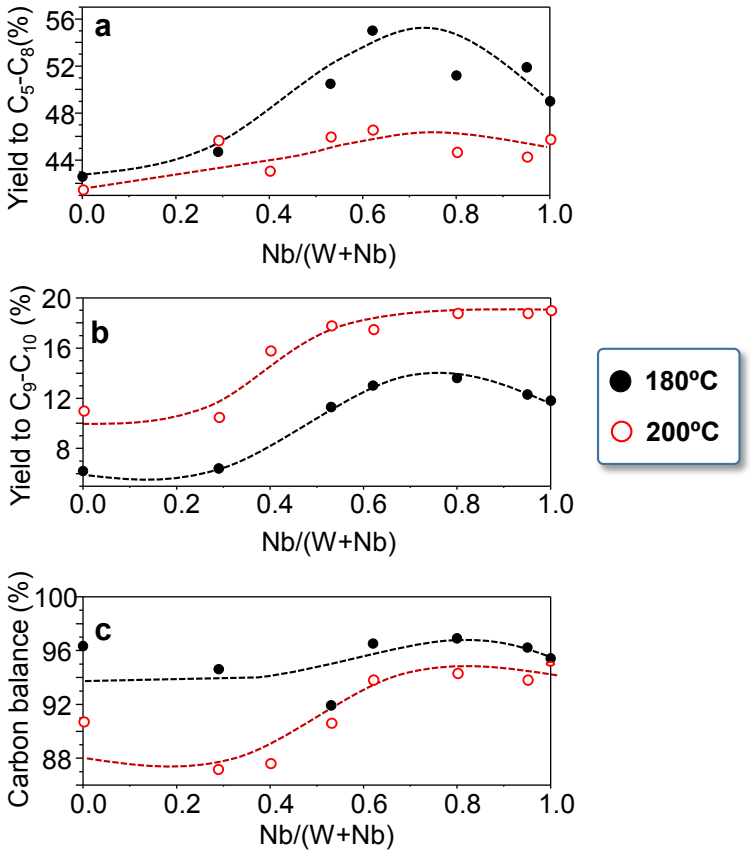

Figure 6.22. Yield to C_5-C_8 products (a), yield to C_9-C_{10} products (b) and carbon balance (c) as a function of Nb content in HT-WNbO samples at 180 ºC and 200 ºC during 7h.

Finally, it is worth noting that H_2O is the only by-product generated during the oxygenated compounds condensation process. Positively, this reaction scheme maximizes atom economy, but the use of H_2O as solvent forcedly decreases reaction rates.

In particular, additional experiments with varying water concentration were performed to study the effect of water and mixture complexity on catalyst activity. In this sense, HT-WNbO series of materials were tested in the condensation of propanal with and without water in the reaction medium (Figure 6.23A), and also in the condensation of the mixture of selected oxygenated compounds in aqueous and non-aqueous systems (Figure 6.23B).

Big detrimental effects on propanal conversion and products yield are observed when H_2O is present in the system (Figure 6.23). Interestingly, smaller differences are detected when high-niobium content catalysts are employed. These water-resistant characteristics, together with improved textural an acid properties drive to the best catalytic results.

Additionally, propanal conversion decreases when complex mixtures are studied if compared to aldehyde condensation individual assessment. Therefore, these experiments confirm that the study of stability and catalytic performance by using complex aqueous mixtures is essential for the development of future industrial applications.

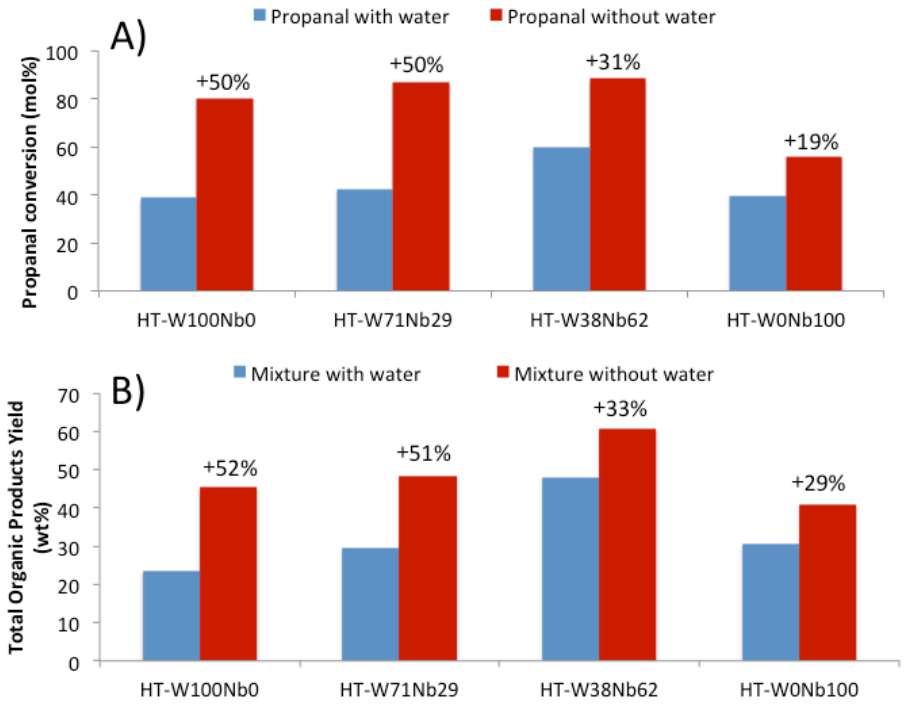

Figure 6.23. Experiments of condensation reactions with varying water concentration: A) Propanal conversion and B) Total organic products yield from aqueous/non aqueous mixture. The effect of water (wt%) on catalytic results is detailed. Reaction conditions: A) propanal (25wt%) + ethanol (75wt%) and B) aqueous model mixture; with water (30wt%) or without water and catalyst (50 mg) in autoclave-type reactor, at 13 bar N_2 and 200 ˚C under continuous stirring during 1 h.

6.3.6. Catalysts post-synthesis optimization

It is well known that both textural and acid properties (total number of acid sites and BAS/LAS ratio) in niobium-containing materials can be tuned by an appropriate combination of hydrothermal synthesis and post-synthesis treatments (as seen in Section 6.2). Thus, the influence of post-synthesis heat-treatment was studied to improve the surface area and acid characteristics, and consequently, the catalytic performance of HT-WNbO catalysts.

HT-$W_{47}Nb_{53}$, HT-$W_{38}Nb_{62}$ and HT-W_0Nb_{100} samples were studied under three different heat-treatment scenarios, where samples were treated under N_2 atmosphere at 300 ºC, 400 ºC and 550 ºC, respectively. Firstly, higher surface areas and higher density of acid sites are observed when decreasing the heat-treatment temperature (see Table 6.14).

Table 6.14. Main textural and physicochemical properties of WNbO materials when different heat-treatment conditions are applied.

Sample	Heat treatment	Surface area (m^2/g)[a]	Total acid sites ($\mu mol_{PY}/g$)[b]
HT-$W_{47}Nb_{53}$	300 ºC	195	99
	400 ºC	175	111
	550 ºC	102	73
HT-$W_{38}Nb_{62}$	300 ºC	195	192
	400 ºC	198	103
	550 ºC	124	89
HT-W_0Nb_{100}	300 ºC	163	177
	400 ºC	152	110
	550 ºC	70	36

[a] *Calculated values from N_2 adsorption isotherms (BET method).*
[b] *Calculated values from FTIR-PY experiments.*

In this way, higher total organic products yields are reached when a higher density of acid sites is achieved (Figure 6.24). Interestingly, in spite of the higher reaction rates observed when the samples are heat-treated at lower temperatures, their higher acidity could also favour undesired polymerization reactions during the process; thus lowering the final total organic products found in the liquid reaction mixture. This effect can be observed by the decrease of total organic products yield

when total acid sites overcome 100-120 $\mu mol_{PY} g^{-1}$ and by the decrease of the carbon balance when lower heat-treatments are applied.

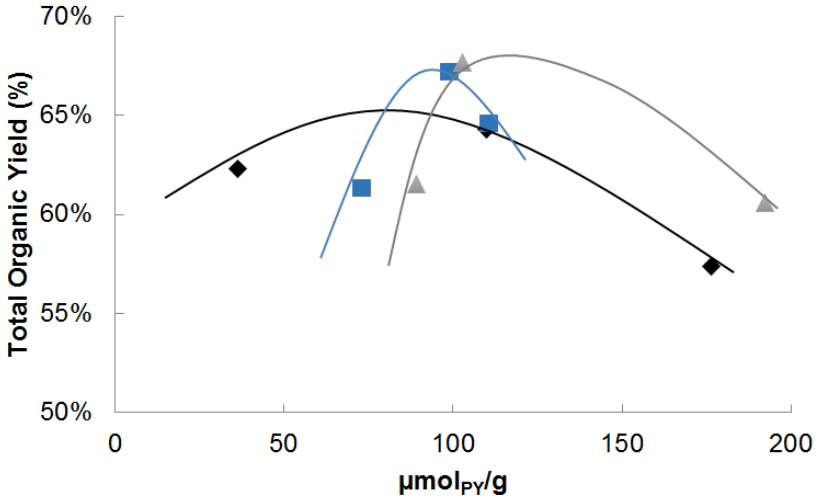

Figure 6.24. Total organic product yield variation with total acid sites per gram ($\mu mol_{PY}/g$) measured by FT-IR. HT-$W_{47}Nb_{53}$ (grey triangles), HT-$W_{38}Nb_{62}$ (blue squares) and HT-W_0Nb_{100} (black diamonds). Reaction Conditions: aqueous model mixture (3000 mg) and catalyst (150 mg) in autoclave-type reactor, at 13 bar N_2 and 200 ºC during 3 h.

Indeed, the higher amount of total acid sites and their right distribution on the catalyst surface leads to increase the organic products yields during the process (Figure 6.25). Therefore, if total organic products yield is analogously plotted with total acid sites normalized by surface area ($\mu mol_{PY}/m^2$), the right distribution of acid sites seems to be a key factor on catalytic results. The optimal combination of hydrothermal synthesis, composition and post-synthesis heat-treatment leads to HT-$W_{47}Nb_{53}$-C300 and $W_{38}Nb_{62}$-C400 as the best catalysts in terms of total organic product yields.

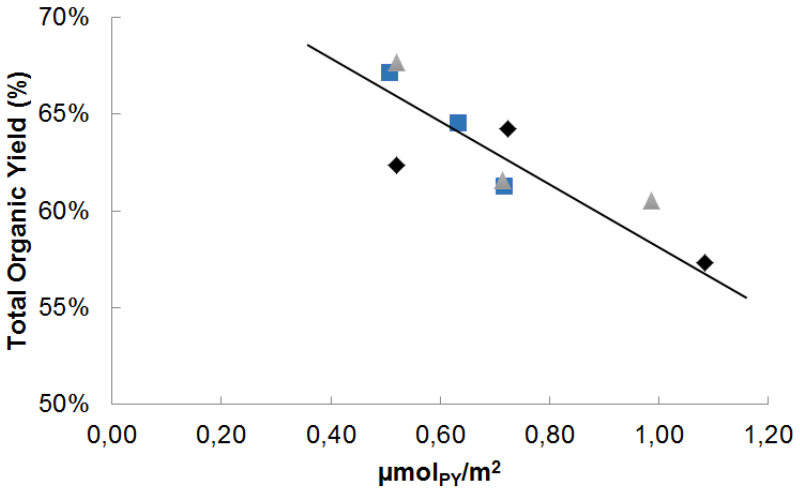

Figure 6.25. Total organic product yield variation with total acid sites normalized per surface area ($\mu mol_{PY}/m^2$). HT-$W_{47}Nb_{53}$ (grey triangles), HT-$W_{38}Nb_{62}$ (blue squares) and HT-W_0Nb_{100} (black diamonds). Reaction Conditions: 3 g aqueous mixture, 150 mg of catalyst, at 13 bar N_2 and 200 ºC during 3 h.

Definitely, surface area and acid properties can be optimized when applying the adequate post-synthesis heat-treatment. In particular, higher total acid sites are favourable, although their correct distribution is essential in order to avoid undesired polymerization reactions and finally optimize total organic products yield.

6.3.7. Stability tests

Recycling experiments of oxygenated compounds condensation reactions were performed testing selected catalysts during three consecutive reuses to corroborate the resistance of WNbO materials under these reaction conditions and the results in terms of total organic product yield attained are given in Figure 6.26.

Recycling experiments were performed by reusing the catalysts several times. Once the catalytic experiment was finished, the solid was separated by centrifugation and washed repeatedly with methanol. Finally, after drying it at 100 ºC overnight, the solid was analysed by elemental analysis (EA) to determine the organic compounds deposition in the surface of the catalyst.

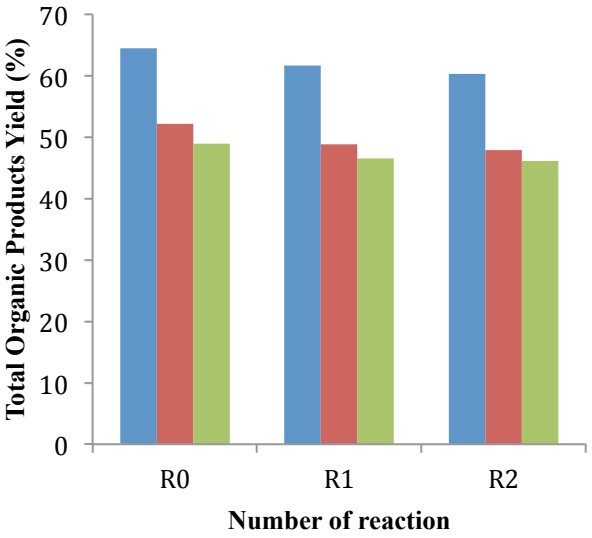

Figure 6.26. Effect of the re-uses (R0, R1 and R2) of different WNbO catalysts on total organic product yield (%) on the condensation of oxygenated compounds in aqueous model mixture: HT-$W_{38}Nb_{62}$ (blue), COP-$W_{50}Nb_{50}$ (red) and WI-$W_{50}Nb_{50}$ (green). Reaction Conditions: 3 g aqueous mixture, 150 mg of catalyst, at 13 bar N_2 and 200 ºC during 7 h.

Firstly, no leaching of tungsten and/or niobium was observed in all the different WNbO catalysts tested. Therefore, differences in stability are completely due to acid sites deactivation by carbon deposition on the surface of the catalysts.

HT-WNbO sample exhibited high stability (structure maintenance), although its catalytic activity slightly decreased during the re-uses, with 6% loss of total organic product yield after the 2nd reuse. This is probably due to carbon deposition on the solid (measured by EA, Table 6.15), as this material possesses both higher surface area and total acid sites.

Analogously, COP-WNb and WI-WNb samples also suffered a similar loss of catalytic activity (6-8% loss), depending on the amount of carbon deposited as measured by EA (Table 6.15).

Table 6.15. Total organic product yield (%) and post-reaction characterization by elemental analysis for different WNbO catalysts in the condensation of oxygenated compounds in aqueous model mixture.

Catalysts	Total Organic Products Yield (%)			E.A. (%)
	R0	R1	R2	
HT-$W_{38}Nb_{62}$	64.5	61.7	60.3	1.4
COP-$W_{50}Nb_{50}$	52.2	48.9	47.9	4.2
WI-$W_{50}Nb_{50}$	49.0	46.6	46.1	1.3

Summarizing, HT-WNbO samples show great catalytic results in the aqueous-phase condensation of oxygenated compound. These catalysts maintain their performance practically invariable after reuses due to the structure preservation and the slight amount of coke deposition on the catalyst surface (measured by EA). Other WNbO mixed oxides also show high stability (low carbon deposition), although they show much lower activity based on their poor surface areas and acid properties. More interestingly, in all the Nb-based catalysts used in the re-cycling experiments, no leaching of Nb was observed.

6.4 Conclusions

- Niobium oxide materials prepared by hydrothermal synthesis with a pseudo-crystalline structure and showing tunable acid properties have shown to be active and selective catalysts for the valorisation of oxygenated compounds in aqueous effluents obtained by phase separation of bio-oils.

- Control of post-synthesis heat-treatments drives to optimized NbO_x materials with higher stability (after several reuses) and catalytic activity than those previously reported by other authors, mainly because they are highly water-resistant catalysts.

- In the same line, hydrothermally synthesized tungsten-niobium mixed oxides have shown the advantage of having crystalline structure, area and acid properties that can be controlled by tailoring their chemical composition. Optimization of W-Nb contents in HT-samples maximized the yield of products in the range of C_5-C_{10} compounds useful for fuel applications. Moreover, HT-WNbO catalysts show much better catalytic results than other WNbO prepared by different procedures.

- High content Nb (i.e. HT-$W_{38}Nb_{62}$) samples drive to the highest total organic product yields, especially due to their activity and stability under complex aqueous environments. Catalytic results can be further optimized by employing adequate post-synthesis heat-treatment conditions.

- A deeper understanding of the reaction network has been achieved by working at different reaction conditions. In this sense, acetic acid low conversion values confirm that most of the organic acid reacts via esterification, while simultaneous oxidation reaction may be occurring at 200 ºC. Finally, reactions at 180 ºC allow correlating catalytic results to catalysts physicochemical properties, whereas higher reaction times and higher process temperatures maximize the yield of products from 2nd condensation steps (C_9-C_{10} products).

6.5 References

1. Nakajima, K. *et al. J. Amer. Chem. Soc.* **133,** 4224–4227 (2011).
2. Tanabe, K. *Catal. Today* **78,** 65–77 (2003).
3. Nowak, I. & Ziolek, M. *Chem. Rev.* **99,** 3603–3624 (1999).
4. Rodrigues, R., Mandelli, D., Gonçalves, N.S., Pescarmona, P.P. & Carvalho, W.A. *J. Mol. Catal. A: Chem.* **422,** 122–130 (2016).
5. Kreissl, H.T. *et al. J. Catalysis.* **338,** 329–339 (2016).
6. Paulis, M. Martín, M. Soria, D.B. Díaz, A. Odriozola, J.A. Montes, A. *Appl. Catal., A. Gen.* **180,** 411–420 (1999).
7. Foo, G.S., Wei, D., Sholl, D.S. & Sievers, C. *ACS Catal.* **4,** 3180–3192 (2014).
8. Omata, K., Matsumoto, K., Murayama, T. & Ueda, W. *Catal. Today* **259,** 205–212 (2016).
9. Murayama, T., Chen, J., Hirata, J., Matsumoto, K. & Ueda, W. *Catal. Sci. Technol.* **4,** 4250–4257 (2014).
10. Soriano, M.D. *et al. Green Chem.* **13,** 2954-2962 (2011).
11. Chieregato, A. *et al. ChemSusChem* **8,** 398–406 (2015).

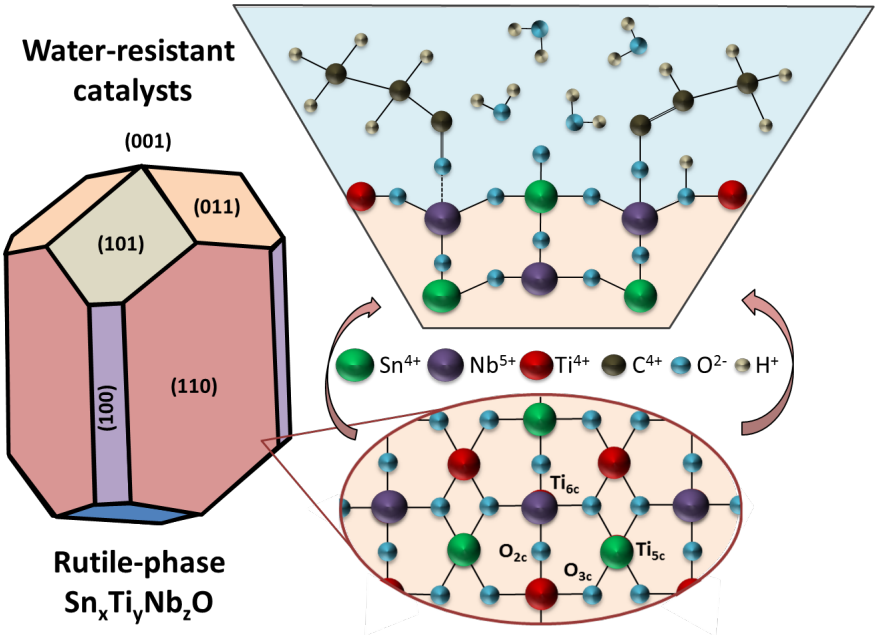

CHAPTER 7

TIN-BASED MIXED OXIDES AS ACID CATALYSTS FOR THE AQUEOUS-PHASE CONDENSATION OF OXYGENATED COMPOUNDS

7.1 Introduction

Isolated Sn^{4+} centers present in homogeneous and heterogeneous catalysts are broadly known as effective Lewis acid sites with high catalytic activity in diverse organic reactions as Baeyer-Villiger reactions[1,2], Meerwein-Ponndorf-Verley reactions[3,4], isomerization reactions[5,6], among others. In the case of solid materials, Sn^{4+} centers need to be well dispersed over supports (i.e. zeolites), which posses higher surface areas, density of acid sites and hydrophobic properties. In particular, Sn-Beta zeolites have been widely employed in above-mentioned organic reactions with outstanding results. Nonetheless, as discussed in Chapter 4, zeolites are not effective catalysts in the aqueous-phase condensation of oxygenate mixtures mainly due to the presence of high-functionalized organic compounds in acidic aqueous environments.

On the other hand, SnO_2 catalysts usually crystallize in a rutile-phase structure with low surface area and reduced number of acid sites. In this regard, the surface science of tin oxide, including crystalline structure, textural properties and potential applications have been widely studied[7]. Moreover, innovative and complex synthesis methods (i.e. high temperature thermal oxidation, hydrothermal, sol-gel method, among others) using organic mediums and several synthesis steps have been attempted in order to obtain high surface area tin oxides[8–10].

In this Chapter, Sn-based mixed oxides prepared via co-precipitation will be studied as potential Lewis acid catalysts in the condensation of light oxygenates in aqueous mixtures. In particular, tin combination with resistant metal oxides as zirconia, titania and niobia will be analysed.

7.2 Sn_xZr_yO mixed oxides

A general co-precipitation procedure (detailed in Section 3.2.4) was used to synthesize Sn_xZr_yO mixed oxides. Tin (IV) chloride pentahydrate and zirconium (IV) oxynitrate were used as metal precursors and dissolved in 100 mL of distilled water. After reaching pH=9 by adding a 28 wt% NH_4OH aqueous solution, the gel was aged, washed, filtered and dried at 100 ºC overnight. Finally, synthesized catalysts were calcined in air at 600 ºC for 2h with a heating rate of 2 ºC/min. Samples are named as SnZr-x, where x is the Sn/(Sn+Zr) molar ratio in the catalyst.

Firstly, Sn_xZr_yO materials were characterized by X-ray diffraction and compared with commercial SnO_2 (Sigma Aldrich) and tetragonal ZrO_2 (Chempur) samples (Figure 7.1). Commercial SnO_2 (SnZr-1.00) presents the characteristic rutile structure of this metal oxide[10]. Incorporation of zirconium in low amounts (i.e. SnZr-0.86 and SnZr-0.72 samples) leads to the formation of homogeneous Sn_xZr_yO mixed oxides with rutile crystalline structure. On the contrary, a higher content of zirconium in these mixed oxides (Sn/(Sn+Zr) <0.72) drives to undefined crystalline structures, where Bragg signals of both rutile and ZrO_2 tetragonal phases can be recognized[11]. Then, only Sn_xZr_yO with a Sn atomic ratio >0.72 can be synthesized with an homogeneous crystalline structure.

These catalysts were also characterized by means of N_2 adsorption to determine their surface area and pore volume (Table 7.1). Higher Zr-contents in the composition increase the surface area and pore volumes of the mixed oxides, reaching a maximum of 91 m^2/g for SnZr-0.19.

Nonetheless, homogeneous rutile-phase samples (Sn/(Sn+Zr) >0.72) show low surface area values (<30 m^2/g) and negligible pore volumes.

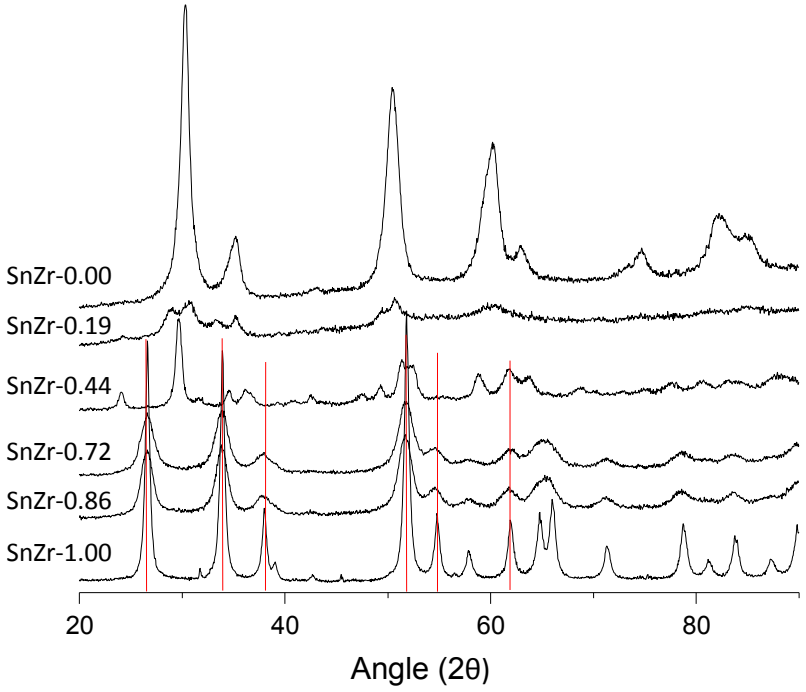

Figure 7.1. XRD profiles of Sn_xZr_yO catalysts (red lines indicate rutile structure).

Table 7.1. Main structural and textural characteristics of Sn_xZr_yO catalysts.

Catalyst	Rutile crystalline phase	Surface area (m^2/g)[c]	Pore volume (cm^3/g)
SnZr-0.00[a]	×	138	0.20
SnZr-0.19	×	91	0.05
SnZr-0.44	×	43	0.08
SnZr-0.72	✓	28	0.03
SnZr-0.86	✓	22	0.01
SnZr-1.00[b]	✓	15	0.01

[a]Tetragonal ZrO_2 (Chempur); [b]SnO_2 (Sigma Aldrich); [c] Calculated from N_2 adsorption isotherms (BET method).

The activity of these Sn_xZr_yO type catalysts was tested in the condensation of C_2-C_3 oxygenated compounds in the aqueous phase (Table 7.2). As can be seen, propanal conversion increases when Sn_xZr_yO mixed oxides are employed compared to SnO_2 and ZrO_2 commercial catalysts, but this enhanced conversion does not drive to a concomitant increase in total product yields. Then, catalytic results are similar to commercial catalysts even when samples with Sn/(Sn+Zr) ratios ≤0.44 (i.e. SnZr-0.44 and SnZr-0.19 samples) show higher surface area values. This can be explained by their non-uniform crystalline structure, where tetragonal zirconium species drive to low carbon balances, as oxygenated compounds may be retained in the catalysts surface due to interactions with strong Zr active sites.

Table 7.2. Catalytic results of Sn_xZr_yO materials in the condensation of oxygenated compounds in the aqueous phase.

Catalyst		Zr	1.00[a]	0.81	0.56	0.28	0.14	0.00
		Sn	0.00	0.19	0.44	0.72	0.86	1.00[b]
Conversion (%)		Acetic acid	7.9	17.2	9.5	9.1	9.4	12.9
		Propanal	63.7	70.0	75.3	81.9	82.2	68.8
		Ethanol	50.8	46.0	49.5	52.0	51.7	48.6
		Acetol	100.0	100.0	100.0	100.0	100.0	100.0
Product Yield (%)		Ethyl acetate	23.3	24.7	20.9	21.8	21.0	24.5
		2M2P[a]	18.9	26.2	25.1	27.0	26.9	29.5
		C5-C8	9.5	9.9	11.7	11.8	12.0	7.8
		C9-C10	8.5	12.5	12.5	13.1	12.5	16.3
		Total	**36.9**	**50.0**	**51.3**	**55.5**	**54.6**	**53.6**
Carbon balance (%)			86.2	91.4	89.7	93.2	93.5	96.7

Reaction conditions: 3 g of aqueous mixture, 150 mg of catalyst; T=200 ºC, P=13 bar N_2, t= 7h. [a]2M2P=2-methyl-2-pentenal.

[a]Tetragonal ZrO_2 (Chempur); [b]SnO_2 (Sigma Aldrich)

7.3 Sn_xTi_yO mixed oxides

Sn-based mixed oxides rutile-phase crystalline structure has arisen as an important factor to possibly increase their catalytic activity. Analogously to SnO_2 monometallic oxides, TiO_2-rutile phase has always been dismissed due to its poor textural and acid properties, although it has been interestingly claimed as the most hydrophobic TiO_2 crystalline phase[12]. In this sense, Sn_xTi_yO mixed oxides, synthesized via hydrothermal and sol-gel methods, with an homogeneous rutile structure and enhanced textural properties, have been studied in literature[13–15]. These materials have been used as proton exchange membranes, in photocatalysis applications and as solid catalysts (i.e. CO oxidation), but their acid characteristics in catalysis and especially in condensation reactions have never been tested. Moreover, it will be of great interest to prepare these materials via easier and cheaper synthesis procedures.

7.3.1. Synthesis of Sn_xTi_yO materials

A general co-precipitation procedure (detailed in Section 3.2.4) was used to synthesize Sn_xTi_yO mixed oxides. Tin (IV) chloride pentahydrate and titanium (IV) oxychloride-HCl acid solution (15wt% Ti) were used as metal precursors and dissolved in 100 mL of distilled water. After reaching pH=9 by adding a 28wt% NH_4OH aqueous solution, the gel was aged, washed, filtered and dried at 100 ºC overnight. Finally, synthesized catalysts were calcined in air at 600 ºC for 2h with a heating rate of 2 ºC/min. Samples are named as SnTi-x, where x is the Sn/(Sn+Ti) molar ratio in the catalyst.

7.3.2. Catalysts characterization

Firstly, Sn_xTi_yO materials were characterized by X-ray diffraction and compared to commercial SnO_2 and RUT-TiO_2 (Sigma Aldrich) samples (Figure 7.2). As above-mentioned, commercial SnO_2 (Figure 7.2a) presents characteristic Bragg peaks of the rutile structure of this metal oxide[10]. X-rays patterns of Sn_xTi_yO co-precipitated materials indicate that titanium is fully incorporated in the same rutile crystalline phase[14]. Thus, peaks shift is completely consistent with the progressive enrichment in Ti along all the range of composition studied (Fig. 7.2a-e).

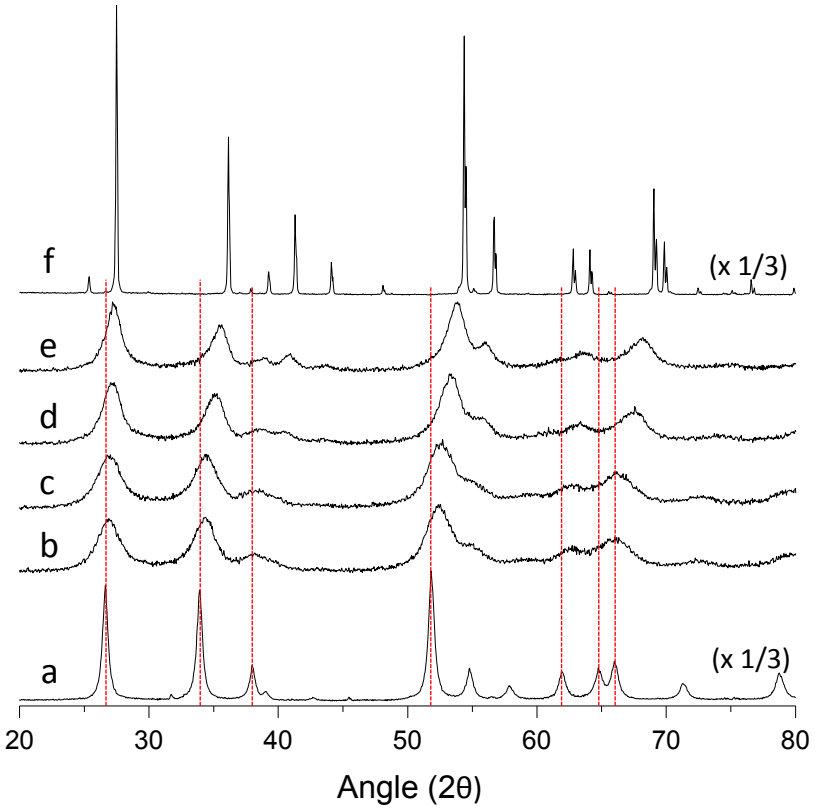

Figure 7.2. XRD profiles of Sn_xTi_yO catalysts: a) SnTi-1.00; b) SnTi-0.74; c) SnTi-0.64; d) SnTi-0.33; e) SnTi-0.18 and f) SnTi-0.00.

The concomitant variation of unit cell parameters (a and c) of the crystalline structure of Sn_xTi_yO catalysts can be calculated from XRD profiles (Figure 7.3). This figure shows that homogeneous Sn_xTi_yO materials can be prepared by co-precipitation even for low Sn/(Sn+Ti) molar ratios (i.e. SnTi-0.05 and SnTi-0.09 in Figure 7.3)[14]. It is worth noting that commercial RUT-TiO_2 catalyst is used as reference, because SnTi-0.00 prepared by co-precipitation and calcined under the same conditions (i.e. 600 ºC) is the only exception and drives to an anatase phase TiO_2 material.

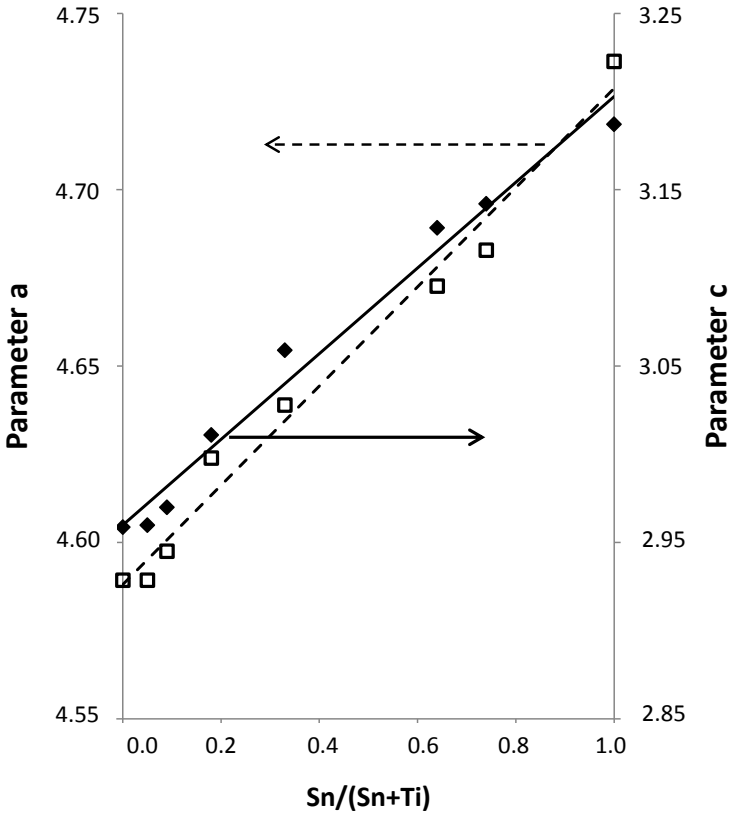

Figure 7.3. Variation of unit cell parameters of Sn_xTi_yO catalysts from XRD diffraction measurements.

An equivalent behavior can be observed during Raman spectroscopy measurements of these samples. Characteristic signals assigned to rutile-phase SnO_2 are observed for commercial SnO_2 catalyst (Figure 7.4a). Progressive incorporation of titanium in the crystalline structure drives to the disappearance of B_{2g} mode (775 cm^{-1}) and the analogous shift of E_g (473 cm^{-1}) and A_{1g} (639 cm^{-1}) modes in the Raman spectra of all the Sn_xTi_yO catalysts studied (Figure 7.4b-e)[14]. Finally, commercial RUT-TiO_2 catalyst shows the characteristic Raman signals of this crystalline structure (Figure 7.4f)

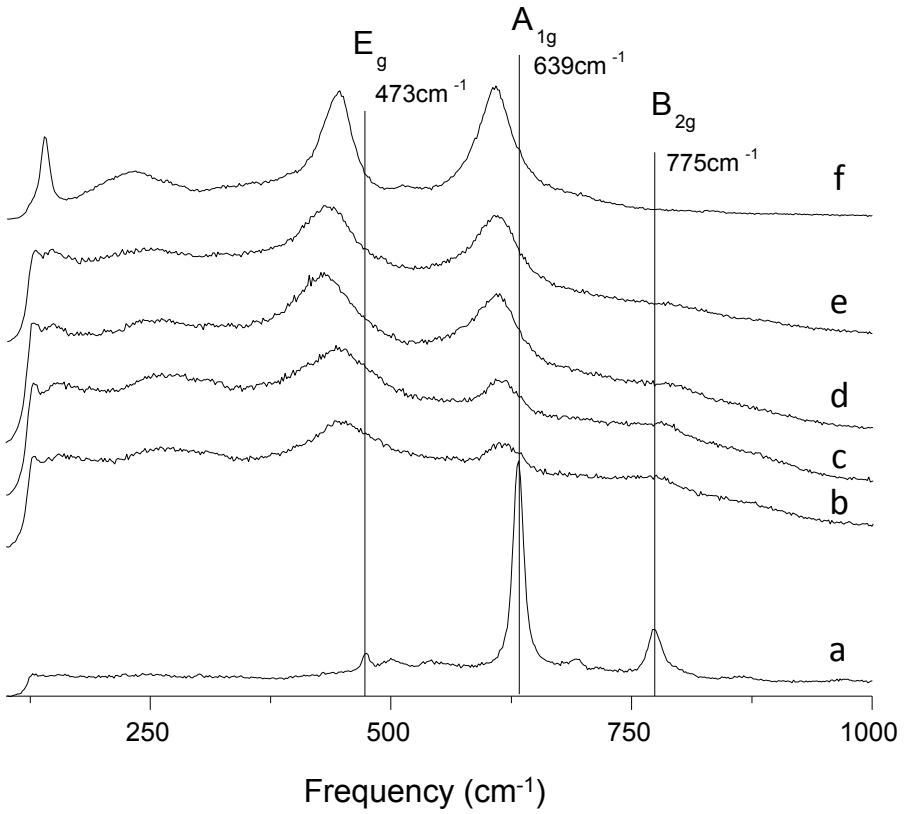

Figure 7.4. Raman spectra of Sn_xTi_yO catalysts: a) SnTi-1.00; b) SnTi-0.74; c) SnTi-0.64; d) SnTi-0.33; e) SnTi-0.18 and f) SnTi-0.00.

Then, the preparation of these catalysts via co-precipitation allows obtaining homogeneous solid mixed oxides (elucidated by elemental mapping from SEM-EDS) in all the range of composition (Fig. 7.5B-C). Moreover, Sn_xTi_yO mixed oxides present less intense and broad signals in both XRD diffraction (Figure 7.2b-e) and Raman spectroscopy (Figure 7.4b-e), which can be ascribed to the formation of nanoparticles[10]. TEM images (Figure 7.5D), where agglomerated nanoparticles of Sn-Ti ranging from 5 to 15 nm are observed, confirm these structural features.

In particular, estimated particle size (nm) for Sn_xTi_yO materials from Scherrer´s equation and TEM images analyses can be compared in Table 7.3, where equivalent values are achieved by both methods.

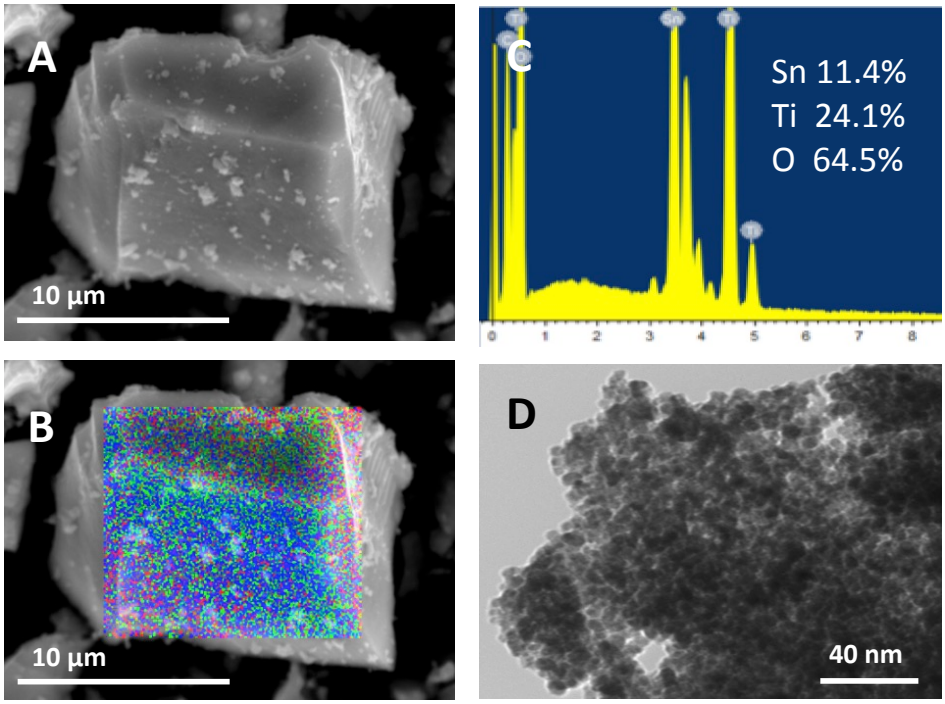

Figure 7.5. Electron microscopy techniques of SnTi-0.33 catalyst: A) SEM image; B) SEM-EDS mapping image: Sn (blue),Ti (green), O (red); C) SEM-EDS spectra and D) TEM image.

Finally, textural and acid characteristics of these materials were elucidated by N_2 adsorption isotherms and FT-IR with pyridine adsorption-desorption at 150 ºC (Table 7.3). In this sense, the synthesis of Sn_xTi_yO mixed oxides via co-precipitation drives to catalysts, which show enhanced surface areas (85-120 m^2/g), pore volumes (0.12-0.16 cm^3/g) and acid properties (85-150 $\mu mol_{PY}/g$) compared to commercial catalysts or analogous Ti/SnO_2 and Sn/TiO_2 mixed oxides prepared by incipient wetness impregnation (2-15 m^2/g, <0.01 cm^3/g and 10-30 $\mu mol_{PY}/g$, respectively). More interestingly, acid characteristics in these materials completely rely on Lewis acid sites.

Table 7.3. Main textural and physicochemical characteristics of Sn_xTi_yO materials.

Catalyst	Surface area (m^2/g)[a]	Pore volume (cm^3/g)	Lewis acid sites (mmol/g)[b]	Particle size (nm)	
				Scherrer equation	TEM images
SnTi-0.00[c]	2	0.00	12	-	-
SnTi-0.18	87	0.15	85	5	10
SnTi-0.33	116	0.16	84	4	8
SnTi-0.64	118	0.13	132	6	7
SnTi-0.74	103	0.12	148	8	8
SnTi-1.00[d]	15	0.01	29	20	-
Sn/TiO_2	2	0.00	-	-	-
Ti/SnO_2	13	0.01	-	-	-

[a]Calculated from N_2 adsorption isotherms (BET method); [b]FT-IR with pyridine adsorption-desorption at 150 ºC; [c] Commercial RUT-TiO_2 (Sigma Aldrich); [d] Commercial SnO_2 (Sigma Aldrich).

Therefore, Sn_xTi_yO preparation via co-precipitation is essential to obtain homogeneous solid mixed oxides, with a higher concentration of Lewis acid sites, adequate for aqueous-phase condensation reactions.

7.3.3. Catalytic results

7.3.3.1. Catalytic performance of Sn_xTi_yO materials in the condensation of a mixture of oxygenated compounds in aqueous phase

Catalytic results of Sn_xTi_yO materials in the consecutive condensation of oxygenated compounds in aqueous mixture containing: 30wt% H_2O, 30wt% acetic acid, 25wt% propanal, 10wt% ethanol and 5wt% acetol (See Section 3.4) are shown in Table 7.4 and Table 7.5. Results are expressed in terms of oxygenated compounds conversion and yields to main reaction products: ethyl acetate, 2-methy-2-pentenal, C_5-C_8 and C_9-C_{10} products.

In general, co-precipitated Sn-Ti mixed oxides show higher yields to the main condensation organic products. In particular, catalysts containing low amounts of Sn (i.e. molar ratio from 0.18 to 0.33) maximize reactants conversion: acetol (≈90%), propanal (≈58%), ethanol (≈40%) and acetic acid (8-12%). Therefore, higher total organic products yields (sum of first condensation and C_5-C_{10} products in wt%) of 40-46% are achieved up to 1h on stream, whereas other Sn-Ti oxides drive to lower catalytic results (Table 7.5).

Figure 7.6 specifically shows how catalyst composition optimization (i.e. $0.18<Sn/(Sn+Ti)<0.33$) allows maximizing both C_9-C_{10} (2^{nd} condensation step) products yield and total organic products yield, always analyzing results attained at 1 h of reaction.

Table 7.4. Catalytic results of Sn_xTi_yO materials in the condensation of oxygenated compounds in the aqueous phase.

Catalyst		Ti	1.00[a]	0.82	0.67	0.36	0.26	0.00
		Sn	0.00	0.18	0.33	0.64	0.74	1.00[b]
Conversion (%)		Acetic acid	9.9	7.5	12.2	6.7	9.0	0.0
		Propanal	27.2	56.4	57.8	55.7	51.9	19.2
		Ethanol	26.9	42.4	38.4	41.0	38.0	20.1
		Acetol	85.2	92.4	93.1	91.1	92.6	84.0
Product Yield (%)		Ethyl acetate	17.8	21.5	15.6	22.6	18.2	15.0
		2M2P[c]	9.4	17.9	18.8	19.3	16.4	13.6
		C5-C8	14.4	21.3	21.4	17.4	20.3	11.8
		C9-C10	1.6	6.9	5.1	5.3	3.9	5.4
		Total	**25.4**	**46.0**	**45.3**	**42.0**	**40.7**	**30.8**
Carbon balance (%)			98.3	98.8	93.4	98.7	97.4	99.5

Reaction conditions: 3 g of aqueous mixture, 150 mg of catalyst; T=200 ºC, P=13 bar N_2, t= 1h. [a]RUT-TiO_2; [b]Comm. SnO_2; [c]2M2P=2-methyl-2-pentenal.

Table 7.5. Catalytic results of Sn_xTi_yO materials in the condensation of oxygenated compounds in the aqueous phase.

Catalyst		Rut-TiO_2	4%Sn/TiO_2	**SnTi-0.33**	7%Ti/SnO_2	Rut-SnO_2
Conversion (%)	Acetic acid	9.9	0.8	**12.2**	8.2	0.0
	Propanal	27.2	34.8	**57.8**	38.1	19.2
	Ethanol	26.9	37.5	**38.4**	28.6	20.1
	Acetol	85.2	78.9	**93.1**	70.4	84.0
Product Yield (%)	Ethyl acetate	17.8	16.8	**15.6**	16.0	15.0
	2M2P[a]	9.4	13.5	**18.8**	13.4	13.6
	C5-C8	14.4	7.9	**21.4**	16.1	11.8
	C9-C10	1.6	4.9	**5.1**	2.2	5.4
	Total	**25.4**	**26.3**	**45.3**	**31.7**	**30.8**
Carbon balance (%)		98.3	94.5	**93.4**	98.7	99.5

Reaction conditions: 3 g of aqueous mixture, 150 mg of catalyst; T=200 ºC, P=13 bar N_2, t= 1h. [a]2M2P=2-methyl-2-pentenal.

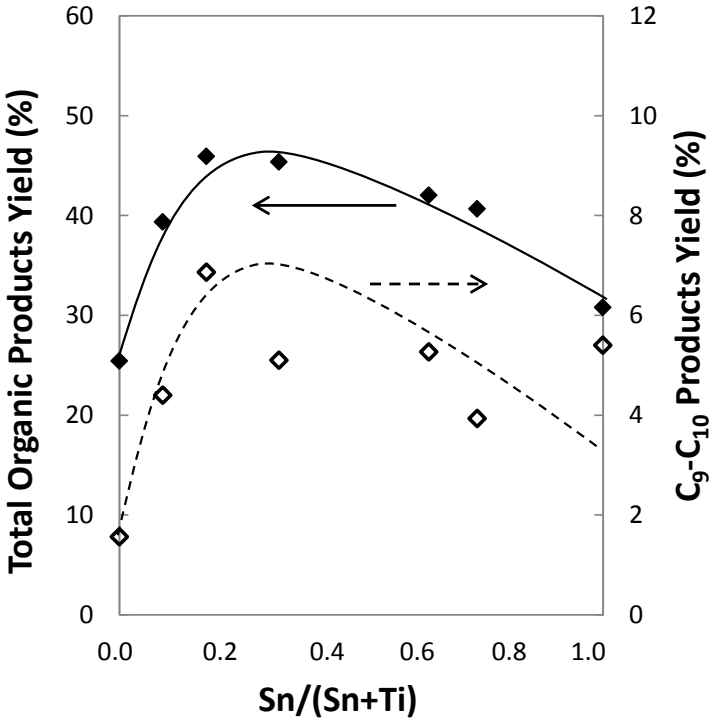

Figure 7.6. Sn/(Sn+Ti) composition effect on total organic products yield (full diamonds) and C_9-C_{10} products yield (empty diamonds) in the condensation of a mixture of oxygenated compounds in aqueous phase.
Reaction conditions: 3 g of aqueous mixture, 150 mg of catalyst; T=200 ºC, P=13 bar N_2, t= 1h.

Thus, Sn_xTi_yO materials prepared via co-precipitation show higher reaction rates at 1h on stream (Table 7.6) and the highest yields to the main condensation organic products at 1h and 7h, when compared to SnO_2 and RUT-TiO_2 commercial materials. More interestingly, only co-precipitated Sn-Ti mixed oxides are able to produce enough heavier products after 7h of reaction, these hydrocarbons becoming spontaneously separated from water and non-converted reactants, which facilitates their isolation and subsequent use.

Table 7.6. Reaction rates calculated at 1h and total organic products yield (%) of Sn_xTi_yO materials at different times on stream.

Catalyst	Reaction rate at 1h ($\mu mol \cdot min^{-1} g^{-1}$)	Total organic products yield (%)	
		1h	7h
SnTi-0.00[a]	941	25.4	48.2
SnTi-0.18	1449	46.0	60.9
SnTi-0.33	1520	45.3	63.5
SnTi-0.64	1412	42.0	60.4
SnTi-0.74	1373	40.7	59.5
SnTi-1.00[b]	610	30.8	53.6
Sn/TiO_2	961	26.3	46.4
Ti/SnO_2	1049	31.7	51.4

[a]Commercial RUT-TiO_2 (Sigma Aldrich); [b]Commercial SnO_2 (Sigma Aldrich)
Reaction conditions: 3 g of aqueous mixture, 150 mg of catalyst; T=200 ºC, P=13 bar N_2, t= 1h and 7h.

7.3.3.2. H_2O and acetic acid effect on the catalytic performance of Sn_xTi_yO materials in light oxygenates condensation reactions

As previously commented, higher reaction rates and total products yields shown by co-precipitated Sn_xTi_yO materials are directly related to their enhanced textural and acid properties (Table 7.3). In this sense, additional experiments (analogous to those carried out during Chapter 5 for TiO_2 materials) were studied in order to obtain further information about water and acetic acid effect on the conversion of light oxygenates for this type of materials.

On one hand, the effect of water is studied. Three different scenarios are considered: a) water is eliminated and relative concentration of all reactants is kept constant; b) the amount of water is replaced by ethanol and c) reference aqueous model mixture is used.

As can be seen in Figure 7.7 (left side), high conversion of propanal (74%) is reached in only 1h when SnTi-0.33 is used in the absence of water in the reaction medium. Propanal conversion slightly decrease (22% decay) when a higher concentration of ethanol is added, as esterification reactions are maximized, whereas no further detrimental effects are observed when 30wt% of water is added to the mixture. Both, commercial SnO_2 and RUT-TiO_2 show analogous trends, although in these cases, the addition of water drives to worse catalytic results compared to the Sn-Ti mixed oxide. It is worth noting that the presence of water has a tremendous impact on SnO_2 (SnTi-1.00) catalyst (64% decay), whereas RUT-TiO_2 suffers an intermediate effect (31% decay).

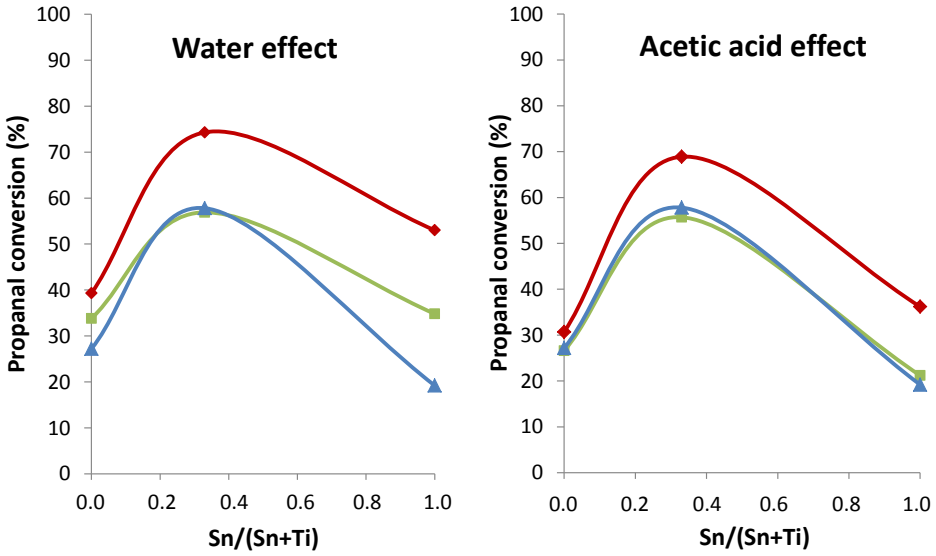

Figure 7.7. Water effect and acetic acid effect on propanal conversion for different Sn_xTi_yO catalysts. Scenario A (red lines); scenario B (green lines) and scenario C (blue lines).
Reaction conditions: 3 g of aqueous mixture, 150 mg of catalyst; T=200 ºC, P=13 bar N_2, t= 1h.

In this regard, the water effect on total organic products yield (%) for the whole Sn_xTi_yO series of catalysts was studied (Figure 7.8). It can be seen that RUT-TiO_2 and high Ti-content Sn_xTi_yO materials approximately maintain their activity (products yield) when 30wt% of water is added to the mixture, whereas bigger detrimental effects are observed for high Sn-content samples and commercial SnO_2 catalyst.

On the other hand, three different scenarios are considered to study acetic acid effect on propanal conversion: a) propanal aldol condensation in an ethanol/H_2O system; b) 30wt% of acetic acid is added to the previous medium and c) reference aqueous model mixture is used.

As can be seen in Figure 7.7 (right side), high conversion of propanal (69%) is reached in only 1 hour when SnTi-0.33 is used in the absence of acetic acid in the reaction medium, being propanal conversion slightly decreased (16% decay) when 30wt% of acetic acid is added. Once again, the presence of acetic acid in the system has a bigger impact on SnO_2 (SnTi-1.00) catalyst (i.e. 47% decay), whereas RUT-TiO_2 suffers the lowest detrimental effect (i.e. 11% decay).

These experiments allow explaining previous results using complex aqueous mixtures in more detail, as catalytic results can be more easily correlated to textural and acid properties of the materials.

On one hand, high Sn-content Sn_xTi_yO catalysts present a higher concentration of acid sites. Nonetheless, these materials show lower resistance to water and organic acid addition in the reaction mixture. On the other hand, high Ti-content Sn_xTi_yO materials possess lower amounts of acid sites, but they are more resistant to the presence of water (see

water-resistant catalysts in Figure 7.8) and organic acids in the media. These balanced characteristics explain why similar reaction rates and total organic products yields are achieved with all the Sn_xTi_yO catalysts.

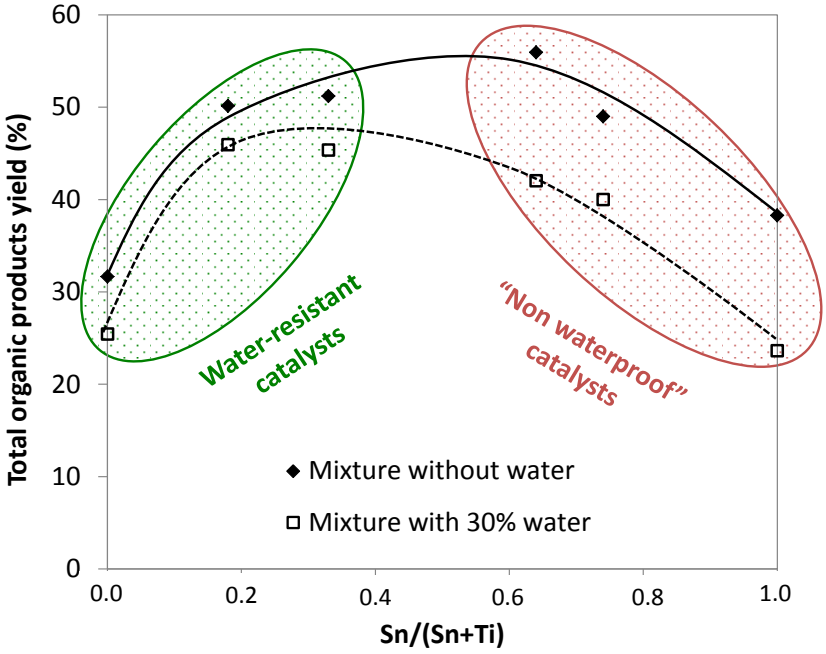

Figure 7.8. Water effect on total organic products yield (%) for different Sn_xTi_yO catalysts. Reaction conditions: 3 g of mixture, 150 mg of catalyst; T=200 ºC, P=13 bar N_2, t= 1h.

Moreover, commercial RUT-TiO_2 and Sn_xTi_yO mixed oxides have shown better resistance to the addition of water and acetic acid in the medium compared to other anatase phase TiO_2 materials previously studied in Chapter 5 (Table 7.7).

In this regard, commercial RUT-TiO_2 shows low propanal conversion (i.e. 39%) when organic solvents are used, whereas anatase phase TiO_2 samples show the highest propanal conversions (89-92%).

Nonetheless, when complex aqueous mixtures are employed, similar reactions rates are achieved for TiO_2-ANA and RUT-TiO_2 (see

calculated reaction rates in Table 7.7), in spite of rutile TiO_2 presents much lower surface area and acid properties than other TiO_2 materials. This data matches previous results in literature, which affirm that rutile TiO_2 materials posses hydrophobic characteristics compared to anatase phase TiO_2 catalysts[12].

As it was previously discussed (see Chapter 5), TiO_2-ISO material with anatase structure and enhanced textural and acid properties mainly due to preferentially exposed {001} TiO_2 facets offers better catalytic results (higher reactions rates in Table 7.7) than both commercial TiO_2-ANA and RUT-TiO_2 materials.

Table 7.7. Water and acetic acid effect on TiO_2 and Sn_xTi_yO catalysts.

Catalyst	Propanal conversion at 1h[a]	Decay effect (%)		Reaction rate at 1h ($\mu molmin^{-1}g^{-1}$)[b]
		Water addition	Acetic acid addition	
TiO_2-ANA	89%	-65%	-63%	1086
TiO_2-ISO	92%	-51%	-42%	1345
SnTi-0.00[c]	39%	-31%	-11%	941
SnTi-0.33	**85%**	**-22%**	**-16%**	**1520**

[a]Reaction mixture: 25wt% of propanal, 75wt% of ethanol; . [b]Model aqueous mixture [c]Commercial RUT-TiO_2 (Sigma Aldrich)

More interestingly, SnTi-0.33 catalyst (with rutile structure and enhanced surface and acid properties) drives to the best catalytic results among all the Ti-based materials studied during this work, when condensation reactions are performed in aqueous systems and in the presence of organic acids and other oxygenates mixtures (see the lowest decay effects caused by water and acetic acid addition on this material).

7.3.3.3. Stability tests of Sn_xTi_yO materials in the condensation of a mixture of oxygenated compounds in aqueous phase

Recycling experiments were performed testing a selected Sn_xTi_yO catalyst (i.e. SnTi-0.33) to corroborate its resistance under reaction conditions. Results in terms of reactants conversion and products yield are given in Table 7.8. Despite its higher catalytic activity, especially under complex aqueous environments, SnTi-0.33 progressively deactivates after three consecutive reuses. Propanal conversion slightly decreases (from 88% to 78%) and thus, lower total organic products yields are observed after the second reuse (63% to 57%). These results can be explained by the carbon deposition (≈2.8%) on the catalyst surface measured by elemental analysis.

Table 7.8. Stability results of the reuse of SnTi-0.33 catalyst in the condensation of oxygenated compounds in the aqueous phase.

Catalyst			Reference	R0	R1	R2
Conversion	(%)	Acetic acid	10.2	7.0	7.9	8.6
		Propanal	87.6	85.3	81.5	78.2
		Ethanol	51.4	46.1	53.5	46.2
		Acetol	100.0	100.0	100.0	100.0
Product Yield	(%)	Ethyl acetate	22.4	20.2	21.6	21.8
		2M2P[a]	30.7	30.5	28.2	26.4
		C5-C8	16.3	16.7	16.6	15.3
		C9-C10	16.5	16.1	15.7	15.8
		Total	**63.5**	**63.3**	**60.5**	**57.5**
Carbon balance (%)			95.0	95.8	95.4	95.8

Reaction conditions: 3 g of aqueous mixture, 150 mg of catalyst; T=200 ºC, P=13 bar N_2, t= 7h. [a]2M2P=2-methyl-2-pentenal.

Reference and R0: 1st use; R1: 2nd use and R2: 3rd use

7.4 Sn_xNb_yO mixed oxides

Sn_xTi_yO catalysts with homogeneous rutile-phase structure and enhanced textural and acid properties have shown better catalytic results in the aqueous-phase condensation of oxygenated compounds than previous TiO_2-based catalysts due to their high stability against acidic aqueous environments. In this sense, it would be of great interest to combine these hydrophobic properties displayed by Sn-based rutile-phase catalysts with the inherent high activity and stability of niobium-based materials in this type of applications (see Chapter 6).

There is only one document in literature where Sn-Nb mixed oxides have been employed as solid catalysts[16]. These solids were prepared by co-precipitation and studied in CO oxidation reactions. These catalysts show much higher surface areas than monometallic oxides and Nb^{5+} can be incorporated into the lattice of rutile SnO_2 to form homogeneous Sn-Nb mixed oxides. This is a promissory start point, although the acid properties of these catalysts have never been studied, so its potential application in these processes should be examined. Moreover, additional characterization to fully comprehend catalysts structure, morphology and physicochemical characteristics will be carried out.

Then, this work is the first time Sn_xNb_yO mixed oxides are tested on condensation reactions, particularly in the condensation of oxygenated compounds in aqueous mixtures. Synthesis parameters will be optimized and special emphasis will be given to the effect of acid and water on the activity of Lewis acid sites present in these catalysts.

7.4.1. Synthesis of Sn_xNb_yO materials

The general co-precipitation synthesis procedure has been specifically optimized for Sn_xNb_yO mixed oxides in order to improve their textural and physicochemical characteristics. In this sense, the following factors have been considered:

- Tin (IV) chloride pentahydrate and niobium oxalate monooxalate were used as metal precursors. Tin (II) oxalate and niobium (V) chloride precursors were also tested, but less crystalline and low surface area mixed oxides were achieved.
- Metal ions concentration in the gel mixture was adjusted (i.e. 25 mmol metal species in 100 mL of distilled water) to maximize catalysts textural properties.
- A 28wt% NH_4OH aqueous solution was used as the precipitation agent and a final pH=9-10 is preferred. Complete co-precipitation was not achieved for pH <7 whereas pH >11 drove to Sn_xNb_yO mixed oxides with lower surface areas and acid properties.
- The gel was aged, washed, filtered and dried at 100 ºC overnight. Finally, synthesized catalysts were calcined in air at 600 ºC for 2h with a heating rate of 2ºC/min. Samples are named as SnNb-x, where x is the Sn/(Sn+Nb) molar ratio in the catalyst.

With respect to the post-synthesis thermal treatment (calcination), 600 ºC was adopted because this is the required temperature to remove all the water and mainly organic matter derived from metal precursors, as can be seen in the TG analysis displayed in Figure 7.9.

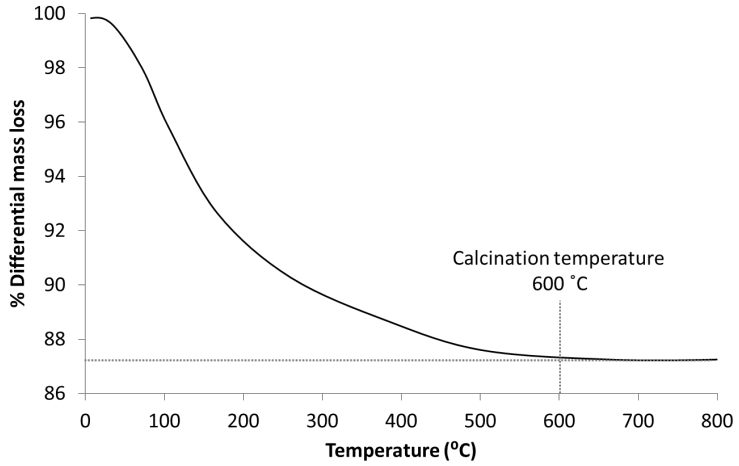

Figure 7.9. TG analysis of SnNb-0.58 catalyst before calcination.

Moreover, this calcination temperature allows obtaining Sn_xNb_yO mixed oxides, which show intermediate surface area (80-100 m^2/g), and more importantly, higher amounts of acid sites (Figure 7.10).

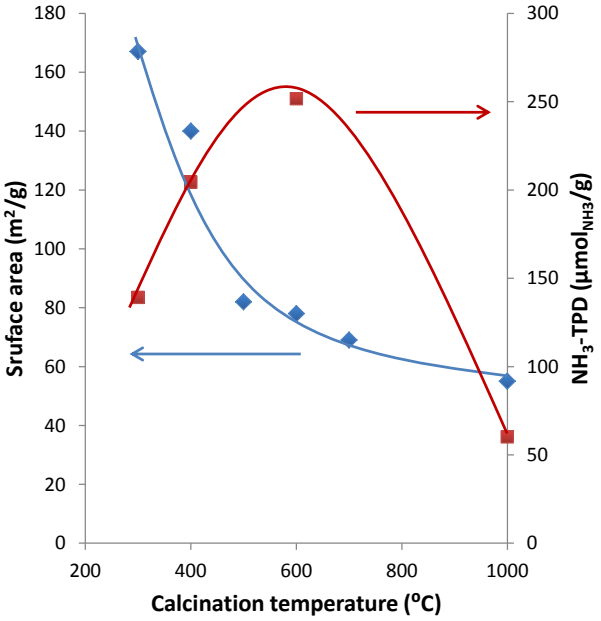

Figure 7.10. Effect of calcination temperature (ºC) on surface area[a] and acid sites[b] of Sn_xNb_yO catalysts. [a] Calculated from N_2 adsorption isotherms (BET method). [b] Calculated from NH_3-TPD measurements.

7.4.2. Catalysts detailed characterization

Firstly, Sn_xNb_yO materials were characterized by X-ray diffraction and compared to commercial SnO_2 and Nb_2O_5 catalysts (Figure 7.11). Commercial SnO_2 (Figure 7.11a) presents characteristic Bragg peaks of the rutile structure, whereas co-precipitated SnO_2 (Figure 7.11b) shows the same structure, but broader Bragg signals are observed[10]. Addition of Nb-precursor during the co-precipitation synthesis allows niobium incorporation in the rutile crystalline phase and diffraction peaks shift is completely consistent with the progressive enrichment in Nb along the range of composition studied (Figure 7.11c-g)[16].

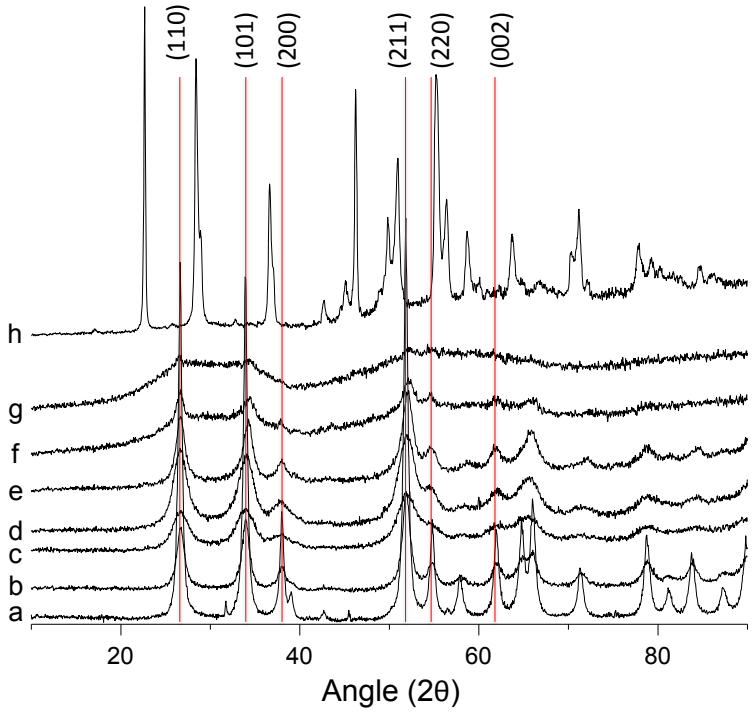

Figure 7.11. XRD profiles of Sn_xNb_yO catalysts: a) Commercial SnO_2; b) SnNb-1.00; c) SnNb-0.86; d) SnNb-0.77; e) SnNb-0.58 and f) SnNb-0.43; g) SnNb-0.29 and h) SnNb-0.00.

Shift in the Bragg signal at 26.5º corresponding to (110) plane is not observed and a and b unit cell parameters keep constant (4.74 Å) along all the range of composition. Nonetheless, Bragg signals at 33.9º and 51.8º corresponding to (101) and (211) planes progressively shift and c unit cell parameter decreases when Nb is added into the structure, due to its lower ionic radius (i.e. 3.19-3.12 Å) (Figure 7.12)[16].

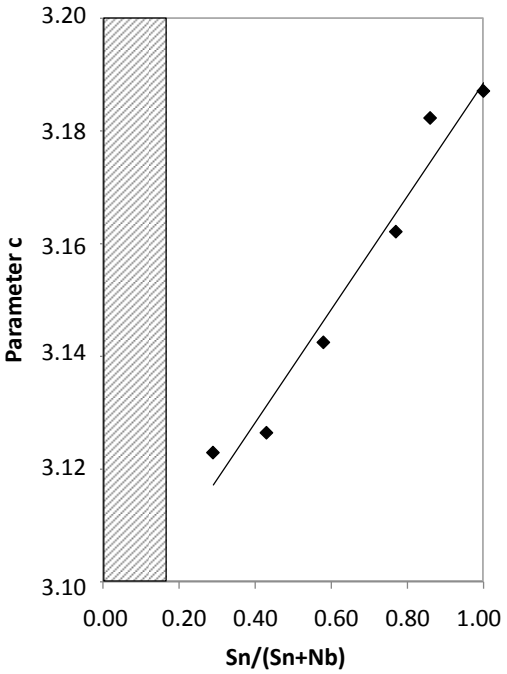

Figure 7.12. Variation of unit cell parameter (c) of Sn_xNb_yO catalysts.

Niobium incorporation in the mixed oxide composition causes a progressive loss of crystallinity (the intensity of the Bragg signals decreases) as seen in Figure 7.11c-g. SnNb-0.29 sample (Figure 7.11g) already shows a pseudo-crystalline rutile phase, whereas further addition of Nb in the mixed oxide gives rise to amorphous mixed oxides (i.e. SnNb-0.17). Finally, very low Sn-content catalysts (Sn/(Sn+Nb) <0.10) show the characteristic T-Nb_2O_5 crystalline structure (Figure 7.12).

These features were also confirmed by Raman spectroscopy (Figure 7.13). Main bands centered at 473, 639 and 775 cm^{-1} assigned to E_g, A_{1g} and B_{2g} vibrational modes of rutile SnO_2 structure are observed (Figure 7.13a)[10]. Then, introduction of Nb within SnO_2 rutile structure promotes a progressive broadening and shift of these signals (Figure 7.13b-d). SnNb-0.43 to SnNb-0.17 samples (Figure 7.13e-g) show notably broad signals, where a new contribution at 709 cm^{-1} ascribed to symmetric stretching mode of distorted NbO_6 octahedra in bulk oxides can be slightly noticed. By contrast, Sn low-content catalysts (Figure 7.13h-i) only show the characteristic Raman signals of T-Nb_2O_5 structure.

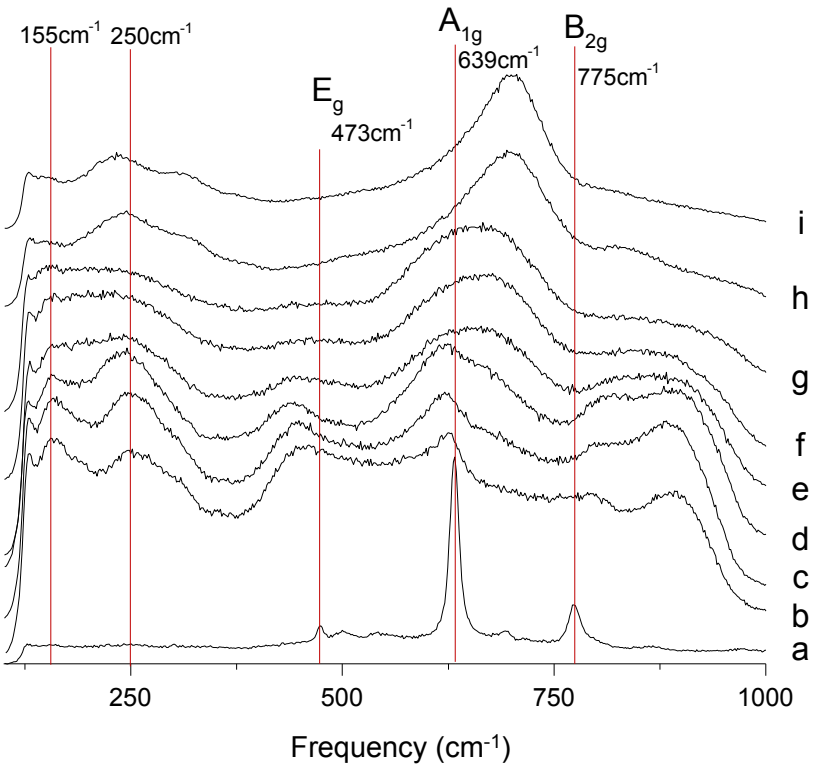

Figure 7.13. Raman spectra of Sn_xNb_yO catalysts: a) SnNb-1.00; b) SnNb-0.86; c) SnNb-0.77; d) SnNb-0.58; e) SnNb-0.43; f) SnNb-0.29; g) SnNb-0.17; h) SnNb-0.10 and i) SnNb-0.00.

Broad diffraction and Raman peaks, together with the shift of A_{1g} signals to lower frequencies and the appearance of deformation modes at 150-250 cm^{-1} (due to the increasing disorder in the crystalline structure) suggest the presence of Sn-Nb mixed oxide nanoparticles[7]. TEM images (Figure 7.14) confirm these structural features. Agglomerated Sn-Nb nanoparticles ranging from 3 to 40 nm depending on the catalyst composition are observed. In particular, SnNb-0.86 to SnNb-0.58 samples (Figure 7.14b-d) show the lowest average particle size, whereas further introduction of Nb gives rise to more heterogeneous systems, where bigger nanoparticles can be found (Figure 7.14e-f).

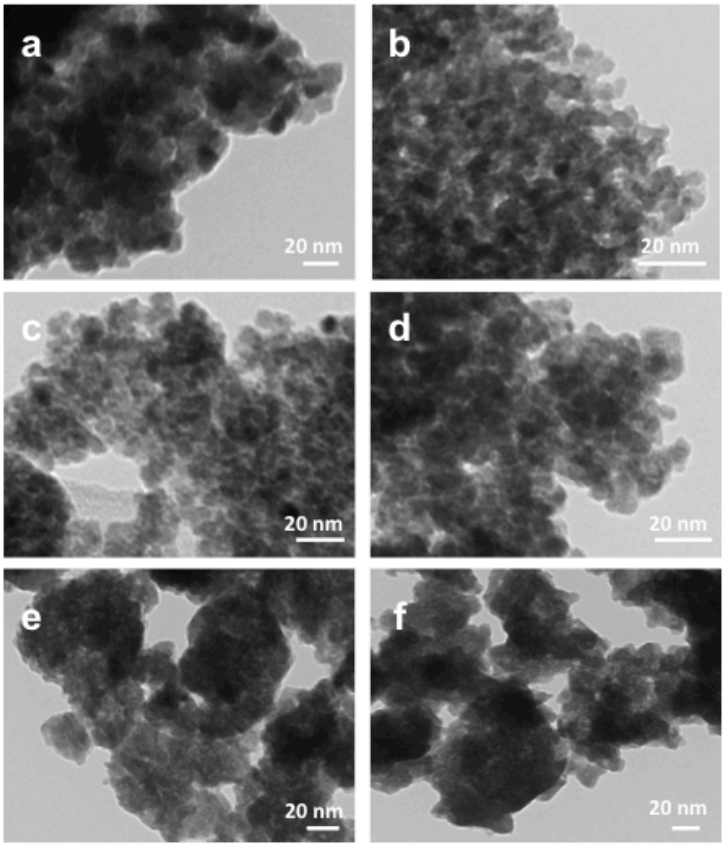

Figure 7.14. TEM images of Sn_xNb_yO catalysts: a) SnNb-1.00; b) SnNb-0.86; c) SnNb-0.77; d) SnNb-0.58; e) SnNb-0.43 and f) SnNb-0.29.

In this sense, estimated particle size (nm) for co-precipitated Sn_xNb_yO materials from Scherrer´s equation and TEM images analyses can be compared in Table 7.9, where equivalent values are achieved by both procedures.

Table 7.9. Main textural properties of Sn_xNb_yO materials.

Catalyst	Surface area (m^2/g)[a]	Pore volume (cm^3/g)	Average pore size (Å)	Particle size (nm)	
				Scherrer equation	TEM images
SnNb-0.00[b]	13	0.01	-	-	-
SnNb-0.00	29	0.03	-	-	-
SnNb-0.10	19	0.04	-	-	-
SnNb-0.17	22	0.05	-	-	-
SnNb-0.29	35	0.09	-	20	28
SnNb-0.43	59	0.10	-	10	13
SnNb-0.58	103	0.16	75	8	9
SnNb-0.77	128	0.14	57	5	7
SnNb-0.86	101	0.09	48	4	6
SnNb-1.00	15	0.01	-	-	-
SnNb-1.00[c]	15	0.01	-	20	16
Sn/Nb_2O_5	15	0.02	-	-	-
Nb/SnO_2	13	0.03	-	-	-

[a]Calculated from N_2 adsorption isotherms (BET method); [b]Commercial Nb_2O_5 (Sigma Aldrich); [c]Commercial SnO_2 (Sigma Aldrich).

Moreover, the synthesis of Sn_xNb_yO mixed oxides via co-precipitation (i.e. SnNb-0.86 to SnNb-0.58) drives to catalysts, which show enhanced surface areas (100-130 m^2/g) and pore volumes (0.09-0.16 cm^3/g). In this regard, a transition between type II isotherms to type IV (typical of mesoporous materials) is observed in this range of composition (Figure

7.15b-d). N_2 adsorption isotherms of these catalysts are indicative of disordered mesoporosity caused by small nanoparticles agglomeration. Indeed, these changes are also accompanied by a concomitant variation in average pore sizes and pore volumes (Table 7.9). From this point, surface area and pore volumes progressively decrease if further niobium is incorporated in the catalyst composition. Finally, commercial catalysts or analogous mixed oxides prepared by incipient impregnation show the lowest surface area values (<15 m^2/g) and negligible porosity (<0.03 cm^3/g).

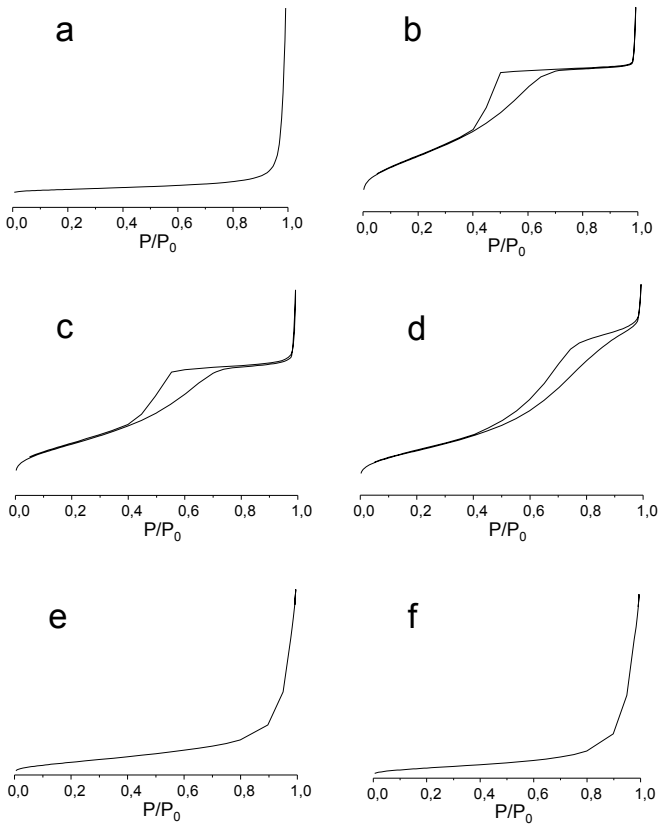

Figure 7.15. N_2 adsorption isotherms of Sn_xNb_yO catalysts a) SnNb-1.00; b) SnNb-0.86; c) SnNb-0.77; d) SnNb-0.58; e) SnNb-0.29 and f) SnNb-0.00.

Then, the preparation of these catalysts via co-precipitation allows obtaining homogeneous solid mixed oxides (elucidated by elemental mapping from SEM-EDS) in all the range of composition (Figure 7.16). On the other hand, Sn-Nb mixed oxides prepared by incipient wetness impregnation (i.e. Nb/SnO_2 and Sn/Nb_2O_5) show mixed crystalline phases more similar to a physical mixture between both monometallic oxides. XRD diffraction profiles and elemental mapping by SEM-EDS of different Sn-Nb mixed oxides (Figure 7.16) confirmed these tremendous differences depending on the synthesis procedures.

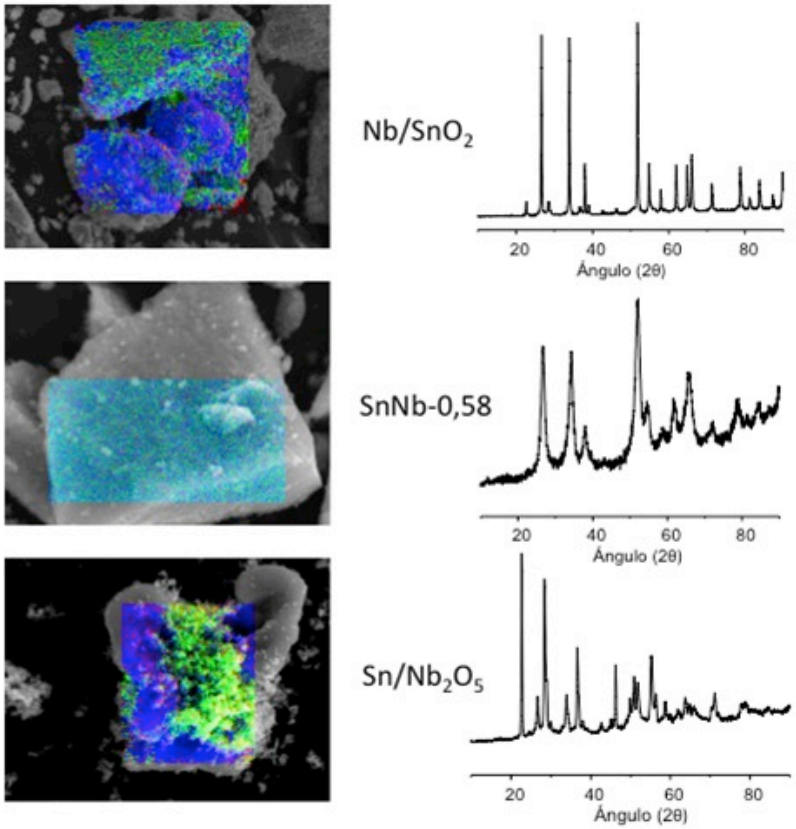

Figure 7.16. Elemental mapping by SEM-EDS and XRD profiles of SnNb-mixed oxides prepared by different procedures: a) Nb/SnO_2; b) SnNb-0.58 and c) Sn/Nb_2O_5.

Considering the acid properties of the materials, co-precipitated Sn_xNb_yO samples remarkably exhibit higher number of acid sites than monometallic and commercial SnO_2 and Nb_2O_5 samples (Table 7.10 and Figure 7.17). In particular, samples with Sn(Sn+Nb) ratios >0.58 show the greatest number of acid sites, reaching a maximum of 250-280 $\mu mol_{NH3}/g$ for SnNb-0.58 and SnNb-0.77 catalysts. From this point, acidity decreases with further Nb content, being these changes consistent with the reduction of surface areas and pore volumes in these samples.

Table 7.10. Acid characteristics of Sn_xNb_yO materials

Catalyst	NH_3-TPD ($\mu mol_{NH3}/g$)	FT-IR pyridine	
		Lewis acid sites ($\mu mol_{PY}/g$)	Brönsted acid sites ($\mu mol_{PY}/g$)
SnNb-0.00[a]	-	10	5
SnNb-0.00	34	10	7
SnNb-0.29	49	14	2
SnNb-0.43	64	17	3
SnNb-0.58	252	99	13
SnNb-0.77	278	110	13
SnNb-0.86	218	81	7
SnNb-1.00	24	28	1
SnNb-1.00[b]	-	29	0
Sn/Nb_2O_5	49	-	-
Nb/SnO_2	55	-	-

[a]*Commercial Nb_2O_5 (Sigma Aldrich);* [b]*Commercial SnO_2 (Sigma Aldrich).*

Moreover, acid properties of co-precipitated Sn_xNb_yO mixed oxides were elucidated by FT-IR of adsorbed pyridine to achieve additional information. In this sense, the general trend of the acid properties values of co-precipitated SnNb-mixed oxides is similar to that observed by

means of NH_3-TPD measurements (see Table 7.10 and Figure 7.17). More interestingly, Lewis/Brönsted (LAS/BAS) acid sites ratios >7 are observed in all Sn_xNb_yO samples, especially in those with higher amount of acid sites. Then, acid properties of these catalysts also rely on Lewis acid centers, which are preferred in aldol condensation reactions.

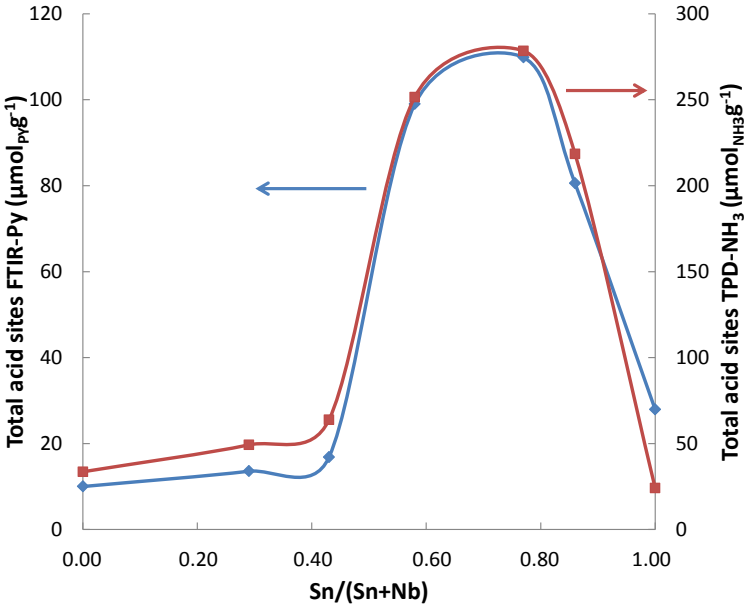

Figure 7.17. Total acid sites of Sn_xNb_yO catalysts measured by FT-IR (with pyridine adsorption) and NH_3-TPD.

Summarizing, homogeneous rutile-phase Sn_xNb_yO catalysts can be easily prepared by co-precipitation. Synthesis conditions and tailoring the Nb composition and its incorporation in the SnO_2 rutile structure can modify material crystallinity, surface area and acid properties. In general, co-precipitation method drives to mixed oxides conformed by Sn-Nb agglomerated nanoparticles with enhanced textural and acid properties compared to SnO_2 and Nb_2O_5 commercial catalysts or analogous mixed oxides prepared by different procedures.

7.4.3. Catalytic results

7.4.3.1. Catalytic performance of Sn_xNb_yO materials in the condensation of a mixture of oxygenated compounds in aqueous phase

Catalytic results of Sn_xNb_yO materials in the consecutive condensation of oxygenated compounds in aqueous mixture containing: 30wt% H_2O, 30wt% acetic acid, 25wt% propanal, 10wt% ethanol and 5wt% acetol (See Section 3.4) are shown in Table 7.11 and Table 7.12. Results are expressed in terms of oxygenated compounds conversion and yields to main reaction products: ethyl acetate, 2-methy-2-pentenal, C_5-C_8 and C_9-C_{10} products.

In general, co-precipitated Sn-Nb mixed oxides show higher yields to the main condensation organic products than monometallic oxides (Table 7.11). In particular, catalysts containing high amounts of Sn (i.e. molar ratio from 0.58 to 0.77) maximize reactants conversion: acetol (≈100%), propanal (65-75%), ethanol (42-45%) and acetic acid (≈8%). Therefore, higher total organic products yield (sum of first condensation and C_5-C_{10} products in wt%) of 50-54% are achieved after 1h on stream, whereas other Sn-Nb oxides (Table 7.12) drive to lower catalytic results (i.e. 20% propanal conversion).

Figure 7.18 specifically shows how catalyst composition optimization (i.e. $0.55<Sn/(Sn+Nb)<0.80$) allows maximizing both C_9-C_{10} (2^{nd} condensation step) products yield and total organic products yield, being these results directly correlated to catalysts with the lowest particle size, highest surface area and maximum concentration of Lewis acid sites.

Table 7.11. Catalytic results of Sn_xNb_yO materials in the condensation of oxygenated compounds in the aqueous phase.

Catalyst		Nb	1.00[a]	0.57	0.42	0.23	0.14	0.00
		Sn	0.00	0.43	0.58	0.77	0.86	1.00[b]
Conversion	(%)	Acetic acid	8.4	7.5	7.1	8.1	10.6	0.0
		Propanal	21.3	63.2	74.8	65.6	48.3	19.2
		Ethanol	27.3	43.0	42.7	45.4	43.8	20.1
		Acetol	87.2	92.3	100.0	97.1	88.8	84.0
Product Yield	(%)	Ethyl acetate	18.6	19.1	20.8	20.6	21.1	15.0
		2M2P[c]	11.5	23.1	28.7	26.2	18.8	13.6
		C5-C8	15.1	17.7	17.6	19.6	19.0	11.8
		C9-C10	5.7	9.3	10.7	7.7	7.0	5.4
		Total	**32.3**	**50.1**	**57.1**	**53.5**	**44.8**	**30.8**
Carbon balance (%)			95.5	97.4	99.9	100.5	97.6	99.5

Reaction conditions: 3 g of aqueous mixture, 150 mg of catalyst; T=200 ºC, P=13 bar N_2, t= 1h.

[a]Commercial Nb_2O_5 (Sigma Aldrich); [b]Commercial SnO_2 (Sigma Aldrich); [c]2M2P=2-methyl-2-pentenal.

Table 7.12. Catalytic results of Sn_xNb_yO materials in the condensation of oxygenated compounds in the aqueous phase.

Catalyst			RUT-SnO_2	Sn/Nb_2O_5	Nb/SnO_2	SnNb-0.29	SnNb-0.58
Conversion	(%)	Acetic acid	0.0	14.2	3.3	2.1	7.1
		Propanal	19.2	20.6	20.8	60.7	74.8
		Ethanol	20.1	24.7	23.3	47.0	42.7
		Acetol	84.0	78.5	88.9	91.5	100.0
Product Yield	(%)	Ethyl acetate	15.0	15.3	14.6	20.8	20.8
		2M2P[a]	13.6	14.7	13.9	21.5	28.7
		C5-C8	11.8	11.3	14.5	18.3	17.6
		C9-C10	5.4	5.5	5.0	8.0	10.7
		Total	**30.8**	**31.5**	**33.4**	**47.9**	**57.1**
Carbon balance (%)			99.5	97.6	98.1	98.3	99.9

Reaction conditions: 3 g of aqueous mixture, 150 mg of catalyst; T=200 ºC, P=13 bar N_2, t= 1h. [a]2M2P=2-methyl-2-pentenal.

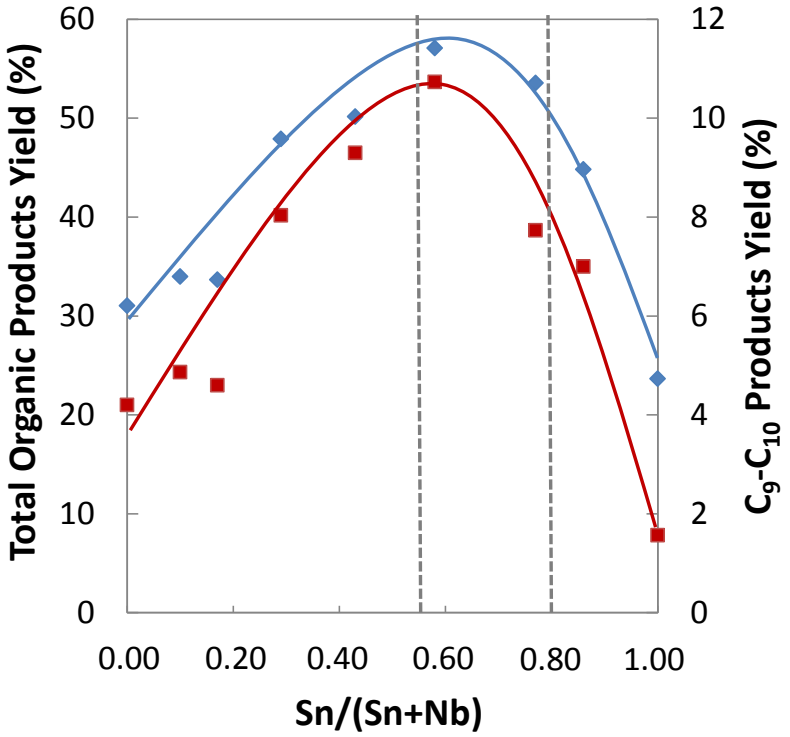

Figure 7.18. Sn/(Sn+Nb) composition effect on total organic products yield (blue diamonds) and C_9-C_{10} products yield (red squares) in the condensation of a mixture of oxygenated compounds in aqueous phase.
Reaction conditions: 3 g of aqueous mixture, 150 mg of catalyst; T=200 ºC, P=13 bar N_2, t= 1h.

Thus, Sn_xNb_yO materials prepared via co-precipitation show higher reaction rates at 1h on stream (Table 7.13) and the highest yields to the main condensation organic products at 1h and 7h. On the other hand, commercial SnO_2 and Nb_2O_5 catalysts, monometallic oxides prepared by the same precipitation procedure, SnO_2-Nb_2O_5 physical mixtures and Sn/Nb_2O_5 or Nb/SnO_2 samples prepared by incipient wetness impregnation drive to low reaction rates and low total organic products yield at 1h and 7h.

Table 7.13. Reaction rates calculated at 1h and total organic products yield (%) of Sn_xNb_yO materials at different times on stream.

Catalyst	Reaction rate at 1h ($\mu mol \cdot min^{-1} g^{-1}$)	Total organic products yield (%)	
		1h	7h
SnNb-0.00[a]	839	32.3	49.1
SnNb-0.00	746	31.0	51.7
SnNb-0.10	-	-	55.0
SnNb-0.17	-	-	59.1
SnNb-0.29	1452	47.9	64.5
SnNb-0.43	1550	50.1	63.8
SnNb-0.58	1725	57.1	65.7
SnNb-0.77	1623	53.5	65.9
SnNb-0.86	1386	44.8	61.2
SnNb-1.00	1010	36.4	57.8
SnNb-1.00[b]	610	30.8	53.6
Sn/Nb_2O_5	887	31.5	48.2
Nb/SnO_2	722	33.4	56.3
SnO_2-Nb_2O_5	-	-	53.1

[a]Commercial Nb_2O_5 (Sigma Aldrich); [b]Commercial SnO_2 (Sigma Aldrich)

Reaction conditions: 3 g of aqueous mixture, 150 mg of catalyst; T=200 ºC, P=13 bar N_2, t= 1h and 7h.

Afterwards, and analogously to the strategy followed in Chapter 6, experiments under different temperature conditions (180 ºC – 200 ºC) were carried out using the whole series of Sn_xNb_yO materials. Reactions at 180 ºC show a similar behavior for all Sn-Nb mixed oxides. C_5-C_8 products yield keep constant regardless Nb-content, whereas 2nd condensation step products (i.e. C_9-C_{10} products) and total products yield are maximized when Sn_xNb_yO mixed oxides are employed.

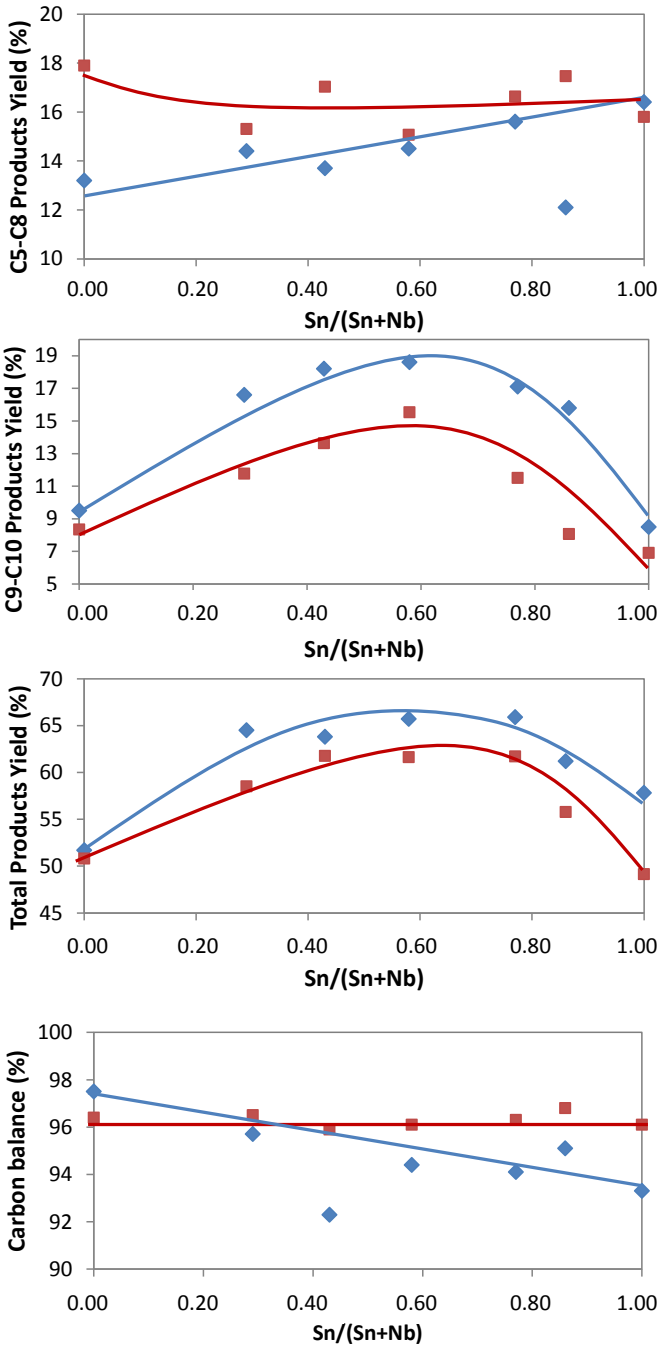

Figure 7.19. Effect of Sn/(Sn+Nb) composition on: C_5-C_8 products yield, C_9-C_{10} products yield, total products yield and carbon balance at 180 ºC (red squares) and 200 ºC (blue diamonds).

Increasing the reaction temperature improves 2nd condensation reaction steps. Then, yield to intermediates (2M2P and C_5-C_8 products) decreases when increasing the Nb-content in the catalyst, while C_9-C_{10} oxygenated products and total organic products yield are optimized in the same range of SnNb mixed oxides composition, this meaning Sn/(Sn+Nb) ratios between 0.58 and 0.77. In this regard, carbon balances (i.e. >94%) are obtained in all the cases, although a slight decrease with Sn-content is observed when experiments are carried out at 200 ºC.

More interestingly, only selected co-precipitated Sn-Nb mixed oxides are able to produce enough heavier products after 7h of reaction, these hydrocarbons becoming spontaneously separated from water and non-converted reactants, which facilitates their isolation and subsequent use (Figure 7.20). In this sense, higher temperatures promote higher C_9-C_{10} products yields and better organic products separation.

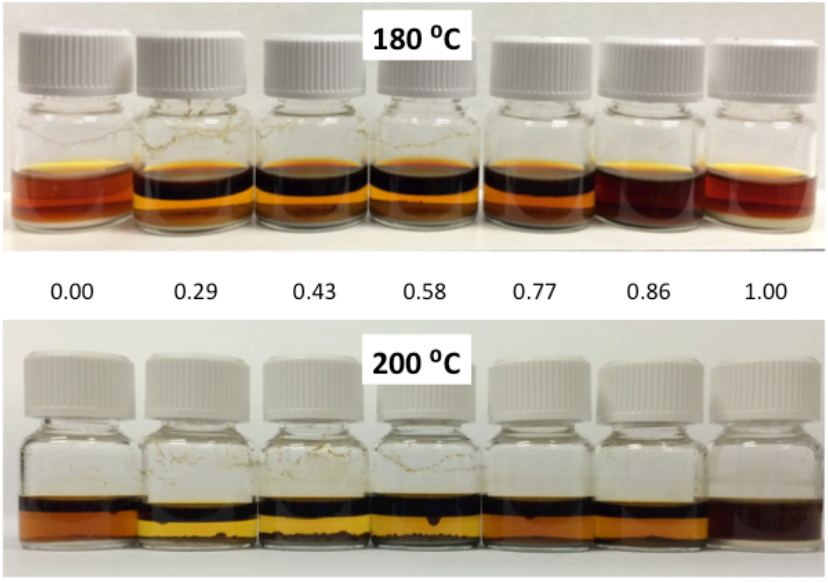

Figure 7.20. Effect of Sn/(Sn+Nb) ratios in SnNb-catalysts on organic phase separation in the final mixture in the condensation of oxygenated compounds in an aqueous mixture at 180 ºC and 200 ºC.

7.4.3.2. Catalytic performance of supported K/ and Cs/Sn_xNb_yO materials in the condensation of a mixture of oxygenated compounds in aqueous phase

K and Cs supported on Sn_xNb_yO catalysts were prepared by incipient wetness impregnation of the corresponding aqueous solutions of K and Cs salt precursors to attain different alkaline metal loadings in the final solid and these catalysts were tested in the same reaction conditions. In this sense, K impregnation over SnNb-0.58 samples drives to lower total products yields, even though C_9-C_{10} products yields are increased. This data confirm that condensation reactions on Sn_xNb_yO mixed oxides are based on acid catalysis, although the presence of acid-base pair sites can promote additional 2nd condensation steps. Finally, Cs incorporation drives to excessive acid sites blocking and lower C_9-C_{10} products and total yields are observed, possibly due to polymerization reactions are taking place (lower carbon balance).

Table 7.14. Catalytic results of supported K/ and Cs/SnNb-0.58 in the condensation of oxygenated compounds in the aqueous phase.

Catalyst		Ref.	2.3% K	4.9% K	9.3% K	6.1%Cs
Conversion (%)	Acetic acid	4.9	8.6	8.4	11.4	13.2
	Propanal	96.1	79.6	77.7	78.7	78.4
	Ethanol	55.6	51.9	50.5	50.6	49.9
	Acetol	100.0	100.0	100.0	100.0	100.0
Product Yield (%)	Ethyl acetate	17.3	25.5	26.5	21.7	22.9
	2M2P[a]	32.6	33.2	29.8	26.7	28.2
	C5-C8	14.5	10.7	10.1	9.2	11.6
	C9-C10	18.6	17.1	19.8	21.3	15.3
	Total	**65.7**	**61.0**	**59.7**	**57.2**	**55.1**
Carbon balance (%)		94.4	98.6	98.4	95.0	93.1

Reaction conditions: 3 g of aqueous mixture, 150 mg of catalyst; T=200 ºC, P=13 bar N_2, t= 7h. [a]2-methyl-2-pentenal

7.4.3.3. Acetic acid and H_2O effect on the catalytic performance of Sn_xNb_yO materials in light oxygenates condensation reactions

Higher reaction rates and total products yields shown by co-precipitated Sn_xNb_yO materials in the aqueous-phase condensation of oxygenated compounds are directly related to their enhanced textural and acid properties (see Figure 7.17 and Figure 7.18). Afterwards, additional experiments were carried out to obtain further information about water and acetic acid effect on the conversion of light oxygenates for this type of materials. As in the case of SnTi-based samples, three different scenarios are considered in this study: a) water is eliminated and relative concentration of all reactants is kept constant; b) the amount of water is replaced by ethanol and c) reference aqueous model mixture is used.

On one hand, as can be seen in Figure 7.21 (left side), the highest conversion of propanal (90%) is reached in only 1h when SnNb-0.58 is used in the absence of water in the reaction medium. Slight decrease (15-17% decay) on propanal conversion is observed when a higher concentration of ethanol or 30%wt of water is added to the mixture for both SnNb-mixed oxides. On the other hand, the addition of ethanol and water drives to worse catalytic results for commercial SnO_2 and Nb_2O_5 catalysts (>60% decay). More interestingly, negligible detrimental effects are observed for Nb_2O_5 and SnNb-mixed oxides when acetic acid is added (Figure 7.21, right side). However, as previously mentioned, the presence of acetic acid in the system has a bigger impact on SnO_2 (SnTi-1.00) catalyst (47% decay). This experimental data confirms the outstanding performance and stability of Nb-based catalysts, particularly of these novel Sn_xNb_yO mixed oxides on acidic aqueous environments.

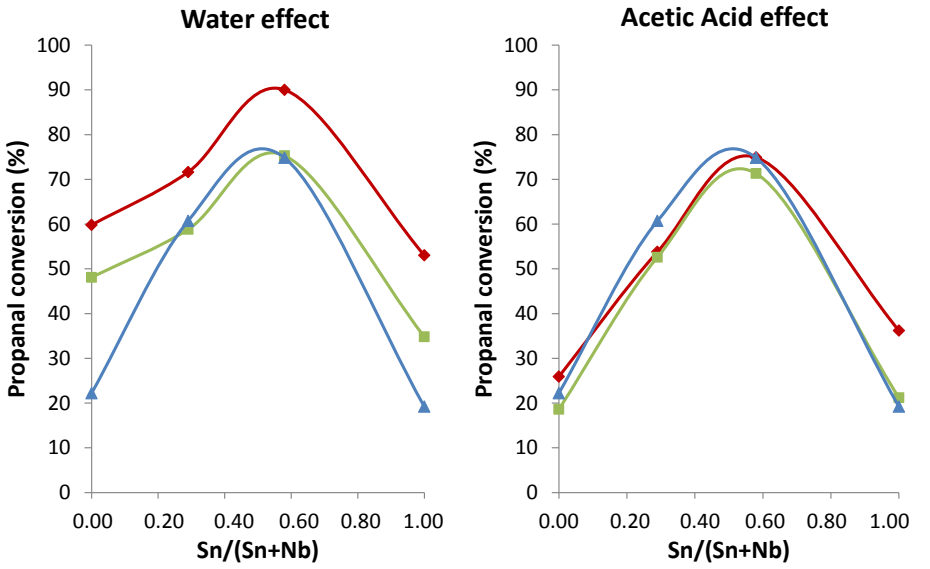

Figure 7.21. Water effect and acetic acid effect on propanal conversion for different Sn_xNb_yO catalysts. Scenario A (red lines); scenario B (green lines) and scenario C (blue lines). Reaction conditions: 3 g of aqueous mixture, 150 mg of catalyst; T=200 ºC, P=13 bar N_2, t= 1h.

These experiments (especially those performed in the absence of water) allow correlating catalytic results to surface area and main acid properties of the materials in a simpler way (Figure 7.22).

Firstly, total organic products yield is directly related to the acid properties ($\mu mol_{NH3}/g$) of all the co-precipitated SnNb materials (Figure 7.22A). In particular, SnNb-0.58 and SnNb-0.77 samples show the greatest number of acid sites, reaching a maximum of total organic products yield. It is also worth noting how SnNb-0.29 catalyst achieves high total products yield, in spite of the lower surface area and number of acid sites observed for this sample. In this sense, Nb better resistance to organic acids and aqueous environments combined with the special activity observed for pseudo-crystalline Nb-based catalysts can explain these catalytic results for SnNb-mixed oxides (see also Section 6.2).

Moreover, the vast differences among co-precipitated SnNb-mixed oxides and Sn/Nb_2O_5 or Nb/SnO_2 samples prepared via incipient wetness impregnation can be repeatedly noticed (Figure 7.22B). The importance of the synthesis method to obtain homogeneous rutile-phase SnNb-mixed oxides with enhanced textural and acid properties is newly highlighted.

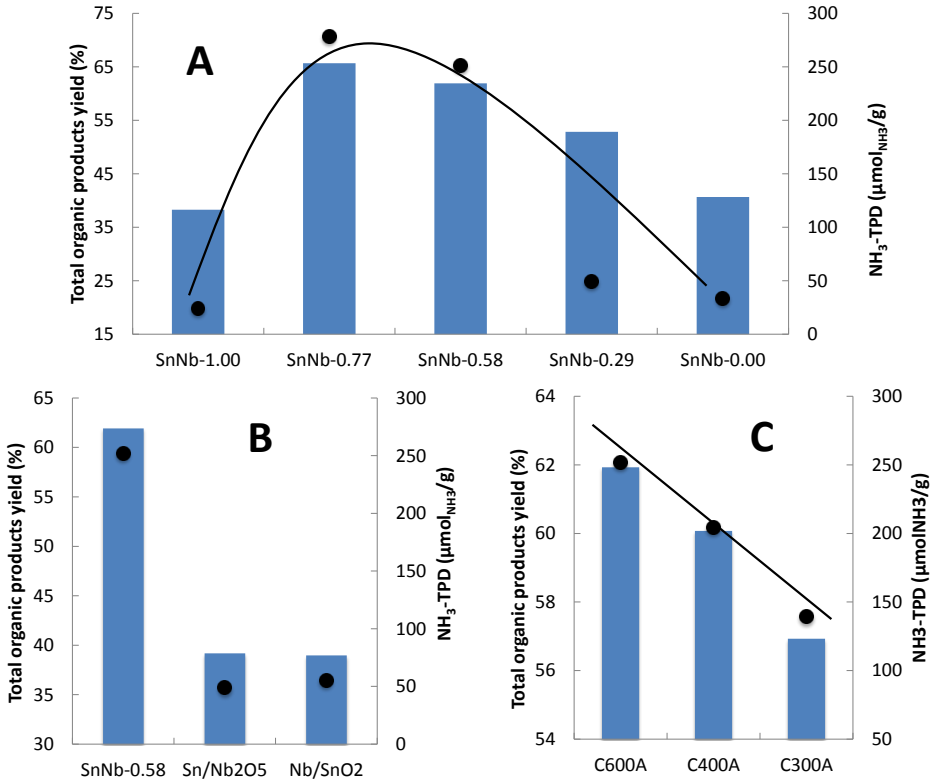

Figure 7.22. Correlation among total organic products yield (bars) and acid properties of Sn_xNb_yO catalysts in the condensation of oxygenated compounds in a mixture without water: A) Sn_xNb_yO prepared by co-precipitation; B) SnNb mixed oxides prepared by different procedures and C) Calcination temperature optimization of SnNb-0.58 catalyst.
Reaction conditions: 3 g of aqueous mixture, 150 mg of catalyst; T=200 ºC, P=13 bar N_2, t= 1h.

Finally, calcination temperature optimization in the range of 300 to 600 ºC for Sn_xNb_yO catalysts (see Figure 7.10) leads to higher total organic products yields, which correlate with the higher amount of acid sites for the SnNb sample calcined at 600 ºC (Figure 7.22C).

More remarkably, these SnNb mixed oxides exhibit the best activity among all the different type of catalysts studied along this work. SnNb-mixed oxides show better catalytic results than SnTi-mixed oxides in the condensation of light oxygenates in an aqueous mixture, having all these catalyst the same crystalline structure and similar textural and acid characteristics. Then, the better performance of rutile SnNb-mixed oxides can be explained based on their outstanding resistance to aqueous environments and the presence of organic acids.

In this sense, the greater stability of SnNb-mixed oxides compared to SnTi samples can be observed in Figure 7.23, where different scenarios, up to 60%wt of water content were studied. Firstly, both catalysts show comparable activity in the condensation reaction of oxygenates performed in the absence of water. Then, the activity of the SnTi-based catalyst progressively decreases when higher amounts of water are added in the reaction medium, whereas a smaller decrease on the total organic products yield is observed for the SnNb-based material.

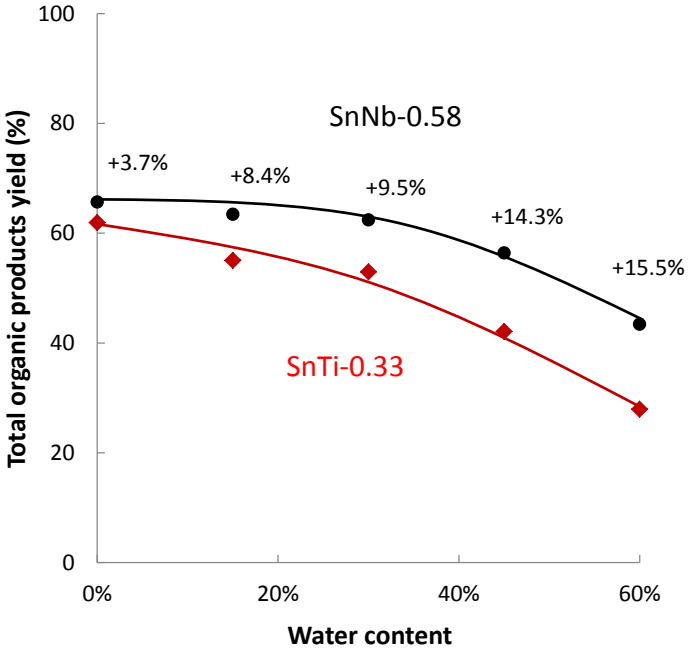

Figure 7.23. Water effect on total organic products yield (%) for SnNb-0.58 and SnTi-0.33 catalysts. Reaction conditions: 3 g of mixture, 150 mg of catalyst; T=200 ºC, P=13 bar N_2, t= 1h.

7.4.3.4. Stability tests of Sn_xNb_yO materials in the condensation of a mixture of oxygenated compounds in aqueous phase

Lastly, and most importantly, Sn_xNb_yO materials show an incredible stability under these process conditions and maintain their activity (expressed as total organic products yield) after several reuses (Figure 7.24). In this sense, SnNb-0.58 and SnNb-0.77 samples maintain their activity practically invariable after three reuses, whereas total organic products yield slightly decrease when SnTi-0.33 is studied.

This great stability is based on the reduced amount of carbon deposits on the catalyst surface compared to other SnTi catalysts, which suffer from a deeper carbon deposition and deactivation (Table 7.15).

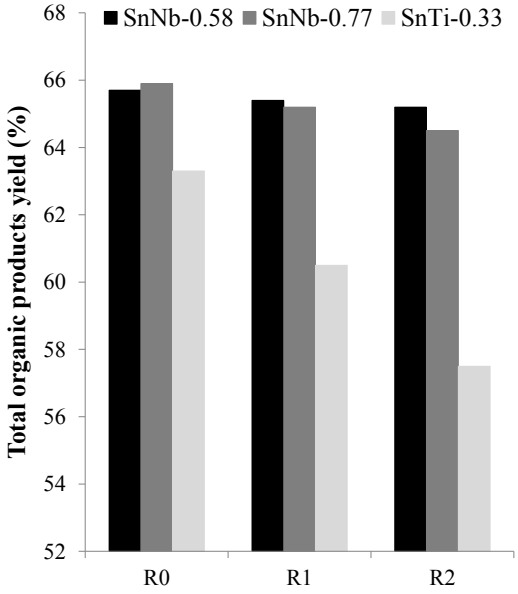

Figure 7.24. Stability tests (expressed as total organic products yield) of SnNb-0.58, SnNb-0.77 and SnTi-0.33 catalysts. R0: 1st use; R1: 2nd use and R2: 3rd use Reaction conditions: 3 g of mixture, 150 mg of catalyst; T=200 ºC, P=13 bar N_2, t= 7h.

Table 7.15. Catalyst characterization by elemental analysis (EA) and thermogravimetric measurements (TG) after reuses.

Catalyst	Organic product deposition	
	%C (E.A.)	% (TG)
SnNb-0.58	0.5	1.5
SnNb-0.77	0.6	2.1
SnTi-0.33	2.8	-

Summarizing, SnNb-based mixed oxides showing a homogeneous rutile-phase structure and enhanced textural and acid properties have great activity in the condensation of oxygenated compounds due to their high performance in aqueous environments, even in the presence of organic acids. Moreover, these materials show an outstanding stability under these reaction conditions.

7.5 $Sn_xTi_yNb_zO$ mixed oxides

7.5.1. Synthesis of $Sn_xTi_yNb_zO$ materials

With the idea of taking advance of the enhanced properties of SnTi and SnNb mixed oxides in only one solid, ternary Sn-Ti-Nb mixed oxides were also studied. Thus, in an attempt to achieve more information of these rutile-phase ternary mixed oxides, $Sn_xTi_yNb_zO$ catalysts were synthesized following the same co-precipitation procedure (detailed in Section 3.2.4). These catalysts were also calcined in air at 600 ºC for 2h with a heating rate of 2 ºC/min and samples are named as SnTiNb-x/y/z, where x is the Sn/(Sn+Ti+Nb) molar ratio in the catalyst.

7.5.2. Catalysts characterization and catalytic results

$Sn_xTi_yNb_zO$ catalysts were characterized by X-ray diffraction and Raman spectroscopy and compared to representative SnNb and SnTi binary mixed oxides (i.e. SnNb-0.58 and SnTi-0.33). Figure 7.25 shows that all Sn-Ti-Nb tertiary mixed oxides present broad signals, characteristic of the rutile crystalline structure. Bragg signals shift and Raman peaks shape is consistent with differences in the catalyst composition. These tertiary mixed oxides present a homogeneous rutile structure (SEM-EDS) comprised of agglomerated nanoparticles (TEM images). These oxides show enhanced surface areas (type IV isotherms), pore volumes and acid properties compared to commercial monometallic oxides. As example, the most relevant characterization data above-mentioned of SnTiNb ternary mixed oxides are shown for the SnTiNb (35:39:26) sample (see Figure 7.26).

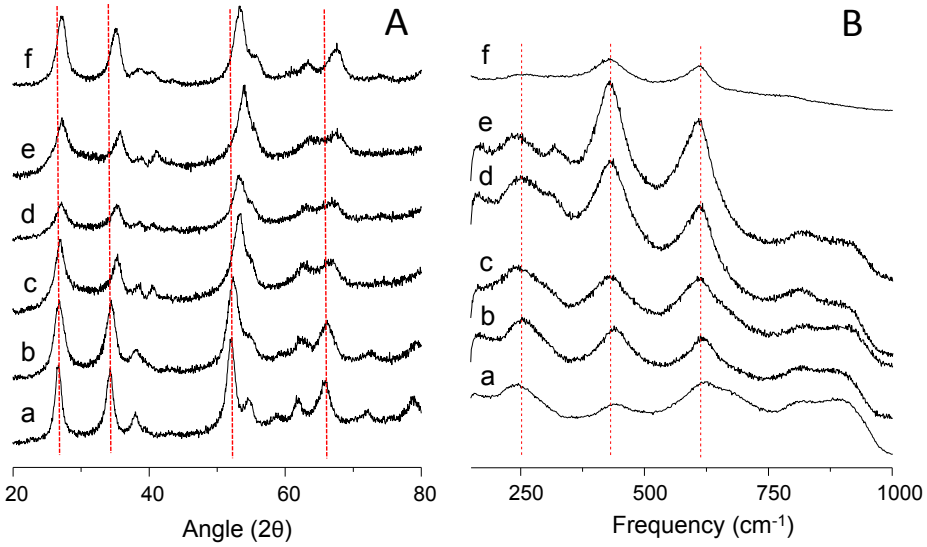

Figure 7.25. XRD profiles (A) and Raman spectra (B) of $Sn_xTi_yNb_zO$ catalysts: a) SnNb-0.58; b) SnTiNb-60/15/25; c) SnTiNb-29/29/42; d) SnTiNb-35/39/26; e) SnTiNb-16/56/28 and f) SnTi-0.53.

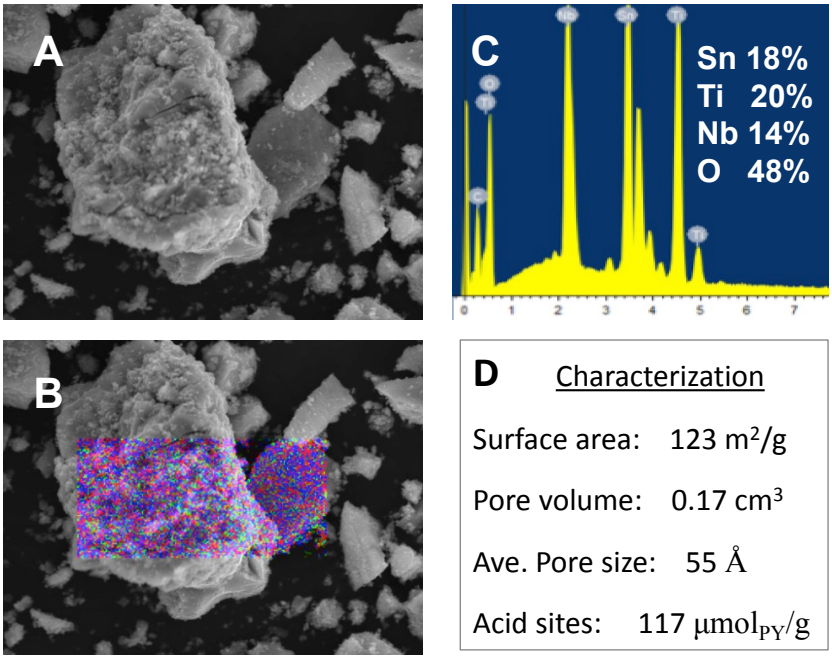

Figure 7.26. Detailed characterization of SnTiNb (35:39:26) catalyst: A) SEM image, B) SEM-EDS mapping image; C) SEM-EDS spectra and D) Main textural and acid characteristics

Catalytic results of $Sn_xTi_yNb_zO$ materials in the consecutive condensation of oxygenated compounds in the same aqueous mixture (See Section 3.4) were studied. Tertiary diagrams displayed in Figure 7.27 are used to condense all the information achieved from this family of catalysts and main textural and catalytic properties are discussed.

Firstly, homogeneous rutile structure is achieved in most of the compositions studied for $Sn_xTi_yNb_zO$ materials (Figure 7.27a). There are only two exceptions: i) on one hand, TiNb mixed oxides (without Sn) present anatase crystalline phase, like pure TiO_2 synthesized by co-precipitation and calcined under the same conditions; ii) on the other hand, high Nb-content catalysts (Nb/(Sn+Ti+Nb) ratios >0.90) drive to T-Nb_2O_5 crystalline structures.

Moreover, tailoring the composition of SnNb-, SnTi-, and SnTiNb mixed oxides drives to catalysts, which show enhanced surface areas (>100 m^2/g) characterized by disordered mesoporosity caused by small nanoparticles agglomeration (Figure 7.27b). Indeed, these textural changes are also accompanied by a concomitant increase in the total acid sites of these catalysts.

Therefore, total organic products yields are maximized (Figure 7.27c) and especially, SnNb and tertiary SnTiNb mixed oxides with intermediate contents of Sn (0.5 <Sn/(Sn+Ti+Nb) <0.8) also maximize C_9-C_{10} products yield (Figure 7.27d).

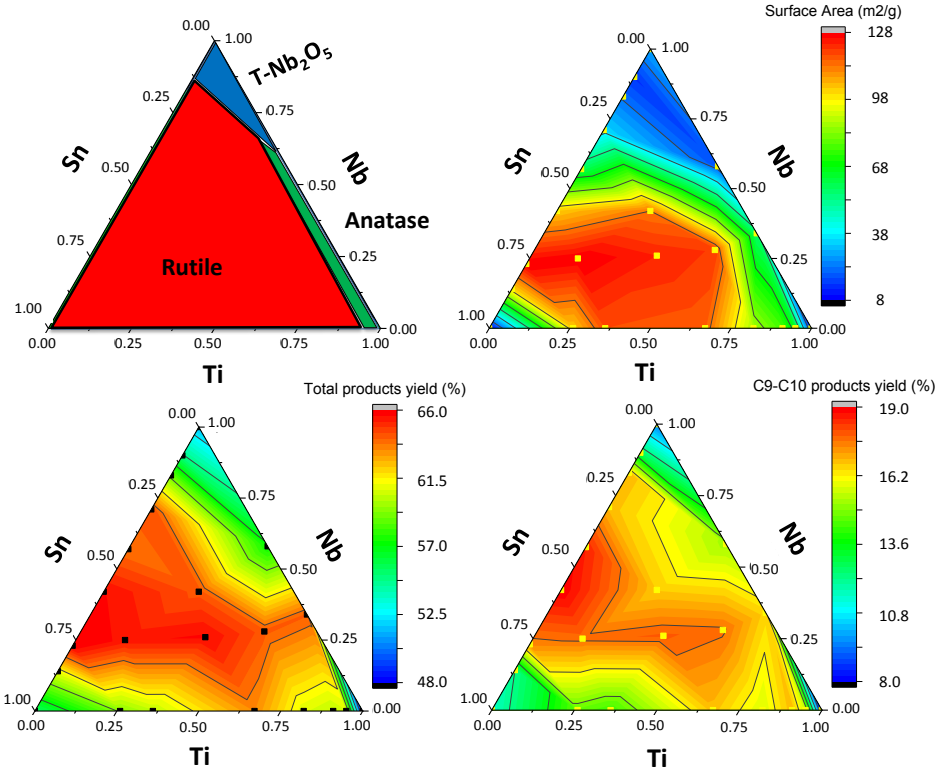

Figure 7.27. $Sn_xTi_yNb_zO$ catalysts: a) Crystalline structure; b) Surface area (m^2/g); c) Total organic products yield (%) at 7h; and d) C_9-C_{10} products yield (%) at 7h.

Summarizing, tertiary $Sn_xTi_yNb_zO$ catalysts also show homogeneous rutile-phase structures, enhanced surface areas and high number of acid sites. In this sense, these catalysts show similar total products yields compared to SnNb-based materials. Specifically, intermediate contents of Sn in these tertiary mixed oxides also maximize C_9-C_{10} products yield, whereas intermediate stability behaviour against aqueous environments was observed when compared to SnNb- and SnTi-based materials. Therefore, SnNb-0.58 catalyst continues displaying the best catalytic results along this work.

7.6 Process application and intensification

7.6.1. Organic phase characterization: Partition coefficients

The highest reactants conversions and total organic products yields have been achieved by using SnNb-0.58 catalyst in the consecutive condensation of oxygenated compounds in an aqueous mixture. These results have been explained by the enhanced textural and acid properties, together with the extraordinary resistance of this material against organic acids and aqueous environments. High products yields drive to formed hydrocarbons become spontaneously separated from water and non-converted reactants, which facilitates their isolation and subsequent use. Therefore, this organic phase was characterized in detailed.

First of all, GC analyses of aqueous and organic phases after 7h of reaction are displayed in Figure 7.28. On one hand, the aqueous phase mainly contains water and non-converted reactants (i.e. propanal, ethanol and acetic acid), together with low amounts of C_5-C_{10} organic products. On the other hand, the organic phase is enriched with these heavier products C_5-C_{10}, although water and light oxygenates (C_2-C_3) can be also observed.

In this sense, partition coefficients of both, reactants and organic products can be calculated considering their concentration (wt%) in the two separated phases (Table 7.16).

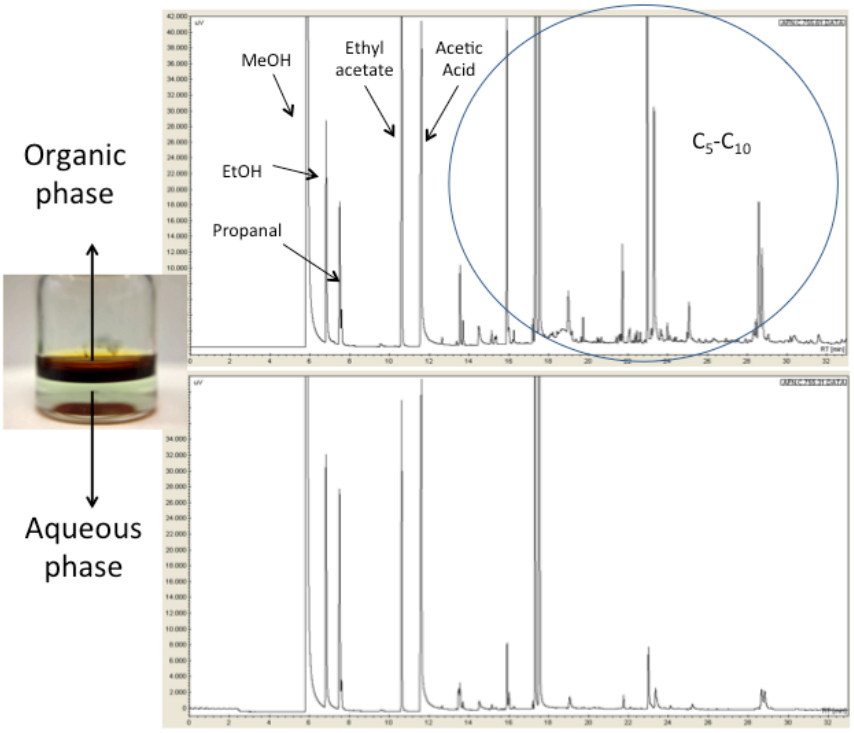

Figure 7.28. GC analysis of organic and aqueous phases obtained with SnNb-0.58 catalyst. Reaction conditions: 3 g of mixture, 150 mg of catalyst; T=200 ºC, P=13 bar N_2, t= 7h.

It is worth noting that partition coefficients for light oxygenates in the organic phase is approximately 45-60%. Then, non-converted reactants can be equally found in both aqueous and organic phases. More interestingly, C_5-C_{10} organic products are favourably separated into the organic phase, being their partition coefficients >75%. As can be seen in Table 7.16, longer reaction times promote higher yields to heavier products and a better isolation of these products in the organic phase. GCxGC analysis of the organic phase (Figure 7.29) confirms these data and groups of short-chained oxygenated compounds (i.e. acetic acid and ethyl acetate), C_5-C_6 intermediate products and C_8-C_{12} aromatic oxygenated compounds are detected.

Table 7.16. Reactants and organic products partition coefficients in the aqueous and organic phase after reaction with SnNb-0.58 catalyst at different times on stream.

Compounds	Partition coefficients (at 3h)		Partition coefficients (at 7h)	
	Aqueous phase %	Organic phase %	Aqueous phase %	Organic phase %
Ethanol	54	46	**61**	39
Propionaldehyde	46	54	**68**	32
Acetic Acid	56	44	51	49
Ethyl Acetate	40	60	46	54
2M2P	30	70	25	**75**
C_5-C_8 products	30	**70**	22	**76**
C_9-C_{10} products	22	**78**	21	**78**
Total products	29	**71**	24	**76**

Reaction conditions: 3 g of mixture, 150 mg of catalyst; T=200 ºC, P=13 bar N_2, t= 3-7h. Partition coefficients for each time are calculated as: K_a=Aqueous(wt%)/Total(wt%) and K_o=Organic(wt%)/Total(wt%).

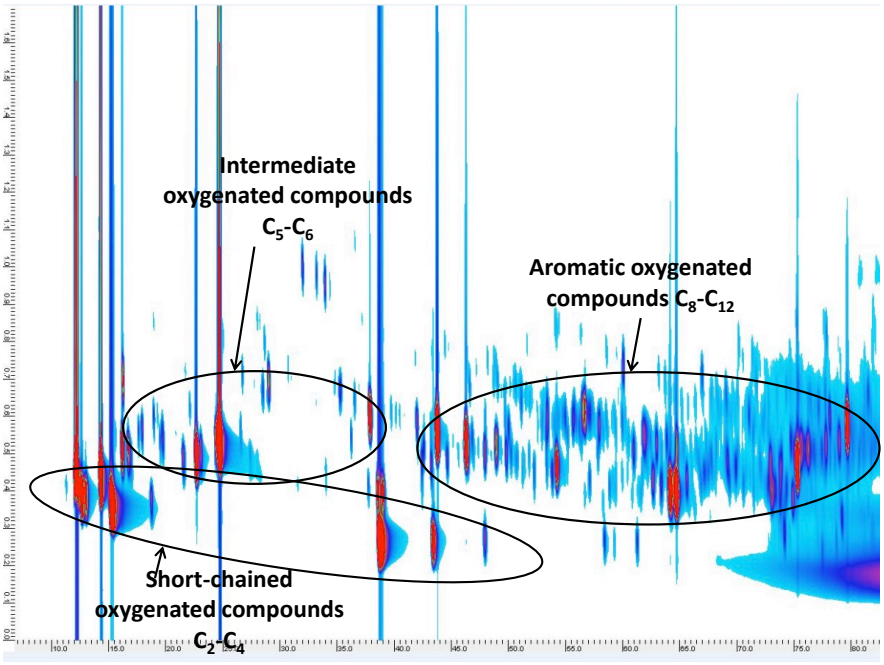

Figure 7.29. GCxGC analysis of the organic phase obtained after reaction with SnNb-0.58 catalyst. Reaction conditions: 3 g of mixture, 150 mg of catalyst; T=200 ºC, P=13 bar N_2, t= 7h.

Therefore, in these conditions, the organic phase in mainly composed by: 26-28% of C_2-C_3 non-converted reactants (mainly acetic acid), 32-34% of H_2O, 6-7% of esters (i.e. ethyl acetate) and 32-35% of C_5-C_{12} organic products. Figure 7.30 shows simulated distillation GC analyses of organic phases obtained after 3h and 7h of reaction when SnNb-0.58 catalyst was used. In this sense, longer reaction times are preferred to promote higher yields of heavier products. Temperatures observed in these curves fall in the range of gasoline and jet fuels. Unfortunately, even when O/C ratios have been diminished, average molecular weights have been increased and total products yields have been maximized, this organic phase still contains large amounts of light oxygenated compounds (non-converted acetic acid) observed in this first plateau of the distillation curves, which hinder their direct application.

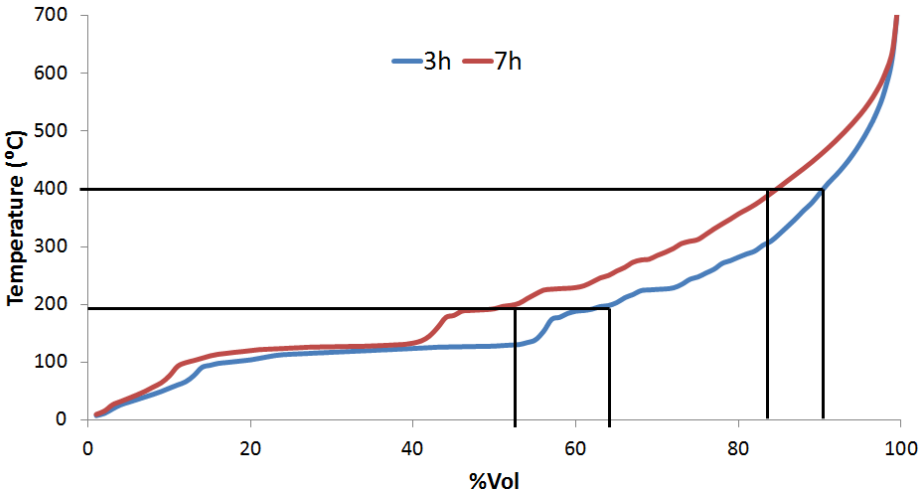

Time	<100 ºC	100-200 ºC	200-400 ºC	>400 ºC
3h	14%	51%	26%	9%
7h	10%	43%	30%	17%

Figure 7.30. Simulated distillation analysis of the organic phase obtained with SnNb-0.58 catalyst. Reaction conditions: 3 g of mixture, 150 mg of catalyst; T=200 ºC, P=13 bar N_2, t= 3-7h.

7.6.2. Process intensification: ABE mixtures valorisation

Taking in consideration the results discussed in the previous section, a final process intensification strategy to improve organic phase applicability was attempted. The idea is to perform the liquid-liquid separation of bio-oils employing ABE (acetone-butanol-ethanol) aqueous mixtures instead of process water streams. These mixtures usually present a high content of water, so phase separation can be easily accomplished. Moreover, light oxygenates functionality can be exploited. On one hand, acetone can easily react with propanal and acetol via aldol condensation to produce C_6 products, meanwhile alcohols can be useful to increase acetic acid conversion to esters via esterification reactions. In this way, bio-oils aqueous phases and ABE aqueous mixtures can be upgraded in "one pot" into hydrocarbons and aromatic products useful in fuel applications and process water necessity in bio-refineries is reduced. In this regard, compositions for model bio-oil aqueous mixture and ABE aqueous mixture used in this section are detailed in Table 7.17.

Table 7.17. Model bio-oil derived aqueous mixture and ABE mixture composition.

Compound	Bio-oil mixture (wt%)	ABE mixture (wt%)
Water	30.0	84.6
Acetic	30.0	-
Propanal	25.0	-
Acetol	5.0	-
Ethanol	10.0	1.6
Butanol	-	9.3
Acetone	-	4.5

Selected SnNb-0.58 catalyst was used again as reference because of the outstanding resistance of this material against aqueous environments. As it was just demonstrated in this study, SnNb-mixed oxides have shown better stability compared to SnTi samples (Figure 7.23). In this sense, a slight decrease in total organic products yield was observed when scenarios up to 60%wt of water content were studied.

In this regard, ABE mixture incorporation was tried in different stages:

- 90% bio-oil mixture + 10% ABE mixture = 35%wt H_2O
- 80% bio-oil mixture + 20% ABE mixture = 40%wt H_2O
- 70% bio-oil mixture + 30% ABE mixture = 45%wt H_2O

Catalytic results expressed as propanal conversion (%) at different reaction times and total organic products yield are detailed in Table 7.18 for the different scenarios studied.

Table 7.18. Propanal conversion and total organic products yield for different bio-oil/ABE mixtures depending on water content using SnNb-0.58 as catalyst.

Aqueous mixture			Propanal conversion (%)			Total products yield (%)
Bio-oil	ABE	Total water	1h	3h	7h	3h
0% H_2O	-	0% H_2O	90.0	95.5	98.0	65.7
15% H_2O	-	15% H_2O	76.9	89.2	94.9	63.5
30% H_2O	-	30% H_2O	74.8	92.2	96.1	62.4
30% H_2O	10%	35% H_2O	69.7	81.3	90.6	60.3
30% H_2O	**20%**	**40% H_2O**	**62.2**	**78.4**	**87.4**	**50.4**
30% H_2O	30%	45% H_2O	53.0	61.6	78.5	42.9
45% H_2O	-	45% H_2O	58.3	81.5	89.2	56.4

Reaction conditions: 3 g of mixture, 150 mg of catalyst; T=200 ºC, P=13 bar N_2, t= 1-7h.

ABE mixtures incorporation drives to initial mixtures with higher water contents. Then, propanal conversion and total products yield progressively decrease. Nonetheless, good propanal conversion and total products yield were achieved up to 20% ABE incorporation (40wt% water), being these results very similar to the ones achieved when a simple 45% bio-oil aqueous model mixture was employed.

More interestingly, the use of more diluted initial mixtures promotes a better separation of the organic products into the organic phase. Then, partition coefficient for acetic acid in the organic phase decrease when 20% of ABE mixture is incorporated, whereas esters and C_5-C_{10} products partition coefficients increase from 75-78% to 86-89% (Table 7.19).

Table 7.19. Partition coefficients of reactants and organic products in the organic phase for different bio-oil/ABE mixtures.

Compounds	**0% ABE**	**10% ABE**	**20% ABE**	**30% ABE**
	30% H_2O	35% H_2O	**40% H_2O**	45% H_2O
Acetone	44	48	**47**	50
Butanol	-	67	**75**	73
Ethanol	39	43	**44**	45
Propionaldehyde	32	60	**63**	62
Acetic Acid	49	36	**37**	44
Ethyl Acetate	54	69	**74**	75
Butyl Acetate	-	84	**94**	92
2-methyl-2-pentenal	75	81	**86**	87
C_5-C_8 products	76	76	**86**	88
C_9-C_{10} products	78	85	**89**	88
Total organic products	76	82	**87**	88
Water	38	37	**31**	34

Reaction conditions: 3 g of mixture, 150 mg of catalyst; T=200 ºC, P=13 bar N_2, t= 7h.

Therefore, a 20% ABE incorporation is found to be the optimum composition in this strategy. This initial aqueous mixture drives to lower global total products yields, but organic phase composition is greatly improved compared to the reference scenario.

Then, lower amounts of high-quality organic phase are obtained (Table 7.20). This way, 20% ABE incorporation (40%wt total initial water) allows obtaining an organic phase where acetic acid and water content has decreased (25% to 12% and 32 to 29%, respectively), whereas higher amounts of esters (6.5% to 15%) and C_5-C_{10} products (32% to 35%) are observed.

Table 7.20. Organic phase composition (wt%) for different bio-oil/ABE mixtures depending on water content.

Compounds	**0% ABE**	**10% ABE**	**20% ABE**	**30% ABE**
	30% H_2O	35% H_2O	**40% H_2O**	45% H_2O
Acetone	0.4	1.3	**1.2**	1.2
Butanol	-	0.8	**1.8**	3.0
Ethanol	3.2	3.2	**3.4**	3.3
Propionaldehyde	1.1	2.1	**3.4**	7.0
Acetic Acid	24.6	13.0	**11.7**	8.7
Ethyl Acetate	6.5	10.8	**11.7**	9.6
Butyl Acetate	-	1.6	**3.2**	4.8
2-methyl-2-pentenal	14.9	16.6	**17.2**	16.4
C_5-C_8 products	6.8	6.8	**9.1**	5.9
C_9-C_{10} products	8.6	8.2	**7.6**	3.7
Total organic products	32.0	33.1	**34.8**	26.0
Water	32.2	32.1	**28.8**	36.4

Reaction conditions: 3 g of mixture, 150 mg of catalyst; T=200 ºC, P=13 bar N_2, t= 7h.

Summarizing, the strategy combining the use of ABE mixtures and bio-oil aqueous fractions in the catalytic condensation of oxygenated compounds present in diluted aqueous systems derived from biomass primary treatments allow attaining acceptable total organic products yields and affordable separation of organic compounds from the aqueous fraction when efficient and highly water-resistant catalytic materials are employed. The SnNb-mixed oxides catalysts here developed accomplish these requirements and open the doors for their future application in industrial systems.

7.7 Conclusions

- Sn_xZr_yO mixed oxides drive to similar catalytic results than SnO_2 and ZrO_2 commercial catalysts, even when these samples show higher surface areas. This can be explained by their non-uniform crystalline structure. Then, rutile-phase structure is a key point for developing active Sn-based mixed oxides.

- Sn_xTi_yO materials preparation via co-precipitation allows obtaining homogeneous rutile-phase mixed oxides, with enhanced textural properties and a higher concentration of Lewis acid sites. These materials show better catalytic results than monometallic SnO_2 and RUT-TiO_2 catalysts. More interestingly, RUT-TiO_2 and specially Sn-Ti mixed oxides show better resistance to the addition of water and acids in the medium compared to other anatase TiO_2 materials studied in Chapter 5.

- Sn_xNb_yO and $Sn_xTi_yNb_zO$ materials can also be prepared via co-precipitation, where both Nb and Ti can be partially or fully incorporated into the rutile structure of SnO_2. SnNb mixed oxides with enhanced textural and acid properties and outstanding resistance to acidic aqueous environments drive to the best catalytic results observed along all this work. Moreover, these catalysts can be reused with negligible loss of activity due to the small deposition of coke on their surface.

- Bio-oils aqueous phases and ABE mixtures can be upgraded in "one-pot" into hydrocarbons and aromatic products useful in fuel applications. Moreover, this innovative strategy allows reducing associated costs derived from process water streams and improves the organic phase quality and its further application.

7.8 References

1. Corma, A., Nemeth, L.T., Renz, M. & Valencia, S. *Nature* **412,** 423–425 (2001).
2. Corma, A *et al. Chem. Eur. J.* **51,** 4708–4717 (2002).
3. Corma, A., Domine, M.E. & Valencia, S. *J. Catalysis* **215,** 294–304 (2003).
4. Jiménez-Sanchidrián, C. & Ruiz, J.R. *Appl. Catal. A., Gen.* **469,** 367–372 (2014).
5. Lew, C.M., Rajabbeigi, N. & Tsapatsis, M. *Microp. Mesop. Mater.* **153,** 55–58 (2012).
6. Moliner, M., Roman-Leshkov, Y. & Davis, M.E. *Proc. Natl. Acad. Sci.* **107,** 6164–6168 (2010).
7. Batzill, M. & Diebold, U. *Prog. Surf. Sci.* **79,** 47–154 (2005).
8. Hagemeyer, A. *et al. Appl. Catal. A., Gen.* **317,** 139–148 (2007).
9. Marakatti, V., Manjunathan, P., Halgeri, A. & Shangbhag, G. *Catal. Sci. Technol.* **6,** 2268–2280 (2016).
10. Kumar, V. *et al. Mater. Res. Bull.* **85,** 202–208 (2017).
11. Wang, Y., Tong, X., Yan, Y., Xue, S. & Zhang, Y. *Catal. Commun.* **50,** 38–43 (2014).
12. Aranda-Pérez, N., Ruiz, M.P., Echave, J. & Faria, J. *Appl. Catal. A., Gen.* **531,** 106-118 (2017).
13. Trotochaud, L. & Boettcher, S.W. *Chem. Mater.* **23,** 4920–4930 (2011).
14. Dong, L. *et al. Appl. Catal. B., Environ.* **180,** 451–462 (2016).
15. Gao, Y. *et al. J. Energ. Chem.* **23,** 331–337 (2014).
16. Xu, X. *et al. Catal. Sci. Technol.* **6,** 5280–5293 (2016).

CHAPTER 8

GENERAL CONCLUSIONS

This work has shown the necessity of designing and developing new solid catalysts with high activity and stability against complex aqueous environments (containing diverse oxygenated compounds in varying concentration) similar to those they will face in actual bio-refinery scheme processes. In this context, the catalytic behaviour of catalysts has been tested by using different aqueous mixtures of representative C_2-C_3 oxygenated compounds with varying water content, which are closer to faithful industrial operation conditions and differing from the usual probe molecules studies performed even in the absence of water.

From the results attained during this thesis with the different solid catalysts specifically designed and tested for the valorisation of oxygenated compounds in aqueous mixtures, the following general conclusions are established:

CeZrO, hydrotalcites and other metallic oxides (Chapter 4):

$Ce_xZr_{1-x}O$ mixed oxides were selected as reference materials for the condensation of oxygenated compounds in aqueous mixtures, and catalysts deactivation by Ce partial leaching and coke deposition was found an issue for their application under these operation conditions.

Binary and tertiary hydrotalcite-derived mixed oxides showed better catalytic results than $Ce_xZr_{1-x}O$ mixed oxides, but Mg^{2+} and Zn^{2+} leaching was also observed in all these type of samples, even when the chemical composition of the materials was optimized.

These active species (i.e. Mg^{2+}, Zn^{2+}) could not be stabilized on resistant ZrO_2 and TiO_2 supports by different synthesis methods, whereas poor catalytic results were obtained when traditional metal oxides, such as SiO_2 or Al_2O_3 were employed. Therefore, new solid materials must be designed to operate under these conditions.

In this context, three different novel acid materials have been studied and applied as catalysts for the condensation of oxygenated compounds in aqueous mixtures:

Faceted TiO_2 materials (Chapter 5):

Hydrothermally synthesized faceted titanium oxides have shown high activity and outstanding stability in the valorization of these light oxygenated compounds present in aqueous model mixtures.

The addition of aqueous HF during TiO_2 catalysts synthesis is essential to selectively control the preferential growth of catalytic more reactive {001} TiO_2 facets. Tailoring of crystal facets of titanium oxide completely influences the catalytic behaviour of these materials.

Moreover, Lewis acid sites on faceted TiO_2 have great stability on condensation reactions, especially in the presence of organic acids under aqueous environments. Thus, these materials have shown better results than other commercial titanium oxides when complex reaction mixtures are tested under moderated operation conditions.

Nb- and WNb-mixed oxides (Chapter 6):

Nb-based materials were studied in depth for the aqueous-phase condensation of oxygenated compounds, as Nb_2O_5 is widely known for its resistance against organic acids and aqueous environments.

In this sense, NbO_x materials prepared by hydrothermal synthesis with a pseudo-crystalline structure and showing tunable acid properties are active and selective catalysts for the valorization of oxygenated compounds present in aqueous effluents. Control of post-synthesis heat-treatments drives to optimized NbO_x materials with higher activity and stability than others catalysts previously reported by other authors.

In the same line, hydrothermally synthesized WNb-mixed oxides have shown the advantage of having crystalline structure, area and acid properties modified by tailoring their composition. Optimization of W-Nb contents and post-synthesis conditions in HT-samples maximized the yield of final organic products useful for fuel application. Moreover, HT-WNbO catalysts show much better catalytic results than other WNbO samples prepared by different procedures.

Sn-based mixed oxides (Chapter 7):

Finally, Sn-based mixed oxides were studied as Sn^{4+} centers are known to be effective Lewis acid sites and because rutile-phase crystalline structures have been claimed to have interesting hydrophobic characteristics. Both properties could allow facilitating condensation reactions in aqueous phase.

Poor catalytic results in aqueous-phase condensations shown by Sn_xZr_yO mixed oxides confirmed the importance of synthesizing uniform rutile-phase mixed oxides for developing active Sn-based mixed oxides.

In this sense, Sn_xTi_yO materials preparation via co-precipitation allows obtaining homogeneous SnTi mixed oxides with rutile-phase structure, with enhanced textural properties and a higher concentration of Lewis acid sites. These materials have shown better catalytic results in the aqueous-phase condensation of light oxygenates than monometallic SnO_2 and TiO_2-rutile catalysts. More interestingly, rutile TiO_2 and specially Sn-Ti mixed oxides showed better resistance to the addition of water and acids in the medium compared to other anatase TiO_2 materials (including faceted TiO_2 catalysts developed in Chapter 5).

Remarkably, Sn_xNb_yO and $Sn_xTi_yNb_zO$ materials can also be prepared via co-precipitation, where both Nb and Ti can be partially or fully incorporated into the rutile structure of SnO_2. SnNb mixed oxides with enhanced textural and acid properties and outstanding resistance to acidic aqueous environments drive to the best catalytic results observed along all this work. Moreover, these catalysts can be reused with negligible loss of activity due to the small deposition of coke on their surface.

Finally, bio-oils aqueous fractions and ABE aqueous mixtures can be upgraded via “one-pot” consecutive condensations of oxygenated compounds into hydrocarbons and aromatic products useful in fuel applications. This innovative strategy allows reducing associated costs derived from process water streams and improves the organic phase quality and its further application when these catalysts are employed.

CHAPTER 9

LIST OF FIGURES AND TABLES

9.1 List of Figures

Chapter 1. Introduction

Chapter 3. Experimental Procedure

Chapter 4. Ceria-Zirconia and hydrotalcite-derived mixed oxides as acid catalysts for the aqueous-phase condensation of oxygenated compounds

Page

Chapter 5. {001} Faceted TiO_2 materials as acid catalysts for the aqueous-phase condensation of oxygenated compounds

Chapter 6. Niobium and tungsten-niobium oxides as acid catalysts for the aqueous-phase condensation of oxygenated compounds

Chapter 7. Tin-based mixed oxides as acid catalysts for the aqueous-phase condensation of oxygenated compounds

9.2 List of Tables

Chapter 1. Introduction

Chapter 3. Experimental Procedure

Chapter 4. Ceria-Zirconia and hydrotalcite-derived mixed oxides as acid catalysts for the aqueous-phase condensation of oxygenated compounds

Chapter 5. {001} Faceted TiO_2 materials as acid catalysts for the aqueous-phase condensation of oxygenated compounds

Page

Chapter 6. Niobium and tungsten-niobium oxides as acid catalysts for the aqueous-phase condensation of oxygenated compounds

Chapter 7. Tin-based mixed oxides as acid catalysts for the aqueous-phase condensation of oxygenated compounds